Exponent®

PG&E's Composite Risk Model for Overhead Electric Transmission Components:

A White Paper

DRAFT: 31 March 2022, Revision 1

Exponent®

PG&E's Composite Risk Model for Overhead Electric Transmission Components:

A White Paper

Prepared for

Mr. [redacted]
Dr. [redacted]
Pacific Gas and Electric Company

Prepared by

Exponent
149 Commonwealth Drive
Menlo Park, CA 94025

DRAFT: 31 March 2022, Revision 1

Doc. no. 2102746.000 - 9462

DRAFT: 31 March 2022, Revision 1

Contents

List of Figures

DRAFT: 31 March 2022, Revision 1

Definitions

Definitions used in risk assessments vary by industry and application. The definitions used herein are specific to this application and may differ from those used elsewhere.

Annual Exceedance Frequency (AEF): The number of times, on average, a hazard intensity is exceeded in one year. AEF is the reciprocal of the mean return period of a hazard intensity.

Annual Failure Rate*:** The expected number of unwanted outcomes (e.g., failures) in a year. It is the reciprocal of the mean time between failures (mtbf). For low annual failure rates (less than 0.02), it is approximately equal to the ***annual probability of failure.

***Annual Probability of Failure*:** The probability of at least one unwanted outcome (e.g., failure) occurring in a single year.

***Asset*:** The combination of a transmission line structure (e.g., a lattice tower or a wood pole) and all components supported by the structure (e.g., conductors, hardware and equipment).

Component grouping: A group of components with similar lifecycle, sensitivity to threats/hazards, and asset management strategy.

***Composite Annual Probability of Failure*:** Annual probability of failure combined across multiple component groupings and/or multiple hazards.

***Degradation*:** Reduction in capacity, or increase in uncertainty, over time caused by a threat.

Design Life: The theoretical age of a component or structure at which the uncertainty regarding whether it remains fit for purpose is so high (or, conversely, the confidence is so diminished) that it would be scheduled to be either replaced, hardened or re-certified based on engineering analysis.

***Expected Useful Life (EUL)*:** The age of a component or structure, based on average degradation rates and external hazards, at which the risk of failure outweighs the benefits of continued inspection, maintenance, repair and/or hardening.

***Failure (or Unwanted Outcome)*:** The inability of the asset to perform its expected function. Examples of failures could include support collapse, heat- or flood-induced equipment failure, clearance violation, or the inability to provide service due to any number of underlying causes.

***Failure Rate Tolerance (or Failure Rate Appetite)*:** A failure rate above which the risk associated with a component or asset is unacceptably high.

***Fragility*:** The conditional probability of an unwanted outcome given the intensity of a hazard (e.g., the likelihood of pole groundline failure given a peak wind gust of 100 miles per hour).

Fragility function: The locus of fragilities for all hazard intensities. Fragility functions are conventionally expressed as lognormal cumulative distribution functions defined by a median, μ, corresponding to the median hazard intensity at which the unwanted outcome occurs, and a dispersion parameter, β, which defines the shape of the fragility function, i.e., the probabilities of unwanted outcomes corresponding to all hazard intensities.

***Hazard*:** An event that causes a failure or other unwanted outcome. Events can be external (environmental) or internal (design flaw, operation error, etc.). Examples of external hazards include wind loads, wildfire, and earthquake ground shaking.

***Hazard Curve*:** A locus of points that defines the annual exceedance frequency (or equivalently, mean return period) of a hazard intensity. The term hazard is often used to describe the numerical value of the annual exceedance frequency at a particular intensity such as design level, for example 0.01 would be the hazard associated with the 100-year return period wind speed.

Intensity: The measure of a particular hazard used to predict how the asset will perform and the probability of an unwanted outcome (failure). For instance, the intensity measure for a wind hazard is typically the peak gust speed averaged over 3 seconds.

Mean return period (MRP): The time, on average, between events of a given hazard intensity. MRP is the reciprocal of the annual exceedance frequency of a hazard intensity.

***Risk*:** The combined effect of probability of an unwanted outcome (failure) and the consequence (cost) of that outcome, considered in an overall context (e.g., failure during high wildfire threat conditions). In quantitative risk assessments, risk is often calculated by combining the hazard with fragility and cost functions; cost functions are outside the scope of this report, but the framework herein is formulated so that it can be expanded to include probabilistic cost functions.

***Risk Integral*:** An equation that is used to determine an annual failure rate by combining the hazard and fragility functions in the context of the Total Probability Theorem. The risk integral can be expanded to include probabilistic definitions of the cost and downtime, but those extensions are outside the scope of this report.

***Threat*:** A phenomenon that reduces an asset's ability to resist the effects of a hazard. Examples of threats include wood decay, steel corrosion, wear, and metal fatigue. A threat will typically affect the fragility such that, over time, the probability of an unwanted outcome (failure) increases for a given hazard intensity.

1. Architecture of the Transmission Composite Model

The fundamental purpose of the work described herein is to provide a scientifically sound framework by which Pacific Gas and Electric Company (PG&E) can incorporate asset health and site-specific hazards into their risk-informed overhead electric transmission asset management. This paper describes the technical basis for the framework, while the software that applies this model is referred to as the Composite Risk Tool. For convenience, and consistent with current parlance within PG&E, the framework and its software implementation are collectively referred to herein as the Transmission Composite Model (TCM).

The technical basis of this framework is often attributed to Dr. C. Allin Cornell's original research at M.I.T. and later work while at Stanford. The framework has been applied for decades to the quantitative seismic assessment of nuclear structures, and virtually all nuclear power plants and Department of Energy nuclear structures in the U.S. have been designed and assessed using these methods. More recently, the fundamental aspects of the framework have been adopted into more general structural engineering standards, and now form the basis of the seismic design provisions of building codes. Moreover, building codes now allow direct application of the method for building design as an alternative to the prescriptive requirements of the codes. This new design paradigm is termed Performance Based Engineering (PBE), and it is becoming more common. In fact, many new California high rise buildings have been designed using PBE in lieu of the seismic design provisions of the building code. The framework described in this paper uses the principles of PBE to evaluate the risk to assets that suffer environmental degradation that, over time, reduces their ability to resist external hazards.

The framework is built upon a number of key underlying principles, described briefly here and in more detail in later sections:

- *Assets* are put to use in environments that are not benign, and asset health will degrade with time. The *degradation* of asset health is accompanied by an increase in the probability the asset will fail due to an external *hazard*. The probability of asset failure is a function of its original design, its current health, and the site-specific nature of the hazards (e.g., probabilities of failure are higher at windier sites).

- At some point in its life, an asset will have degraded to the degree that the probability of failure becomes unacceptably high. This point describes the end of its useful life, that is, the risk of failure outweighs the benefits of continued inspection, maintenance, repair and/or hardening. An asset put into service has an *expected useful life* (EUL) based on average degradation rates and external hazards. For instance, wood poles may have an EUL of 60 years, though many poles in less aggressive environments can last much longer, and those in more aggressive environments might be replaced earlier (Figure 1).

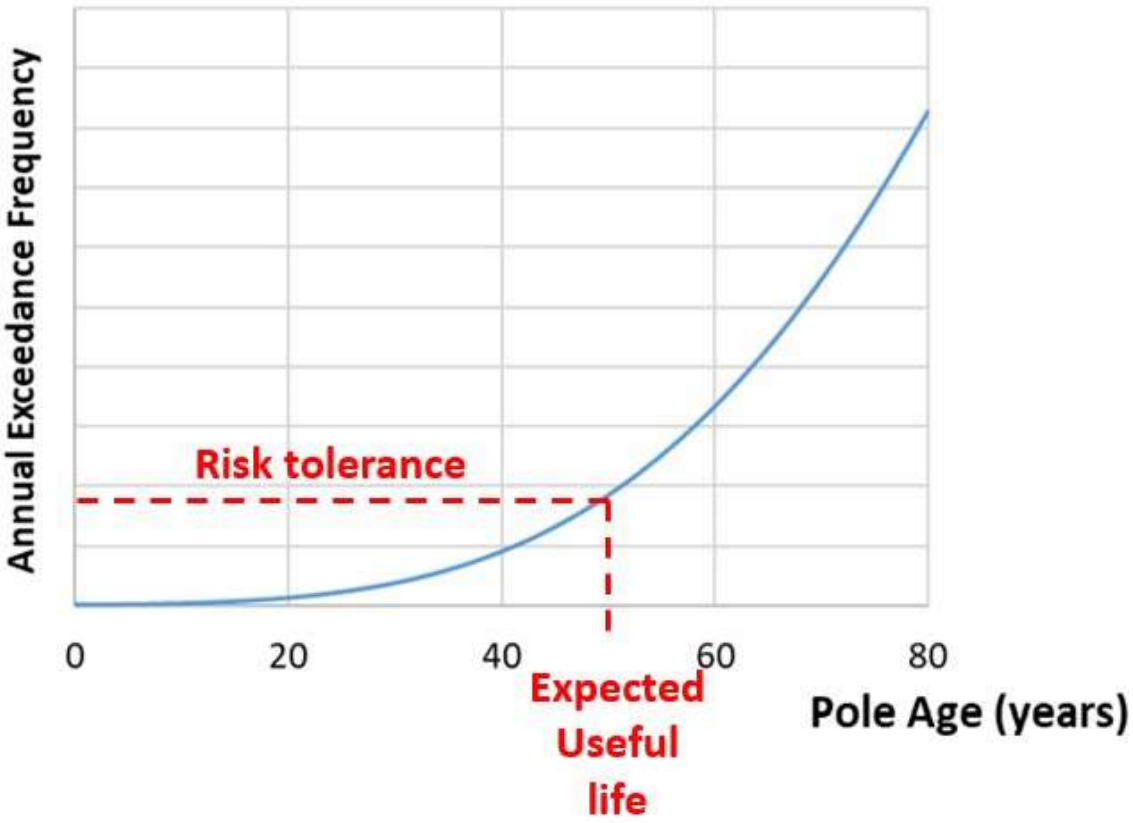

Figure 1. Increasing failure rate with time and the relation to useful life

- One way to calculate the failure rate is by the *Risk Integral* (described in a subsequent section). The Risk Integral takes as input the asset health (in the form of a *fragility function*) and the likelihood of experiencing an extreme external load (in the form of a *hazard curve*). The Risk Integral can be evaluated based on projected future health as determinized by degradation

models to determine the increase in failure rates with time, and the end of useful life when the failure rate crosses an acceptance threshold or *failure rate tolerance*.

- Herein we assume that the failure rate will increase with time due to degradation that begins at the time of installation. Readers familiar with the bathtub curve for product failure rates will note that this neglects early failure rates due to product design and manufacturing defects (the so-called infant mortality portion of the curve). High early failure rates from those causes are outside the scope of the current framework.
- The probability that an asset will fail at a given hazard intensity (e.g., wind speed, or ground shaking acceleration) is termed *fragility*. Low hazard intensities result in low probabilities of failure, while high intensities increase that probability. As such, when *fragility functions* are plotted, they resemble an "S" curve, and are conventionally defined by lognormal cumulative distribution functions, which are defined by a median, μ, corresponding to the median hazard intensity at which the unwanted outcome occurs, and a dispersion parameter, β, which defines the shape of the fragility function, i.e., the probabilities of unwanted outcomes corresponding to all hazard intensities.
- Fragility functions can evolve with time as an asset degrades. The underlying causes of the degradation mechanisms are referred to as *threats*. Threats could include fungal decay for wood poles, or atmospheric corrosion for steel components. The degradation mechanisms associated with these threats are modeled to predict future fragility functions and associated failure rates.
- The likelihood that an asset will be subjected to an external load of a given intensity during a given time period is known as the site hazard, and is typically given in the form of a *hazard curve*. The notion of hazard curves is somewhat familiar because we use the phrase return period to describe the intensity of floods and windstorms. For instance, a wind of 60 miles per hour may have a mean return period of 50 years,[1] whereas a 90-mph wind may have a return period of 100 years. The locus of the return periods associated with all wind speeds forms a hazard curve. Hazard curves are conventionally expressed in terms of the reciprocal of return period, which is termed the annual exceedance frequency (AEF), and are commonly fit to extreme value probability distributions, such as the Gumbel distribution for wind hazard.

For some assets and hazards, there is sufficient information regarding failure rates to preclude the need for evaluation of the Risk Integral, and it is more appropriate to simply estimate failure

[1] A wind with a mean return period of 50 years is exceeded, on average, once every 50 years.

rates directly rather than model fragilities or hazards that may not be amenable to mathematical models. An example of this is vehicle impacts to transmission line structures, for which the hazard is not amenable to modeling, and direct modeling of the failure rates based on past impacts is more appropriate.

More detailed descriptions of the hazards, fragilities, threats, and failure rates are provided in the following sections.

Limitations of the Framework

This report is a living document intended to record the continuous, teamwork-driven process of framework development based on input, recommendations and guidance from diverse groups and subject matter experts. The contents of this document should be considered the current, consensus view of the team rather than the opinions of the authors. As such, the contents of this document may change significantly throughout the course of the development of the framework in both the long and short terms.

Exponent's work was undertaken to assist PG&E in their efforts to reduce the risk of future wildland fire ignitions from overhead electric transmission lines. The framework described herein is based on a diverse set of mostly qualitative data, which necessitates substantive simplifications and assumptions throughout. Although Exponent has exercised usual and customary care in the conduct of its work, it is understood and agreed that the responsibility for reviewing and implementing the framework described herein, including the incorporation of risk tolerances and recognition of the framework limitations, remains fully with PG&E. The framework underlying this work is based on mathematical and statistical modeling of physical systems limited to collection and processing of descriptions of the relative physical health of overhead transmission line assets. Given the nature of the underlying data, significant uncertainties are inherent, and any results from using this framework should be interpreted as indicators rather than facts or predictions of the behavior of specific assets or circuits. The actual performance of specific assets in extreme hazard conditions can be materially different than indicated by the framework.

2. Component Groupings and Assets

A PG&E Failure Mode and Effects Analysis (FMEA) in 2019 identified 47 critical transmission line components such that a failure of a single component had the potential to result in a wildfire ignition. In 2021, a cross-functional team of subject matter experts (SME's) divided these components in *component groupings* based on similarities in lifecycle, sensitivity to threats/hazards, and asset management strategy.[2] This resulted in the following nine component groupings:

- Conductors
- Insulators
- Non-steel structures
- Steel structures
- Foundations
- Switches
- Above grade hardware
- Below grade hardware
- Splices

With the exception of switches, which are addressed by others, the framework described herein is applied to each of these component groupings. The failure rate estimated by the TCM for a component grouping is intended to conservatively estimate the failure rate for the most vulnerable component of the grouping.

At a given structure, the combination of the structure and all components supported by the structure is referred to herein as an *asset*. Failure rates estimated by the TCM for component groupings of an asset can be combined, resulting in an asset-level failure rate. This supports risk-informed asset management at the component grouping level (e.g., a program intended to address wildfire risk associated with wood pole failure), as well as at the asset level (e.g., enhanced inspection programs targeting high risk assets).

[2] For a detailed discussion of the components and component groupings, see "Transmission Line Critical Component Grouping," dated September 7, 2021, by PG&E Transmission Line Asset Strategy.

3. Hazards

Hazard curves are used to quantify how frequently external hazards of various intensities will occur. For instance, consider points on a flood hazard curve representing 100, 200, 500 and 2500-year flood elevations; the locus of these points forms a hazard curve. These points are often fit to an extreme value statistical distribution such as Gumbel, as is done herein for wind hazards.

A hazard curve can take two equivalent forms, either showing the intensity as a function of annual exceedance frequency (AEF),[3] or its reciprocal Mean Return Period (MRP), as shown in Figure 2 and Figure 3, respectively. In the figures, the green curve represents a site with a lower hazard than the site represented by the red curve, as equal intensities have greater frequency (or equivalently shorter return periods) for the red curve. Given two identical assets, the asset located at the site represented by the red curve would experience higher rates of failure because of the higher hazard (higher frequency of intense loading). In this way, the failure rates calculated herein are site-specific.

The TCM currently considers hazards associated with wind and seismic loading, as well as so-called third-party hazards associated with vehicle impacts, metallic balloons/kites, and gunshots/vandalism. Hazard curve formulations for each of these is described in the following subsections.

[3] In some instances, annual *probability* of exceedance is used rather than exceedance *rate*. For the hazard intensities of interest this distinction will not have a measurable effect on calculated failure rates.

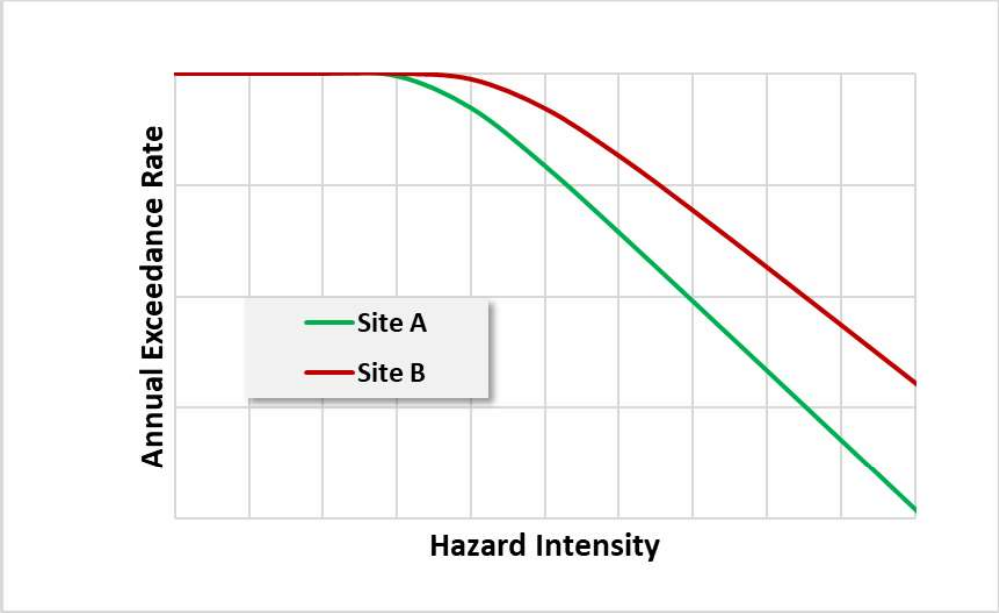

Figure 2. Generic hazard curve showing hazard intensity versus annual exceedance frequency.

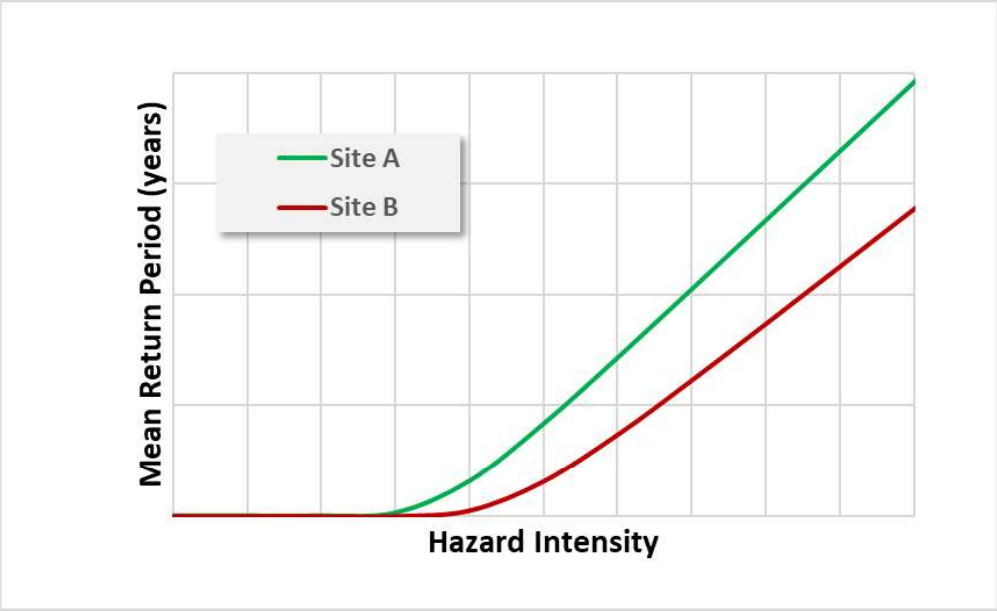

Figure 3. Generic hazard curve showing hazard intensity versus mean return period.

Wind Hazard

The annual failure rates and useful life for many assets are defined by their ability to resist wind loads. As such, expected failure rates for many assets are calculated based on wind hazard, though the threats (degradation) come from multiple sources. In California, the minimum strength requirements for utility structures are prescribed by General Order 95 (G.O. 95), although California utilities may design to internal standards that exceed G.O. 95 requirements.

The wind hazard for assets considered herein are site-specific, based on meteorological data provided by PG&E. The data is provided for the entire service area on a 2km × 2km grid, and is based on 31 years of data collection and modelling of maximum hourly wind each day, converted to 3-second gust equivalent. Data provided includes ordered pairs of wind velocity and the percentage of days over 31 years for which the velocity was not exceeded (i.e., the maximum recorded wind speed was lower than the given velocity).[4] For example, a pair of 40 mph and 60% would indicate that, at this site, on 60% of the days the recorded peak 3-second gust was lower than 40 mph. This empirical wind data is fit to an Extreme Value Type I (Gumbel) distribution by determining the Gumbel location and scale factors that minimize the error in the percentiles for all wind speeds weighted equally (Figure 4). The percentiles associated with the fit allow direct calculation of mean return periods and annual exceedance frequencies (Figure 5),[5] which are used directly in the failure rate calculations.

The resulting wind speed maps for the PG&E service area showing the 50, 100 and 150-year mean return period gust speeds appear in Figure 6, Figure 7, and Figure 8, respectively.

[4] The data records the highest wind speed regardless of direction. Herein we make the conservative assumption that the wind comes from the most adverse direction for each asset.

[5] Note that the annual exceedance frequency of the lowest recorded wind speed from the dataset will be 365, since that wind speed was exceeded on every day of every year.

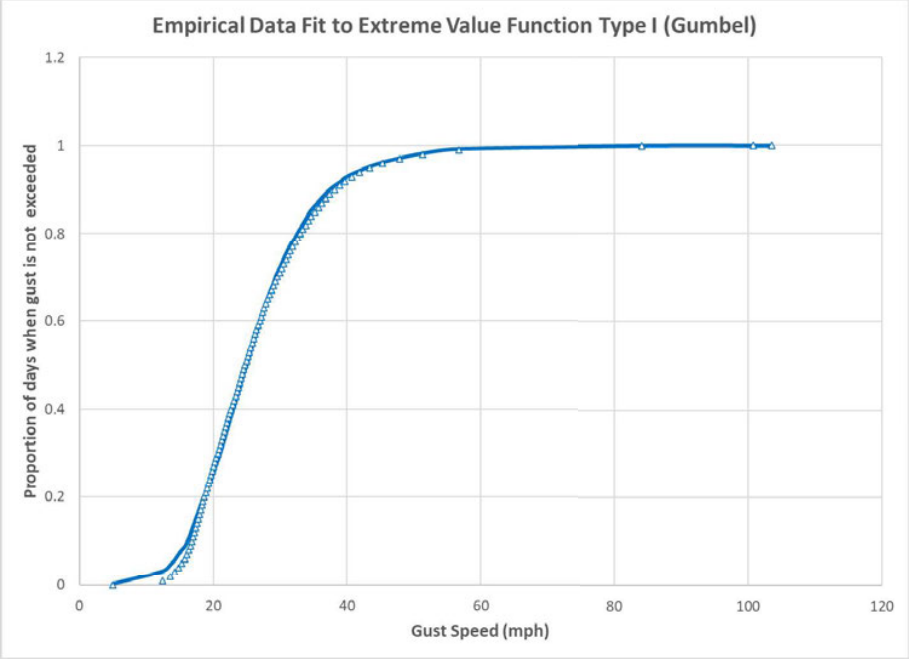

Figure 4. Example of Gumbel distribution fit to PG&E wind percentiles.

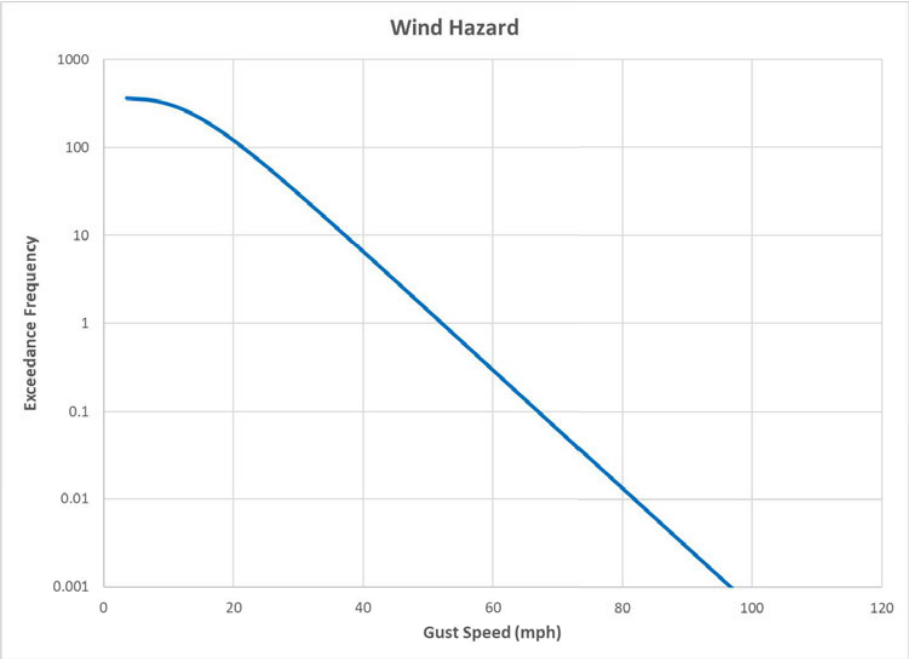

Figure 5. Wind hazard curve based on fit shown in Figure 4.

DRAFT: 31 March 2022, Revision 1

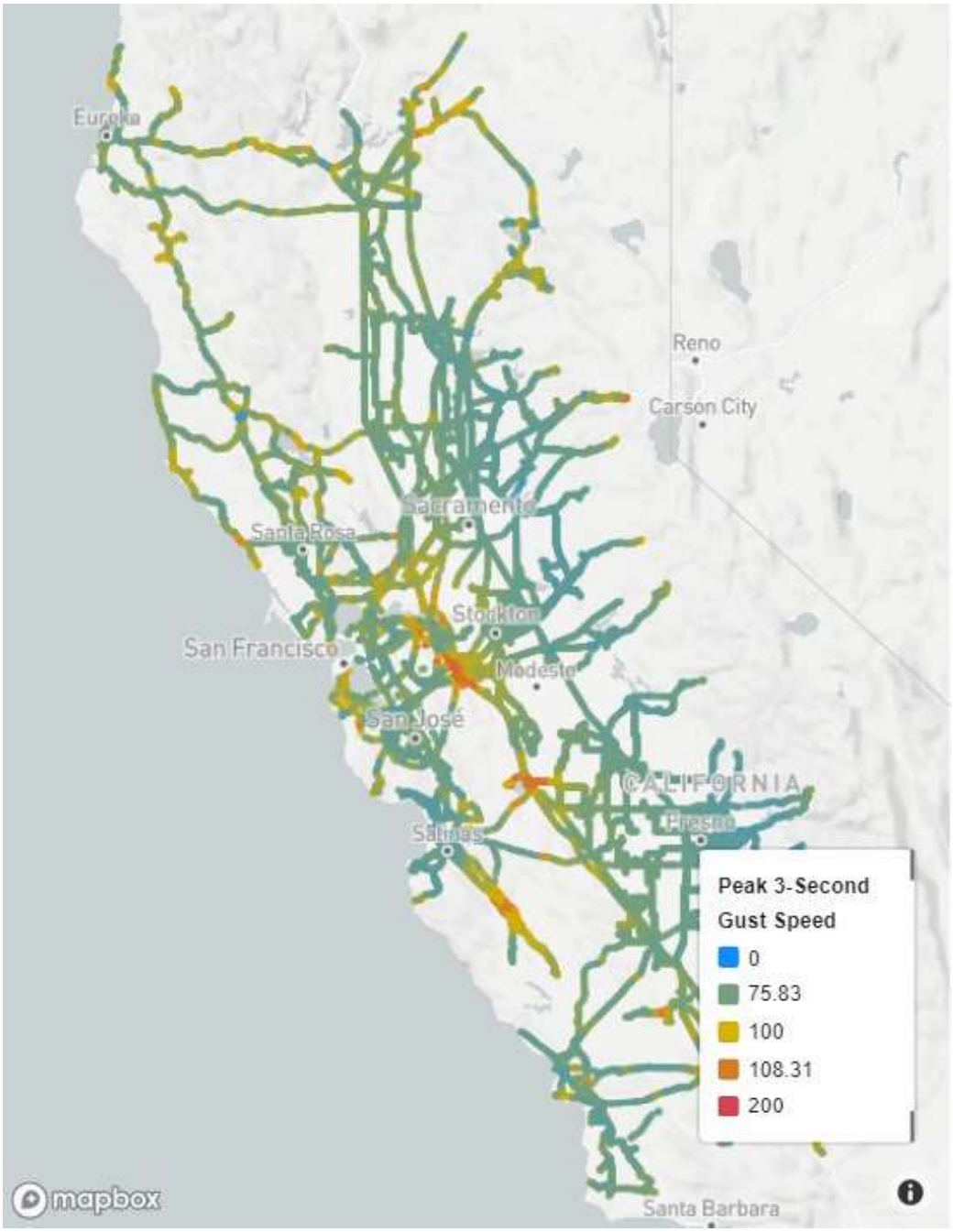

Figure 6. 50-year mean return period 3-second gust speed mapped at each transmission structure.

DRAFT: 31 March 2022, Revision 1

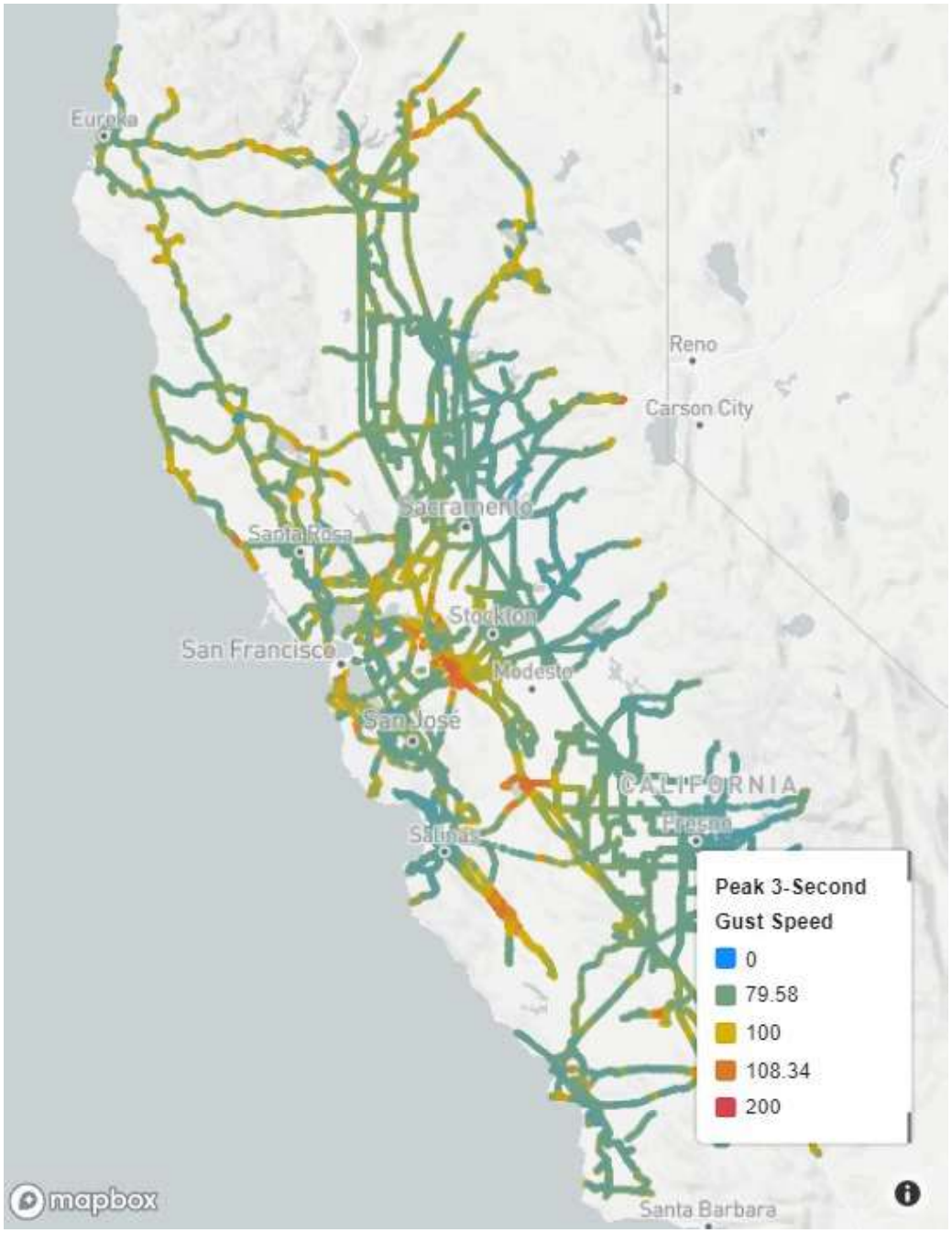

Figure 7. 100-year mean return period 3-second gust speed at each transmission structure.

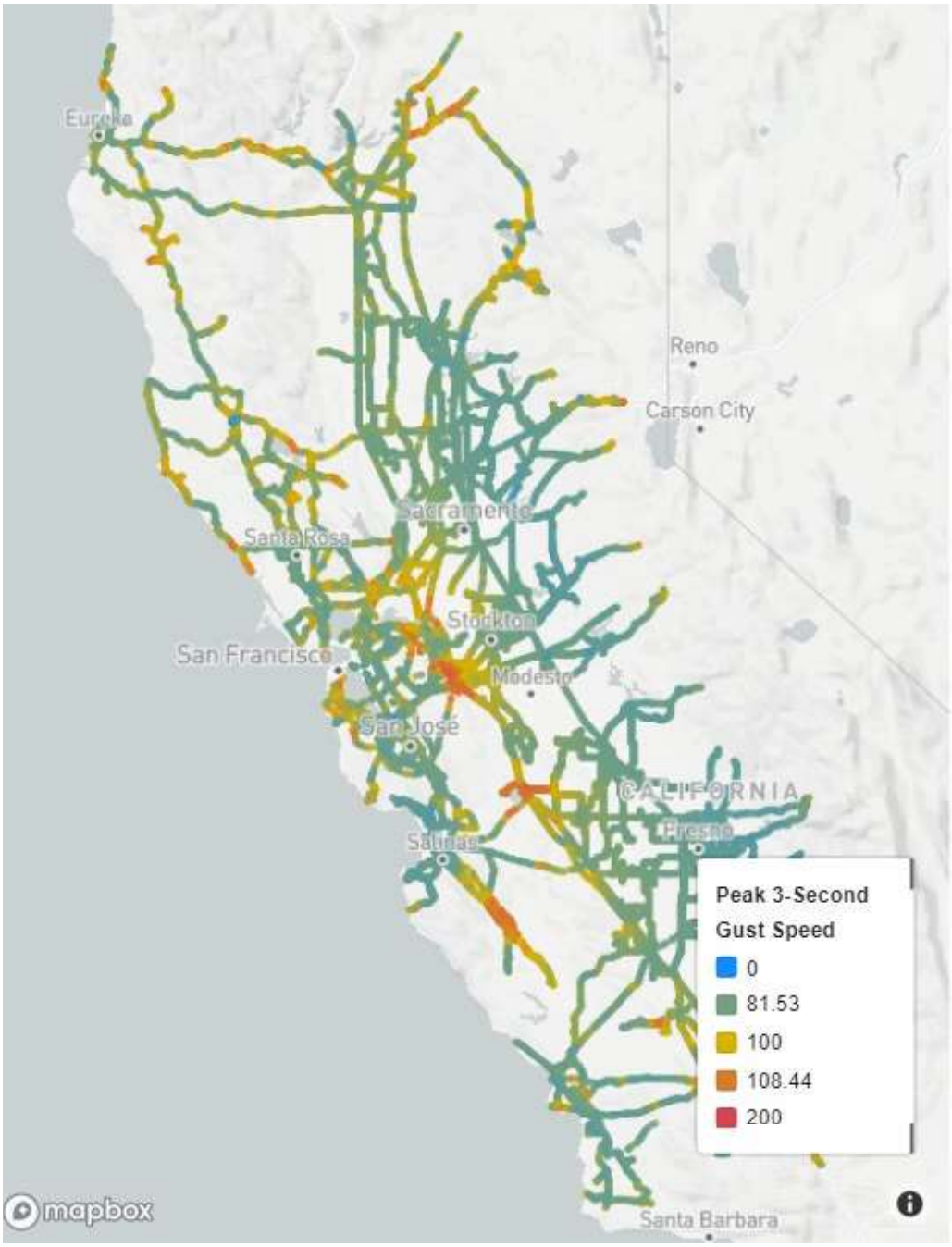

Figure 8. 150-year mean return period 3-second gust speed at each transmission structure.

Figure 9 shows a histogram of the 100-year mean return period wind speed at each structure location. The substantial variability across the PG&E service territory is an indication of how important it is to consider the wind environment when risk-ranking similar assets.

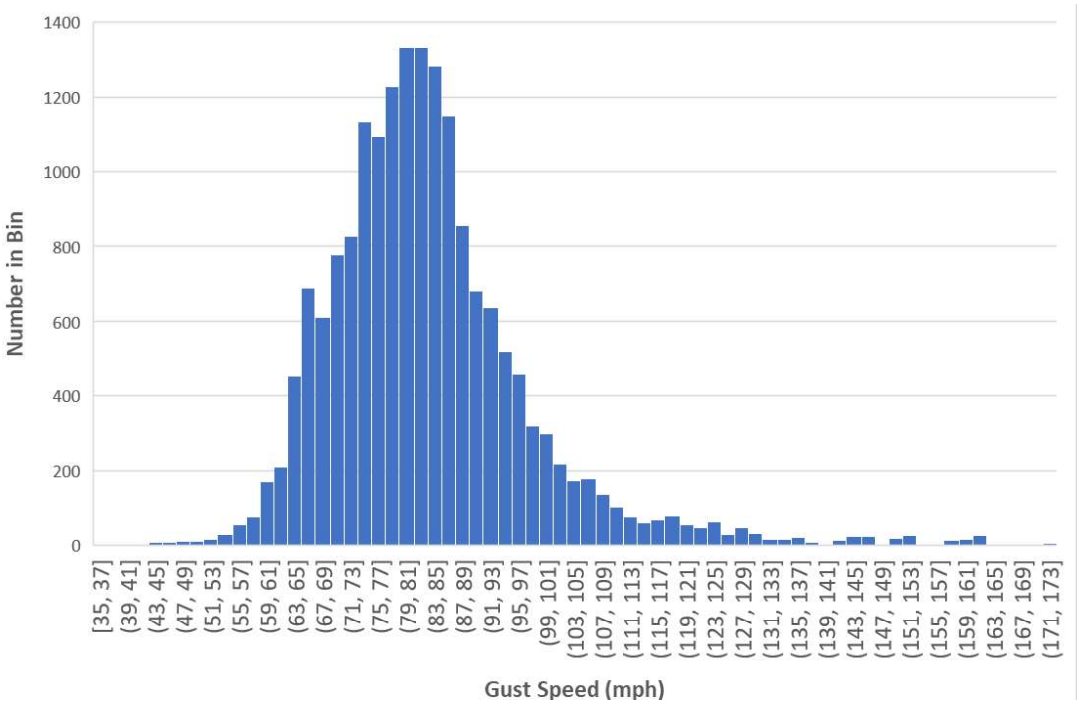

Figure 9. Histogram of 100-year mean return period winds for all structures.

Seismic Hazard

The TCM estimates annual probabilities of failure of wood poles and steel transmission towers due to inertial forces and landslides. For the inertial force models, peak ground acceleration (PGA) is used as the intensity measure for wood poles because they are expected to be relatively rigid, while spectral acceleration at the first mode period, Sa(T1), is used for steel towers due to the potential for flexibility of the towers. The first mode period of several transmission tower types was calculated by performing a modal analysis of the towers. Site-specific hazard curves for both PGA and Sa(T1) are taken from the USGS 2018 dynamic conterminous model based on

the soil site class at each location. These hazard curves are integrated with fragility curves to determine the annual failure probabilities of wood poles and steel towers due to inertial forces.

The landslide analysis uses the joint probability distribution of PGA and earthquake moment magnitude (M) as its intensity measures because expected landslide displacements, which are used to determine failure probabilities, are a function of both PGA and M. The joint probability distribution is determined from the USGS 2018 dynamic conterminous model at numerous return periods such that a hazard curve for PGA can be defined, and the distribution of M at each PGA intensity level on the hazard curve is also defined. This enables probabilistic estimates of landslide displacement hazard curves that consider jointly distributed intensity measures.

For a detailed description of the seismic hazard data used by the TCM, see Appendix A, which includes information related to the following component/hazard combinations:

- Wood pole inertial force
- Steel tower inertial force
- Wood pole landslide (in progress)
- Steel tower landslide (in progress)

Hazards for which Failure Rates are Otherwise Estimated

There are some external events that can cause failures or outages that are not amenable to hazard curve formulation or failure rate calculation using the Risk Integral. Failure rates from these hazards are modeled directly based on past performance, subject matter expert input, and engineering judgment. Such hazards are described below.

Third-Party Hazards

The TCM currently considers third-party hazards associated with vehicle impacts, metallic balloons/kites, and gunshots/vandalism. Annual probabilities of the occurrence of damage events caused by these hazards were estimated by Urbint using machine learning models that

ingest work order, outage, and inspection data related to each hazard. Probabilities were provided for hexagonal grid cells throughout the PG&E service territory.[6]

Because the TCM estimates failure rates at the asset and component grouping levels, results from the third-party hazard models are apportioned to the relevant assets and component groupings so that the results can be combined with those of other hazards. For car impact hazard, probabilities of damage events are apportioned equally to the structure component groupings (steel structure or non-pole structure) of all assets in a hexagonal grid cell. For metallic balloon/kite hazard, probabilities of damage events are apportioned equally to the conductor component groupings of all assets in a hexagonal grid cell. For gunshot/vandalism hazard, probabilities of damage events are apportioned equally to the conductor and insulator component groupings of all assets in a hexagonal grid cell.

According to Urbint, results from their third-party hazard models are intended to be evaluated at the hexagonal grid level, and results have been apportioned to relevant themes and component groupings in the TCM solely for the purpose of combining with results associated with other hazards. See documentation by Urbint for details regarding their third-party hazard models.

[6] Results provided by Urbint represent the annual probability of at least one damage event associated with the hazard of interest within the grid cell. For purposes of the TCM, a third-party damage event is considered equivalent to a failure due to one of the other hazards (e.g., wind). In other words, annual probability of at least one damage event is considered equivalent to annual probability of failure.

4. Fragility Functions

Transmission assets are designed to withstand various external (environmental) hazards such as high winds and ice accretion. It is possible, based on engineering principals or past performance of similar assets, to estimate the capacity to resist each hazard (e.g., the wind speed at which we expect the pole to snap at its base). However, material properties and construction practices vary, and therefore the capacities of nominally identical assets will vary. Moreover, our engineering models are imprecise, and we cannot predict failure loads with 100% accuracy. As such, we can never know an asset's capacity to withstand a given hazard intensity with complete certainty. A benefit of using *fragility functions* is that both the asset's capacity, as well as the degree of certainty with which it can be predicted, are quantified and tracked.

Fragility functions quantify the probability of some unwanted outcome (failure)[7] given that the asset is subjected to a hazard of some intensity. For instance, the increasing probabilities that a wood pole will break at the ground line due to transverse wind could be estimated for peak gusts of 50, 100, and 200 mph. The locus of these points forms a fragility function that is conventionally expressed as a lognormal cumulative distribution function defined by a median, μ, corresponding to the median hazard intensity at which the unwanted outcome occurs, and a dispersion parameter, β, which defines the shape of the fragility function, i.e., the probabilities of unwanted outcomes corresponding to all hazard intensities.[8]

The fragility functions for new component groupings in the TCM subjected to wind hazard are derived from publicly available technical literature describing reliability studies of electric transmission structures. The basis for new metallic components was obtained from the document *Reliability-Based Design of Transmission Line Structures: Final Report*, Publication EL-4793 by the Electric Power Research Institute. Based on calibration studies, that document

[7] Failure is put in quotes here because it is the common terminology in quantitative risk assessments, even when the outcome is not a failure in the usual sense (collapse or broken component). Fragility can represent the probability of exceeding any limit state, such as noncompliance with standards, or the onset of a condition that requires further inspection.

[8] The median strength by definition is the wind speed at which half of the assets would be expected to fail. The dispersion represents the uncertainty in our strength estimation and is reflected in the width of the bell-shaped curve of the probability distribution.

recommends that utilities developing new design standards for lattice transmission structures target a reliability (annual probability of failure) of 2.7×10^{-5} (based on a 50-year reliability index of 3.0). The basis for new wood and polymer components was obtained from the document *Reliability-based Design of Utility Pole Structures*, a 2006 publication by ASCE, which suggests a higher annual probability of failure of 4.6×10^{-4} (based on a 50-year reliability index of 2.0) for existing wood poles. Based on technical literature and engineering judgement, values for the standard deviation of the natural logarithms of strength for new metallic and wood/polymer component groupings are taken as 0.2 and 0.3, respectively. The corresponding new component grouping fragilities based on these calibration studies are shown in Figure 10.[9]

The calibrated fragility functions described above assume all component groupings have been sized/selected based on the minimum design wind loads for transmission structures. This assumption is in the process of being refined by computer-aided structural analyses by others, using the software PLSCADD. While PLSCADD results are available for only a limited number of assets at this time, the median strength parameter of the fragility functions is adjusted for component groupings where results are available.[10]

Fragility functions are typically not constant over time, but will evolve as the asset degrades. For instance, wood poles can be weakened by fungal decay, or metallic conductors can be weakened by small fatigue cracks due to Aeolian vibration. The threats to different asset types and modeling of the degradation mechanisms are described in the next section.

---

[9] For a more detailed description of fragility curve development, see *A Framework for Risk-Based Transmission Line Asset Management and Operability Assessment, Revision 6*, by Exponent, dated June 1, 2021.

[10] Where PLSCADD results indicate a component grouping has been "overdesigned" with respect to the minimum design wind loads, the median of the fragility function is increased, and vice versa. To account for the possibility of failure modes not analyzed by PLSCADD, the increase in the fragility is capped at a value associated with doubling the minimum wind-related design strength.

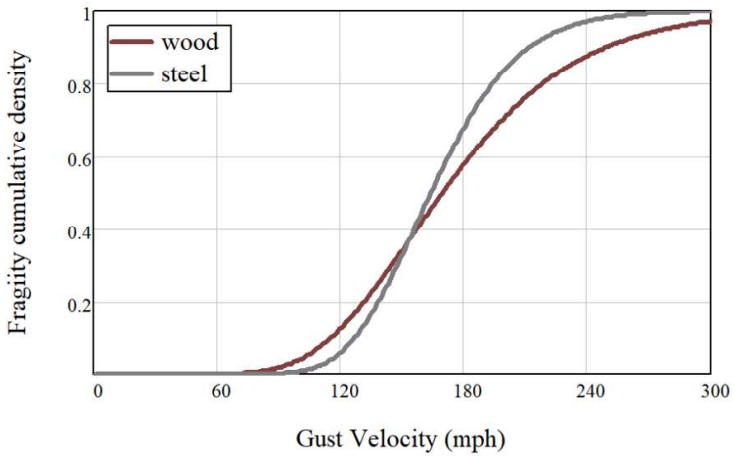

Figure 10. Fragilities for metallic and wood/polymer component groupings with median strength based on EPRI and ASCE calibration studies, respectively.

While overhead electric transmission and distribution assets are typically not designed for seismic hazard,[11] inertial forces imparted to these assets during an earthquake are similar in nature to lateral forces caused by wind. In the same way, the threats that weaken an asset relative to wind hazard also weaken the asset relative to seismic (inertial) hazard. For this reason, the fragility functions for new component groupings in the TCM subject to seismic (inertial) hazard are derived from calibrated wind fragility functions as detailed in Appendix A.

[11] G.O. 95 Rule 43 specifies temperature, wind, ice and dead weight as the loads to be considered in the design of components and structures.

5. Threats

In this framework, externalities that affect the fragilities over time are referred to as *threats*. Either decreased capacity (median strength) or increased uncertainty (dispersion) will cause the probability of failure for a given hazard intensity of interest to increase, thereby increasing the risk associated with that asset. For instance, wood poles can decay over time, thus reducing their structural capacity. However, we lose confidence in a wood pole's capacity to resist wind as the pole approaches the end of its design life, even if it is in visually good condition. Strength reduction shifts the bell curve model of capacity to the left, and increased uncertainty (higher standard deviation) causes it to fatten. As an example, consider the results of strength tests of new and existing poles conducted by the Electric Power Research Institute in the 1980s (Figure 11). The strength distribution of older wood poles has shifted the bell curve to the left, while increased variability (uncertainty) is illustrated by the fattening of the curve.

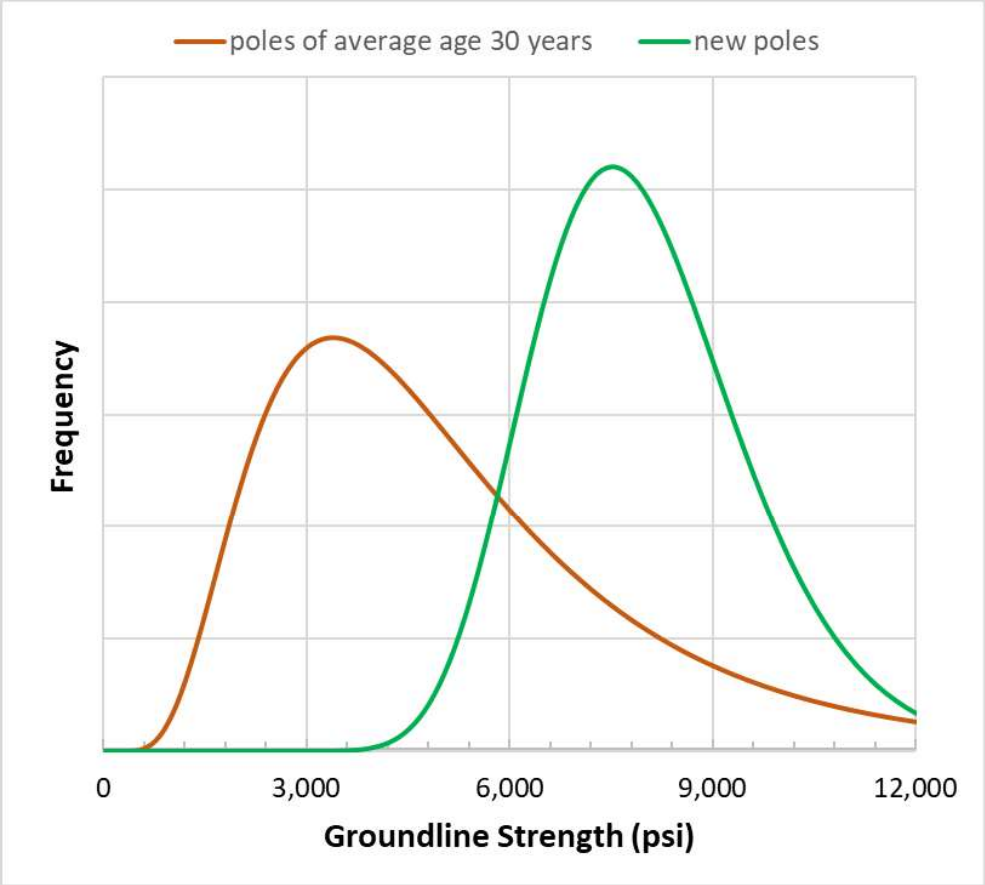

Figure 11. Loss of strength and increased dispersion as wood poles age[12] and the effect on fragility.

Effects of Decreased Capacity or Increased Uncertainty

This section describes the modeling of changes to both capacity and uncertainty due to the effects of external threats.

[12] Reliability-Based Design of Transmission Line Structures: Final Report, Publication EL-4793 by the Electric Power Research Institute, 1986.

Decreased Capacity[13]

Unless the asset is in a perfectly benign environment and made of indefatigable material, the asset's fragility function will change with time in ways that reflect increased probability of asset failure. Consider the wind fragility function for groundline bending failure of an existing wood pole (Figure 12, black curve); in a 100-mph wind there is less than 5% chance of failure. If the base of the pole is subject to the *threat* of decay, in time its capacity to resist wind will be reduced. In this example, after 30 years the probability of failure in a 100-mph wind increases from less than 5% to almost 40% due to the weakened base. The effect of this weakening on the fragility function can be seen as the dashed red curve in Figure 12.

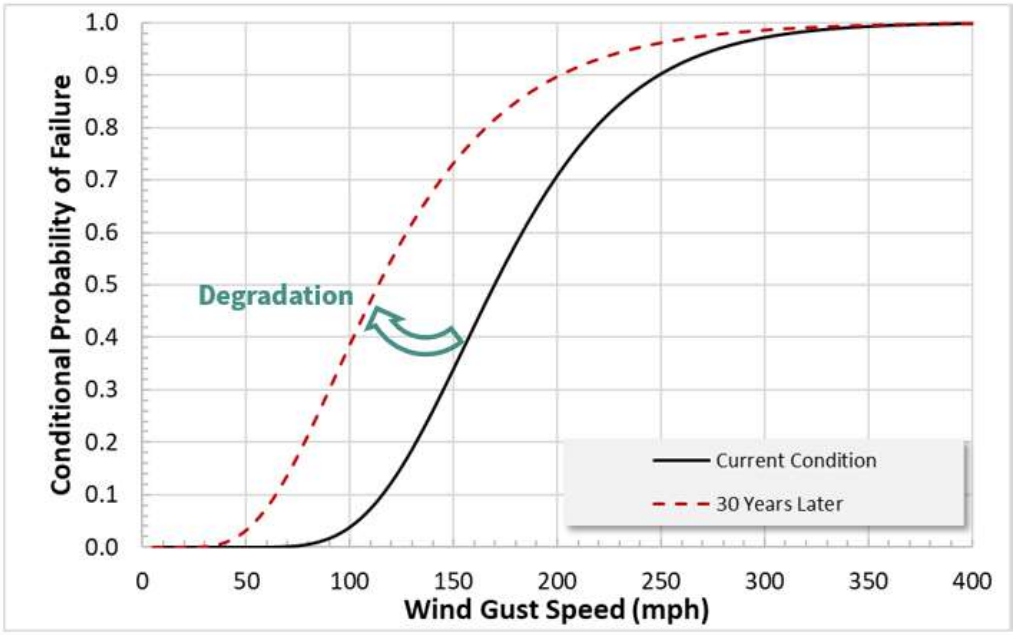

Figure 12. Fragility functions for an existing wood pole (black) and an aged, degraded pole (red dash).

[13] Capacity is defined as the asset's ability to perform its intended function in the presence of hazard(s) of some intensity. In the current context of the TCM, it typically refers to physical strength, but it other contexts it could refer to more generally things like maintaining clearance to avoid flashover, or maintaining the ability to deliver power.

Increased Uncertainty

As mentioned, increased uncertainty surrounding the asset capacity can also affect the fragility function. Consider the case of a tower that is sited in an area of persistent steady winds transverse to the conductor span, that is, under the *threat* of fatigue due to Aeolian vibration. Further suppose that the fatigue damage location is concealed within a connection such that it is difficult to inspect. Thus, as the conductor ages, we will become less confident in its ability to resist load, even though there is no visible indication of strength loss. In this example, after 30 years our estimate of the probability of failure in a 100-mph wind increases from less than 5% to 12% due to increased uncertainty with age. This effect can be seen as the dashed red curve in Figure 13, which is rotated clockwise relative to the black curve as a consequence of fattening the underlying bell curve.

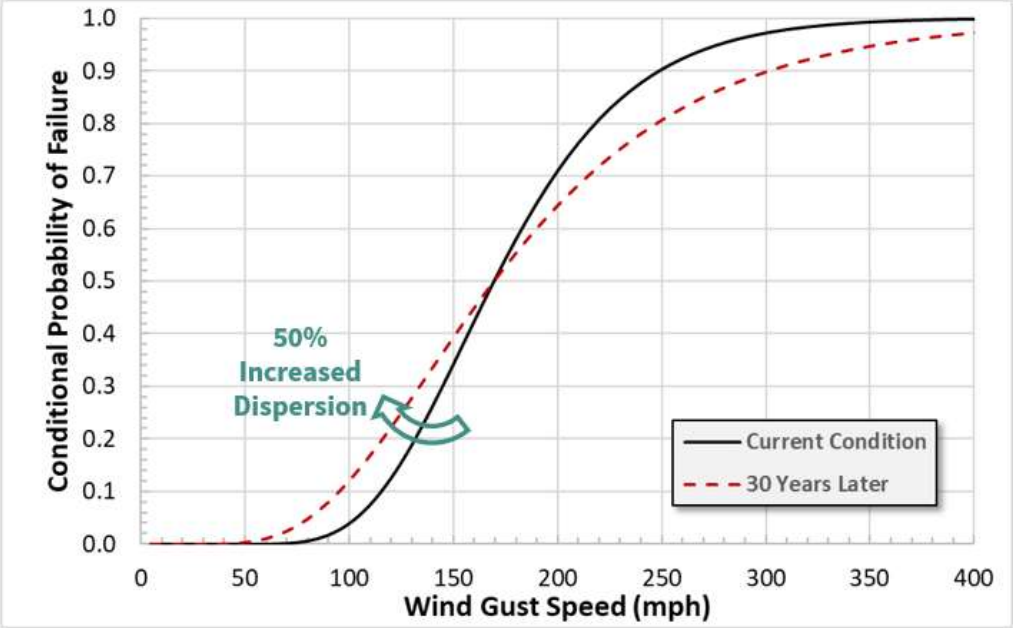

Figure 13. Fragility functions for an existing conductor span (black) and an aged conductor that exhibits no visible degradation (red dash).

Design Life and Design Life Reduction Factors

One of the fundamental concepts used in the framework to track uncertainty is the notion that uncertainty increases with the age of the component, or put differently, we have less confidence in the behavior of older components compared to newer ones. There are two reasons for closely linking uncertainty and age. First, there may be degradation occurring that is not visible and that we cannot easily identify using currently available inspection tools and techniques, such as fatigue damage to a conductor concealed within a connection. Second, design standards and material specifications are presumed to continually improve with time, and newer components or structures should be better fit for purpose with more predictable capacities.

Another fundamental concept used in the framework is that the rate at which uncertainty grows also increases with age. In other words, our confidence in a component does not decrease as quickly in the first third of its design life as it does in the last third. Early in the design life of a component, this assumption is contrary to the so-called bathtub curve often used in product reliability studies in which there is an increased rate of failures early in the life of a product due to design or manufacturing errors. Given the age of the existing transmission line structure stock, it was decided that the early life portion of the bathtub curve had passed for the vast majority of components and that its inclusion would not meaningfully affect the framework results.

The third fundamental concept used in the Framework to address age-related uncertainty is the notion of a design life t_D. The design life is defined herein as the theoretical age of the component or structure at which the uncertainty regarding whether it remains fit for purpose is so high (or, conversely, the confidence is so diminished) that it would be scheduled to be either replaced, hardened or re-certified based on engineering analysis. This defines an important anchor point for our quantification of uncertainty: At t_D, the dispersion of the median strength (as a surrogate for fitness) has increased such that the associated probability of failure when subject to 8 psf wind pressure equals that which would result from a *strength* reduction of 1/3, absent any change in the uncertainty. The 1/3 strength reduction comes from G.O. 95 and is the

strength degradation at which repair or reinforcement is mandated,[14] and 8 psf is the design wind pressure for light loading (no ice accretion).

As discussed above, the engineering parameter used in the framework to quantify the uncertainty is β, which is the standard deviation of the natural logarithms of the strength of a component grouping. Age of the component grouping is currently taken from PG&E's GIS data for the components of a particular component grouping, supplemented with conservative age logic[15] for component groupings without available GIS data. To represent the accelerated rate of uncertainty increase with age, a quadratic uncertainty-versus-age curve is assumed. The quadratic form is adopted because it is simple and exhibits the desired general shape; it is not based on first principles. The quadratic uncertainty curve is anchored at two points (and assumed to have zero slope at time zero):

- At $t = 0$, the dispersion is taken as $\beta = \beta_0$, which is the assumed strength dispersion for new construction based on technical literature and engineering judgement. The values of β_0 for metallic and wood/polymer component groupings are currently taken as 0.2 and 0.3, respectively.
- The second anchor point is at a presumed design life t_D, at which we set $\beta = \beta_R$ such that it results in the same probability of failure subject to 8 psf wind pressure as would a strength reduction of 1/3, all else being equal.

Those three conditions, $\beta_0 = 0.2$ or 0.3 at $t = 0$; $\beta = \beta_R$ at $t = t_D$; and slope = 0 at $t = 0$, are sufficient to solve for the three coefficients of the quadratic form.

The Framework allows for increased uncertainty associated with an aggressive environment by shortening the presumed design life. Reduced design life causes the uncertainty to increase more quickly to β_R thereby increasing the probability of failure at intensities of interest in a shorter time. Based on engineering judgement and review of age information for components across the PG&E network, the TCM currently uses a presumed "no threat" design life of 150 years for all component groupings with the exception of insulators. This design life is a

[14] G.O. 95 Rule 44.3 requires replacement or reinforcement of components when safety factors have been reduced to less than two-thirds of the safety factors associated with new design.

[15] For a description of this logic see "T-Line Asset Data Quality Improvement – Critical Components, Guide to Conservative Assumptions," dated January 14, 2020, by PG&E and GTS.

theoretical value for an asset in a perfectly benign environment, and should not be confused with actual useful life for a given component. The design life is reduced to 100 years and 50 years for non-polymer and polymer insulators, respectively.

Threats can accelerate the increase in uncertainty with time through the use of a "design life reduction factor" (DLRF). In other words, a threat will cause the uncertainty of a component grouping to increase to a given level more quickly than an otherwise identical component grouping that is not subject to the threat. Figure 14 presents graphically the increase in uncertainty with time, including the effect of a DLRF.

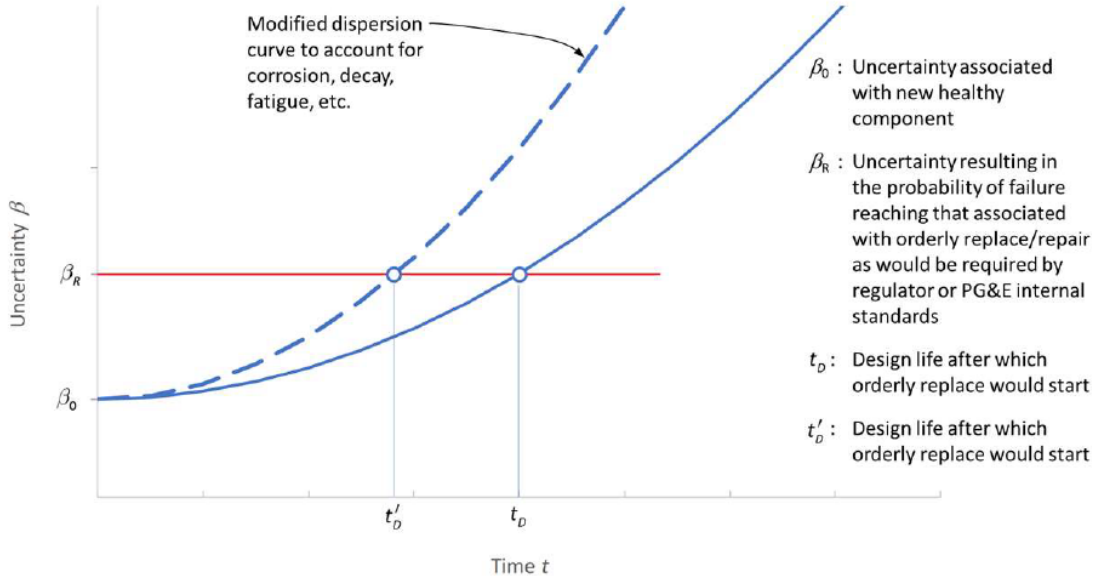

Figure 14. Model of uncertainty increase with time, and the effect on the rate of increase in the uncertainty with shortening the design life.

Currently, based on engineering judgement, the maximum DLRF applied for any single threat in the TCM is 1/3 the notional design life of the component grouping. The effects of multiple DLRF's for a single component grouping are combined by the square root of the sum of the squares method. For example, a component grouping with a DLRF of 1/3 for both corrosion and fatigue would have an overall design life reduction of $\sqrt{(1/3)^2 + (1/3)^2} = 0.47$.

In summary, fragility measures the health of an asset considering both its median strength and the uncertainty in our ability to predict that strength. The fragility of an asset subject to various threats will evolve with time: loss of capacity is demonstrated by a shift in the fragility curve to the left, while increased uncertainty is demonstrated by rotating the curve clockwise. Both of these effects increase the probability of failure at hazard intensities of interest.

Specific Threat Models

Currently, the TCM includes the threat models shown in Table 1, which apply to the component groupings indicated in the table. Threats apply to wind and seismic (inertial) hazards, with the exception of insulator contamination, which applies to the hazard of critical moisture events.

Table 1. Threat model and component grouping matrix

Threat Model	Component Grouping							
	Conductor	Insulator	Non-Steel Structure	Steel Structure	Foundation	Above Grade Hardware	Below Grade Hardware	Splice
Wood decay			✓					
Atmospheric corrosion	✓	✓		✓		✓		✓
Underground corrosion					✓		✓	
Fatigue	✓					✓		
Wear						✓		
Insulator contamination		✓						

A summary of each threat model is included in the following subsections, with more detailed descriptions included in the referenced appendices.

Wood Decay

Relevant hazards: wind, seismic (inertial)

Relevant component groupings: non-steel structure

Effect on fragility function: reduction in median strength, increased uncertainty (Cellon treatment)

The principal threat to wood poles is fungal decay, and wood pole replacement or hardening is most often due to strength loss from fungal decay (Figure 15). Decay reduces the cross-section of a wood pole that is effective in resisting load, typically at or near the groundline but also where water can be trapped at crossarms or at the pole top. PG&E assesses the potential for decay through its Pole Test & Treat (PT&T) program, which involves field testing of each pole on a nominal 10-year cycle. PT&T results include an effective circumference, which can be used to estimate current remaining groundline bending capacity to that of the pole when new. Both the literature and PT&T results indicate that a significant population of wood poles begins to decay several years after installation, while another significant population does not decay even after many decades.

The wood decay model used by the TCM adjusts the median strength of a wood pole's fragility function based on PT&T results for that pole. Depending on the date of the last PT&T results, the model predicts the remaining strength at current and future dates by estimating a decay rate from successive PT&T results, or in the case of a pole with only one PT&T inspection, guidance from the literature regarding how long after installation of the pole appreciable decay is likely to begin.

For a detailed description of the wood decay model used by the TCM, see Appendix B.

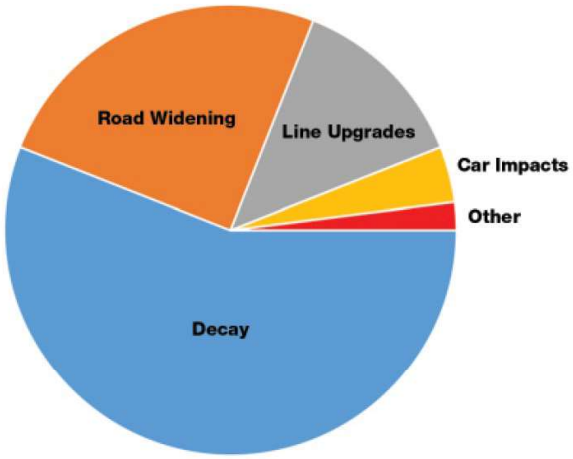

Figure 15. Reasons for pole removal.[16]

Poles are treated using various preservatives to inhibit decay. One of these preservatives, pentachlorophenol in liquified petroleum gas (referred to by its trade name *Cellon*), has been found to provide less effective treatment compared to other common preservatives. Furthermore, decay of poles treated with Cellon often occurs just below the groundline and is therefore concealed to inspectors absent excavation or drilling down from the surface. A comparison of pole replacements by PG&E indicates a Cellon treated pole has a shorter expected useful life (EUL) than a pole with another treatment method. The TCM accounts for this difference in EUL by a Design Life Reduction Factor of 33% for Cellon treated poles.

For a detailed description of the effect of Cellon treatment on wood poles see Appendix C.

[16] Morrell, Jeffrey, Estimated Service Life of Wood Utility Poles, North American Wood Pole Council Technical Bulletin No. 16-U-10, 2016

Atmospheric Corrosion

Relevant hazards: wind, seismic (inertial)

Relevant component groupings: conductor, insulator, steel structure, above grade hardware, splice

Effect on fragility function: increased uncertainty

One of the principal threats to above ground metallic components is atmospheric corrosion, which results in a loss of cross-section that is effective in resisting load. The rate of corrosion depends on environmental factors such as temperature, the presence of water on the surface of the component, and atmospheric pollutants. It also depends on properties of the component such as metal alloy and the presence of paint or other protective coatings.

Systematic measurements of cross-section reduction associated with atmospheric corrosion are generally not available for PG&E components, and corrosion may occur at faying surfaces that are difficult to inspect. For these reasons, the adverse effect of atmospheric corrosion is modeled in the TCM as an increase in uncertainty (dispersion) of fragility functions for metallic component groupings. In other words, the useful life of a component in a highly corrosive environment is expected to be shorter than that of an otherwise identical component in a less corrosive environment.

For a detailed description of the atmospheric corrosion models used by the TCM, see Appendix D.

Underground Corrosion

Relevant hazards: wind, seismic (inertial)

Relevant component groupings: foundation, below grade hardware

Effect on fragility function: increased uncertainty

One of the principal threats to below ground metallic components is underground corrosion, which results in a loss of cross-section that is effective in resisting load. The rate of corrosion depends on environmental factors such as soil pH and the presence of groundwater. It also

depends on properties of the component such as metal alloy and, in the case of foundations, the use of concrete to encase metallic components.

Systematic measurements of cross-section reduction associated with underground corrosion are generally not available for PG&E components, and the corrosion is typically concealed by soil. For these reasons, the adverse effect of underground corrosion is modeled in the TCM as an increase in uncertainty (dispersion) of fragility functions for metallic component groupings located below ground. In other words, the useful life of a component in a highly corrosive environment is expected to be shorter than that of an otherwise identical component in a less corrosive environment.

For a detailed description of the underground corrosion models used by the TCM, see Appendix E.

Fatigue

Relevant hazards: wind

Relevant component groupings: conductor, above grade hardware

Effect on fragility function: increased uncertainty

Steady winds perpendicular to a conductor span cause vibrations due to vortex shedding, referred to as Aeolian vibrations. These high cycle, low amplitude vibrations can result in fatigue damage to conductors and the supporting hardware. The damage accumulates over time, reducing the capacity of the conductor and/or hardware. The occurrence of Aeolian vibrations depends on the wind environment, such as wind speed, direction and turbulence intensity. It also depends on properties of the conductor such as span length, span orientation, conductor type/size, and conductor tension.

Fatigue damage may ultimately result in broken conductors or fractured connecting hardware. Advance detection of fatigue damage by visual inspection, however, can be difficult because the damage is often concentrated near the connection of the conductor and the hardware, and may therefore be concealed from view. For these reasons, the adverse effect of Aeolian vibration is modeled in the TCM as an increase in uncertainty (dispersion) of fragility functions for conductors and their associated above ground hardware. In other words, the useful life of a

component with a configuration and in an environment prone to Aeolian vibrations is expected to be shorter than that of an otherwise identical component less prone to Aeolian vibrations.

For a detailed description of the Aeolian vibration model used by the TCM, see Appendix F.

Mechanical Wear

Relevant hazards: wind

Relevant component groupings: above grade hardware

Effect on fragility function: increased uncertainty

Wear is chiefly due to large deflections and associated rubbing when relatively light, unbraced components are buffeted in turbulent (gusting) wind. Damage associated with wear accumulates over time, reducing the capacity of hardware used to connect light, unbraced spans such as jumpers. The occurrence of wear depends on the wind environment, such as wind speed, wind direction and frequency content of the wind turbulence. It also depends on the properties of the components buffeted by the wind, such as mass, length, stiffness, and damping. Finally, wear depends on the thickness and material properties of the hardware components that are ultimately subject to material loss.

Currently, details regarding hardware and jumper components are not sufficiently available across the PG&E network to develop asset-specific structural models of the components. For this reason, Exponent's first-principles wear model assumes reasonable values for component properties relevant to the calculation of wear, and applies site-specific wind properties to a structural model based on these reasonable values. The results of the wear model include the depth of wear for a typical metal hanger plate. For a detailed description of Exponent's first-principles wear model, see Appendix G.

The results of Exponent's first-principles wear model is used as an input parameter for a machine learning model by Urbint. This model is used to predict the likelihood of wear at assets throughout the PG&E network, sorted by Urbint into bins of high, medium, and low wear potential. These results are the basis of the design life reduction factor for wear used in the TCM. See documentation by Urbint for details regarding their wear model.

Insulator Contamination

Relevant hazards: critical moisture event

Relevant component groupings: insulator

Effect on fragility function: increased probability of failure with accumulation

As contamination from dust, wildland fires, etc., accumulates on insulators, they become susceptible to flashover when a heavy fog or light rain occurs that generates ionized solution on the insulators. Over time, increased accumulation makes insulators more susceptible to flashover, while washing of the insulators from heavy rain removes the depositions and makes them less susceptible to flashover. Exponent has developed a first-principles model to calculate the annual rates of insulator flashover from this mechanism, as follows:

- Estimate the deposition rate of contaminants on insulators;
- Estimate the distribution of precipitation amount in a given period to determine the expected washing of the insulators;
- Estimate the rate that critical rainfall events occur, that is, heavy fog or light rain;
- Determine the relationship between probability of flashover given a deposition total accumulation quantity and the voltage stress of the insulator, by insulator type, conditioned on the occurrence of a critical rainfall event;
- Simulate the accumulation of depositions, washing, and critical rainfall events to determine the rate of insulator flashover.

For a detailed description of the insulator contamination model used by the TCM, see Appendix H (in progress).

6. The Risk Integral and Projected Failure Rates

The hazard and fragility functions can be combined to calculate the annual rate λ at which the unwanted outcomes will occur (i.e., the frequency at which the limit state will be exceeded, or failure rate for short). This equation is known as the *Risk Integral*. For low exceedance frequencies, the annual rate λ approximates the annual probability of failure; annual exceedance frequency, annual failure rate, and annual probability of failure are often used synonymously in this context. This is not technically correct but is normally very close for practical ranges of failure probabilities. For example, for annual failure rates less than 0.02, the different between the annual failure rate and annual probability of failure is less than 1%, assuming failures follow a Poisson process.

The Risk Integral is:

$$\lambda = \int_0^\infty p(f|im) \left| \frac{\mathrm{d}h}{\mathrm{d}im} \right| \mathrm{d}im$$

Where $p(f|im)$ is the probability of an outcome f conditioned on the intensity of the hazard im, $\left| \frac{\mathrm{d}h}{\mathrm{d}im} \right|$ is the absolute value of the derivative of the hazard curve (i.e., the slope of the hazard curve), and the integration is performed over all possible intensities of the hazard. In words, the Risk Integral is the integration of the fragility curve with the derivative of the hazard curve.

At the request of PG&E, results of the TCM are presented as annual probabilities of failure, which are calculated from λ assuming failures follow a Poisson process:[17]

$$P(f) = 1 - e^{-\lambda}$$

where $P(f)$ is the annual probability of failure, which is the probability of at least one failure occurring in a single year.

Annual failure rate, λ, and annual probability of failure, $P(f)$, are useful measures by which assets can be risk-ranked, even for assets of different types and for different hazards. The Risk

[17] The Poisson process assumes failures are independent with respect to time, which is a common assumption for failures associated with natural hazards.

Integral provides a failure rate that reflects the underlying hazard and fragility functions. As discussed in the next section, the Risk Integral is evaluated for each component grouping subject to each applicable hazard, and the results can be combined across multiple hazards and/or multiple component groupings.

Both the fragilities and hazards might evolve with time, due to asset degradation and climate change,[18] respectively. As an example, consider the wood pole represented above in Figure 12; the pole groundline bending strength decreased by one third in 60 years due to decay. If we use the wind hazard curve shown in Figure 5, the failure rate λ can be evaluated at any time in the future to show how the failure rate is expected to increase (Figure 16). The curve is similar to the conceptual model in Figure 1.

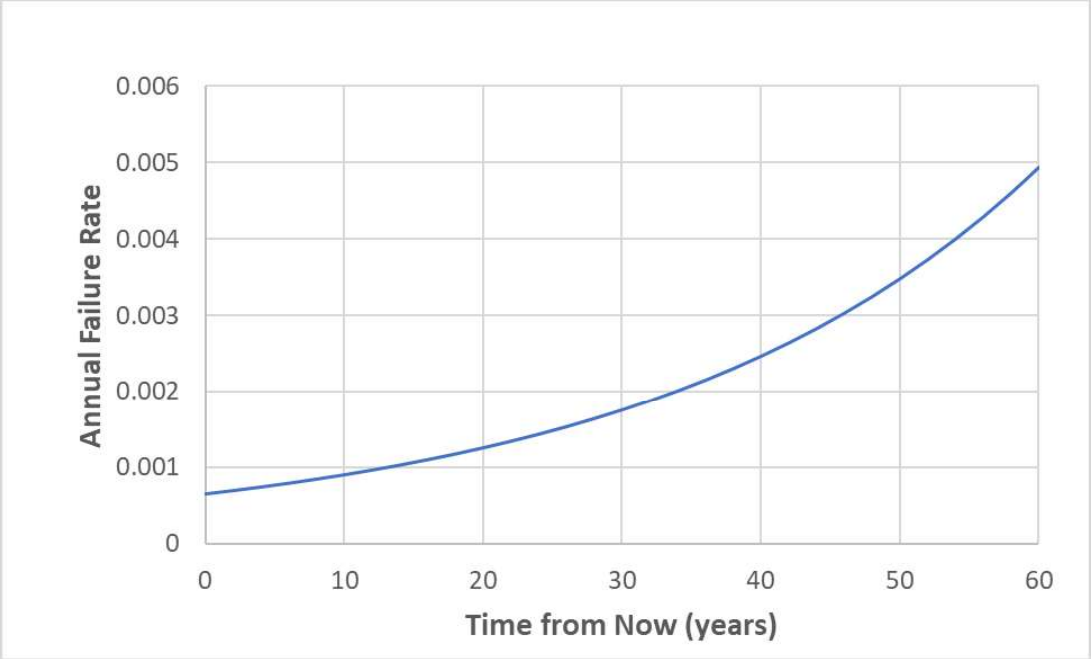

Figure 16. Increased failure rate with time for the example wood pole (Figure 12) and hazard curve (Figure 5) used for illustration in preceding sections.

[18] The effect of climate change is currently outside the scope of the TCM.

The TCM currently evaluates the risk integral for five states of the fragility functions: current state, as well as forecast condition in 5, 10, 25 and 50 years. This allows users of the TCM to evaluate the increase in risk associated with an asset over time, or to predict the time at which a risk threshold will be exceeded.[19]

[19] Future predictions of the Risk Integral assume decreased capacity continues to occur at its current rate, and increased uncertainty continues to follow the quadratic form discussed above.

7. Combining Annual Probabilities of Failure

The annual probabilities of failure described in the preceding section are combined in the TCM in three primary ways:

1. For a single hazard (e.g., wind), annual probabilities of failure for all component groupings of an asset are combined. The resulting probability of failure represents the annual likelihood that at least one component grouping of the asset will fail due to the hazard of interest. This is referred to herein as the *single hazard, asset-level, annual probability of failure.*
2. For all hazards, annual probabilities of failure for a single component grouping of an asset (e.g., conductor) are combined. The resulting probability of failure represents the annual likelihood that the component grouping will fail due to at least one hazard. This is referred to herein as the *multi-hazard, component grouping-level, annual probability of failure.*
3. For all hazards, annual probabilities of failure for all component groupings of an asset are combined. The resulting probability of failure represents the annual likelihood that at least one component grouping of the asset will fail due to at least one hazard. This is referred to herein as the *multi-hazard, asset-level, annual probability of failure.*

The procedures used to combine annual probabilities of failure for these three cases are described below.

Single Hazard, Asset-Level, Annual Probability of Failure

For a single hazard, the asset-level annual probability of failure can be computed in several ways, based on assumptions regarding the correlation between component groupings. For the uncorrelated (mutually independent) case, the annual probability of failure is computed based on the product of the survival rates for each component grouping subject to the hazard of interest:

$$P(f)_{single\ hazard,asset,uncorrelated} = 1 - \prod_{i=1}^{m}(1 - P(f)_{single\ hazard,component\ grouping_i})$$

where m is the total number of component groupings. The uncorrelated case represents the upper bound annual probability of failure.

For the assumption of fully correlated component groupings, the annual probability of failure is equal to the maximum of the annual probabilities of failure for all component groupings:

$$P(f)_{single\ hazard,asset,fully\ correlated} = maximum(P(f)_{single\ hazard,component\ grouping_{i=1\ldots m}})$$

The uncorrelated case represents the lower bound annual probability of failure. Since we currently have no information on which of the upper or lower bound assumptions is more correct in any given circumstance, we average the two bounds:

$$P(f)_{single\ hazard,asset} = average(P(f)_{single\ hazard,asset,uncorrelated}, P(f)_{single\ hazard,asset,fully\ correlated})$$

Multi-Hazard, Component Grouping-Level, Annual Probability of Failure

Because hazards considered to date by the TCM are assumed to be uncorrelated (e.g., wind and earthquake loading are mutually independent), annual failure rates for different hazards can be added within a component grouping:

$$\lambda_{multi\ hazard,component\ grouping} = \sum_{j=1}^{n} \lambda_{single\ hazard_j,component\ grouping}$$

where *n* is the total number of independent hazards. The multi-hazard, component grouping-level annual probability of failure is then computed as:

$$P(f)_{multi\ hazard,component\ grouping} = 1 - e^{-\lambda_{multi\ hazard,component\ grouping}}$$

Multi-Hazard, Asset-Level, Annual Probability of Failure

Again, because hazards considered to date by the TCM are assumed to be uncorrelated, the multi-hazard, asset-level, annual probability of failure is computed based on the product of the survival rates for each single hazard, asset-level annual probability of failure:

$$P(f)_{multi\ hazard,asset} = 1 - \prod_{j=1}^{n} (1 - P(f)_{single\ hazard_j,asset})$$

8. An Example: Wood Pole Decay

The following is an example calculation using the TCM framework to estimate the single hazard, component grouping-level, annual probability of failure for a wood pole subject to wind. The threats of wood decay and Cellon treatment are considered. For illustration purposes, results are combined across multiple hazards and multiple component groupings.

DRAFT: 31 March 2022, Revision 1

Example Calculation for TCM Framework Overview

Asset identifying information

ETL:	2060 Fort Bragg-Elk
Structure number:	016/003
Voltage class:	60
Equipment number:	40666507
Structure type:	ST := "wood"
Latitude/Longitude:	39.334448828329499/-123.798414308094
HFTD:	Tier 2

Age and threat information

Structure age (years): $T := 60 \cdot yr$

PT&T current remaining strength: $SdS_0 := 0.854190101$

PT&T decay rate (strength loss per year): $k_D := \frac{-0.005071528}{yr}$

Cellon treatment?: Cellon := "Y"

Design life reduction factor for Cellon treatment:

$$DLRF_{CT} := \begin{cases} \frac{1}{3} & \text{if Cellon = "Y"} \\ 0 & \text{otherwise} \end{cases} \qquad \boxed{DLRF_{CT} = 0.333}$$

DRAFT: 31 March 2022, Revision 1

Fragility function

Initial median and uncertainty:

$$\mu_{new} := \begin{cases} 163.940459 & \text{if ST = "steel "} \\ 169.57949 & \text{otherwise} \end{cases} \cdot mph \qquad \beta_{new} := \begin{cases} 0.2 & \text{if ST = "steel"} \\ 0.3 & \text{otherwise} \end{cases}$$

$\boxed{\mu_{new} = 169.579 \cdot mph}$ $\boxed{\beta_{new} = 0.3}$

"No threat" design life: $t_D := 150 \cdot yr$

Uncertainty at design life:

$$\beta_D := \begin{cases} 0.246529291 & \text{if ST = "steel"} \\ 0.367186527 & \text{otherwise} \end{cases}$$

$\boxed{\beta_D = 0.367}$

PLSCADD results: $V := 1.0$ no data available for structure

Median adjustment for threat:

Current median: $\mu_0 := \sqrt{SdS_0} \cdot \mu_{new}$ $\boxed{\mu_0 = 156.729 \cdot mph}$

Forecast median in "t_F" years, considering threat: $\mu_F(t_F) := \max\left(0, \min\left(\mu_{new}, \sqrt{SdS_0 + k_D \cdot t_F} \cdot \mu_{new}\right)\right)$

Uncertainty adjustment for threat:

Adjusted design life: $t_{adj} := \left(1 - DLRF_{CT}\right) \cdot t_D$ $\boxed{t_{adj} = 100 \cdot yr}$

Current uncertainty: $\beta_0 := \beta_{new} + \left(\beta_D - \beta_{new}\right) \cdot \left(\frac{T}{t_{adj}}\right)^2$ $\boxed{\beta_0 = 0.324}$

Forecast uncertainty in "t_F" years: $\beta_F(t_F) := \beta_{new} + \left(\beta_D - \beta_{new}\right) \cdot \left(\frac{T + t_F}{t_{adj}}\right)^2$

DRAFT: 31 March 2022, Revision 1

Plot of fragility

New fragility function: $f_{new}(V) := plnorm\left(\frac{V}{mph}, ln\left(\frac{\mu_{new}}{mph}\right), \beta_{new}\right)$

Current fragility function: $f_0(V) := plnorm\left(\frac{V}{mph}, ln\left(\frac{\mu_0}{mph}\right), \beta_0\right)$

Forecast fragility function in "t_F" years: $f_F(V, t_F) := plnorm\left(\frac{V}{mph}, ln\left(\frac{\mu_F(t_F)}{mph}\right), \beta_F(t_F)\right)$

Plot variable: $V_{plot} := 1 \cdot mph, 2 \cdot mph .. 4\mu_0$

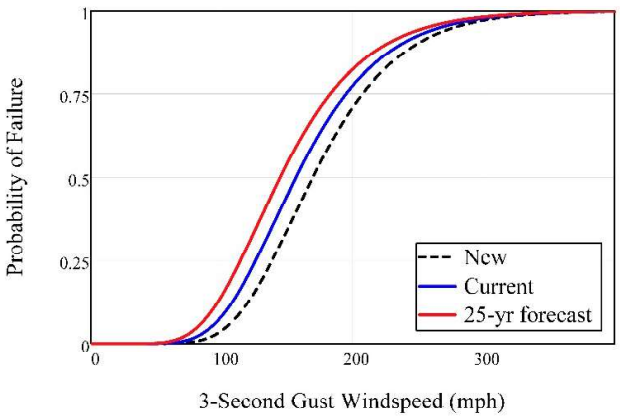

DRAFT: 31 March 2022, Revision 1

Hazard curve

POMMS grid cell: 80_314

Gumbel fit (proportion of days when gust is not exceeded):

$m := 21.36214 \cdot mph$ $s := 6.595705 \cdot mph$ $Fit(V) := e^{-e^{\frac{-(V-m)}{s}}}$

Hazard curve: $H(V) := 365(1 - Fit(V))$

Plot of hazard curve

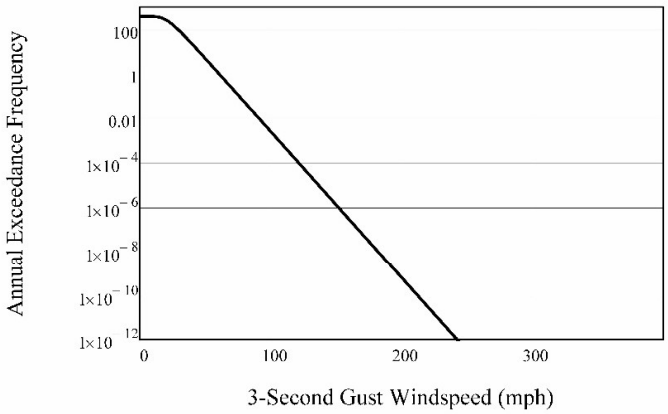

DRAFT: 31 March 2022, Revision 1

Risk integral

Annual failure rate:

New condition: $\lambda_{new} := \int_0^{4\cdot\mu_{new}} f_{new}(V)\cdot\left|\frac{d}{dV}H(V)\right| dV$

Current condition: $\lambda_0 := \int_0^{4\cdot\mu_{new}} f_0(V)\cdot\left|\frac{d}{dV}H(V)\right| dV$

Forecast condition in "t" years: $\lambda_F(t) := \int_0^{4\cdot\mu_{new}} f_F(V,t)\cdot\left|\frac{d}{dV}H(V)\right| dV$

Annual probability of failure:

New condition: $P_{f\_new} := 1 - e^{-\lambda_{new}}$ $\boxed{P_{f\_new} = 2.154\times10^{-3}}$

Current condition: $P_{f\_0} := 1 - e^{-\lambda_0}$ $\boxed{P_{f\_0} = 9.17\times10^{-3}}$

Forecast condition in "t" years: $P_{f\_F}(t) := 1 - e^{-\lambda_F(t)}$

Forecast condition in 25 years: $\boxed{P_{f\_F}(25yr) = 0.033}$

DRAFT: 31 March 2022, Revision 1

Risk integral (continued)

Calculate "no-observed decay" annual probability of failure for comparison purposes

Forecast fragility function in "t_F" years, no observed decay:

$$f_{F\_NT}(V, t_F) := \text{plnorm}\left(\frac{V}{\text{mph}}, \ln\left(\frac{\mu_{new}}{\text{mph}}\right), \beta_F(t_F)\right)$$

Forecast condition in "t" years, no observed decay:

$$\lambda_{F\_NT}(t) := \int_0^{4\cdot\mu_{new}} f_{F\_NT}(V, t)\cdot\left|\frac{d}{dV}H(V)\right| dV$$

Forecast condition in "t" years, no observed decay:

$$P_{f\_F\_NT}(t) := 1 - e^{-\lambda_{F\_NT}(t)}$$

Plot variable:

$$t_{plot} := 0, 5\text{yr} .. 1.5t_D$$

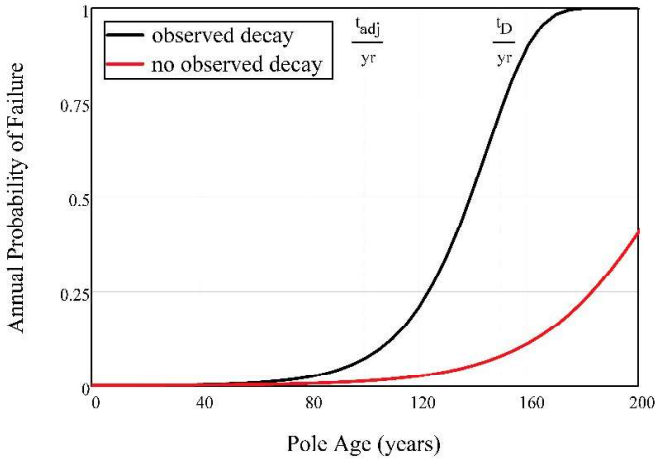

DRAFT: 31 March 2022, Revision 1

Combining annual probabilities of failure

For illustration purposes, the results above are combined with the following hazards and component groupings:

Wind hazard (applies to all component groupings present)

$$\lambda_w := \begin{pmatrix} \lambda_0 \\ 0.001 \\ 0.001 \\ 0.001 \\ 0.001 \\ 0.001 \end{pmatrix}$$

-wood structure
-conductor
-insulator
-splice
-above grade hardware
-below grade hardware

$$Pf_w := 1 - e^{-\lambda_w} \qquad Pf_w = \begin{pmatrix} 9.17 \times 10^{-3} \\ 9.995 \times 10^{-4} \\ 9.995 \times 10^{-4} \\ 9.995 \times 10^{-4} \\ 9.995 \times 10^{-4} \\ 9.995 \times 10^{-4} \end{pmatrix}$$

Seismic hazard (applies only to wood structure component grouping)

$$\lambda_s := \begin{pmatrix} 0.001 \\ 0 \\ 0 \\ 0 \\ 0 \\ 0 \end{pmatrix}$$

-wood structure
-conductor
-insulator
-splice
-above grade hardware
-below grade hardware

$$Pf_s := 1 - e^{-\lambda_s} \qquad Pf_s = \begin{pmatrix} 9.995 \times 10^{-4} \\ 0 \\ 0 \\ 0 \\ 0 \\ 0 \end{pmatrix}$$

Car-Pole hazard (applies only to wood structure component grouping)

$$\lambda_{cp} := \begin{pmatrix} 0.001 \\ 0 \\ 0 \\ 0 \\ 0 \\ 0 \end{pmatrix}$$

-wood structure
-conductor
-insulator
-splice
-above grade hardware
-below grade hardware

$$Pf_{cp} := 1 - e^{-\lambda_{cp}} \qquad Pf_{cp} = \begin{pmatrix} 9.995 \times 10^{-4} \\ 0 \\ 0 \\ 0 \\ 0 \\ 0 \end{pmatrix}$$

DRAFT: 31 March 2022, Revision 1

Combining annual probabilities of failure (continued)

Single hazard, asset-level, annual probability of failure

Wind:

$$Pf_{w\_asset\_ind} := 1 - \prod_{i=1}^{length(\lambda_w)} \left(1 - Pf_{w_i}\right) \qquad Pf_{w\_asset\_ind} = 0.014$$

$$Pf_{w\_asset\_dep} := \max\left(Pf_w\right) \qquad Pf_{w\_asset\_dep} = 9.17 \times 10^{-3}$$

$$Pf_{w\_asset} := mean\left(Pf_{w\_asset\_ind}, Pf_{w\_asset\_dep}\right) \qquad \boxed{Pf_{w\_asset} = 0.012}$$

Seismic:

$$Pf_{s\_asset\_ind} := 1 - \prod_{i=1}^{length(\lambda_s)} \left(1 - Pf_{s_i}\right) \qquad Pf_{s\_asset\_ind} = 9.995 \times 10^{-4}$$

$$Pf_{s\_asset\_dep} := \max\left(Pf_s\right) \qquad Pf_{s\_asset\_dep} = 9.995 \times 10^{-4}$$

$$Pf_{s\_asset} := mean\left(Pf_{s\_asset\_ind}, Pf_{s\_asset\_dep}\right) \qquad \boxed{Pf_{s\_asset} = 9.995 \times 10^{-4}}$$

Car-pole:

$$Pf_{cp\_asset\_ind} := 1 - \prod_{i=1}^{length(\lambda_{cp})} \left(1 - Pf_{cp_i}\right) \qquad Pf_{cp\_asset\_ind} = 9.995 \times 10^{-4}$$

$$Pf_{cp\_asset\_dep} := \max\left(Pf_{cp}\right) \qquad Pf_{cp\_asset\_dep} = 9.995 \times 10^{-4}$$

$$Pf_{cp\_asset} := mean\left(Pf_{cp\_asset\_ind}, Pf_{cp\_asset\_dep}\right) \qquad \boxed{Pf_{cp\_asset} = 9.995 \times 10^{-4}}$$

DRAFT: 31 March 2022, Revision 1

Combining annual probabilities of failure (continued)

Multi-hazard, component group-level, annual probability of failure

$\lambda := \lambda_w + \lambda_s + \lambda_{cp}$ $\quad Pf := 1 - e^{-\lambda}$ $\quad Pf = \begin{pmatrix} 0.011 \\ 9.995 \times 10^{-4} \\ 9.995 \times 10^{-4} \\ 9.995 \times 10^{-4} \\ 9.995 \times 10^{-4} \\ 9.995 \times 10^{-4} \end{pmatrix}$

- wood structure
- conductor
- insulator
- splice
- above grade hardware
- below grade hardware

Multi-hazard, component group-level, annual probability of failure

$Pf\_asset := 1 - \left(1 - Pf_{w\_asset}\right)\cdot\left(1 - Pf_{s\_asset}\right)\cdot\left(1 - Pf_{cp\_asset}\right)$ $\quad \boxed{Pf\_asset = 0.014}$

DRAFT: 31 March 2022, Revision 1

Appendix A

Seismic Hazard Models

Exponent®

EXTERNAL MEMORANDUM

TO:	[redacted] (PG&E)
FROM:	Exponent
DATE:	March 31, 2022
PROJECT:	Transmission Composite Model
SUBJECT:	Wood Pole Seismic Inertial Force Model

This memorandum describes the technical basis for the wood pole seismic inertial force risk model, which is part of the Transmission Composite Model (TCM) project. Often wood pole failures occur at the groundline after weakening from fungal decay or pests (*e.g.*, termites).[1] Groundline failures are triggered by lateral forces acting on the wood pole from windstorms or seismic events. Wind-induced failure is more commonly reported,[2] however the effect of inertial seismic forces on wood poles should be considered in a comprehensive risk analysis. The wood pole seismic inertial force risk model described herein estimates the annual probability of failure for a wood pole using the risk integral to combine a fragility curve and a site-specific seismic hazard curve.

Wind fragility curves for wood poles have been developed for the Operability Assessment (OA) and TCM models and are described in other reports.[3] To account for asset (*e.g.*, wood pole) health, the framework estimates the probability that an asset will fail at a given hazard intensity (*e.g.*, wind speed) through the use of fragility functions, and accounts for degradation over time due to threats (*e.g.*, decay) via adjustments to the fragility functions. The seismic model described herein utilizes two approaches: The first approach (Base Case) accounts for wood decay using collected data from the Pole Test and Treat (PT&T) program including pole diameter measurements and whether the pole was treated using Cellon Gas. The second approach (Multi-Feature Case) builds upon the Base Case by incorporating condition scores and Bayesian updating to adjust for reported wind-outage performance. These two approaches to consider the

[1] Bureau of Reclamation. (1992). Wood Pole Maintenance. *Facilities Instructions, Standards, & Techniques, Volume 4 – 6.*

[2] Engel, M. (2007, May 1). Extreme Winds Test Wood Pole Strength. *T&D World.* https://www.tdworld.com/transmission-reliability/article/20969229/extreme-winds-test-wood-pole-strength

[3] For more detail on the TCM model, see Revision 1 of Exponent's "PG&E's Composite Risk Model for Overhead Electric Transmission Components: A White Paper." For more detail on the OA model, see Revision 6 of Exponent's "A Framework for Risk-Based Transmission Line Asset Management and Operability Assessment."

effects of the pole health (including possibility of decay) are considered in this seismic inertial force risk model framework.

Wind to Seismic Fragility Curve Conversion

Fragility functions, also known as fragility curves, are conditional relationships between the intensity measure of a hazard (*e.g.*, wind speed) or an engineering demand parameter (*e.g.*, displacement at pole top) to the probability of an unwanted outcome (*e.g.*, failure). They are typically modeled as lognormal cumulative distribution functions, which are fully defined by two parameters representing the central tendency (value of the intensity measure at which the probability of the unwanted outcome is 0.5, sometimes referred to as the median) and the dispersion (parameter that defines the shape of the fragility function around the central tendency calculated as the standard deviation of the natural logarithms of the values). The past effort to determine fragility curves for wood poles subjected to wind gust hazard can be leveraged to obtain seismic fragility curves, by converting the wind fragility curve parameters to seismic fragility curve parameters. This concept is appropriate because, not only do both wind and earthquakes cause lateral forces, but it is also expected that failure occurs in similar locations and with similar modes: bending overstress at or just above the groundline. The wind model uses yielding of the pole base as a proxy for failure, and the seismic inertial force model takes this same approach.

Figure 1 shows wind compared to seismic lateral forces and a few parameters needed to convert from wind to seismic fragility curves. It is assumed that both wind and seismic forces cause yielding at the ground line under the same moment. Therefore, the moment caused by the median wind speed ($\mu_{0,wind}$) from the wind fragility curve is calculated, and then the seismic intensity that would cause the same moment ($\mu_{0,PGA}$) is determined. To quantify seismic intensity, peak ground acceleration (PGA) is selected as the ground motion intensity measure (im). PGA is an appropriate im, because wood pole structures are typically light and stiff, and previous studies in the literature use PGA for transmission structures.[4] Once $\mu_{0,PGA}$ is determined, a dispersion parameter is needed to fully establish the relationship between intensity and probability of failure for the seismic fragility function. For this analysis, it is expected that the wind dispersion parameter (β_{wind}) and seismic dispersion parameter ($\beta_{seismic}$) are the same with respect to the moment at the base of the pole.

[4] Lee, T.H. and Parl, H.S. Seismic fragility of transmission towers in Korea. *11th Canadian Conference on Earthquake Engineering*. Canadian Association for Earthquake Engineering.

Xie, L., Tang, J., Tang, H., and Xie, Q. Seismic fragility assessment of transmission towers via performance-based analysis. *15th World Conference on Earthquake Engineering*. Lisbon, 2012.

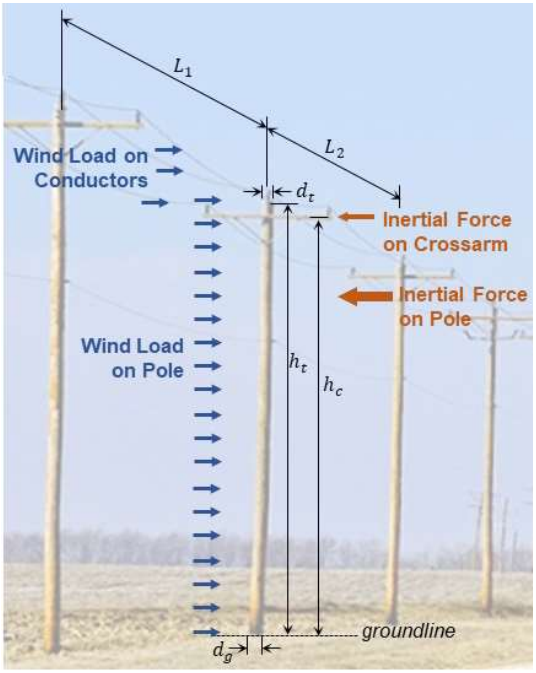

Figure 1: Wood pole showing lateral forces from wind and seismic forces and input parameters to convert a wind fragility curve to a seismic fragility curve.

To calculate the median PGA ($\mu_{0,PGA}$) from the median wind speed ($\mu_{0,wind}$), it is assumed that the moment from wind forces equals the moment from seismic forces:

$$M_{wind} = M_{seismic}$$

To determine M_{wind}, the wind pressure (p_{wind}) at a given height above the groundline, x, is computed from $\mu_{0,wind}$ by assuming laminar flow:[5]

$$p_{wind}(x) = 0.00256 \cdot K_z(x) \cdot \mu_{0,wind}{}^2$$

M_{wind} is then calculated as:

$$M_{wind} = M_{wind,pole} + M_{wind,conductor}$$

where $M_{wind,pole}$ is the moment due to wind load on the wood pole and $M_{wind,conductor}$ is the moment due to wind load on the conductors. $M_{wind,pole}$ is calculated as:

$$M_{wind,pole} = 0.00256 \cdot \mu_{0,wind}^2 \int_0^{h_t} K_z(x) \cdot d(x) \cdot x \cdot dx$$

[5] The equation for wind pressure is a basic form of the established velocity pressure equation 26.10-1 for imperial units found in the standard ASCE 7-22. Equation 26.10-1 has additional factors for velocity pressure exposure that is considered (see footnote 5) and ground elevation and topography that are not considered.

where h_t is the height of the top of the wood pole from the groundline, $d(x)$ is the diameter of the pole at any height, x, above the groundline, and $K_z(x)$ is the velocity-pressure coefficient[6] at height x. $K_z(x)$ is calculated as:

$$K_z(x) = \begin{cases} 2.41\left(\frac{15}{z_g}\right)^{\frac{2}{\alpha}} & x < 15\ ft \\ 2.41\left(\frac{x}{z_g}\right)^{\frac{2}{\alpha}} & x \geq 15\ ft \end{cases}$$

where α and z_g are terrain exposure constants.[7] For each wood pole, the surface roughness category[8] is determined from PG&E land use data according to the table provided in Appendix B. The exposure category[9] is determined using the surface roughness. It is assumed that surface roughness prevails in the upwind direction. If the surface roughness cannot be determined for a wood pole location, Exposure C is assumed. $d(x)$ is calculated according to:

$$d(x) = d_g - x\left(\frac{d_g - d_t}{h_t}\right)$$

where d_g is the wood pole diameter at the groundline and d_t is the wood pole diameter at the top. The values for d_g are found from data collected as part of the Pole Test & Treat (PT&T) program. Since diameter measurements at the top of the wood pole were not found within the collected PT&T data, the values for d_t are estimated using Table 8 from the standard ANSI O5.1. The ANSI standard provides minimum circumference measurements based on the height and class of the wood pole.

$M_{wind,conductor}$ is calculated as:

$$M_{wind,conductor} = p_{wind}(h_{c1})\ L_t n_{c1} d_{c1} h_{c1}$$

where n_{c1} is the number of conductors, d_{c1} is the diameter of the conductor, h_{c1} is the height from the groundline to the crossarm. It is assumed that the crossarm is 2 feet from the top of the wood pole. L_t is the tributary conductor span length computed from the adjacent conductor span lengths:

$$L_t = \frac{L_1 + L_2}{2}$$

where $L_1$is the length of first adjacent conductor span and L_2 is the length of the second adjacent conductor span.

[6] The velocity pressure exposure coefficient is determined according to ASCE7-22 Section 26.10.1 for each increment.

[7] The terrain exposure constants are determined according to ASCE7-22 Table 26.11-1.

[8] The surface roughness categories are described in ASCE7-22 Section 26.7.2.

[9] The exposure categories are described in ASCE7-22 Section 26.7.3.

It is assumed that seismic weight is the combined weight of the wood pole and the estimated weight of the crossarm and equipment at the crossarm, W_{equip}, assumed to be 200 lbs. The weight and influence of the conductors has been neglected for seismic weight, because conductors are flexible and lightweight[10] compared to the wood pole and equipment. The weight of the wood pole (W_{pole}) is calculated assuming a tapered pole:

$$W_{pole} = \frac{\pi}{12}\left({d_g}^2 + d_g d_t + {d_t}^2\right) h_t \cdot \rho_{wood}$$

where ρ_{wood} is the density of the wood pole, which is assumed to be 33 lb/ft^3.[11] $M_{seismic}$ is then computed assuming that the seismic inertial force from the pole acts at 2/3 of the wood pole height:

$$M_{seismic} = \mu_{0,PGA}\left(W_{pole}\frac{2}{3}h_t + W_{equip}h_{c1}\right)$$

Finally, $\mu_{0,PGA}$is calculated by setting $M_{wind} = M_{seismic}$ and rearranging the equation to solve for $\mu_{0,PGA}$:

$$\mu_{0,PGA} = \frac{\left(W_{pole}\frac{2}{3}h_t + W_{equip}h_{c1}\right)}{M_{wind}}$$

The dispersion parameter for fragility curves based on intensity measures that lead to direct calculation of M_{wind} and $M_{seismic}$ should be the same, since both are functions of force times distance. However, the wind fragility curves are defined in terms of wind speed or velocity, which is proportional to the square root of force. Therefore, computing an equivalent seismic fragility curve dispersion parameter ($\beta_{seismic}$) for the seismic im, which is proportional to force, requires doubling the wind fragility curve dispersion parameter:

$$\beta_{seismic} = 2 \cdot \beta_{wind}$$

For reference, more detail can be found in Appendix A.

All wood transmission poles (~90,000) were considered for analysis. For wood transmission poles with available input data (~26,000), a seismic median and dispersion are calculated from the wind median and dispersion. As an example, a representative wood pole was selected, and the calculated parameters are shown in **Table 1** with the associated wind and equivalent seismic fragility curves shown in **Figure 2**.

[10] While the conductors are expected to sway in an earthquake, the swaying will not be in phase with the oscillations of the pole itself, and the associated inertial loads will therefore not be additive.

[11] The specific gravity of Douglas Fir and Southern Pine, wood species commonly used for wood poles, are around 0.5.

Table 1: Representative Wood Pole Properties (Equipment Number 40574887)

Parameter	Description	Value	Unit
$\mu_{0,wind}$	Median wind speed for the wind fragility curve	172.03	mph
Land Use	PG&E land use category	Other Land	-
Exposure Category	Upwind exposure based on ground surface roughness	C	-
α	3-s gust speed power law exponent	9.8	-
z_g	Nominal height of the atmospheric boundary layer used in this standard	2,460	ft
d_t	Wood pole diameter at the top	8.59	in
d_g	Wood pole diameter at the groundline	16.87	in
h_t	Height from the groundline to the top of the wood pole	61	ft
$M_{wind,pole}$	Moment from wind load on the wood pole	135,906	lb-ft
L_1	Adjacent span length	78.9	m
L_2	Adjacent span length	85.5	m
n_{c1}	Number of conductors	3	-
d_{c1}	Conductor diameter	0.723	in
h_{c1}	Height from the groundline to the crossarm	59	ft
$p_{wind}(h_{c1})$	Wind pressure at h_{c1}	85.23	psf
$M_{wind,conductor}$	Moment from wind load on the conductors	245,327	lb-ft
M_{wind}	Total moment from wind load	381,232	lb-ft
ρ_{wood}	Density of the wood pole	33	lb/ft^3
W_{pole}	Weight of the wood pole	1,843	lb
W_{equip}	Weight of the equipment at the crossarm	200	lb
$\mu_{0,PGA}$	Median PGA for the seismic fragility curve	4.40	g
β_{wind}	Dispersion for the wind fragility curve	0.301	-
$\beta_{seismic}$	Dispersion for the seismic fragility curve	0.602	-

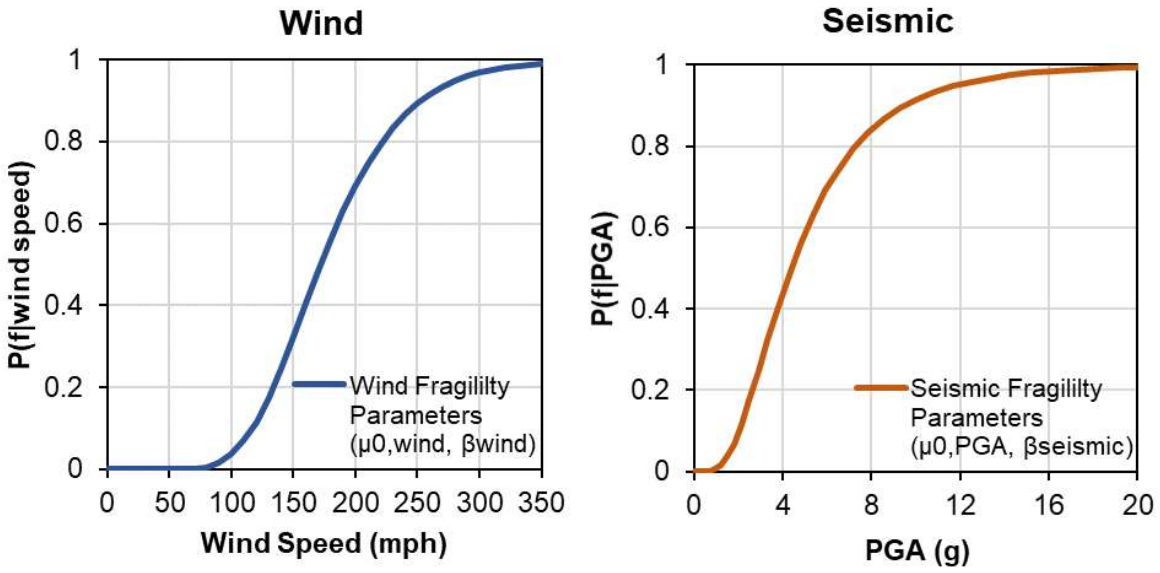

Figure 2: Wind fragility curve (left) and equivalent converted seismic fragility curve (right) for a representative wood pole (**Table 1**)

Seismic Hazard Curves

The site-specific hazard curve, relating the PGA to annual exceedance frequency, is selected from the United States Geological Survey (USGS) database based on the geographic coordinates of the wood pole and the site classification of the wood pole location. The site classification is selected using geographic coordinates and a spatial Vs30 map for California from USGS.[12] As an example, **Figure 3** shows the hazard curve selected for the representative wood pole from **Table 1**. The hazard curves from the USGS database use geometric mean to define the directionality of the PGA intensity measure. Because wood poles are isotropic with respect to horizontal ground shaking (again neglecting the influence of conductors), the geometric mean PGA was converted to RotD100 (maximum direction) PGA using an established ratio:[13]

$$RotD100\ PGA = 1.19 \cdot Geometric\ Mean\ PGA$$

[12] Thompson, E.M. (2018). An Updated Vs30 Map for California with Geologic and Topographic Constraints: U.S. Geological Survey data release. https://doi.org/10.5066/F7JQ108S.

[13] Shahi, S. K., & Baker, J. W. (2014). NGA-West2 models for ground motion directionality. Earthquake Spectra, 30(3), 1285-1300. https://doi.org/10.1193/040913EQS097M.

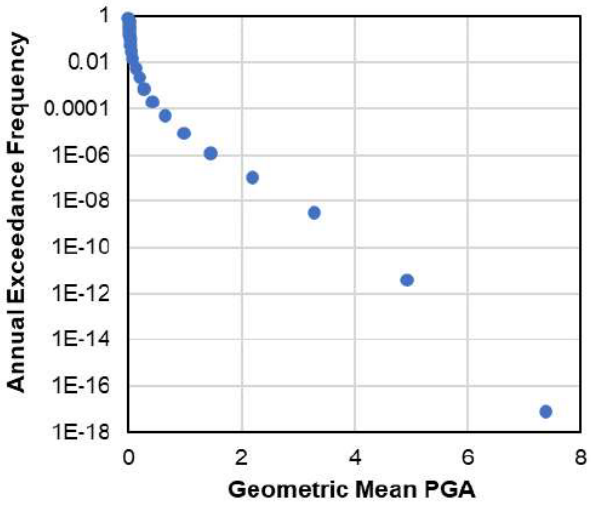

Figure 3: Hazard curve for a representative wood pole (**Table 1**) with a latitude and longitude of 39.1 and -121.7, respectively, and site class D

Seismic Annual Probability of Failure

Once the seismic fragility curve and hazard curve are determined, the risk integral is used to evaluate the annual failure rate:

$$\lambda = \int_0^\infty p(f|im) \left|\frac{dh}{dim}\right| dim$$

where λ is the annual failure rate, $p(f|im)$ is the probability of failure conditioned on the im, RotD100 PGA, $\left|\frac{dh}{dim}\right|$ is the absolute value of the derivative of the seismic hazard curve (i.e., the slope of the hazard curve), and the integration is performed over all possible intensities. For practical purposes, the risk integral can be described as the integration of the fragility curve with the derivative of the hazard curve. Annual failure rate is converted to annual probability of failure by assuming that earthquakes are a Poisson process, and using the equation:

$$P(f) = 1 - e^{-\lambda}$$

where $P(f)$ is the annual probability of wood pole failure at the groundline.

Limitations

The model described herein necessarily relies on simplifying engineering assumptions and idealized representations of complex engineering systems, threats and loads. The implications and limitations of these modeling decisions have been discussed and accepted by PG&E Subject Matter Experts. While we have made every effort to accurately capture key factors related to the effects of seismic inertial forces on wood poles that could adversely affect PG&E's transmission structures based on available information, this model is expected to be further refined as new idealizations, methods and/or data become available. Proper application of this model requires recognition and understanding of the limitations of both the scope and methodology.

The model described herein is intended to be incorporated into a comprehensive PG&E framework (TCM Framework) that was developed to inform PG&E risk mitigation decisions. Neither the Framework nor this model is intended to predict specific failures, and the actual performance of some assets may be materially different from that anticipated by the model.

For limitations associated with the Framework, see Revision 1 of Exponent's "PG&E's Composite Risk Model for Overhead Electric Transmission Components: A White Paper," dated March 31, 2022.

Appendix A: Relationship between dispersion values for function of random variables

The seismic analysis leverages previous work developing wind fragility curves in order to produce seismic fragility curves. While the continuum of the fragility curve could be converted, we have sought to generalize the conversion of the fragility curves so that only the median and dispersion parameters must be converted. The conversion of the median value of the seismic fragility curve is addressed in the main text of this memo. The conversion of the dispersion parameter is derived below, considering that while both wind and seismic failure mechanisms are based on the moment at the base of the pole, the seismic fragility curves are conditioned on PGA which is proportional to seismic moment and the wind fragility curves are conditioned on wind speed which is proportional to the square root of wind moment.

Background for problem

Assume a random variable, X, is normally distributed with mean, μ_X, and standard deviation, σ_X. The coefficient of variation, δ_X, is:

$$\delta_X = \frac{\sigma_X}{\mu_X}$$

The Variance of X is:

$$Var(X) = \sigma_X^2$$

Now let's define a function of the random variable:

$$Y = aX^2$$

where a is a constant. This has the same functional form as the relationship between wind pressure (proportional to wind-induced moment) and wind velocity. We are interested in determining the coefficient of variation of Y as a function of the coefficient of variation of X.

Dispersion for functions of random variables (single variable)

Assume a function, $g(x)$. The variance of $g(x)$ can be approximated:

$$Var[g(x)] \approx (g'(x))^2 Var(X)$$

evaluated at $E[X]$. Now let's evaluate $Var[g(x)]$ at $E[X]$ using the previously defined parameters:

$$E[X] = \mu_X \quad \text{and} \quad g(x) = Y = aX^2 \quad \text{and} \quad Var(X) = \sigma_X^2$$

Consequently, the Variance of Y is:

$$Var[Y] = (2aE[X])^2 \sigma_X^2 = 4a^2 E[X]^2 \sigma_X^2 = 4a^2 \mu_X^2 \sigma_X^2$$

We can now evaluate the coefficient of variation of Y, δ_Y, where the normally distributed mean, μ_Y, is:

$$\mu_Y = E[Y] = a\mu_X^2$$

Solving for δ_Y gives:

$$\delta_Y = \frac{\sigma_Y}{\mu_Y} = \frac{\sqrt{Var[Y]}}{a\mu_X^2} = \frac{\sqrt{4a^2\mu_X^2\sigma_X^2}}{a\mu_X^2} = \frac{2a\mu_X\sigma_X}{a\mu_X^2} = \frac{2\sigma_X}{\mu_X}$$

Finally, it can be seen that the coefficient of variation of the function of the random variable (δ_Y) is twice the coefficient of variation of the original random variable (δ_X) when the random variable (X) is squared and multiplied by a constant (a):

$$\frac{\delta_Y}{\delta_X} = \frac{\frac{2\sigma_X}{\mu_X}}{\frac{\sigma_X}{\mu_X}} = 2$$

Impact on the conversion of wind to seismic fragility curves

It has been seen that the coefficient of variation is *doubled* when a function of random variables squares the original random variable. Similarly, for the wind speed and PGA-based fragility curves to be equivalent, the dispersion parameter on the ground motion intensity measure needs to be twice the dispersion parameter on the wind speed. This has been verified through the example shown in **Figure A1**, in which

1. Each individual ordinate from the wind speed-based fragility curve is converted to an equivalent PGA and assigned the same probability of failure.
2. Only the median wind speed is converted to PGA and it is assumed that the dispersion parameter for PGA is doubled compared to that for wind speed

It can be seen that doubling the wind-speed dispersion parameter matches the ordinate by ordinate conversion exactly.

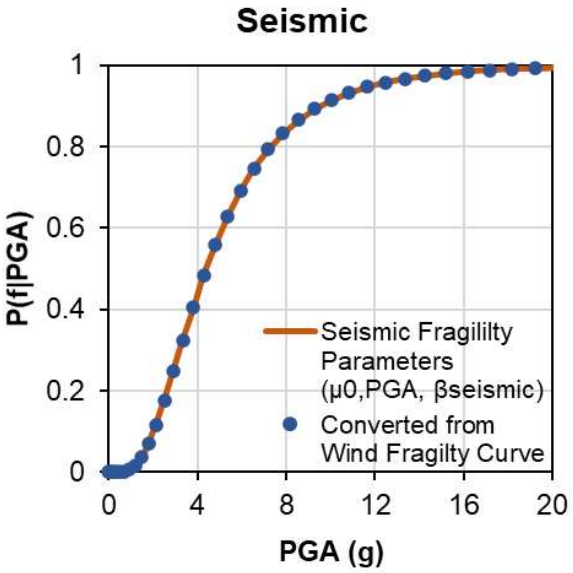

Figure A1: Seismic fragility curve converted from wind speed fragility curve by ordinate vs. converting only the median and assuming the dispersion is doubled.

Appendix B: Assigning Surface Roughness Categories from PG&E Land Use Data

Table B1 shows the surface roughness category assigned to a structure using the land use data from PG&E. Of note, 'Other Land' and 'Not Mapped' land use categories have been assigned a roughness category of 'C' for this analysis. This designation may differ from other analyses within the TCM framework. In ASCE7-22 26.7.3, an exposure category of 'C' is applied for all cases where exposure category B or D does not apply. Considering this instruction, a roughness category of 'C' was selected to categorize the structure location in exposure category 'C' where exposure category 'B' or 'D' does not apply.

Table B1: Surface Roughness Categories Assigned to PG&E Land Use Data

PG&E Land Use Data	Assigned ASCE 7-22 Surface Roughness Category
Confined Animal Agriculture	C
Farmland of Local Importance	C
Farmland of Local Potential	C
Farmland of Statewide Importance	C
Grazing Land	C
Nonagricultural and Natural Vegetation	C
Prime Farmland	C
Rural Residential Land	B
Semi-agricultural and Rural Commercial Land	C
Unique Farmland	C
Urban and Built-up Land	B
Vacant or Disturbed Land	D
Water Area	D
Other Land	C
Not Mapped	C

Exponent®

EXTERNAL MEMORANDUM

TO:	[redacted] (PG&E)
FROM:	Exponent
DATE:	March 31, 2022
PROJECT:	Transmission Composite Model
SUBJECT:	Steel Structure Seismic Inertial Force Model

This memorandum describes the technical basis for the steel structure seismic force inertial risk model, which is part of the Transmission Composite Model (TCM) project. We have received structural drawings for four steel lattice transmission tower structures: 115kV Type AH, 115kV Type BH (0° to 15° diversion angle), 115kV Type CH (15° to 45° diversion angle), and 230kV Type BW. Currently, the steel structure seismic force inertial risk model only considers these tower types, but it can be expanded to other steel structure types as more structural drawings become available. Because steel lattice towers are lightweight and tall, they are expected to be more susceptible to wind-induced failure than seismic inertial force-induced failure; however, for completeness, we have evaluated the probability of failure of steel transmission towers due to seismic inertial forces. Because we have not seen reference to inertial force-induced failures in the literature, it is unclear if the failure modes are comparable for that in wind-induced failures (*e.g.*, buckling of leg members near the base of the tower[1]). While failure modes might not be similar, they should be brought on by actions that cause high moment at the base of the tower. Notably, failure of steel transmission towers subjected to ground movement, is more widely reported in the literature and by PG&E. This failure mode is analyzed separately in the steel structures landslide risk model.[2] The analysis of seismic inertial forces for steel structures is similar to the analysis completed for wood poles.[3] In brief, we compute annual failure probabilities by integrating fragility curves for steel towers (converted from wind fragility curves) with hazard curves for earthquake intensity.

[1] Sad Saoud, K., Langlois, S., Loignon, A., & Lamarche, C. P. (2018). Failure analysis of transmission line steel lattice towers subjected to extreme loading. In Annual conference of the Canadian Society for Civil Engineering (CSCE)/Congrès annuel de la Société canadienne de génie civil (SCGC)(2018: Fredericton, Canada) (Vol. 2018, pp. ST056-1).

[2] For more detail, see Exponent's "Steel Structure Seismic-Induced Landslide Model" memorandum, dated March 31, 2022.

[3] For more detail, see Exponent's "Wood Pole Seismic Inertial Force Model" memorandum, dated March 31, 2022.

Wind fragility curves for steel structures have been developed for the OA and TCM models and are described in other reports.[4] To account for asset (*e.g.*, steel structure) health, the framework estimates the probability that an asset will fail at a given hazard intensity (*e.g.*, wind speed) through the use of fragility functions, and accounts for degradation over time due to threats (*e.g.*, corrosion) via adjustments to the fragility functions. The seismic model described herein utilizes two approaches: The first approach (Base Case) accounts for atmospheric corrosion using an advanced model. The second approach (Multi-Feature Case) builds upon the Base Case by incorporating condition scores and Bayesian updating to adjust for reported wind-outage performance. These two approaches to consider the effects of the steel structure health (including possibility of corrosion) are considered within the seismic inertial force risk model framework.

For the hazard (earthquake ground motion) intensity measure (im), we have tailored the im to each tower type, rather than using the typical peak ground acceleration (PGA), because the steel towers may be relatively flexible. We have conducted a modal analysis for each tower type to determine the first mode period of the structure (T_1). Then, we select earthquake hazard curves using the spectral acceleration of the first mode period ($S_a(T_1)$) as the im.

Wind to Seismic Fragility Curve Conversion

Fragility functions, also known as fragility curves, are conditional relationships between the intensity measure of a hazard (*e.g.*, wind speed) or an engineering demand parameter (*e.g.*, displacement at tower top) to the probability of an unwanted outcome (*e.g.*, failure). They are typically modeled as lognormal cumulative distribution functions, which are fully defined by two parameters representing the central tendency (value of the intensity measure at which the probability of the unwanted outcome is 0.5, sometimes referred to as the median) and the dispersion (parameter that defines the shape of the fragility function around the central tendency calculated as the standard deviation of the natural logarithms of the values). The past effort to determine wind fragility curves for steel structures can be leveraged to obtain seismic fragility curves by calculating the seismic median and dispersion from the wind median and dispersion. For steel towers, the failure modes due to wind and inertial seismic forces may be different. Therefore, the results of converting from wind to seismic fragility curves can provide insight, but also rely on proxy engineering demand parameters (*i.e.*, the base moment due to wind load).

Figure 1 shows wind forces compared to seismic lateral forces on steel structures and the adjacent span lengths (L_1 and L_2). It is assumed that both wind and seismic forces cause failure under the same moment. Therefore, the moment caused by the median wind speed ($\mu_{0,wind}$) from the wind fragility curve is calculated, and then the seismic intensity that would cause the same moment is determined. To quantify seismic intensity, spectral acceleration at the first mode period of the structure ($S_a(T_1)$) is selected as the ground motion intensity measure (im). $S_a(T_1)$ is an appropriate im, because there is some flexibility in the steel towers. To determine the first

[4] For more detail on the TCM model, see Revision 1 of Exponent's "PG&E's Composite Risk Model for Overhead Electric Transmission Components: A White Paper" For more detail on the OA model, see Revision 6 of Exponent's "A Framework for Risk-Based Transmission Line Asset Management and Operability Assessment."

mode period of the structure (T_1), a modal analysis was performed using SAP2000 for each tower type. Higher mode effects were not considered for the purposes of this proxy analysis. Once the median $S_a(T_1)$ ($\mu_{0,S_a(T_1)}$) is determined, a dispersion parameter is needed to fully establish the relationship between intensity and probability of failure for the seismic fragility function. For this analysis, it is expected that the wind dispersion parameter (β_{wind}) and seismic dispersion parameter ($\beta_{seismic}$) are the same with respect to the moment at the base of the pole.

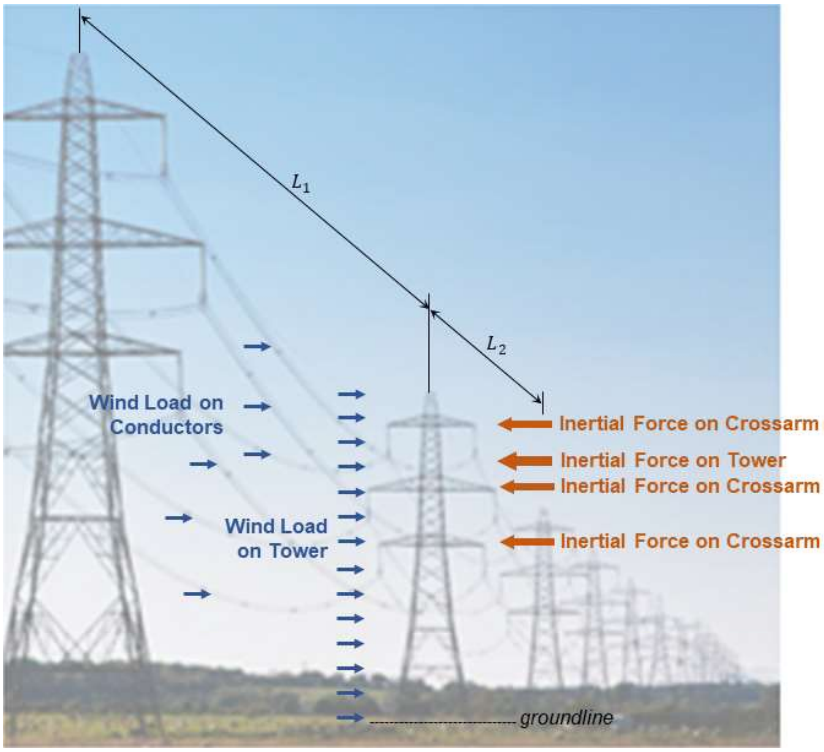

Figure 1: Steel structure showing lateral forces from wind and seismic forces, and input parameters to convert a wind fragility curve to a seismic fragility curve

To calculate the $\mu_{0,S_a(T_1)}$ from $\mu_{0,wind}$, it is assumed that the moment from wind forces equals the moment from seismic forces:

$$M_{wind} = M_{seismic}$$

To determine M_{wind} and $M_{seismic}$, each tower type was analyzed by element according to the structural drawings.[1] The wind area of the element ($A_{wind,elem}$) describes the area of the element face exposed to wind pressure and is calculated using the element dimensions from the structural drawings:

$$A_{wind,elem} = b_{elem} l_{elem}$$

where b_{elem} is the width of the exposed element face typically described by the leg length of an angle member and l_{elem} is the length of the element. The weight of each element (W_{elem}) is then

calculated. Most elements are angle members, but some elements are plates. W_{elem} for angle and plate elements, respectively, is:

$$W_{elem} = \begin{cases} (l_{leg,1} + l_{leg,2} - t_{elem}) t_{elem} l_{elem} \rho_{steel} & for\ angle\ members \\ b_{plate} t_{elem} l_{elem} \rho_{steel} & for\ plate\ members \end{cases}$$

where $l_{leg,1}$ and $l_{leg,2}$ and the lengths of the angle legs, b_{plate} is the width of the plate, t_{elem} is the thickness of the element, and ρ_{steel} is the density of steel. The structural drawings provide two steel options (i.e., medium steel and high elastic limit (HEL) steel) for tower types AH, BH, and CH. For this analysis, the medium steel elements were assumed for tower types AH, BH, and CH and a density of 0.284 lb/in^3 was used for all tower types because of a lack of data on the specific material type used for each tower. Finally, for each element, the midpoint of each element ($\bar{x}_{elem}$) was determined using dimensions provided in the structural drawings.

For each steel tower, the moment due to wind forces on the tower ($M_{wind,tower}$) was calculated by assuming laminar flow:[5]

$$M_{wind,tower} = 0.00256\, {\mu_{0,wind}}^2 \sum_{elem=1}^{n_{elem}} A_{wind,elem} \cdot K_z(\bar{x}_{elem}) \cdot \bar{x}_{elem}$$

where n_{elem} is the total number of elements and $K_z(x)$ is the velocity pressure coefficient at height x:

$$K_z(x) = \begin{cases} 2.41 \left(\frac{15}{z_g}\right)^{\frac{2}{\alpha}} & x < 15\ ft \\ 2.41 \left(\frac{x}{z_g}\right)^{\frac{2}{\alpha}} & x \geq 15\ ft \end{cases}$$

where α and z_g are terrain exposure constants.[6] For each steel tower, the surface roughness category[7] is determined from PG&E land use data according to the table found in Appendix B of Exponent's "Wood Pole Seismic Inertial Force Model" memorandum. The exposure category[8] is determined using the surface roughness, and it is assumed that surface roughness prevails in the upwind direction. If the surface roughness cannot be determined for a steel tower location, Exposure C is assumed. Next, the moment due to wind forces on the conductor ($M_{wind,conductor}$) was calculated assuming the conductor diameter and number of conductors are the same for each adjacent span and the number of conductors is evenly distributed among the crossarm levels:

---

[5] The equation to determine wind pressure is a basic form of the established velocity pressure equation 26.10-1 for imperial units found in the standard ASCE 7-22. Equation 26.10-1 has additional factors for velocity pressure exposure that are considered (see footnote 5) and ground elevation and topography that are not considered.

[6] The terrain exposure constants are determined according to ASCE7-22 Table 26.11-1.

[7] The surface roughness categories are described in ASCE7-22 Section 26.7.2.

[8] The exposure categories are described in ASCE7-22 Section 26.7.3.

$$M_{wind,conductor} = 0.00256\,\mu_{0,wind}{}^2 \left(\frac{L_1 + L_2}{2}\right) d_c \left(\frac{n_c}{n_{levels}}\right) \sum_{i=1}^{n_{levels}} K_z(h_{c,i}) \cdot h_{c,i}$$

where L_1 is the length of first adjacent conductor span and L_2 is the length of the second adjacent conductor span, n_c is the number of conductors, n_{levels} is the number of crossarm levels, and $h_{c,i}$ is the distance from the groundline to each crossarm level i. For the transmission tower types in this analysis, n_{levels} is 3.[9] Then, M_{wind} can be calculated:

$$M_{wind} = M_{wind,tower} + M_{wind,conductor}$$

To determine $M_{seismic}$, it is assumed that seismic weight is the combined calculated weight of the steel tower and the estimated weight of the equipment (W_{equip}) at each crossarm level. It is also assumed that W_{equip} is 200 lbs at each crossarm level. The weight and influence of the conductors has been neglected for seismic weight, because conductors are flexible and lightweight compared to the steel tower and equipment. $M_{seismic}$ is calculated:

$$M_{seismic} = \mu_{0,S_a(T_1)} \left[\left(\sum_{elem=1}^{n_{elem}} W_{elem} \bar{x}_{elem} \right) + \left(W_{equip} \sum_{i=1}^{n_{levels}} h_{c,i} \right) \right]$$

Finally, $\mu_{0,Sa(T_1)}$ is calculated by setting $M_{wind} = M_{seismic}$ and rearranging the equation to solve for $\mu_{0,Sa(T_1)}$:

$$\mu_{0,S_a(T_1)} = \frac{\left(\sum_{elem=1}^{n_{elem}} W_{elem} \bar{x}_{elem}\right) + \left(W_{equip} \sum_{i=1}^{n_{levels}} h_{c,i}\right)}{M_{wind}}$$

The dispersion parameter for fragility curves based on intensity measures that lead to direct calculation of M_{wind} and $M_{seismic}$ should be the same, since both are functions of force times distance. However, the wind fragility curves are defined in terms of wind speed or velocity, which is proportional to the square root of force. Therefore, computing an equivalent seismic fragility curve dispersion parameter ($\beta_{seismic}$) for the seismic im, which is proportional to force, requires doubling the wind fragility curve dispersion parameter:

$$\beta_{seismic} = 2 \cdot \beta_{wind}$$

For reference, more detail can be found in Appendix A of Exponent's "Wood Pole Seismic Inertial Force Model" memorandum.

All transmission steel lattice towers (~35,700) were considered for analysis. For transmission steel lattice towers with available input data (~14,000), a seismic median and dispersion are calculated from the wind median and dispersion. As an example, a representative steel tower was selected, and the calculated parameters are shown in **Table 1** with the associated wind and equivalent seismic fragility curves shown in **Figure 2**. It is noteworthy that the median $S_a(T_1)$ is

[9] The number of conductors at each level reported in the available PG&E data seems low (*e.g.*, 1 conductor per crossarm level). Further investigation may result in updates to the model.

very high, which reflects a very low risk of failure due to seismic inertial forces. This is due to the low mass compared to the tower strength.

Table 1: Representative Steel Structure Properties (Equipment Number 40586445)

Parameter	Description	Value	Unit
$\mu_{0,wind}$	Median wind speed for the wind fragility curve	134.04	mph
Land Use	PG&E land use category	Not Mapped	-
Exposure Category	Upwind exposure based on ground surface roughness	C	-
α	3-s gust speed power law exponent	9.8	-
z_g	Nominal height of the atmospheric boundary layer used in this standard	2,460	ft
Tower Type	Transmission tower type	CH	-
Steel Type	Steel selection from structural drawings	Medium	-
$\sum_{elem=1}^{n_{elem}} A_{wind,elem} \cdot K_z(\bar{x}_{elem}) \cdot \bar{x}_{elem}$	Summation of wind area, the velocity pressure coefficient, and element midpoint over all elements in tower	6,502	ft^2-ft
$M_{wind,pole}$	Moment from wind load on the wood pole	299,038	lb-ft
L_1	Adjacent span length	454.79	m
L_2	Adjacent span length	87.95	m
n_c	Number of conductors	3	-
n_{levels}	Number of crossarm levels	1	-
$\sum_{i=1}^{n_{levels}} K_z(h_{c,i}) \cdot h_{c,i}$	Summation of velocity pressure coefficient and height from groundline to each crossarm level	237	ft
$M_{wind,conductor}$	Moment from wind load on the conductors	7,592,642	lb-ft
M_{wind}	Total moment from wind load	7,891,679	lb-ft
ρ_{steel}	Density of the steel element	0.284	lb/in^3
$\sum_{elem=1}^{n_{elem}} W_{elem}\bar{x}_{elem}$	Seismic weight times moment arm of the tower	283,778	lb-ft
W_{equip}	Weight of the equipment at each crossarm	200	lb
$\mu_{0,S_a(T_1)}$	Median PGA for the seismic fragility curve	24.3	g

β_{wind}	Dispersion for the wind fragility curve	0.243	-
$\beta_{seismic}$	Dispersion for the seismic fragility curve	0.486	-

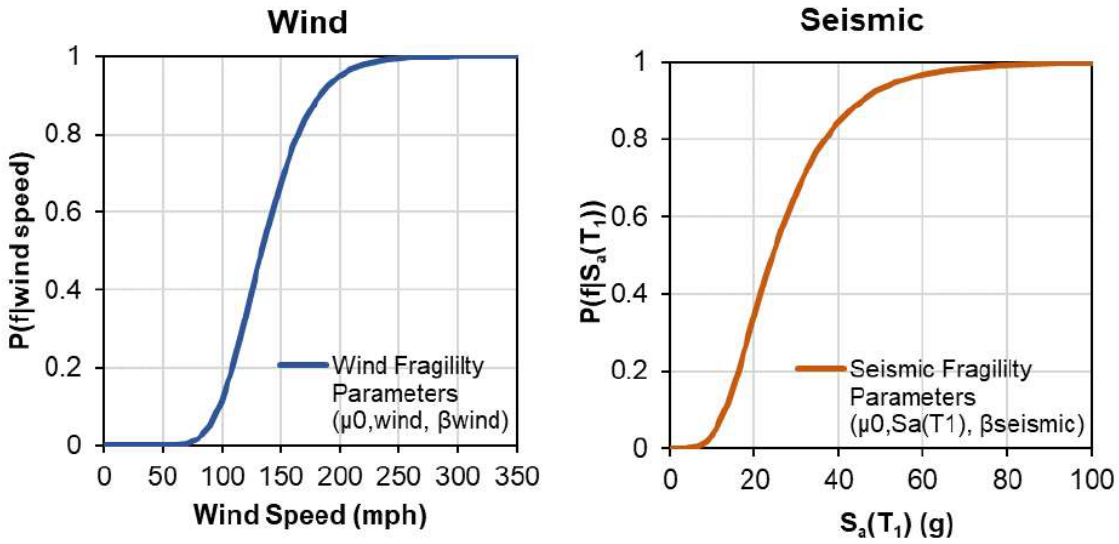

Figure 2: Wind fragility curve (left) and equivalent converted seismic fragility curve (right) for a representative steel structure (**Table 1**)

Seismic Hazard Curve

The site-specific hazard curve for each structure is selected from the USGS database based on the geographic coordinates of the steel tower, the site classification of the steel tower location, and T_1. The site classification is selected using geographic coordinates and a spatial Vs30 map for California from USGS. T_1 for each tower type is determined from a modal analysis using SAP2000, and the results are shown in **Table 2**.

Table 2: Modal Analysis Results for Steel Transmission Towers

Tower Type	Steel Type	Tower Weight [kips]	First Mode Period (T_1) [s]
115kV Type AH	Medium	4.454	0.200
115kV Type BH	Medium	7.254	0.195
115kV Type CH	Medium	7.444	0.143
230kV Type BW	N/A	42.70	0.447

From the SAP model results (**Table 1**), spectral acceleration hazard curves for T_1= 0.2 s were used for tower types 115kV Type AH, 115kV Type BH and 115kV Type CH, and spectral acceleration hazard curves for T_1= 0.5 s were used for tower type 230kV Type BW. These periods are slightly longer than the reported periods for Tower Types CH and BW, but are used because of the availability of hazard curve data at these periods from USGS.

As an example, **Figure 3** shows the hazard curve selected for the representative steel tower from **Table 1**. The hazard curves from the USGS database use geometric mean $S_a(T_1)$ ($GM\ S_a(T_1)$) as the intensity measure (im). For this analysis, the $GM\ S_a(T_1)$ was converted to maximum direction, or $RotD100\ S_a(T_1)$ using established ratios that consider T_1:[10]

$$RotD100\ S_a(T_1) = \begin{cases} 1.21 \cdot GM\ S_a(T_1) & T_1 = 0.2\ s \\ 1.23 \cdot GM\ S_a(T_1) & T_1 = 0.5\ s \end{cases}$$

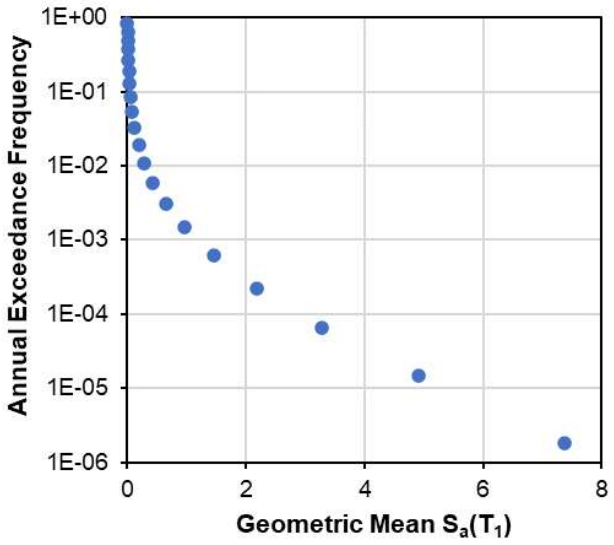

Figure 3: Hazard curve for a representative steel tower (**Table 1**) with a latitude and longitude of 40.4 and -123.4, respectively, site class BC, and T_1 = 0.2 s

[10] Shahi, S. K., & Baker, J. W. (2014). NGA-West2 models for ground motion directionality. Earthquake Spectra, 30(3), 1285-1300. https://doi.org/10.1193/040913EQS097M.

Seismic Annual Probability of Failure

Once the seismic fragility curve and hazard curve are determined, the risk integral is used to evaluate the annual failure rate:

$$\lambda = \int_0^\infty p(f|im) \left|\frac{dh}{dim}\right| dim$$

where λ is the annual failure rate, $p(f|im)$ is the probability of failure conditioned on the im, $RotD100\ S_a(T_1)$, $\left|\frac{dh}{dim}\right|$ is the absolute value of the derivative of the seismic hazard curve (*i.e.*, the slope of the curve), and the integration is performed over all possible intensities of $RotD100\ S_a(T_1)$. For practical purposes, the risk integral can be described as the integration of the fragility curve with the derivative of the hazard curve. Annual failure rate is converted to annual probability of failure by assuming that earthquakes are a Poisson process, and using the equation:

$$P(f) = 1 - e^{-\lambda}$$

where $P(f)$ is the annual probability of steel tower failure.

Limitations

The model described herein necessarily relies on simplifying engineering assumptions and idealized representations of complex engineering systems, threats and loads. The implications and limitations of these modeling decisions have been discussed and accepted by PG&E Subject Matter Experts. While we have made every effort to accurately capture key factors related to the effects of seismic inertial forces on steel structures that could adversely affect PG&E's transmission structures based on available information, this model is expected to be further refined as new idealizations, methods and/or data become available. Proper application of this model requires recognition and understanding of the limitations of both the scope and methodology.

The model described herein is intended to be incorporated into a comprehensive PG&E framework (TCM Framework) that was developed to inform PG&E risk mitigation decisions. Neither the Framework nor this model is intended to predict specific failures, and the actual performance of some assets may be materially different from that anticipated by the model.

For limitations associated with the Framework, see Revision 1 of Exponent's "PG&E's Composite Risk Model for Overhead Electric Transmission Components: A White Paper," dated March 31, 2022.

DRAFT: 31 March 2022, Revision 1

Appendix B

Wood Decay Model

Exponent®

EXTERNAL MEMORANDUM

TO:	[redacted] (PG&E)
FROM:	Exponent
DATE:	March 31, 2022
PROJECT:	Operability Assessment and Transmission Composite Models
SUBJECT:	Wood Decay Model

Exponent has developed a wood decay model to incorporate the results of Osmose Pole Test & Treat (OPTT) data into the Operability Assessment (OA) tool and the Transmission Composite Model (TCM). The purpose of this memorandum is to provide a summary of the technical bases underpinning this model and describe its implementation in the OA tool and TCM.

Motivation for Model Development

The OA tool and TCM provide a similar risk-based framework for evaluating the strength of transmission line assets to resist wind loads (as well as other loads in the case of the TCM). The OA tool and TCM use the results of enhanced inspections, among other data sources, to evaluate the current remaining strength of wood poles relative to the strength of a new pristine wood pole.

In addition to enhanced inspection results, PG&E has results from OPTT inspections of wood poles. These results provide an estimate of the pole's remaining strength based on the undecayed cross-section of the pole near groundline, a well-established indicator of a wood pole's ability to resist bending moments induced by lateral loads. The OPTT results can be incorporated into the OA tool and TCM to more precisely account for decay-related strength loss for Transmission Line Asset Management and Operability Assessment decisions. Further, an understanding of decay progression can be used to predict future decay-related strength loss of wood poles for Asset Management decisions.

Technical Bases for Model Development

Modeling of decay behavior in wood utility poles is a subject of considerable research. Key findings across a broad range of research efforts include the following:

- Some wood poles exhibit negligible decay, even after several decades of service. Such poles are decay resistant (due to species or treatment) and/or located in environments that, for whatever reason, are not conducive to decay formation.
- For wood poles that exhibit decay, the rate of decay is typically very low early in the service life of the pole and then begins to increase at some later date. Researchers have proposed bilinear or similar decay models to account for this phenomenon, whereby the decay-related reduction in pole strength is negligible for several years (estimated as approximately 7 years in a 2005 study by Li[1]), and then proceeds in a linear, or nearly linear, manner thereafter (Figure 1).
- Different regions of the US are generally more prone to decay, as well as higher rates of decay, than others. This forms the basis of decay severity zones for wood utility poles identified by the US Department of Agriculture (USDA).[2] Of the five zones identified by the USDA, PG&E's service area encompasses three: Zones 1, 3 and 4 (Figure 2).

Exponent has reviewed results from 2006 – 2020 OPTT inspections for PG&E wood poles and used them to calculate average decay rates per USDA decay severity zone. This data provides up to two cycles of inspections for some wood poles.[3] In the case of poles with two inspection cycles, a pole-specific decay rate was determined by dividing the difference in remaining strength ratios between inspections by the number of years between inspections. If results from only one inspection cycle was available, the decay rate was calculated in a similar manner by assuming no strength reduction at 7 years. Table 1 summarizes the calculated average decay rate from OPTT results per decay severity zone.[4] The average decay rates are higher in Zone 4 than in Zone 1 or 3, which shows some correlation, though not perfect, with the expected decay rate mapping in Figure 1.

[1] Li, et al. (2005) "Degradation-path Model for Wood Pole Asset Management," IEEE.

[2] USDA RUS Bulletin 1730B-121 (https://www.rd.usda.gov/files/UEP_Bulletin_1730B-121.pdf).

[3] It is Exponent's understanding that OPTT inspections typically occur every 10 years.

[4] The average decay rate for wood poles in Zone 3 is slightly lower than that of Zone 1. Based on currently available information, the reason for this is unknown.

Table 1. Calculated average decay rate per USDA decay severity zone

USDA Decay Severity Zone	Average Decay Rate (Strength Loss Ratio per Year)
Zone 1	0.0111
Zone 3	0.0093
Zone 4	0.0125

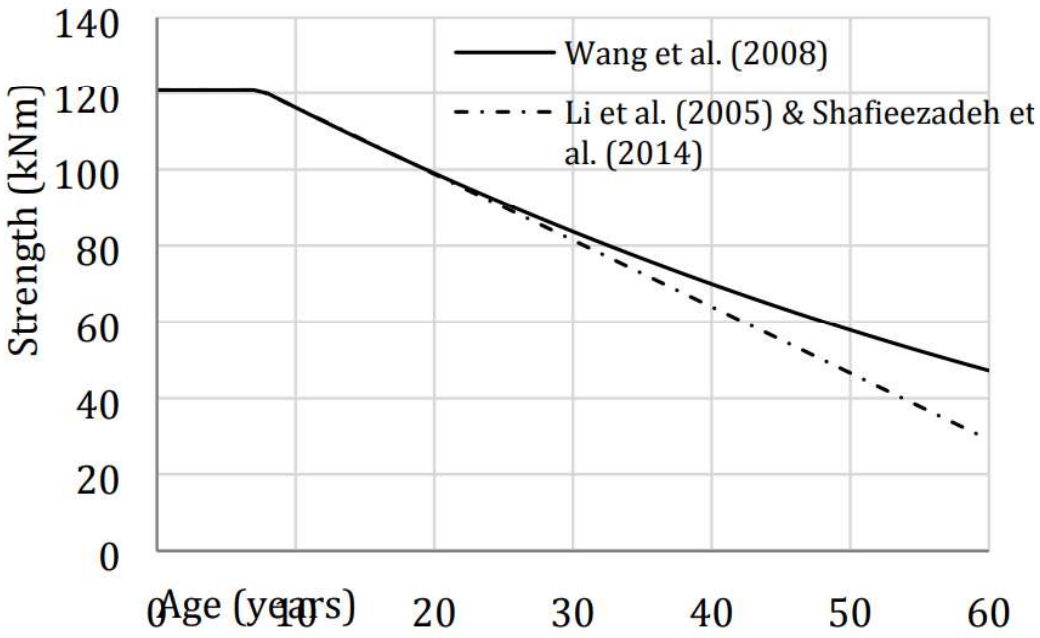

Figure 1. Models for decay-related strength reduction of wood poles.[5]

[5] Abdullahi M. Salman, Yue Li, Emilio Bastidas-Arteaga. (2017) Maintenance optimization for power distribution systems subjected to hurricane hazard, timer decay and climate change. Reliability Engineering and System Safety, Elsevier.

Decay severity zones for wood utility poles as defined by the USDA Rural Utilities Service. Decay is least severe in zone 1, most severe in zone 5.

Figure 2. USDA decay severity zones for wood utility poles. Note that PG&E's service area includes Zones 1, 3 and 4. Source: USDA RUS Bulletin 1730B-121.

Model Implementation in OA Tool and TCM

The wood decay model has been incorporated in the OA tool and TCM by adjusting the median strength for the "Structure" theme/component grouping of each wood pole using the decay rate "k" calculated per Table 2. "S" is the remaining strength ratio determined from the OPTT results and "t" is the age of the pole relative to the pole installation date. In the case of multiple OPTT inspections, the results from the last and second-to-last inspections (n and n-1, respectively) are considered; thus, the decay rate would be updated with each new OPTT result that becomes available.

In a limited number of instances, the following conditions occurred:

- OPTT results for a pole with only one inspection cycle indicated decay for a pole aged less than 7 years. The average decay rate for the USDA decay severity zone was assigned to these poles.
- OPTT results for a pole with multiple inspection cycles indicated *increasing* pole strength (i.e., *decreasing* decay) between cycles. The older OPTT results were disregarded for these poles because more recent results are believed by PG&E SMEs to be more reliable.

As shown in Table 2, the current remaining strength of the pole is estimated by reducing the strength determined using the most recent OPTT results by the product of the calculated decay rate and the number of years since the most recent OPTT inspection. By the same methodology, the future remaining strength of the pole can also be forecast.[6] The value of remaining strength using the wood decay model is compared to that determined by enhanced inspection results from the current OA tool and TCM methodology;[7] the lesser of the two values is used in calculating the fragility of the "Structure" theme/component grouping.

Finally, as a check on possible anomalous decay rates, the decay model flags poles for which the pole-specific decay rate determined from Table 2 is more than one standard deviation greater than the average for all poles in a particular USDA decay severity zone.

[6] The forecast feature of the wood decay model estimates the strength reduction of a pole beyond the most recent OPTT inspection using the decay rate calculated per Table 2. As the time between the forecast date and the most recent OPTT inspection increases, the uncertainty associated with the decay rate also increases.

[7] For estimation of future remaining strength, the remaining strength ratio determined using the enhanced inspection results is also reduced by the product of the calculated decay rate and the forecast time (t_{future} - $t_{current}$). This is to account for the possibility that the enhanced inspection code is associated with the presence of decay.

Table 2. Calculation of wood decay rate and remaining strength for wood poles

Number of T&T Inspections	T&T Decay Results	Decay Rate Calculation (strength reduction per year)	Current Remaining Strength (as a ratio of original strength)	Future Remaining Strength (as a ratio of original strength)
0	N/A	$k = 0$	1.0	1.0
1	No decay	$k = 0$	1.0	1.0
	Decay ($t_{T\&T} > 7$ yrs)	$k = (1 - S_{T\&T}) / (t_{T\&T} - 7 \text{ yrs})$	$S_{current} = S_{T\&T} - k * (t_{current} - t_{T\&T})$	$S_{future} = S_{T\&T} - k * (t_{future} - t_{T\&T})$
	Decay[a] ($t_{T\&T} <= 7$ yrs)	$k = k_{ave}$	$S_{current} = S_{T\&T} - k_{ave} * (t_{current} - t_{T\&T})$	$S_{future} = S_{T\&T} - k_{ave} * (t_{future} - t_{T\&T})$
n (>1)	No decay	$k = 0$	1.0	1.0
	Decay (increasing)	$k = (S_{T\&Tn-1} - S_{T\&Tn}) / (t_{T\&Tn} - t_{T\&Tn-1})$	$S_{current} = S_{T\&Tn} - k * (t_{current} - t_{T\&Tn})$	$S_{future} = S_{T\&Tn} - k * (t_{future} - t_{T\&Tn})$
	Decay[b] (decreasing)	Disregard older OPTT results and calculate using appropriate equations above.		

[a] As discussed above, in a limited number of instances OPTT results for a pole with only one inspection cycle indicated decay for a pole with age less than 7 years. The average decay rate for the USDA decay severity zone was assigned to these poles.

[b] As discussed above, in a limited number of instances OPTT results for a pole with multiple inspection cycles indicated *increasing* pole strength (i.e., *decreasing* decay) between cycles. The older test results are disregarded for these poles because more recent results are believed by PG&E SMEs to be more reliable.

Data Limitations

As described above, the decay model implemented in the OA tool and TCM is based on OPTT inspection results. Some key limitations in the current use of those results are as follows:

- OPTT inspection results from 2006 – 2020 were used for this assessment. These results were partially curated to address line names with spelling errors, extra spaces, etc.
- Only results from inspection/treatment cycles were used for this assessment. Results from restoration cycles were not used, as these cycles typically occur just after an inspection/treatment cycle.
- Wood poles with inspection results dated before the pole installation date or with no installation date were not used for this assessment. Based on currently available information, the reasons for these date discrepancies are unknown. For purposes of determining the installation date, the greater of the pole installation date in ETGIS and the pole manufacture date is used if the pole installation date in ETGIS is available; otherwise, the pole manufacture date as identified by the OPTT inspector is used.
- For multiple wood pole structures, OPTT inspection results typically do not distinguish between poles. Such results were not used for this assessment because they could not be associated with a unique Structure or Equipment number, which prevents calculating the decay rate for the correct pole and mapping to the OA tool and TCM.

Efforts to further incorporate OPTT inspection results into the decay model are ongoing.

Limitations

The model described herein necessarily relies on simplifying engineering assumptions and idealized representations of complex engineering systems, threats and loads. The implications and limitations of these modeling decisions have been discussed and accepted by PG&E Subject Matter Experts. While we have made every effort to accurately capture key factors related to wood decay that could adversely affect PG&E's transmission structures based on available information, this model is expected to be further refined as new idealizations, methods and/or data become available. Proper application of this model requires recognition and understanding of the limitations of both the scope and methodology.

The model described herein is intended to be incorporated into a comprehensive PG&E framework (TCM Framework) that was developed to inform PG&E risk mitigation decisions. Neither the Framework nor this model is intended to predict specific failures, and the actual performance of some assets may be materially different from that anticipated by the model.

For limitations associated with the Framework, see Revision 1 of Exponent's "PG&E's Composite Risk Model for Overhead Electric Transmission Components: A White Paper," dated March 31, 2022.

DRAFT: 31 March 2022, Revision 1

Appendix C

Cellon Gas Preservative Treatment in the TCM

Exponent®

EXTERNAL MEMORANDUM

TO:	[redacted] (PG&E)
FROM:	Exponent
DATE:	March 31, 2022
PROJECT:	Transmission Composite Model
SUBJECT:	Cellon Gas Preservative Treatment in the TCM

This memorandum describes how poles that were originally treated with Cellon Gas are addressed in the Transmission Composite Model (TCM).

Cellon treatment refers to a process by which pentachlorophenol in liquified petroleum gas is used as a preservative to inhibit decay in wood poles. Cellon treatment is known to provide less effective treatment compared to other common preservatives. Decay of poles treated with Cellon is often found at or just below the ground line, and therefore concealed to inspectors absent excavation or drilling down from the surface.

The original preservative treatment is recorded in the PG&E Pole Test and Treat (PT&T) inspection forms for wood transmission poles. Data from 2006 to 2020 comprise about 145,791 transmission poles and more than 190 thousand associated inspections (many poles were visited more than once). Based on the most recent PT&T visit to each pole, about 31,840 poles were treated with Cellon gas (22%); of those, approximately 1,550 were rejected, presumably leaving many Cellon-treated poles in service. Figure 1 provides a summary of the original preservative treatments for PG&E transmission poles using the codes recorded in the PT&T forms. Bars associated with Cellon treatment are colored red. Most Cellon-treated poles are between 20 years and 75 years old (Figure 2).[1]

The PT&T records include a recommendation of whether the pole in its current condition should be replaced or restored, that is, whether the current condition is rejected. Rejection might be triggered if the remaining strength of the pole falls below an action threshold. Loss of strength could be due to decay, mechanical damage, termites, woodpeckers, or other causes. General Order 95 has a rejection threshold of 0.67; PG&E's current rejection threshold is 0.75, and as such is more conservative than General Order 95.

[1] Data is shown only for poles up to 99 years old per the PT&T data. Note that there are 14,981 poles with no installation date information, and those are not shown.

The PT&T data record indication that decay is occurring are 15,256 of 145,791 total poles (10%), as shown in Figure 3. Note that some age data was clearly unrealistic, and those results were screened; Cellon-treated pole data was limited to poles aged 1 to 100 years.

Based on three fields recorded in the PT&T data – pole age, original treatment type, and current rejection status, the rejection rates for Cellon-treated poles are compared to the general population of poles (Figure 4). Two conclusions are immediately apparent. First, the PT&T rejection recommendations clearly show that Cellon-treated poles generally lose strength more quickly and reach the rejection threshold earlier (that is, reach the end of their useful life at a younger age) than their counterparts. Second, the past PT&T inspection methods were capable of capturing this accelerated strength loss, at least often enough that the trend is apparent in the data. It is possible that the number of rejections of Cellon-treated poles would be even higher some decay in Cellon-treated poles is missed, perhaps because it is concealed below grade.

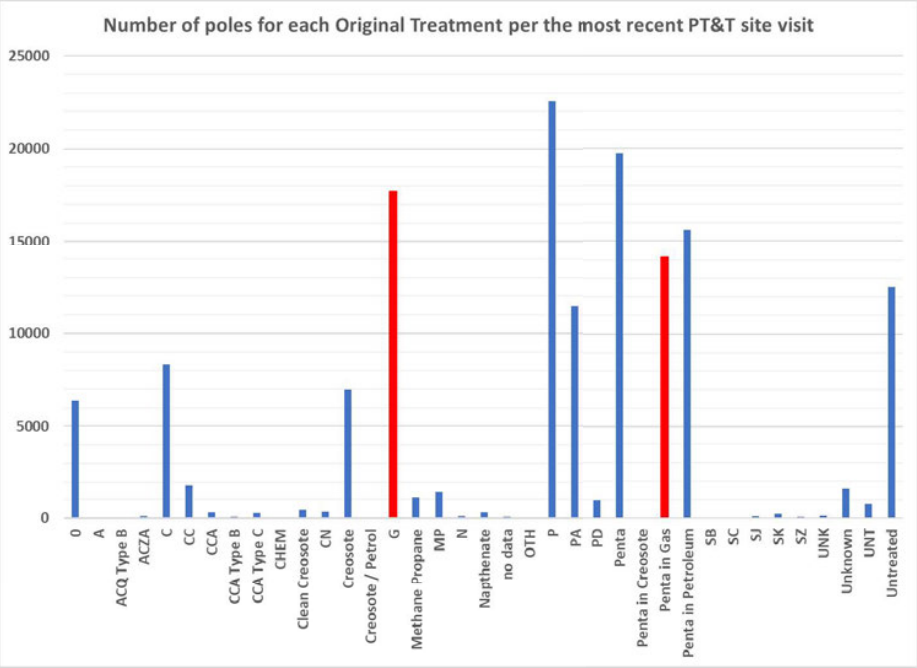

Figure 1. Preservative treatments and pole counts.

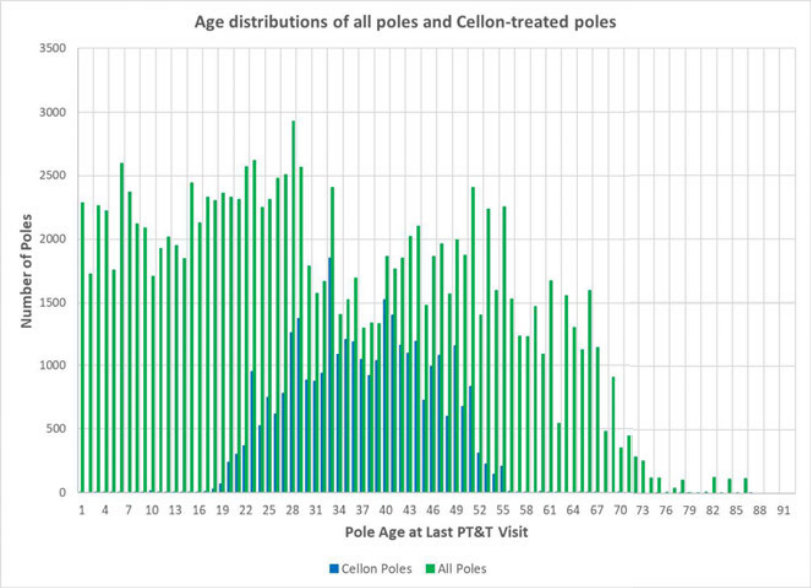

Figure 2. Distribution of Cellon-treated pole ages (2021) compared to the total population of wood poles, based on most recent PT&T record for each pole.

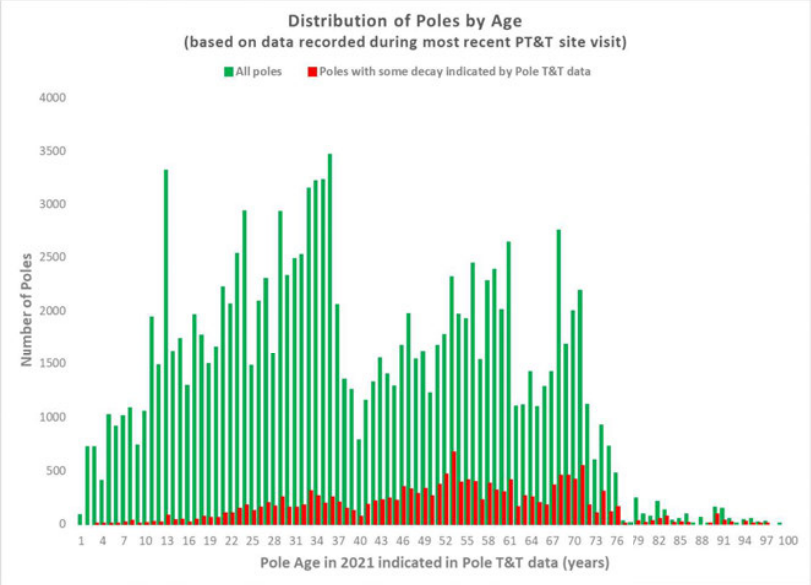

Figure 3. Distribution of poles with decay noted in the PT&T data compared with the distribution for all poles.

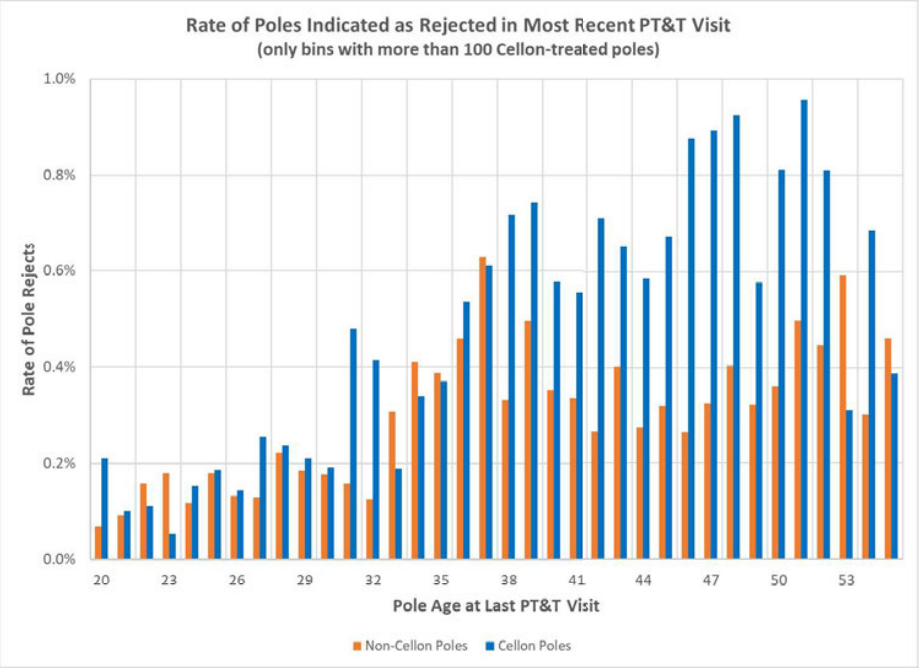

Figure 4. Rejection rates of Cellon and non-Cellon-treated poles as a function of pole age.

The scatter in the PT&T rejection rate data is significant, and in Figure 5 we have fit exponential curves (using Excel's trendline feature) to the data in Figure 4. The plotted rejection rates indicate that, for expected useful life of a decaying pole in the range of 60 years, the Cellon-treated poles reach similar rejection rates at about 75% of the age of non-Cellon-treated poles. For instance, non-Cellon-treated poles reach a rejection rate of 0.5% in about 55 years, whereas Cellon-treated poles reach the same rate in about 43 years.

Based on these findings, the TCM includes a 33% reduction in useful life for Cellon-treated wood poles . (We increase the 25% seen in the graph below to account of the possibility that some below-ground damage is being missed, and to be consistent with other judgment-based adjustments in the model.) Currently, aging of assets and the associated increasing uncertainty is modeled by increasing the fragility dispersion (standard deviation of the natural logarithms of the strengths) with age. The rate at which the dispersion is increased is calibrated such that, for an otherwise healthy asset in a benign environment, the probability of failure at end of design life is equivalent to losing 1/3rd strength. The rate of increase of the dispersion is adjusted for more aggressive environments by adjusting the design life downward. Thus, Cellon-treated

poles are addressed in the same way, that is, all poles identified to have been treated with Cellon Gas have their useful life decreased by 1/3rd, consistent with Figure 4.

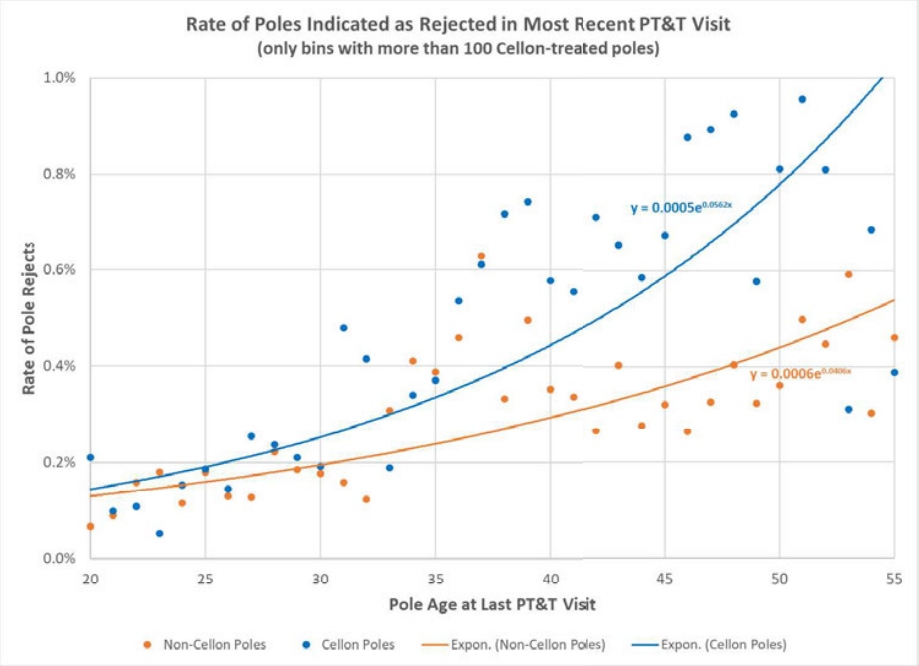

Figure 5. Exponential function fit to rejection rates of Cellon and non-Cellon-treated poles as a function of pole age.

For example, Figure 6 presents the annual failure rates calculated by the TCM using this implementation, comparing the expected failure rates for Cellon-treated poles to non-Cellon-treated poles in an otherwise benign environment in an area of low wind hazard (Figure 7). The curves are based on a non-Cellon-treated design life of 75 years, and a Cellon-treated design life of 50 years. Projected failure rates increase as the dispersion β of the lognormal fragility function is raised (linearly) from 0.3 (new pole) to 0.37 (pole at end of useful life) over the course of the design life (Figure 8). Note that the form of the failure rate increase is similar to the form of the rejection rate increase with age, but lags behind; for any given age the rejection rate is higher than the failure rate. This is to be expected as the failure rates are based on unmitigated degradation until the occurrence of an extreme wind gust, whereas in reality poles are regularly maintained and replaced prior to failure.

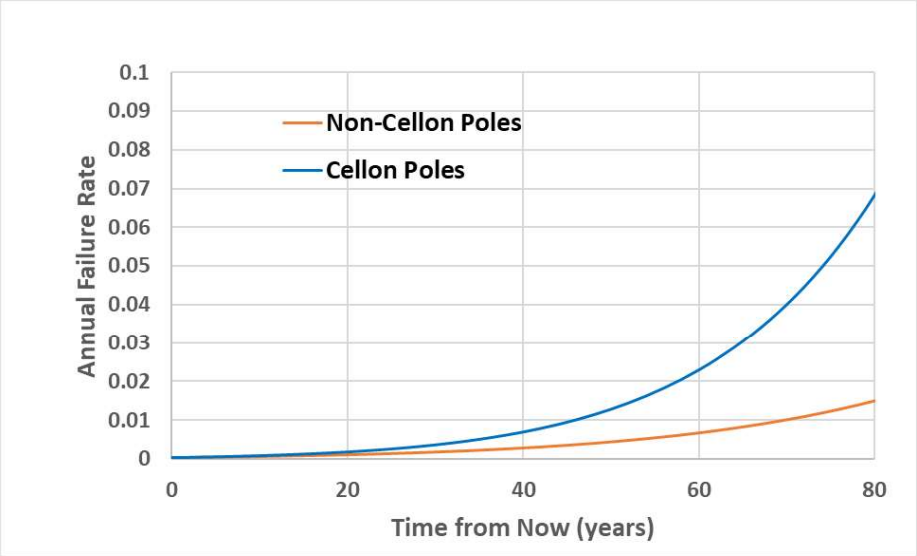

Figure 6. Annual failure rates calculated by the risk integral for Cellon and non-Cellon-treated poles, all else equal.

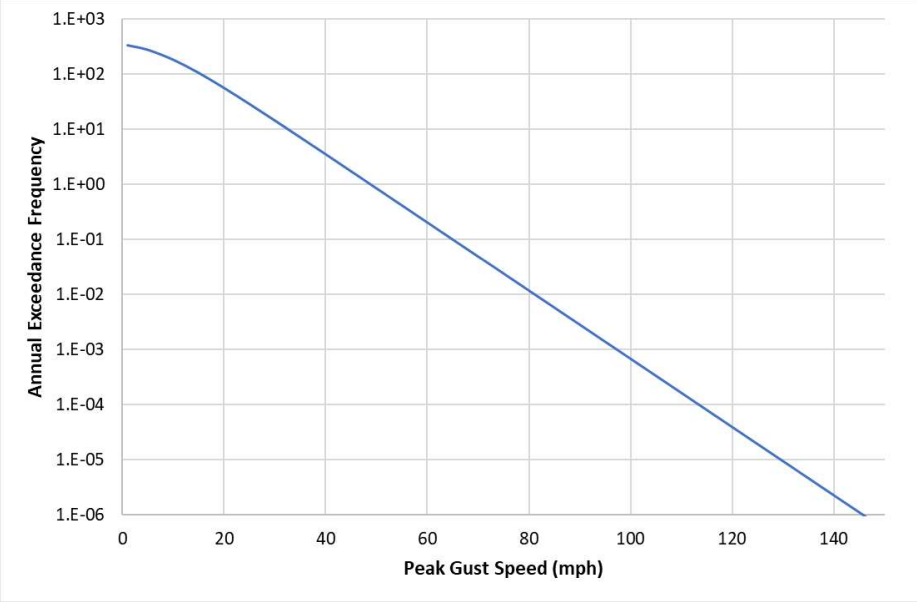

Figure 7. Wind hazard used to create Figure 6.

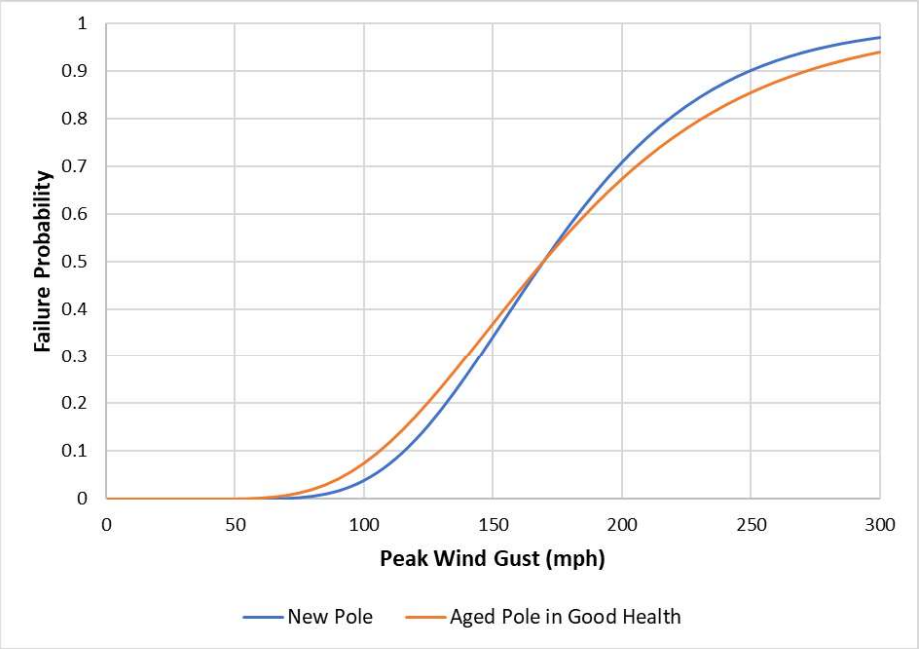

Figure 8. Fragility functions used to create Figure 6.

Limitations

The model described herein necessarily relies on simplifying engineering assumptions and idealized representations of complex engineering systems, threats and loads. The implications and limitations of these modeling decisions have been discussed and accepted by PG&E Subject Matter Experts. While we have made every effort to accurately capture key factors related to Cellon-treated wood poles that could adversely affect PG&E's transmission structures based on available information, this model is expected to be further refined as new idealizations, methods and/or data become available. Proper application of this model requires recognition and understanding of the limitations of both the scope and methodology.

The model described herein is intended to be incorporated into a comprehensive PG&E framework (TCM Framework) that was developed to inform PG&E risk mitigation decisions. Neither the Framework nor this model is intended to predict specific failures, and the actual performance of some assets may be materially different from that anticipated by the model.

For limitations associated with the Framework, see Revision 1 of Exponent's "PG&E's Composite Risk Model for Overhead Electric Transmission Components: A White Paper," dated March 31, 2022.

DRAFT: 31 March 2022, Revision 1

Appendix D

Atmospheric Corrosion Models

Exponent®

EXTERNAL MEMORANDUM

TO: [redacted] PG&E)

FROM: Exponent

DATE: March 31, 2022

PROJECT: Transmission Composite Model

SUBJECT: Advanced Atmospheric Corrosion Model

Section 1: Introduction

Exponent has developed an advanced atmospheric corrosion model (AAC model) as part of the Transmission Composite Model (TCM). The AAC incorporates environmental data and first-principles corrosion estimates to evaluate and predict electric transmission line asset health and susceptibility to atmospheric corrosive attack. The AAC model, and other features of the TCM, significantly refine the original corrosion model used in the Operability Assessment (OA) tool. The purpose of this memorandum is to provide a summary of the technical bases underpinning the AAC model and describe its implementation in the TCM.

1.1 Motivation for AAC Model Implementation in the TCM

The TCM provides a risk-based framework for evaluating the strength of transmission line assets subject to various hazards. The tool uses a variety of data to evaluate the current remaining strength of an asset relative to the strength of a new pristine asset. These data are used to adjust the median strength of an asset and/or the uncertainty (dispersion) associated with the asset strength, resulting in an estimate of the probability of failure at a given wind speed in the form of an asset-specific fragility curve.[1]

Adjustment of the dispersion in strength for an asset within the TCM is based primarily on its age relative to its design life. The design life of an asset is a function of its notional design life,

[1] For a more complete explanation of the OA model / TCM framework see Revision 1 of Exponent's "PG&E's Composite Risk Model for Overhead Electric Transmission Components: A White Paper."

currently set at 150 years for most components in benign environments, and the aggressiveness of its environment with respect to degradation mechanisms such as decay, corrosion, fatigue and wear. Assets exposed to more aggressive environments are assigned greater "design life reduction factors" (DLRFs) than assets in more benign environments (e.g., the actual life of an asset in a highly corrosive environment will be significantly less than the notional design life of 150 years). For above-ground steel structures (Section 2), metallic components of insulator hardware (Section 3), conductors (Section 4), and above grade metallic hardware (Section 5) atmospheric corrosion is one of the primary degradation mechanisms resulting in reductions in useful design life. Thus, the goal of the AAC is to provide a nuanced analysis of this degradation mechanism across these four component groupings.

1.2 AAC Model Development Overview

Atmospheric corrosion is likely to be accelerated in areas where higher concentrations of airborne salts (such as near the sea), specific gases (e.g., H_2S from geothermal sources), and particulate pollutants can combine with moisture on the surface of electric transmission asset components. The extent and rate of corrosive attack is dependent on an asset's properties (e.g., the materials used, its maintenance history, etc.) and its local environment. Thus, the AAC considers both factors when estimating the DLRF.

While there are slight differences in the four implementations discussed in the subsequent sections, at a high level, the AAC model consistently follows the process flow outlined in Figure 1.1. In each case, the model starts by collecting structure information from PG&E's Electric Transmission Geographic Information System (ET GIS) to understand the asset's identifying number, age, and location. Using the asset's location and the materials used in its components, the potential for atmospheric corrosion is determined using local climate information (e.g., average temperature and wetness) and information about the presence of a variety of corrosive species in the environment (e.g., deposition of Cl^- particles). Atmospheric corrosion estimates are quantified by determining the corrosion rate and corresponding corrosion category in accordance with the relevant ISO standards for atmospheric corrosion of metals and alloys.[2,3] Certain types of assets may require additional geometrical normalization steps in determining the corrosion category (e.g., helical conductor spans), in which case, those corrections are also applied. Once the corrosion category has been identified for the asset, an asset-type-specific figure of merit calculation is performed. The figure of merit calculation takes into consideration specific features of the asset (e.g., painting history etc.) and applies adjustments as needed. From the figure of merit, an asset-type-specific DLRF is then determined. Finally, the model outputs a

[2] International Organization for Standards (ISO). (2012) 9223:2012 Corrosion of metals and alloys - Corrosivity of atmospheres - Classification, determination and estimation

[3] International Organization for Standards (ISO). (2012) 9224:2012 Corrosion of metals and alloys - Corrosivity of atmospheres – Guiding values for the corrosivity categories.

list of SAP Equipment IDs, their corrosion categories, and corresponding DLRFs. These values are input to the TCM to adjust the dispersion of the fragility curves for each asset.

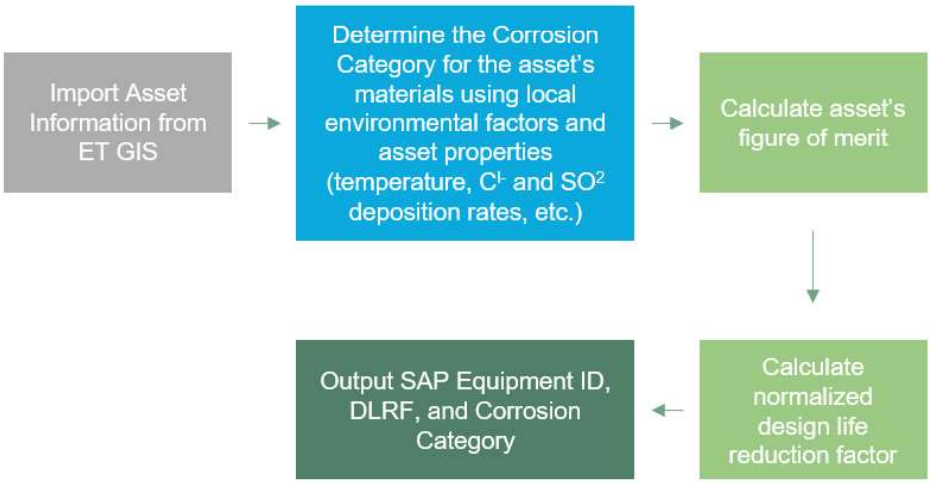

Figure 1.1 AAC Process Overview. The model uses ET GIS to identify information about the structure. It uses this information to calculate the corrosion categories for the materials in use. Using this corrosion category, it calculates a figure of merit which it then uses to assign the DLRF.

1.3 Corrosion Category Assignment Overview

The various implementations of the AAC all rely on the ISO 9223 international standard to estimate the atmospheric corrosivity of an asset's local environment. Atmospheric corrosivity can be divided into six categories, ranging from very low to extreme corrosivity, as shown in Figure 1.2. Most of California is within a C2 corrosion category; however, higher corrosion categories are present near coastal or urban areas.

Corrosion Category	Corrosivity
C1	Very Low
C2	Low
C3	Medium
C4	High
C5	Very High
CX	Extreme

(Map of ISO Corrosivity Categories taken from < https://www.wbdg.org/tools/corrdefense/map.html>)

Figure 1.2 Corrosion Categories as defined by ISO 9223 and map of approximate corrosion categories across the continental US.

Each corrosion category has a corresponding corrosion rate range for the first year of exposure for different metal types, such as carbon steel, zinc, copper, and aluminum, as shown in Figure 1.3 (from ISO 9223). For each implementation, an asset's uniform corrosion rate was calculated. These calculations are laid out in Section 1.4.

Corrosivity category	Corrosion rates of metals r_{corr}				
	Unit	Carbon steel	Zinc	Copper	Aluminium
C1	g/(m²·a)	$r_{corr} \leq 10$	$r_{corr} \leq 0,7$	$r_{corr} \leq 0,9$	negligible
	µm/a	$r_{corr} \leq 1,3$	$r_{corr} \leq 0,1$	$r_{corr} \leq 0,1$	—
C2	g/(m²·a)	$10 < r_{corr} \leq 200$	$0,7 < r_{corr} \leq 5$	$0,9 < r_{corr} \leq 5$	$r_{corr} \leq 0,6$
	µm/a	$1,3 < r_{corr} \leq 25$	$0,1 < r_{corr} \leq 0,7$	$0,1 < r_{corr} \leq 0,6$	—
C3	g/(m²·a)	$200 < r_{corr} \leq 400$	$5 < r_{corr} \leq 15$	$5 < r_{corr} \leq 12$	$0,6 < r_{corr} \leq 2$
	µm/a	$25 < r_{corr} \leq 50$	$0,7 < r_{corr} \leq 2,1$	$0,6 < r_{corr} \leq 1,3$	—
C4	g(m²·a)	$400 < r_{corr} \leq 650$	$15 < r_{corr} \leq 30$	$12 < r_{corr} \leq 25$	$2 < r_{corr} \leq 5$
	µm/a	$50 < r_{corr} \leq 80$	$2,1 < r_{corr} \leq 4,2$	$1,3 < r_{corr} \leq 2,8$	—
C5	g/(m²·a)	$650 < r_{corr} \leq 1\,500$	$30 < r_{corr} \leq 60$	$25 < r_{corr} \leq 50$	$5 < r_{corr} \leq 10$
	µm/a	$80 < r_{corr} \leq 200$	$4,2 < r_{corr} \leq 8,4$	$2,8 < r_{corr} \leq 5,6$	—
CX	g/(m²·a)	$1\,500 < r_{corr} \leq 5\,500$	$60 < r_{corr} \leq 180$	$50 < r_{corr} \leq 90$	$r_{corr} > 10$
	µm/a	$200 < r_{corr} \leq 700$	$8,4 < r_{corr} \leq 25$	$5,6 < r_{corr} \leq 10$	—

NOTE 1 The classification criterion is based on the methods of determination of corrosion rates of standard specimens for the evaluation of corrosivity (see ISO 9226).

NOTE 2 The corrosion rates, expressed in grams per square metre per year [g/(m²·a)], are recalculated in micrometres per year (µm/a) and rounded.

NOTE 3 The standard metallic materials are characterized in ISO 9226.

NOTE 4 Aluminium experiences uniform and localized corrosion. The corrosion rates shown in this table are calculated as uniform corrosion. Maximum pit depth or number of pits can be a better indicator of potential damage. It depends on the final application. Uniform corrosion and localized corrosion cannot be evaluated after the first year of exposure due to passivation effects and decreasing corrosion rates.

NOTE 5 Corrosion rates exceeding the upper limits in category C5 are considered extreme. Corrosivity category CX refers to specific marine and marine/industrial environments (see Annex C).

Figure 1.3 Corrosion rates, r_{corr}, for the first year of exposure for different corrosion categories (from ISO 9223).

1.4 Calculating First Year Corrosion Rates

The AAC Conductor model relies on ISOCORRAG rate equations to estimate the uniform corrosion rate during the first year of exposure for a given environment.[4] Equations 1.1 - 1.4 give the uniform environmental first-year corrosion loss for carbon steel, zinc, copper, and aluminum, respectively.

For carbon steel:

$$r_{corr,St} = (0.085P_d^{0.56})(TOW^{0.53})exp(f_{St}) + (0.24S_d^{0.47})(TOW^{0.25})exp(0.049T)$$
$$f_{St} = 0.098(T-10)\ when\ T \leq 10°C; otherwise\ \ -0.087(T-10) \qquad \textbf{Equation 1.1}$$

For zinc:

$$r_{corr,Zn} = (0.0053P_d^{0.43})(TOW^{0.53})exp(f_{Zn}) + (0.00071S_d^{0.68})(TOW^{0.3})exp(0.11T)$$
$$f_{Zn} = 0\ when\ T \leq 10°C; otherwise - 0.032(T-10) \qquad \textbf{Equation 1.2}$$

For copper:

$$r_{corr,Cu} = (0.00013P_d^{0.55})(TOW^{0.84})exp(f_{Cu}) + (0.0024S_d^{0.31})(TOW^{0.57})exp(0.03T)$$
$$f_{Cu} = 0.047(T-10)\ when\ T \leq 10°C; otherwise\ \ -0.029(T-10) \qquad \textbf{Equation 1.3}$$

For aluminum:

$$r_{corr,Al} = (0.00068P_d^{0.87})(TOW^{0.38})exp(f_{Al}) + (0.00098S_d^{0.49})(TOW^{0.38})exp(0.057T)$$
$$f_{Al} = 0\ when\ T \leq 10°C; otherwise - 0.031(T-10) \qquad \textbf{Equation 1.4}$$

where $r_{corr,X}$ is the first-year corrosion rate of the given metal 'X' (µm/a), T is the annual average temperature (°C) at the location of interest, TOW is the "Time of Wetness" (defined as the fraction of the year in which the temperature is above 0°C and the relative humidity is ≥ 80%, P_d is the annual average SO_2 deposition (mg/(m^{2}d)), and S_d is the annual average Cl^- deposition (mg/(m^{2}d)).

Note that these equations can only be used to model uniform corrosion rates, however, these metals may also be subject to localized corrosion processes (e.g., pitting, crevice corrosion, etc.). Thus, relying solely on these rates may underestimate the total penetration that may occur on certain components.[5,6] Additional laboratory studies would be required to better model pitting in these systems.

---

[4] Knotkova, D., Kreislova, K., Dean, S.W., "ISO CORRAG International Atmospheric Exposure Program: Summary of Results", ASTM Data Series 71. ASTM International, PA, USA, 2010.

[5] International Organization for Standards (ISO). (2012) 9223:2012 Corrosion of metals and alloys - Corrosivity of atmospheres - Classification, determination and estimation

[6] International Organization for Standards (ISO). (2012) 9224:2012 Corrosion of metals and alloys - Corrosivity of atmospheres – Guiding values for the corrosivity categories.

To calculate the corrosion rate, the annual average temperature, TOW, SO_2 deposition, and Cl^- deposition are needed. Data from PG&E's Meteorology Analytics Group was used to assess the TOW; the California Energy Commission Building Climate Zones were used to obtain the annual average temperature for each asset;[7] and the EPA National Atmospheric Deposition Program was used to obtain the annual average SO_2 deposition (dry) and annual average Cl^- deposition (dry).[8] Figure 1.4 shows maps of the TOW, annual average SO_2 and Cl^- deposition rates, and the California Climate Zones. All transmission structures were superimposed onto the TOW map, climate zones, P_d, and S_d GIS layers to assign the geolocation information of each layer onto each asset. The resulting geoprocessed dataset contained the T, TOW, P_d, and S_d for each structure.

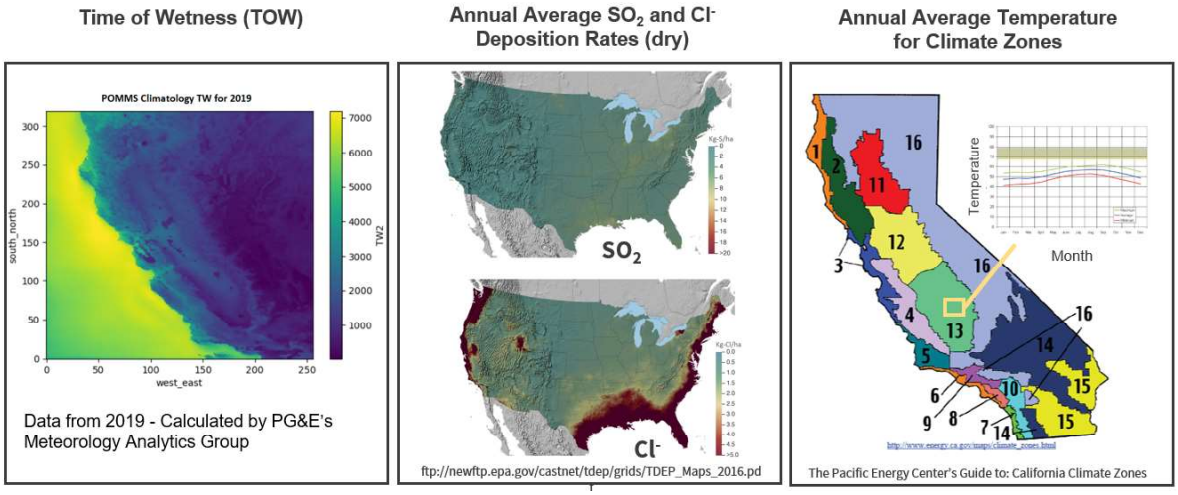

Figure 1.4 Maps of the (*left*) Time of Wetness from PG&E's Meteorology Analytics Group (*middle*) annual average SO_2 and Cl^- deposition rates from the EPA National Atmospheric Deposition Program and (*right*) annual average temperature for each climate zone in California from the California Energy Commission Building Climate Zones.

The calculated corrosion rates are subsequently adjusted by empirical factors to account for real-world measurements of pollutant concentrations and local corrosion rates found in literature.[9]

For all metal types:

[7] Documentation and data from the California Energy Commission can be found at <https://www.energy.ca.gov/programs-and-topics/programs/building-energy-efficiency-standards/climate-zone-tool-maps-and >. Documentation on the temperature and relative humidity for each climate zone can be found at < https://www.pge.com/includes/docs/pdfs/about/edusafety/training/pec/toolbox/arch/climate/california_climate_zones_01-16.pdf>.

[8] The EPA National Atmospheric Deposition Program documentation can be accessed at < ftp://newftp.epa.gov/castnet/tdep/grids/TDEP_Maps_2016.pdf>.

[9] Thomas, H.E, Alderson, H.N., "Corrosion Rates of Mild Steel in Coastal, Industrial, and Inland Areas of Northern California", ASTM International, Metal Corrosion in the Atmosphere, PA, USA, 1968.

$$r_{corr\_adj,X} = (3.91)(2.41)r_{corr,X} \qquad \textbf{Equation 1.5}$$

These normalized values are then compared to the values in Figure 1.3 to assign an interim corrosion category for flat samples. Note that an additional normalization is required for certain sample geometries. This is explored in more detail in Section 4.2. The steel structure model relies on a slightly different normalization. The rationale for this is discussed in Section 2.2.

The interim corrosion categories calculated to this point have relied on local SO_2 deposition rates from the EPA National Atmospheric Deposition Program.[10] However, other sulfurous compounds can act as corrosive agents as well. Geothermal power plants are a major source of sulfur emissions. Figure 1.5 shows two maps from the California Air Resources Board, one of SO_x emissions and one of H_2S emissions statewide.[11] As shown in Figure 1.5, a major H_2S hot spot is observed near The Geysers Geothermal Field (denoted by the white box) but this area has relatively low corresponding SO2 deposition rates.

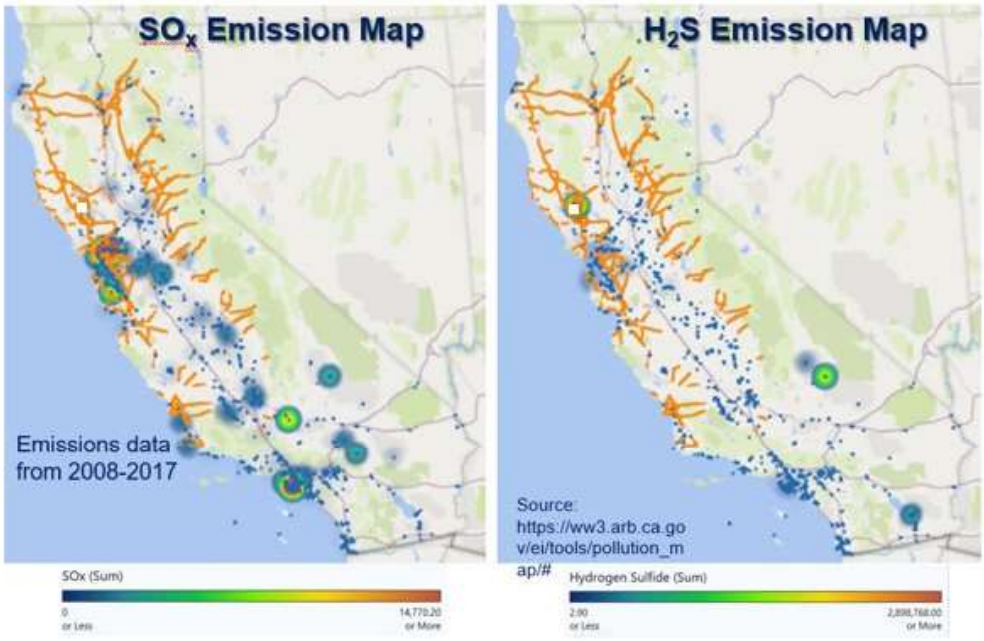

Figure 1.5 Maps of SO_x emission (left) and H_2S emissions across the state of CA. The white box shown on both maps denotes the location of the Geysers Geothermal Field.

Calculation of corrosion rates due to H_2S emissions requires converting these values into deposition rates, which are highly dependent on topography, weather patterns, etc. While doing

[10] The EPA National Atmospheric Deposition Program documentation can be accessed at < ftp://newftp.epa.gov/castnet/tdep/grids/TDEP_Maps_2016.pdf>.

[11] California Air Resources Board documentation can be accessed at <https://ww3.arb.ca.gov/ei/tools/pollution_map/#>

so for the entire PG&E system would be possible using AERMOD (**A**merican Meteorological Society/**E**nvironmental Protection Agency **R**egulatory **Mod**el) software[12], it would be highly resource intensive. Nevertheless, the geothermal plants in The Geysers are a key source of H_2S emissions in CA that should be considered in the model. This is due to the presence of 18 active geothermal energy plants (as of 2009), as reported by the Department of Energy "The Geysers Geothermal Field: Update 1990-2010".[13] Figure 1.6 presents map of the locations of these plants from the same source.

Figure 1.6 Map of active, offline, and dismantled geothermal power plant locations in The Geysers region.

Exponent conducted a pilot study to better understand the impact of these geothermal plants on local corrosion rates. The results of this study, presented in Figure 1.7, suggest that H_2S deposition (and corresponding corrosion categories) can be approximated by the distance from the nearest geothermal source. The results also suggest that corrosion rates return to baseline at approximately 10 km from the nearest geothermal source. Thus, all assets within 10 km of a Geysers geothermal source require additional corrosion category evaluation. The corrosion category adjustments for proximity to a Geysers plant are reported in Figure 1.8. The higher of the two possible corrosion categories (i.e., the interim corrosion category assigned after Equation

[12] AERMOD is the U.S. EPA's preferred aerial pollutant dispersion modeling software. Additional information is available here: https://www.epa.gov/scram/aermod-modeling-system-development

[13] Brophy, P, Lippmann, M, Dobson, P F, & Poux, B. *The Geysers Geothermal Field Update1990/2010.* United States. https://doi.org/10.2172/1048267

1.5 has been applied, and the tabulated geothermal category in Figure 1.8) is assigned as the final corrosion category.

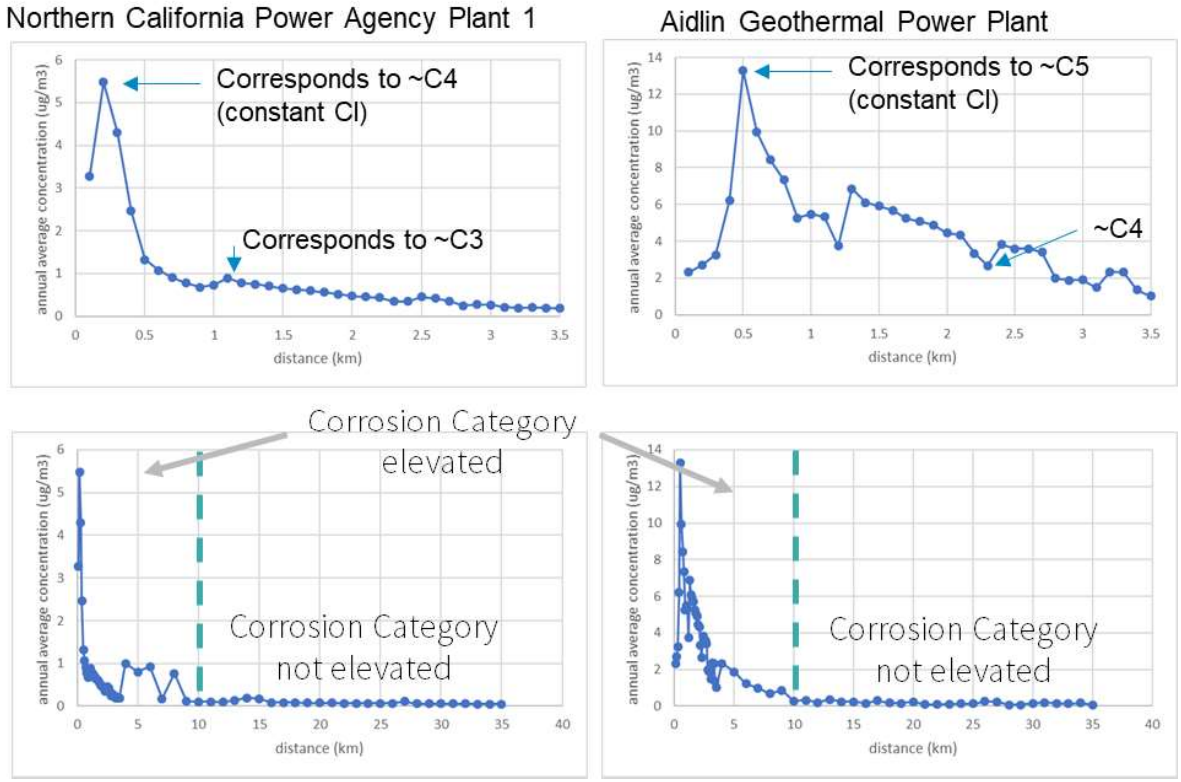

Figure 1.7 Corrosion Category as a function of Distance from two geothermal plants in The Geysers.

Distance from Plant	Corrosion Category
1 km	C5
3 km	C4
5 km	C3
10 km	C2

Figure 1.8 Corrosion Category assignment based on distance from nearest geothermal plant. Note that that the larger category of the two possible categories should be used.

1.5 Calculating Material Loss due to Atmospheric Corrosion

Once the corrosion categories are determined for each structure, the age, alloy type, maintenance history, and coating type are considered to determine the expected material loss due to atmospheric corrosion over time. As metals age in outdoor environments, their corrosion rates decrease over time as corrosion product accumulates on their surfaces. The ISO 9224 standard provides guidance on modeling the total metal attack due to corrosion over time, which can be estimated using the following equations.

For structures less than 20 years old:

$$D = r_{cc,X} t^b \qquad \textit{Equation 1.6}$$

For structures over 20 years old:

$$D(t > 20) = r_{cc,X}[20^b + b(20^{b-1})(t - 20)] \qquad \textit{Equation 1.7}$$

where D is the total corrosion attack in either mass loss per unit area or penetration depth, $r_{cc,X}$ is the maximum first year corrosion rate for metal 'X' in the previously identified corrosion category in accordance with ISO 9223 (g/(m^{2}a) or µm/a), t is the exposure time (years), and b is a metal specific time exponent. Note that after 20 years, the total material loss rate linearizes as the removal rate of the corrosion product increases and the corrosion product layer thickness becomes constant. As the AAC model intends to provide a conservative estimate, the value b_2 is used for these calculations. The value b_2 is the value of b plus two standard deviations. ISO 9224 gives the values of b_2 for the metals associated with the component groupings of the TCM. These values are reported in Table 1.1.

Metal	b_2
Carbon Steel	0.575
Zinc	0.873
Copper	0.726
Aluminum	0.807

Table 1.1 b_2 values for the metals considered by the AAC model

As the specific implementations for calculating materials loss have some asset-type-specific considerations (e.g., steel structures are often painted, while conductors are not), Sections 2 – 5 contain specific information on how any variations to this procedure were implemented. Although certain component groups (e.g., above grade hardware) use aluminum and copper alloys, the AAC treats all aluminum alloyed and copper alloyed components as pure aluminum and pure copper respectively. For copper alloys, this is a reasonably good assumption as ISO

9224 notes that copper alloys have similar or lower atmospheric corrosion rates than pure copper.[14] As noted previously, due to the potential for pitting in aluminum and its alloys, the maximum penetration in aluminum-based components can locally exceed the estimates provided by Equations 1.6 and 1.7. Additionally, certain aluminum alloys, especially those with relatively large copper and copper-zinc fractions, may be susceptible to other corrosion-based failure modes.[15] Nevertheless, as many of the aluminum and copper alloys used in electrical transmission components are proprietary, the AAC model treats all aluminum and copper-based components as pure materials.

1.6 Calculating Figures of Merit and Design Life Reduction Factors

As mentioned in Section 1.1, the AAC model is incorporated into the TCM by adjusting the dispersion of an asset's fragility curve using a calculated design life reduction factor (DLRF). Consistent with the methodology of the TCM, in general, the AAC model implementations use an asset's corrosion rates (as determined by its corrosion category) to determine the time to reduce the fastest corroding component by 1/3 its total thickness.[16] This metric corresponds to approximately 1/3rd reduction in strength, consistent with guidelines from the California Public Utilities Commission General Order 95 (GO-95). Thus, the time to 1/3 wall loss, t_{atm_corr}, serves as the figure of merit for three out of the four implementations. For additional information on the conductor implementation's figure of merit, see Section 4.4. In calculating the time to 1/3 wall loss, the model considers both specific features of the full system (e.g., calculating the times to corrode the thicker steel components and thinner aluminum and copper components and choosing the shortest time) and features of individual components (e.g., painting histories and galvanizing layer thicknesses).

Using the calculated t_{atm_corr} the DLRF was found using Equation 1.8. If the time to corrode was greater than 150 years, the notional design life for electrical transmission towers, the DLRF was set to zero. The DLRF was capped by setting any DLRF greater than 0.33 to 0.33 (i.e., the maximum DLRF was set to correspond to a 1/3 reduction in design life). The following equations were used to determine the atmospheric corrosion DLRF, atm_corr_{DLRF}:

$$atm\_corr_{DLRF} = \begin{cases} 0, t_{atm\_corr} > 150 \\ 1 - \frac{t_{atm\_corr}}{t_D}, \ t \leq 150 \end{cases}$$

Equation 1.8

[14] International Organization for Standards (ISO). (2012) 9224:2012 Corrosion of metals and alloys - Corrosivity of atmospheres – Guiding values for the corrosivity categories.
[15] International Organization for Standards (ISO). (2012) 9224:2012 Corrosion of metals and alloys - Corrosivity of atmospheres – Guiding values for the corrosivity categories.
[16] The model assumes the structure thickness is 3/16th inch, based on the CPUC GO95 standard requiring a minimum thickness of 3/16th inch.

where t_D is the notional design life of 150 years. The AAC model was developed into software that can automatically update the DLRF into the TCM. Note that, like the figure of merit assignment, the DLRF assignment is performed differently in the conductor implementation. Additional details on this process can be found in Section 4.4.

Section 2: Steel Structures

The AAC model implementation described below is intended specifically for structural components of steel towers and poles along PG&E electric transmission lines, since it incorporates steel alloy and painting/coating considerations that are relevant to structural components (e.g., steel angles of a lattice transmission tower), but not to other metallic components (e.g., ACSR conductors).

2.1 Steel Structures AAC Model Overview

An overview of the AAC model implementation process for steel structures is shown in Figure 2.1. The process starts by collecting structure information from ET GIS to understand the structure identifying number, age, and location. Using the location of the structure, the potential for atmospheric corrosion is determined using the annual average temperature, TOW, and deposition rates of SO_2 and Cl^-. Atmospheric corrosion estimates are quantified by determining the corrosion rate and corresponding corrosion category in accordance with the ISO 9223 and 9224 standards.[17,18] Inspection forms and the Tower Painting Program datasets are used to determine the metal alloy type (galvanized or weathering steel) and painting history. The model's figure of merit for above-ground steel structures, the time to corrode 1/3rd of the member thickness, is calculated from the corrosion category, metal alloy type, and painting history. Note that to provide a conservative estimate, this value is used for all steel structures. This includes steel poles, which may have a larger critical thickness. However, as pole thicknesses can vary, for simplicity, the model currently assumes the same critical thickness in all cases. The DLRF is then determined using the procedure outlined in Section 1.6. A list of structures with the corrosion category and DLRF are the final AAC model output which are input to the TCM to adjust the dispersion of the fragility curves for each structure.

[17] International Organization for Standards (ISO). (2012) 9223:2012 Corrosion of metals and alloys - Corrosivity of atmospheres - Classification, determination and estimation

[18] International Organization for Standards (ISO). (2012) 9224:2012 Corrosion of metals and alloys - Corrosivity of atmospheres – Guiding values for the corrosivity categories.

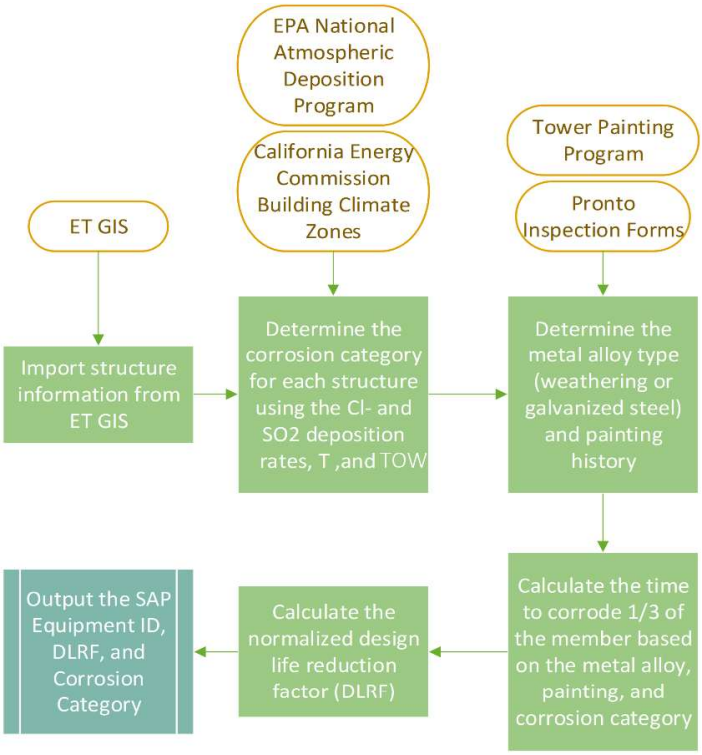

Figure 2.1 AAC model process overview.

2.2 Calculating the Corrosion Category of the Local Environment for Steel Structures

The corrosion rate during the first year of exposure can be estimated for a given environment. Equation 1.1 and 1.2 in Section 1.4 give the first-year corrosion loss for carbon steel and zinc for a given environment, from ISO 9223:

The AAC model adapted Equation 1.1 and Equation 1.2 to calculate the corrosion rate and corresponding corrosion category for each structure within the overhead transmission system. The calculated corrosion rates obtained from these equations were compared to the expected corrosion rate ranges listed in Figure 1.3 for each corrosion category, and the corresponding corrosion category was assigned.

To calculate the corrosion rate, the annual averages of temperature, relative humidity, SO_2 deposition, and Cl^- deposition are needed. The California Energy Commission Building Climate Zones were used to obtain the annual average temperature and annual TOW for each structure (see Figure 1.4).[19] The EPA National Atmospheric Deposition Program was used to obtain the

[19] Documentation and data from the California Energy Commission can be found at <https://www.energy.ca.gov/programs-and-topics/programs/building-energy-efficiency-standards/climate-zone-

annual average SO_2 deposition (dry) and annual average Cl^- deposition (dry) (see Figure 1.4).[20] The resulting geoprocessed dataset contained the T, TOW, P_d, and S_d for each structure.

The T, TOW, P_d, and S_d values for each structure were used to calculate the corrosion rate for carbon steel, according to Equation 1.1.

The calculated corrosion rate for each structure is normalized by Equation 1.5 and is then compared with the carbon steel corrosion rates in Figure 1.3 to determine the appropriate corrosion category. Figure 2.2 shows the calculated corrosion categories for each steel structure. Coastal, urban, and industrial areas have structures with the highest corrosion categories (C4 and C5). This corresponds to the elevated levels of Cl^- and SO_2 in these areas.

Figure 2.2 Steel Structure Corrosion Categories as determined by the AAC model.

tool-maps-and >. Documentation on the temperature and relative humidity for each climate zone can be found at < https://www.pge.com/includes/docs/pdfs/about/edusafety/training/pec/toolbox/arch/climate/california_climate_zones_01-16.pdf>.

[20] The EPA National Atmospheric Deposition Program documentation can be accessed at < ftp://newftp.epa.gov/castnet/tdep/grids/TDEP_Maps_2016.pdf>.

2.3 Calculating the Material Loss Due to Atmospheric Corrosion and Design Life Reduction Factor

As described previously, the AAC model is incorporated into the TCM by adjusting the dispersion in median strength through the design life reduction factor (DLRF). Consistent with the methodology of the TCM, the corrosion rates of the AAC model (as determined by the corrosion categories) are used to determine the time to reduce the lattice steel member thickness by 33%, or 1/16th inch.[21] Solving Equation 1.7 for time, t, and substituting 1/16th inch for D gives the amount of time to corrode 33% of the member, as shown by Equation 2.2 through Equation 2.4. For galvanized steel structures, the zinc layer is assumed to corrode away before corrosion occurs on the carbon steel.[22] Therefore, D in Equation 2.2 is set as 75 microns to represent the zinc layer. After the zinc layer is completely consumed by corrosion, corrosion begins on the carbon steel and the time to corrode 1/16th inch (1587 micron) is calculated. For weathering steel, corrosion begins immediately on the structure, however, weathering steel is a corrosion-resistant alloy. Thus, the value of b_2 for weathering steel is modified to represent the corrosion resistant nature of the alloy, as described in Section 2.3.2.

For zinc (age over 20 years):

$$Zn_{20}(corr_{cat}) = \frac{75 - r_{high\_Zn} 20^{b_{2\_Zn}} + 20 b_{2\_Zn} r_{high\_Zn} 20^{b_{2\_Zn}-1}}{b_{2\_Zn} r_{high\_Zn} 20^{b_{2\_Zn}-1}} \qquad \textit{Equation 2.2}$$

For carbon steel over 20 years old:

$$CS_{20}(corr_{cat}) = \frac{(1587-75) - r_{high\_CS} 20^{b_{2\_CS}} + 20 b_{2\_CS} r_{high\_CS} 20^{b_{2\_CS}-1}}{b_{2\_CS} r_{high\_CS} 20^{b_{2\_CS}-1}} \qquad \textit{Equation 2.3}$$

For weathering steel over 20 years old:

$$WS_{20}(corr_{cat}) = \frac{1587 - r_{high\_CS} 20^{b_{2\_WS}} + 20 b_{2\_WS} r_{high\_CS} 20^{b_{2\_WS}-1}}{b_{2\_WS} r_{high\_CS} 20^{b_{2\_WS}-1}} \qquad \textit{Equation 2.4}$$

where $Zn_{20}(corr_{cat})$ is the number of years to corrode 75 microns of zinc as a function of the corrosion category; $CS_{20}(corr_{cat})$, and $WS_{20}(corr_{cat})$ are the number of years (greater than 20) to uniformly corrode 1/3rd of the member as a function of each corrosion category for carbon steel and weathering steel, respectively; r_{high_Zn} and r_{high_CS} are the high-end corrosion rates for zinc and carbon steel, respectively, for each corrosion category as given in Figure 1.3; b_{2_Zn}, b_{2_CS}, and b_{2_WS} are the metal-environment-specific time exponent for zinc, carbon steel, and weathering steel, as given in Table 2.2; $CS(corr_{cat})$ is the number of years to uniformly corrode 1/3rd of the member as a function of each corrosion category for carbon steel when the number of years is less than 20.

[21] The model assumes the structure thickness is 3/16th inch, based on the CPUC GO95 standard requiring a minimum thickness of 3/16th inch.

[22] The galvanic effects between the zinc layer and carbon steel are not accounted for in this model, as this is not addressed by ISO 9224.

The time to corrode 33% of the member (or 75 micron of zinc) for each corrosion category is shown in Table 2.1.

Corrosion Category	$Zn_{20}(corr_{cat})$ Years to corrode 75 um Zinc Layer	$CS_{20}(corr_{cat})$ Years to corrode 1/16 inch Carbon Steel	$WS_{20}(corr_{cat})$ Years to corrode 1/16 inch Weathering Steel
C1	1254	7211	34859
C2	177	361	1767
C3	57	173	859
C4	27	103	519
C5	12	32	178
C6	2	4	16

Table 2.1 Years to corrode 75 um of Zinc or 1/16 inch carbon or weathering steel, calculated using Equation 2.2, Equation 2.3, and Equation 2.4 for each corrosion category, where r_{high} comes from Figure 1.3 and b_2 comes from Table 2.2. [ISO 9224, Section 7, Equation 3]

However, the time to 1/3 wall loss can be further refined by accounting for the structural properties of the asset, such as the metal alloy composition and painting history and maintenance as alluded to previously. Each of these factors affect how quickly, and severely atmospheric corrosion can occur. The structure properties and corresponding data sources used by the AAC model are listed below:

- *Metal alloy composition* – galvanized steel or weathering steel as indicated by ET GIS or the inspection data
- *Painting history and maintenance* – Painting layer indicated on inspection forms and Tower Painting Program dataset indicating the structure has been or will be painted

Thus, the total time to corrode 1/3rd of the member, t_{atm_corr}, was estimated for each structure. The following three cases were used depending on the metal alloy and painting history and maintenance:

***Weathering Steel*: time to corrode for the member in the weathering steel column of Table 2.1 using the structure's corrosion category $corr_{cat}$:**

$$t_{atm\_corr} = WS_{20}[corr_{cat}] \qquad \textit{Equation 2.5}$$

***Galvanized Steel or Unknown*: time to corrode for the member in the zinc and carbon steel columns of Table 2.1 using the structure's corrosion category $corr_{cat}$:**

$$t_{atm\_corr} = Zn_{20}[corr_{cat}] + CS_{20}[corr_{cat}] \qquad \textit{Equation 2.6}$$

***Painted Galvanized Steel*: the time to corrode for the member in the zinc and carbon steel columns of Table 2.1 and the paint life in Table 2.5 using the structure's corrosion category $corr_{cat}$:**

$$t_{atm\_corr} = paint_{life[corr_{cat}]} + Zn_{20}[corr_{cat}] + CS_{20}[corr_{cat}] \qquad \textbf{Equation 2.7}$$

The modifications to the time to 1/3 wall loss calculations for varying metal alloy composition and painting histories are outlined in Sections 2.3.1 and 2.3.2, respectively.

2.3.1 Metal Alloy Composition

The metal alloy of the steel structure was identified through ET GIS or inspection data. The two metal alloys considered in this implementation of the AAC model are galvanized steel and weathering steel. Galvanized steel was assumed if the structure alloy composition was unknown.[23] As previously mentioned, galvanized steel was assumed to have a 75-micron Zn layer on top of carbon steel.

The metal alloy composition is accounted for in Equation 1.6 and Equation 1.7 through the variable b, the metal-environment-specific time exponent. To provide a conservative estimate, the model uses a value of b_2. For more information on this, see Section 1.5. ISO 9224 gives the values of b_2 for carbon steel and zinc, shown in Table 2.2.[24]

The value of b_2 for weathering steel can be calculated according to Annex C of ISO 9224. If the steel composition is known or can be estimated, the value of b_2 can be calculated for the specific steel composition using Equation 2.8 and Table 2.3 for the alloying element multipliers. The exact type of weathering steel alloy is unknown based on the datasets from ET GIS and the inspection data; however, the alloy composition was estimated. Cor-Ten B, a common weathering steel used for load bearing structures, can have a range of compositions, as shown in Table 2.3. The b_2 value was calculated for both the minimum and maximum alloy compositions of Corten B and the arithmetic mean was taken as the value of b_2 for weathering steel. The value for b_2 for weathering steel was calculated to be 0.292 by using Equation 2.8, Table 2.3, and Table 2.4. Note that this generates a conservative estimate of b2; however, typical alloys will have non-zero concentrations of the elements with specified minimums of 0 wt. % (e.g., C, S, P, and Ni).

[23] Galvanized steel was assumed for unknown structures based off SME conversations and review of PG&E standards.

[24] International Organization for Standards (ISO). (2012) 9224:2012 Corrosion of metals and alloys - Corrosivity of atmospheres – Guiding values for the corrosivity categories.

Metal	b_2
Carbon Steel	0.575
Weathering Steel*	0.292
Zinc	0.873

Table 2.2 Time exponent values for predicting and estimating corrosion attack. *The b value for weathering steel is calculated as the arithmetic mean of Equation 2.10, using Table 2.3 and Table 2.4. [ISO 9224]

$$b_a = 0.569 + \sum b_i w_i \qquad \textit{Equation 2.8}$$

where b_a is the alloy-specific value of b in non-marine exposures, b_i is the multiplier for the *i*th alloying element (taken from Table 2.3), and w_i is the mass fraction of the *i*th alloying element (taken from Table 2.4[25] for weathering steel).

Element	Multiplier b_i
C	–0,084
P	–0,490
S	+1,440
Si	–0,163
Ni	–0,066
Cr	–0,124
Cu	–0,069

Table 2.3 Alloying element multipliers for Equation 2.8, from ISO 9224.

[25] As ISO 9224 does not give a multiplier for vanadium or manganese, these are not included in the b_2 calculation performed using Equation 2.10

Weathering Steel Cor-Ten B		
Alloy	Maximum Conc. (wt. %)	Minimum Conc. (wt. %)
C	0.16	0.00
P	0.03	0.00
S	0.03	0.00
Si	0.50	0.30
Ni	0.40	0.00
Cr	0.65	0.40
Cu	0.40	0.25
Mn	1.25	0.80
V	0.10	0.02

Table 2.4 Compositional range (wt.%) of Cor-Ten B weathering steel from[https://www.totalmateria.com/page.aspx?ID=CheckArticle&site=kts&NM=274]

2.3.2 Painting History and Maintenance

Many steel structures are manufactured or maintained with protective coatings that extend the expected service lifetime. Two sources were used to determine if a structure had been or will be painted: the inspection forms and Tower Painting Program. Inspection forms were mined to determine if there was indication that the structure had been painted in the past. The Tower Painting Program is an on-going effort to paint towers starting in 2019 and indicates when the tower was painted. The AAC model assumes the paint was applied when the tower was first installed. The model assumes no corrosion was present at the time of painting and the paint layer provided full corrosion protection during the painting service lifetime.

The NACE 4088 paper describes how to estimate the service lifetime of commonly used paints and coatings.[26] The NACE standard defines the practical life of the coating as the "time until 5 to 10% coating breakdown occurs (SSPC-Vis 2 Grade 4), and active rusting of the substrate is present." Acrylic waterborne paints that are hand applied were assumed for the PG&E system. Figure 2.3 shows the estimated practical life for coating systems in different atmospheric corrosion categories.

[26] Jelsel, J., Reina, M., Lanterman, R. (2014) 4088: Expected Service Life and Cost Considerations for Maintenance and New Construction Protective Coating Work. NACE International.

Type	Coating Systems for Atmospheric Exposure (primer/midcoat/topcoat)	Surface Preparation[2]	Number of Coats	DFT Minimum (mils)	Service Life[1,3]			
					Mild (rural)/C2	Moderate (industrial)/C3	Severe (heavy industrial)/C5-I	Seacoast Heavy Industrial/C5-M
Acrylic	Acrylic Waterborne/Acrylic WB/ Acrylic WB	Hand/Power	3	6	12	8	5	5
Acrylic	Acrylic Waterborne/Acrylic WB/ Acrylic WB	Blast	3	6	17	12	9	9

NOTES:

1. Service Life Estimates:
   All estimates (in years) are for the "Practical" life of the system. Practical life is considered to be the time until 5 to 10% coating breakdown occurs (SSPC-Vis 2 Grade 4), and active rusting of the substrate is present.

2. Surface preparation definitions:
   Hand/Power - Requires SSPC-SP 3 "Power Tool Cleaning" or SP 2 "Hand Tool Cleaning"
   Blast - Requires SSPC-SP 6 "Commercial Blast" or SP 10 "Near White Blast"

3. Service Life Environments per ISO 12944-2, "Classification of Environments"
   C2: Low - Atmospheres with low levels of pollution; mostly rural areas
   C3: Medium - Urban and industrial atmospheres, moderate sulfur dioxide pollution; coastal areas with low salinity
   C5-I: Very High, Industry - Industrial areas with high humidity and aggressive atmosphere
   C5-M: Very High, Marine - Coastal and offshore areas with high salinity

Figure 2.3 Estimated service life for practical maintenance coating systems for atmospheric exposure (from NACE paper 4088).

The lifetime of the paint or time until the structure needs a full repaint can be estimated by the following equations:

$$Full\ Repaint = P_M + 0.5P \qquad \textbf{Equation 2.9}$$

$$P_M = 0.33P \qquad \textbf{Equation 2.10}$$

where P_M is the maintenance repaint time and P is the practical life of the painting. Using the values for P from Figure 2.3, the full repaint time for each corrosion category was determined and is shown in Table 2.5.

Corrosion Zone	Full Repaint
C6	9.15
C5	9.15
C4	9.15
C3	14.64
C2	21.96

Table 2.5 Expected Service Life for Maintenance and New Construction Protective Coating Work in Years (calculated from NACE paper 4088).27

2.4 Calculating Design Life Reduction Factor

Using the calculated t_{atm_corr} the DLRF was found as described in Section 1.6. The standard 150-year notional design life was used for all steel structures. However, two additional non-standard scenarios occur in certain cases resulting in slightly modified outputs. The first scenario occurs when the model cannot calculate a corrosion category for a given structure. In this case, no DLRF will be assigned and the DLRF output will be recorded as N/A. Data limitations, such as regions with unknown Cl^- deposition rates, lead to this output. The second case occurs when the model can calculate the corrosion category, but it cannot calculate a time to 1/3 wall loss for some reason. In that case, the DLRF is assigned based solely on the corrosion category. Table 2.6 presents the DLRF assignments for each corrosion category in this case. For example, this occurs for painted steel structures in areas with C1 corrosion categories; NACE paper 4088 does not provide information on paint service life in these locations meaning a lifetime cannot be calculated. Note also that if data limitations make it impossible to calculate a DLRF for other component groups subject to atmospheric corrosion (e.g., above grade hardware), the model relies on Table 2.6 to assign DLRFs to those components.

[27] Distribution of the coating breakdown, type of corrosion present, and physical characteristics of the coating should be considered to determine when a full re-paint is required. A more refined analysis maybe necessary to determine the most appropriate painting maintenance schedule for assets.

CORROSION CATEGORY	DLRF
C1	0
C2	.083
C3	.167
C4	.25
C5	.333

Table 2.6 DLRF assignment for cases where a corrosion category can be calculated but time to 1/3 wall loss cannot be.

2.5 Example Calculations

2.5.1 Galvanized Steel Structure

An example structure is presented in the following section to demonstrate the AAC model calculations. A structure with a SAP Equipment number of 40804616 is used for this example. This asset is a lattice steel tower that was installed in 1959 and made from galvanized steel. The location of the asset is shown below in Figure 2.4. Referencing the EPA National Atmospheric Deposition Program, the SO_2 and Cl^- deposition rates at that location are 2.47 mg/m^2/day and 1.04 mg/m^2/day, respectively. This location is within Zone 12 of the California Energy Commission Building Climate Zone. Within Zone 12, the annual average temperature is 18 °C;

the TOW at this location is 2908 h. These values are used in Equation 1.1 to determine the carbon steel corrosion rate for the structure location.

Figure 2.4 Location of structure 40804616.

$$r_{corr,St} = 0.085(2.47^{0.56})(2908^{0.53})exp(f_{St}) + 0.24(1.04^{0.47})(2908^{0.25})exp(0.049 * 18)$$
$$= 9.09\ \mu m/a$$
$$(f_{St} = -0.087(18 - 10) = -0.725$$

The corrosion rate was normalized using the following equation:

$$r_{corr\_adj} = 9.09\frac{\mu m}{a} * 3.91 * 2.41\ = 85.7\ \mu m/a$$

Comparing the calculated adjusted corrosion rate to Figure 1.3, the corrosion category for this location is determined to be C5, as the corrosion rate in C5 ranges from 80 to 200 µm/a.

Using Table 2.1, the time to corrode 33% of the carbon steel members and the time to corrode the zinc layer can be determined for a C5 corrosion category. These values are used to determine the total time to corrode 1/3rd of the member using Equation 1.8

$$t_{atm\_corr} = 12 + 32 = 44\ years$$

The atmospheric corrosion DLRF is calculated for the structure.

$$atm\_corr_{DLRF} = 1 - \frac{44}{150} = 0.71 \rightarrow 0.33$$

2.5.2 Weathering Steel Structure:

A structure with a SAP Equipment number of 44664794 is used for this example. This asset is a lattice steel tower that was installed in 2018 and made from weathering steel. The location of the asset is shown below in Figure 2.5. Referencing the EPA National Atmospheric Deposition Program, the SO_2 and Cl^- deposition rates at that location are 0.08 mg/m^2/day and 0.46 mg/m^2/day, respectively. This location is within Zone 13 of the California Energy Commission Building Climate Zone. Within Zone 13, the annual average temperature is 17°C. The TOW at this location is 1480 h. These values are used in Equation 1.1 to determine the carbon steel corrosion rate for the structure location.

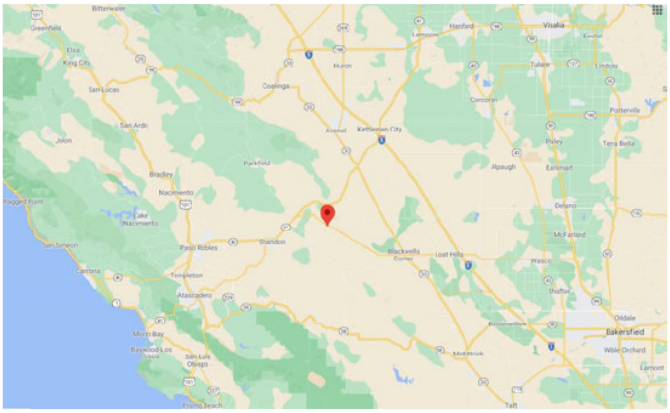

Figure 2.5 Location of structure 44664794.

$$r_{corr,St} = 0.085(0.08^{0.56})(2908^{0.53})exp(f_{St}) + 0.24(0.46^{0.47})(1480^{0.25})exp(0.049 * 18)$$
$$= 2.92\ \mu m/a$$
$$(f_{St} = -0.087(17 - 10) = -0.628$$

The corrosion rate was normalized using the following equation:

$$r_{corr\_adj} = 2.92\frac{\mu m}{a} * 3.91 * 2.41 = 27.6\ \mu m/a$$

Comparing the calculated adjusted corrosion rate to Figure 1.3, the corrosion category for this location is determined to be C3, as the corrosion rate in C3 ranges from 25 to 50 µm/a.

Using Table 2.1, the time to corrode 33% of the weathering steel members for a C3 corrosion category can be determined.

$$t_{atm\_corr} = 859\ years$$

The atmospheric corrosion DLRF is calculated for the structure.

$$atm\_corr_{DLRF} = 1 - \frac{150}{150} = 0$$

2.5.3 Painted Galvanized Steel Structure:

A structure with SAP Equipment number of 40740005 is used for this example. This asset is a lattice steel tower that was installed in 1946 and made from galvanized steel that has been painted. The location of the asset is shown below in Figure 2.6. Referencing the EPA National Atmospheric Deposition Program, the SO_2 and Cl^- deposition rates at that location are 2.47 $mg/m^2/day$ and 1.04 $mg/m^2/day$, respectively. This location is within Zone 12 of the California Energy Commission Building Climate Zone. Within Zone 12, the annual average temperature and relative humidity are 18°C and 57%, respectively. The TOW at this location is 3387 h. These values are used in Equation 1.1 to determine the carbon steel corrosion rate for the structure location.

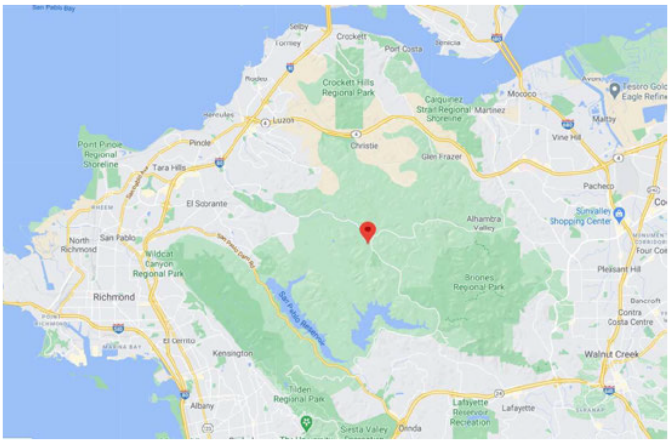

Figure 2.6 Location of structure 40740005.

$$r_{corr,St} = 0.085(2.47^{0.56})(2908^{0.53})exp(f_{St}) + 0.24(1.04^{0.47})(3387^{0.25})exp(0.049 * 18)$$
$$= 9.66\ \mu m/a$$
$$(f_{St} = -0.087(18 - 10) = -0.725$$

The corrosion rate was normalized using the following equation:

$$r_{corr\_adj} = 9.66\frac{\mu m}{a} * 3.91 * 2.41 \ = 91.0\ \mu m/a$$

Comparing the calculated adjusted corrosion rate to Figure 1.3, the corrosion category for this location is determined to be C5, as the corrosion rate in C5 ranges from 80 to 200 µm/a. Using Table 2.1, the time to corrode 33% of the carbon steel members and the time to corrode the zinc layer can be determined for a C5 corrosion category. The painting lifetime is determined from 2.5. These values are used to determine the total time to corrode 1/3rd of the member.

$$t_{atm\_corr} = 9.2 + 12 + 32 = 53.2\ years$$

The atmospheric corrosion DLRF is calculated for the structure.

$$atm\_corr_{DLRF} = 1 - \frac{53.2}{150} = 0.645 \rightarrow 0.33$$

Section 3: Insulator Hardware Corrosion

The AAC model implementation described below is intended specifically for metallic components of insulator hardware present on PG&E electric transmission lines, since it considers factors that are relevant to metallic components of insulators (e.g., the presence of cast iron components), but not to other metallic systems (e.g., steel structures and conductors).

3.1 Insulator Hardware AAC Model Overview

An overview of the AAC model process for insulators is shown in Figure 3.1. The process starts by collecting structure information from ET GIS to understand the structure identifying number, age, and location. Using the location of the structure, the potential for atmospheric corrosion is determined using the annual average temperature, Time of Wetness (TOW), deposition rates of SO_2 and Cl^-, and proximity to geothermal sources for steel, cast iron, and zinc. Atmospheric corrosion estimates are quantified by determining the corrosion rate and corresponding corrosion category in accordance with the ISOCORRAG and the ISO 9223 standard.[28,29] Subsequently, the model identifies the thinnest ferrous component based using ET-GIS information. The model then calculates its figure of merit, time to 1/3 wall loss for the thinnest ferrous component, and a DLRF is calculated. A list of assets with the corrosion category and DLRF are the final AAC model output which are input to the TCM to adjust the dispersion of the fragility curves for each structure.

[28] Knotkova, D., Kreislova, K., Dean, S.W., "ISO CORRAG International Atmospheric Exposure Program: Summary of Results", ASTM Data Series 71. ASTM International, PA, USA, 2010.
[29] International Organization for Standards (ISO). (2012) 9223:2012 Corrosion of metals and alloys - Corrosivity of atmospheres - Classification, determination and estimation

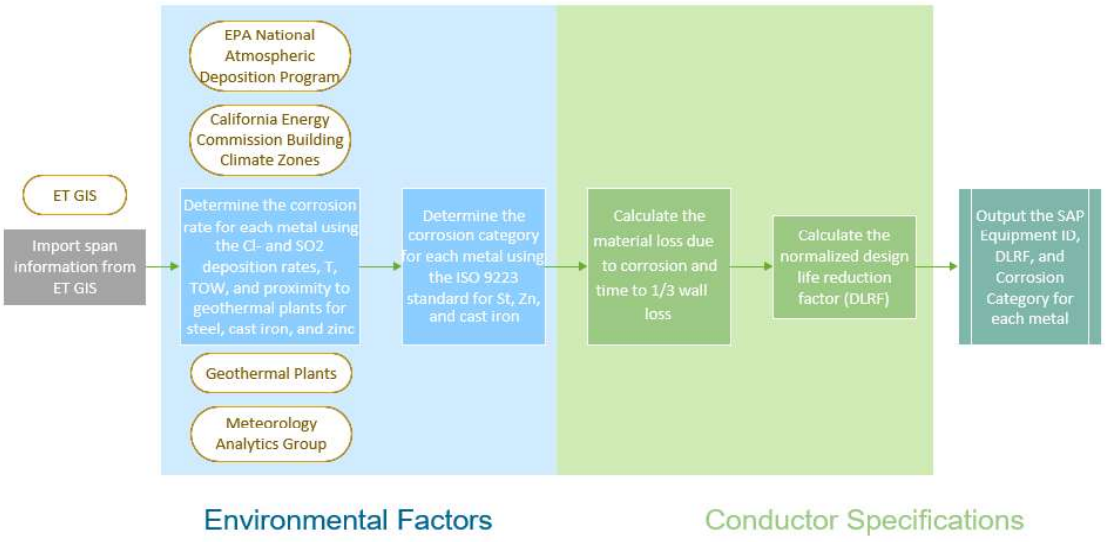

Figure 3.1 Insulator Corrosion Process Flow

3.2 Calculating the Corrosion Category of the Local Environment

In general, the corrosion category assignment for insulators follows the process flow outlined in Section 1.3. The insulator hardware implementation of the AAC considers the possibility for corrosion on both suspension-type insulators and post-type insulators. The metallic components on ceramic suspension insulators consist of, at minimum, a galvanized forged steel shaft and a galvanized cast iron cap. Suspension insulator hardware installed beginning in the 1990s generally also includes an additional metallic component, specifically a zinc sleeve, however, as this likely represents a relatively small fraction of the total hardware in use over PG&E's transmission system, the current implementation of the model simply assumes the presence of the first two components. For post-type insulators, the model considers only a single metallic component—the galvanized steel bolts used for tower attachment. The corrosion categories for steel and zinc are calculated as described in Section 1.3. Research suggests that the first-year corrosion rates of cast irons and mild steels are relatively similar, although there is some indication that the presence of scale on cast irons may provide an additional barrier to corrosion.[30,31] Thus, for the purpose of corrosion category assignment, the cast iron components are assumed to have the same corrosion category as the steel components.

[30] R.E. Melchers / Corrosion Science 68 (2013) 186–194.
[31] M. Sykora, et al., Int. J. Comp. Meth. and Exp. Meas., Vol. 8, No. 2 (2020).

3.3 Calculating the Material Loss Due to Atmospheric Corrosion

As with corrosion category assignment, to calculate the material loss due to corrosion, the model treats both the steel and cast-iron components as mild steels. This aims to provide a conservative estimate, as the studies mentioned in Section 3.2 suggest that the long-term corrosion rates for cast irons are, in general, slower than those of mild steels. Further, as the galvanized steel shaft components consistently have critical dimensions greater than or equal to those of the galvanized cast iron cap, the model assumes that the cast iron cap is the thinnest member, and therefore, most susceptible to failure from corrosion in all cases. The process used to determine these critical dimensions is described in additional detail in Section 5.3. In short, PG&E standards and ATS reports were reviewed in detail to determine the minimum thicknesses possible for a unique group of components (e.g., dead end 230 kV structures). Figure 3.2 presents the process flow employed by the model to identify the cast iron cap's critical thickness. Relying on information from ET GIS, the model determines whether the tower is a suspension or dead-end tower, whether it uses post or suspension insulators, and its operating voltage. Using this information, the model identifies the component of interest's critical thickness, presented in Figure 3.2. Note that the AAC model insulator hardware implementation assumes that zinc galvanizing layers are 75 µm in all cases, consistent with the assumptions made in the steel structures implementation (Section 2) and the Above Grade Hardware implementation (Section 5). As the thinnest galvanizing layer thickness among components in these various groups should be 79 µm, a 75 µm thickness is assumed to account for possible manufacturing variance[32]. Using the steel shaft thickness and zinc layer thickness, the time to 1/3 wall loss is then calculated using the process outlined in Section 1.5 and 1.6.

[32] ASTM International. (2016) A153/A153M-16a Standard Specification for Zinc-Coated (Hot-Dip) on Iron and Steel Hardware.

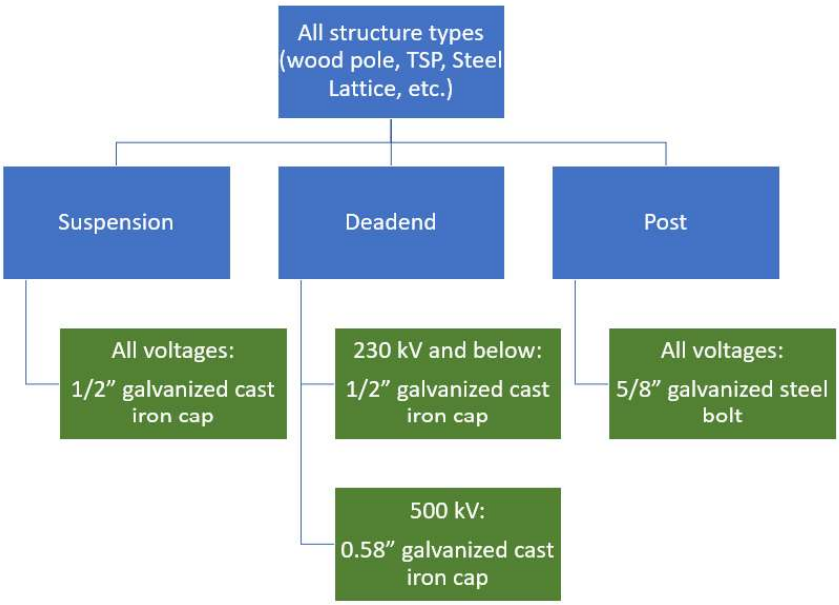

Figure 3.2 Process flow used to identify critical thickness for metallic components of insulators on different types of structures.

3.4 Calculating Design Life Reduction Factor

To calculate the DLRF, the insulator implementation relies on the process outlined in Section 1.6. For insulators, the model assumes a nominal design life of 150 years for the metallic hardware components, consistent with the notional design life for the steel structure. Note that in certain cases the insulating components of the insulator system, rather than the metallic components considered here, may be the most susceptible to environmental degradation. This is especially true for polymeric insulators. In these cases, the degradation of those components is treated elsewhere in the larger composite model.

3.5 Example Insulator Hardware Calculation

This section presents an example calculation for the Insulator Hardware implementation. For this example, we consider structure with SAP Equipment ID 40594046. This asset is a 230 kV double dead end lattice steel tower that was installed in 1979. The location of the asset is shown below in Figure 3.3; it is ~ 0.4 km from the nearest plant in the Geysers. Referencing the EPA National Atmospheric Deposition Program, the SO_2 and Cl^- deposition rates at that location are 0.09 mg/m^2/day and 0.54 mg/m^2/day, respectively. This location is within Zone 2 of the

California Energy Commission Building Climate Zone. Within Zone 2, the annual average temperature is 14.4 °C. The TOW at this location is 2131 hours.

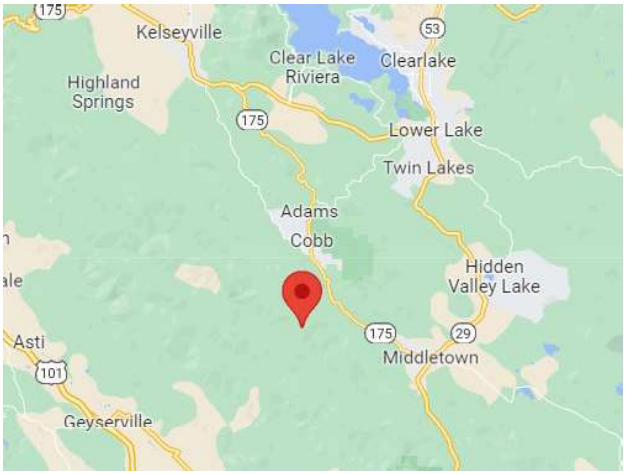

Figure 3.3 Location of structure 40594046 (located with The Geysers' affected area).

Using the equations from Sections 1.3 and 1.4, we calculate the non-normalized corrosion rates for steel and zinc. We assume that cast iron can be modeled as a mild steel, as before.

For carbon steel:

$$r_{corr,St} = (0.085 \times 0.09^{0.56})(2131^{0.53})e^{f_{St}} + (0.24 \times 0.54^{0.47})(2131^{0.25})e^{0.049 \times 14.4} = 3.35\ \mu m/year$$
$$f_{St} = -0.087(14.4 - 10)$$

For zinc:

$$r_{corr,Zn} = (0.0053 \times 0.09^{0.43})(2131^{0.53})e^{f_{Zn}} + (0.00071 \times 0.54^{0.68})(2131^{0.3})e^{0.11 \times 14.4} = 0.12\ \mu m/year$$
$$f_{Zn} = -0.032(14.4 - 10)$$

The corrosion rates were normalized to experimental data using the following equation:

$$r_{corr\_adj,X} = 3.91 \times 2.41 \times r_{corr,X}$$

$$r_{corr\_adj,St} = 31.60\ \mu m/year$$

$$r_{corr\_adj,Zn} = 1.12\ \mu m/year$$

Comparing the calculated adjusted corrosion rates to Figure 1.3, the interim corrosion categories are determined to be C3 for steel and C3 for zinc. However, as the distance from this structure to the nearest plant in The Geysers is less than 1 km, the corrosion categories for both steel and zinc are adjusted to C5.

As this structure is a 230 kV dead end lattice steel tower, the critical dimension is 0.5" (from Figure 3.2). Thus, 1/3 wall loss for this structure is 75 µm of zinc and 4158 µm of carbon steel.

Setting the 1/3 wall losses to (D) from Equation 1.7 and solving for t yields the time to 1/3 wall loss.

$$D(t > 20) = r_{cc,X}[20^{b_2} + b_2(20^{b_2-1})(t - 20)]$$

The values of b_2 for steel and zinc are available in Table 1.1. Note that the time to corrode the zinc and the time to corrode the carbon steel must be solved for separately and then added together. Thus, the time to 1/3 loss is:

$$t_{atm\_corr} = 12 + 114 = 126\ years$$

To calculate the DLRF, the shortest time is chosen (126 years) and the DLRF is calculated for the structure.

$$atm\_corr_{DLRF} = 1 - \frac{126}{150} = 0.157$$

Section 4: Conductor Corrosion

The AAC model implementation described below is intended specifically for conductor spans of PG&E electric transmission lines, since it incorporates various metals, corrosion mechanisms (e.g., galvanic corrosion along ACSR and ACSS conductors), and asset geometric considerations (e.g., helical wire structures) that are relevant to conductor spans, but not to other metallic components (e.g., steel angles of a lattice transmission tower).

4.1 Conductor AAC Model Overview

An overview of the AAC model process for conductors is shown in Figure 4.1. The process starts by collecting structure information from ET GIS to understand the structure identifying number, age, and location. Using the location of the structure, the potential for atmospheric corrosion is determined using the annual average temperature, Time of Wetness (TOW), deposition rates of SO_2 and Cl^-, and proximity to geothermal sources for steel, zinc, aluminum, and copper. Atmospheric corrosion estimates are quantified by determining the corrosion rate and corresponding corrosion category in accordance with the ISOCORRAG and the ISO 9223 standard.[33,34] The model applies two important normalizations at this step which are discussed in Section 4.2. Subsequently, the model calculates the material lost due to corrosion to calculate the conductor model's figure of merit: critical strength loss. The DLRF is then assigned based on the extent of critical strength loss from 0 to 0.33. A list of assets with the corrosion category and DLRF are the final AAC model output which are input to the TCM to adjust the dispersion of the fragility curves for each structure.

[33] Knotkova, D., Kreislova, K., Dean, S.W., "ISO CORRAG International Atmospheric Exposure Program: Summary of Results", ASTM Data Series 71. ASTM International, PA, USA, 2010.
[34] International Organization for Standards (ISO). (2012) 9223:2012 Corrosion of metals and alloys - Corrosivity of atmospheres - Classification, determination and estimation

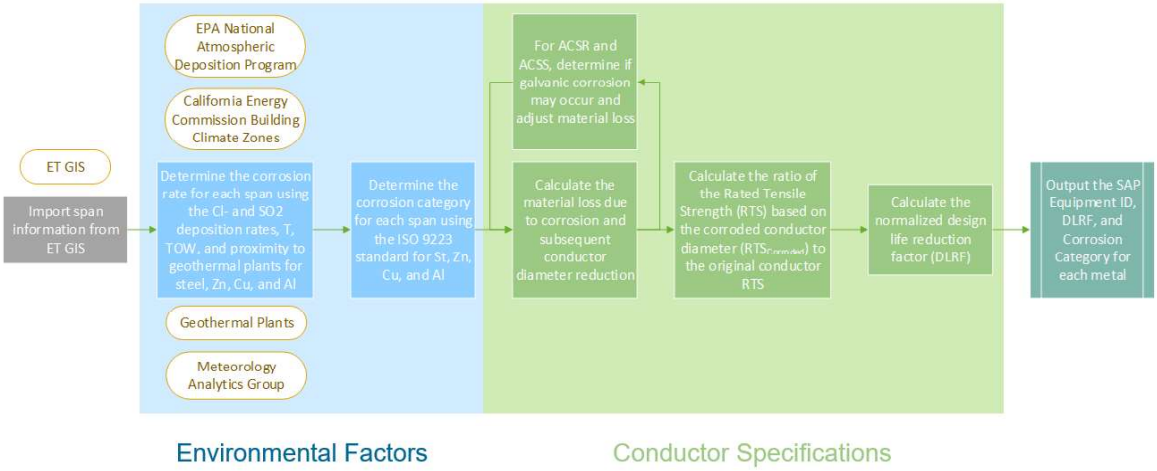

Figure 4.1 AAC conductor model process overview.

4.2 Calculating the Corrosion Category of the Local Environment for Conductors

Most of the corrosion category assignment process employed in the conductor implementation is consistent with the process outlined in Sections 1.3 and 1.4. However, the conductor model employs one additional step during corrosion category determination, as compared to other implementations, to account for corrosion rate increases due to wire geometries, as shown in Figure 4.2.

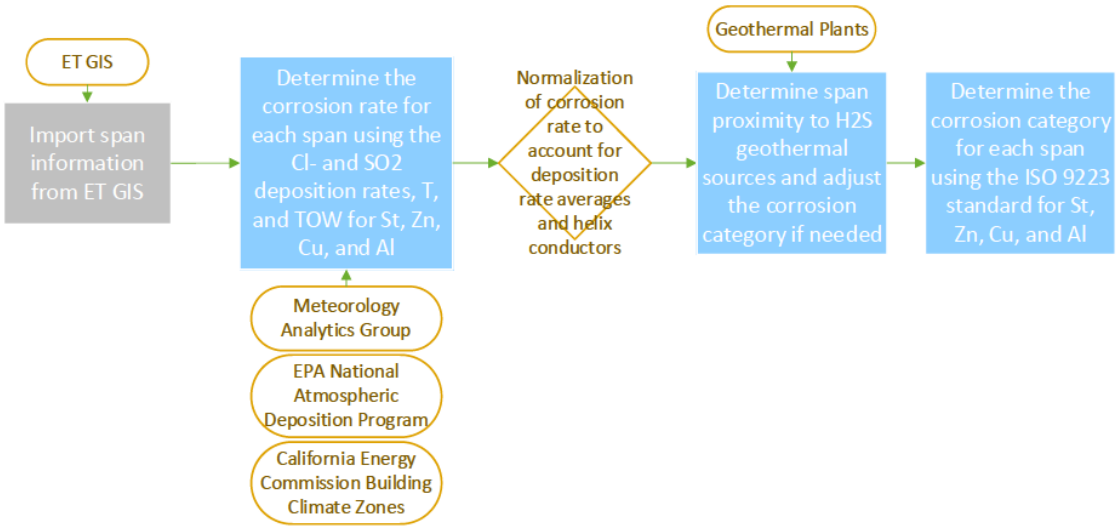

Figure 4.2 Full Corrosion Category Determination Process Flow for Conductors.

The additional step, represented by the diamond in Figure 4.2 was added because ISOCORRAG data show that helical sample geometries corrode more quickly than flat panels.[35] The standard notes that these sample geometries are "more effective at collecting the gaseous and particulate pollutants." For this reason, a helical corrosion factor was determined using the mean increase from the ISOCORRAG data set. These factors, reported in Table 4.1, were then used to adjust the calculated first year corrosion rate as shown in Equations 4.1:

$$r_{h,X} = h_X(r_{corr,X})$$

Equation 3.1

Where $r_{h,X}$ is the helical adjusted corrosion rate for a given metal 'X', h_X is the helical corrosion factor for a given metal 'X', and $r_{corr,X}$ is the previously calculated flat panel corrosion rate for metal 'X'.

35 Knotkova, D., Kreislova, K., Dean, S.W., "ISO CORRAG International Atmospheric Exposure Program: Summary of Results", ASTM Data Series 71. ASTM International, PA, USA, 2010.

METAL TYPE	HELICAL CORROSION FACTOR
Steel	1.51
Zinc	1.73
Aluminum	1.6
Copper	2.14

Table 4.1 Helical Corrosion Factors for Conductor Wire Metals

The helical adjusted corrosion rates for each span were compared with the corrosion rates in Figure 1.3 to determine an interim corrosion category. Note that while the helical acceleration should increase with decreasing wire diameter size, wire diameter size was excluded from the ISOCORRAG study. Thus, the current AAC model excludes this variable as well. To better characterize this effect additional laboratory testing would be required.

4.3 Calculating Material Loss due to Atmospheric Corrosion

Once the corrosion categories are determined for each span, the conductor specifications are evaluated to determine the extent of material loss. The expanded process flow for this portion of the conductor AAC model is presented in Figure 4.3. First the conductor type is determined from the imported ET GIS information. Based on the corrosion category, conductor type, and span age the model computes the expected material loss due to atmospheric corrosion.

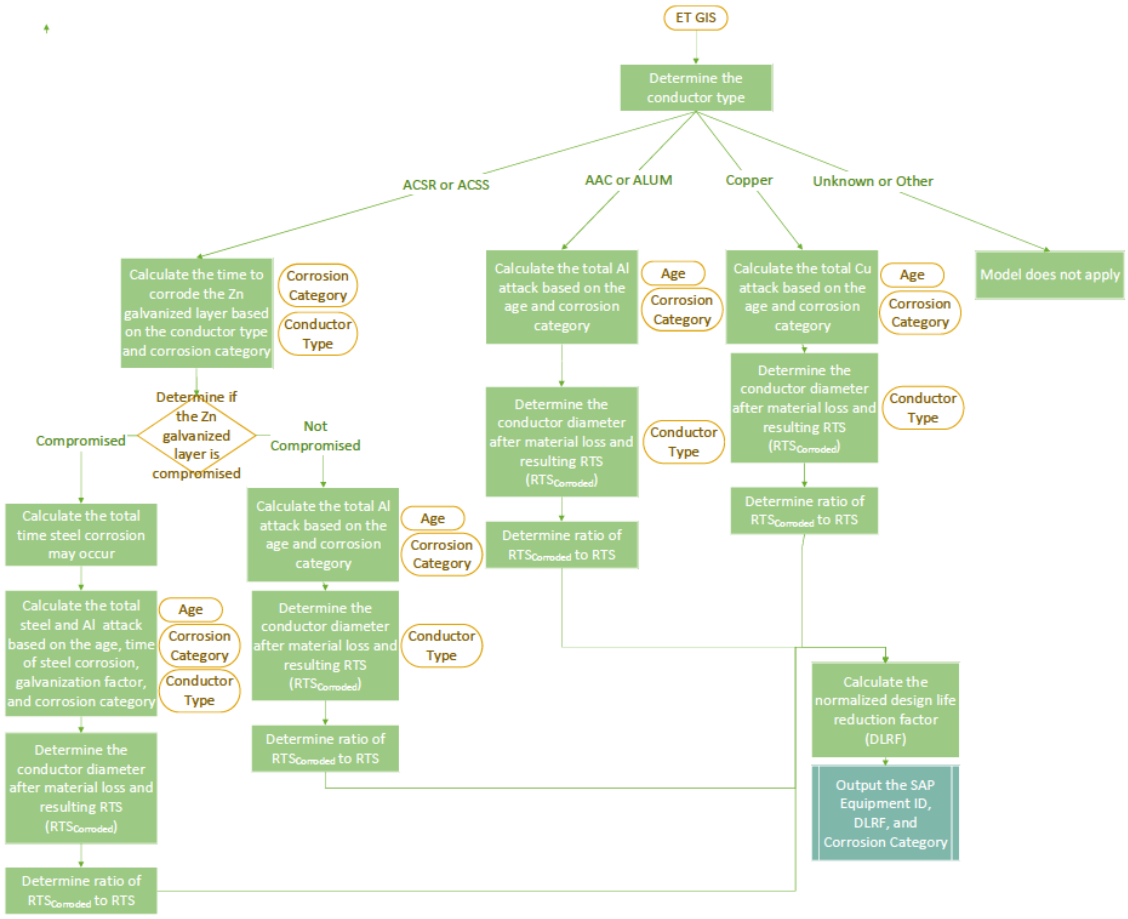

Figure 4.3 Process flow for calculating material loss due to corrosion for conductor spans.

For the case of aluminum and copper conductors, the process for calculating the total metal attack is straightforward and proceeds as outlined in Section 1.5. However, ACSR and ACSS conductors are susceptible to galvanic attack, an additional corrosion process that increases their rate of mass loss. Figure 4.4 presents a plot of conductor strength (a function of mass loss) over time for two ACSR conductors of different sizes. As shown in Figure 4.4, after the zinc galvanizing layer is compromised, the conductor strength drops off very quickly due to the onset of galvanic corrosion.

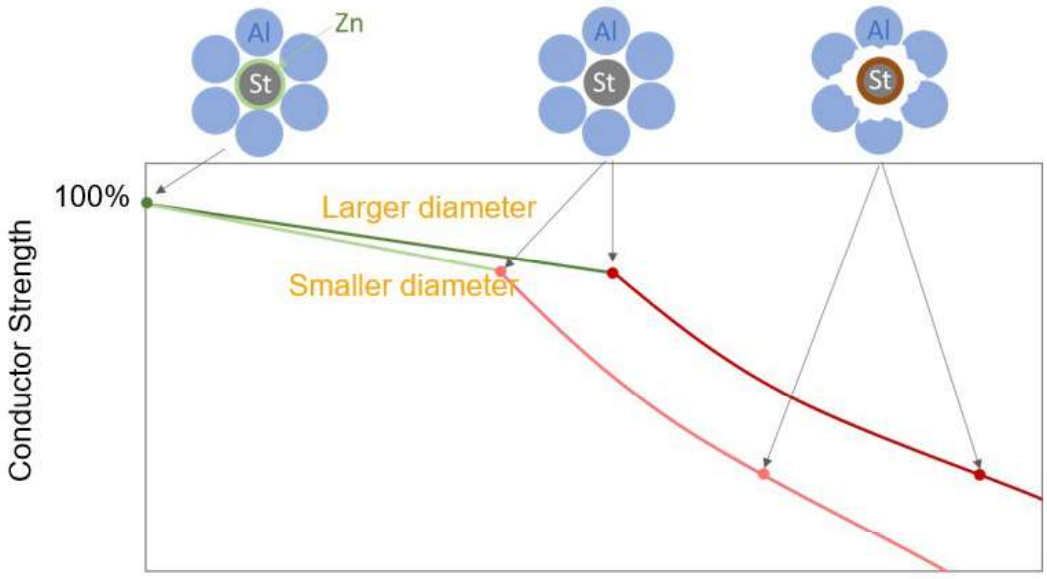

Figure 4.4 ACSR conductor strength as a function of time due to atmospheric corrosion and galvanic attack. The onset of galvanic attack leads to a significant decrease in conductor strength.

Thus, to determine the material loss for ACSR and ACSS spans, it is first necessary to determine whether the zinc galvanizing layer has been compromised. This can be done by determining the time to compromise the zinc layer using the corrosion category, zinc galvanizing layer thickness (ranging from 30.00 – 42.76 μm dependent on conductor size), and conductor age consistent with the process in Section 1.5. If the zinc galvanizing layer *has not* been compromised, which the model defines to be completely gone, the total aluminum loss is calculated using the process outlined in Section 1.5 as well. However, if the zinc layer *has* been compromised, the model calculates the total time steel corrosion may have occurred, relying on the span age and time to compromise the zinc to determine this value. From there the model calculates the total material loss by calculating the steel loss and aluminum loss relying on the span age, time the steel was susceptible to corrosion, corrosion category, and galvanization factor.

To determine the galvanization factor, first, data from the National Research Council of Canada were used to model the increase in corrosion rate with the onset of galvanic corrosion.[36] Neglecting an outlier site and a site whose SO_2 levels exceed that of the ISO standard, aluminum corrodes approximately four times faster when it is in a 1:1 area ratio bimetallic couple with carbon steel than by itself. Next the model considers the geometry of the wire itself to determine the overall mass loss acceleration factor. Figure 4.5 presents the two aluminum corrosion zones on a simple 6/1 stranded ACSR conductor. At the outer diameter, where the aluminum is only in contact with itself and the atmosphere, the corrosion rate remains the same, represented here by the light orange circle. However, at the inner diameter, where the aluminum wires are in contact

[36] Gibbons, E.V., "Corrosion Behavior of the Major Architectural and Structural Metals in Canadian Atmospheres: Summary of Ten-Year Results of Group 1,"

with the steel, their corrosion rate increases by approximately fourfold, represented schematically by the dark orange circle. Thus, the overall corrosion rate of the aluminum has increased by 5x radially as compared to its initial rate. Using this basic procedure, a galvanic acceleration factor was determined for each of the ACSR and ACSS wire geometries.

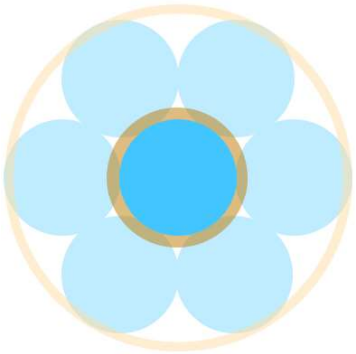

Figure 4.5 Schematic representation of two different corrosion zones on a 6/1 stranded ACSR conductor. Where the light blue aluminum wires contact the dark blue steel wire, they experience a fourfold increase in their corrosion rate (dark orange circle) over the atmospheric rate (light orange circle) they continue to experience where they are exposed to the atmosphere. This results in a fivefold increase radially at the onset of galvanic corrosion.

Although the model assumes a single b_2 value for steel across all ACSR and ACSS conductors, the composition of steels used in overhead conductors is not always identical.[37] Figure 4.6 presents the range of ASTM B498/B498M-19 compliant steel alloys that may be used. Using the procedure outlined in Section 2.3.1, the b_2 values for these alloys are found to be slightly less than the ISO 9224 carbon steel value (0.575) used by the model. Thus, this approximation should provide a conservative estimate in all cases.

Element	Composition, %
Carbon	0.50 to 0.88
Manganese	0.50 to 1.10
Phosphorus, max	0.035
Sulfur, max	0.045
Silicon	0.10 to 0.35

Figure 4.6 Compositions of acceptable steel alloys for zinc coated steel core wires for use in overhead conductors from ASTM B498/B498M-19.

[37] ASTM International. (2019) B498/B498M-19 Standard Specification for Zinc-Coated (Galvanized) Steel Core Wires for Use in Overhead Electrical Conductors.

4.4 Determining Critical Strength Factor and Design Life Reduction Factor

To calculate the DLRF, in each implementation, the model calculates a Figure of Merit. Unlike in the other implementations, the conductor model uses a critical strength factor as its figure of merit. To calculate the critical strength factor, the model converts the mass loss into a reduction in the wire diameter. This reduced wire diameter is described as $d_{corroded}$ shown schematically in Figure 4.7.

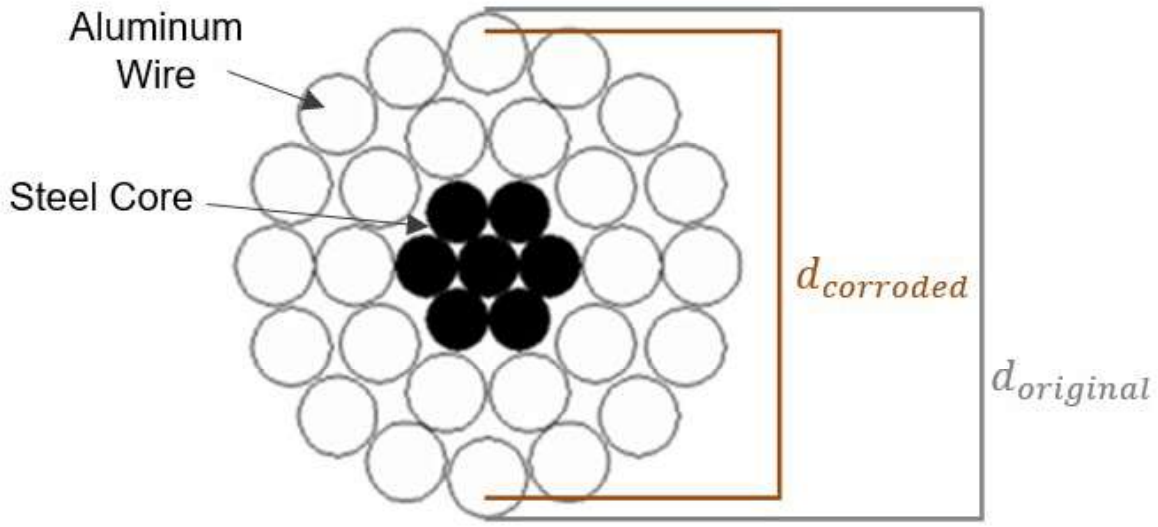

Figure 4.7 Change in wire diameter due to corrosion.

The span's tensile breaking load, $P_{corroded}$, at any given time can be calculated from Equation 4.2

$$P_{corroded} = \sigma_{UTS}(a_{corroded})$$
$$a_{corroded} = \pi\left(\frac{d_{corroded}}{2}\right)^2 \qquad \textbf{Equation 4.2}$$

Where $P_{corroded}$ is the force required to break the wire after a given time, σ_{UTS} is the ultimate tensile stress of the material (a material constant), $a_{corroded}$ is the wire's cross-sectional area at that time. The rated tensile loads (P_{rated}) for different wires and bundles are provided by their manufacturers. Using these values, the model computes the critical strength factor using Equation 4.3.

$$Critical\ Strength\ Factor = \frac{P_{corroded}}{P_{rated}}$$ ***Equation 4.3***

From there, the model uses the critical strength loss to assign a DLRF. Table 4.2 shows that three possible DLRF values are assigned based on the calculated critical strength loss. As with the implementation for steel structures, the maximum DLRF is 0.33 while the minimum is 0. These values are meant to be used as guidelines, with the goal of indicating low, medium, and high corrosion risk. To move from a qualitative high / medium / low assessment to a quantifiable metric, additional laboratory and environmental studies would be required to normalize the model. However, as the overarching goal of the AAC is to stratify corrosion risk across PG&E's ET assets, the final DLRF assignment in this implementation delineates the highest and moderate risk spans from lower risk assets.

CRITICAL STRENGTH FACTOR	DLRF
1.0 – 0.7	0
0.69 – 0.3	0.16
0.29 - 0	0.33

Table 4.2 Design Life Reduction Factor assignments for different calculated Critical Strength Factor values.

4.5 Splices

Conductor splices are used to join two conductors together such that mechanical and electrical integrity is maintained between the two conductors. Of the two main types of splices, compression and automatic, compression splices are now more frequently used for electrical transmission because automatic splices can be prone to improper installation. A compression splice consists of a thick metallic sleeve that is hydraulically tightened and deformed around the conductor ends. To avoid material incompatibility, the splice material should match the conductor material (i.e., aluminum splices should be used on aluminum conductors). In the case of ACSR conductors, splices employ two sleeves: an inner steel sleeve connecting the central steel stranding and an outer aluminum sleeve connecting the aluminum stranding. Based on a review of available failure data and SME input, in-service failures at splices occur for a variety of reasons including annealing of the strands due to overheating (i.e., poor electrical connection), fatigue failure, and tensile creep failure. However, as splices must be at least as new as the conductor that they are applied to (likely even newer), the AAC predicts that the conductor will always fail more quickly than the splice due to corrosion. Therefore, the AAC model does not calculate the corrosion of the splice explicitly, given that it not likely to be the limiting condition or failure mode. Rather, the model considers the effect of the splice on the surrounding

conductor. Specifically, moisture is expected to accumulate and concentrate in the areas adjacent to the splice on the conductor. To account for this, the conductor model doubles the TOW for spans with known splices. This adjustment assumes that crevices and spaces around the spliced segment will trap moisture far more than the bare conductor, resulting in locally-enhanced corrosion rates. Note that the splice adjustment is capped at 8760 h (i.e., one year) for any span with an original TOW $\geq$ 4380 h. Due to splice installation record limitations, the model currently applies this factor over the entire life of the conductor. If additional data becomes available, this methodology may be refined. Note also that additional failure modes of splices are treated elsewhere in the TCM.

4.6 Example Conductor Calculation

An example structure is presented in the following section to demonstrate the AAC conductor implementation calculations. A span with SAP Equipment ID 43701329 is used for this example. This span is an ACSR_2_6/1 type conductor that was installed in 1998. The location of the asset is shown below in Figure 4.8; it is ~ 95 km from the nearest plant in the Geysers. Referencing the EPA National Atmospheric Deposition Program, the SO_2 and Cl^- deposition rates at that location are 0.13 mg/m^2/day and 0.10 mg/m^2/day, respectively. This location is within Zone 11 of the California Energy Commission Building Climate Zone. Within Zone 11, the annual average temperature is 17.8 °C. The TOW at this location is 1677 hours.

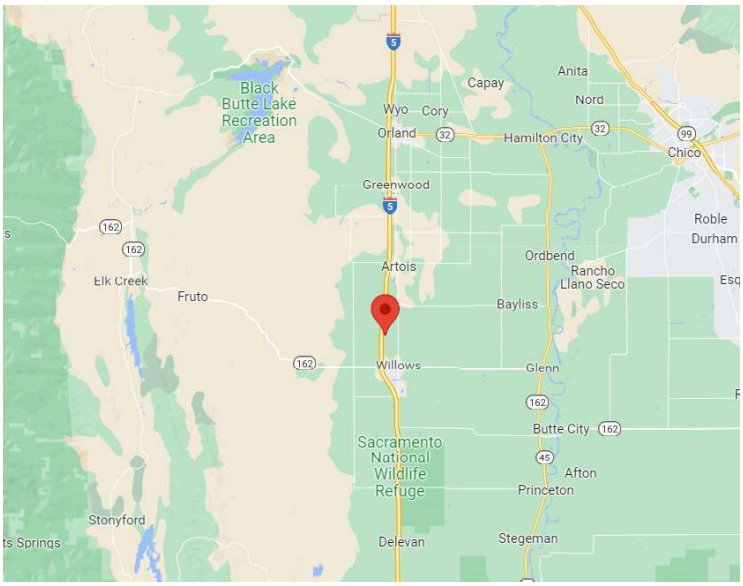

Figure 4.8 Location of span 43701329.

Using the equations from Sections 1.3 and 1.4, we calculate the non-normalized corrosion rates for steel, zinc, copper, and aluminum.

For carbon steel:

$$r_{corr\,St} = (0.085 \times 0.13^{0.56})(1677^{0.53})e^{f_{St}} + (0.24 \times 0.10^{0.47})(1677^{0.25})e^{0.049 \times 17.8} = 1.94\ \mu m/year$$
$$f_{St} = -0.087(17.8 - 10)$$

For zinc:

$$r_{corr\,Zn} = (0.0053 \times 0.13^{0.43})(1677^{0.53})e^{f_{Zn}} + (0.00071 \times 0.10^{0.68})(1677^{0.3})e^{0.11 \times 17.8} = 0.10\ \mu m/year$$
$$f_{Zn} = -0.032(17.8 - 10)$$

For aluminum:

$$r_{corr\,Al} = (0.00068 \times 0.13^{0.87})(1677^{0.38})e^{f_{Al}} + (0.00098 \times 0.10^{0.49})(1677^{0.38})e^{0.057 \times 17.8} = 0.02\ \mu m/year$$
$$f_{Al} = -0.031(17.8 - 10)$$

The corrosion rates were normalized to experimental data using the following equation:

$$r_{corr\_adj,X} = 3.91 \times 2.41 \times r_{corr,X}$$

$$r_{corr\_adj,St} = 18.26\ \mu m/year$$

$$r_{corr\_adj,Zn} = 0.91\ \mu m/year$$

$$r_{corr\_adj,Al} = 0.15\ \mu m/year$$

Using Table 4.1, we find that the helical factors are 1.51 (steel), 1.73 (zinc), and 1.6 (aluminum). Inserting these values into Equation 4.1,

$$r_{h,X} = h_X(r_{corr,X})$$

we find that the helical rates are:

$$r_{h,St} = 27.57\ \mu m/year$$

$$r_{h,Zn} = 1.58\ \mu m/year$$

$$r_{h,Al} = 0.33\ \mu m/year$$

Comparing the calculated adjusted corrosion rates to Figure 1.3 and confirming that the nearest plant at The Geysers is $\geq$ 10 km, the corrosion categories for steel, zinc, and aluminum are all determined to be C3.

If the zinc galvanizing layers in an ACSR conductors are compromised, the aluminum strands are subject to galvanic attack. Thus, we must first check whether the zinc layer has been compromised. ACSR_2_6/1 type conductors have a zinc layer thickness of 34.21 µm.

Setting 34.21 µm to D from Equation 1.7 and solving for t yields the time required to compromise the zinc, t_{comp}. The values of b_2 are available in Table 1.1.

$$34.21 = r_{C3,Zn}\left[20^{b_2} + b_2(20^{b_2-1})\left(t_{comp} - 20\right)\right]$$

$$t_{comp} = 24.4\ years$$

As the structure is currently 24 years old, the zinc is not yet entirely removed, so the aluminum is not subject to galvanic attack at this time. Again taking Equation 1.7, but this time solving for aluminum loss, using the current span age ($t = 24$) we find that $D_{Al}(t = 24) = 9.64\ \mu m$. Next, solving for the total zinc loss at the current span age, we find that $D_{Zn}(t = 24) = 33.72\ \mu m$.

To calculate the critical strength factor, we next calculate the reduction in diameter of the wire, subtracting the two values we calculated in the prior step from the original diameter (8026.4 µm) to get the current wire diameter, $d_{corroded}$, which is 7983.04 µm. As σ_{UTS} is a materials constant, Equation 4.3 simplifies to a ratio of the corroded cross-sectional area to the original cross-sectional area:

$$CSF = \frac{\pi(\frac{7983.04}{2})^2}{\pi(\frac{8026.4}{2})^2} = .99$$

Using Table 4.2, we assign a final DLRF of 0 for this span.

Section 5: Above Grade Hardware Corrosion

The AAC model implementation described in this section is intended specifically for above-grade, load bearing hardware components along PG&E electric transmission lines. As such, it considers specific factors relevant to above grade hardware such variable component parameters (e.g., size, composition, and age) and the possibility of failure occurring at either the "Hot-End" (energized hardware) or "Cold-End" (non-energized hardware). Table 5.1 presents an overview of the components that the AAC model considers for this analysis.

Cold-End Hardware	Hot-End Hardware	Guy system
Anchor Shackle	Power-actuated connectors	EHS Steel Guys
Ball Hook	U-bolt type parallel groove clamp	Preformed grips
Oval-eye ball, and similar	Corona ring	Alumoweld Guys
Mounting Brackets	Hold-down shackle	
Mounting Bases	Socket Y-clevis	
Clamp Adaptor	Socket-ball	
Fasteners	Y-clevis eye	
Y-Clevis Ball	Yoke Plates	
U-bolt	Suspension clamp/Shoe clamp	
	Strain clamps	

Table 5.1 Hardware components considered in the current iteration of the AAC model.

5.1 Above Grade Hardware Corrosion Overview

An overview of the AAC model process for above grade hardware is shown in Figure 5.1. The process starts by collecting structure information from ET GIS to understand the asset identifying number, age, and location. Using the location of the structure, the potential for atmospheric corrosion is determined using the annual average temperature, Time of Wetness (TOW), deposition rates of SO_2 and Cl^-, and proximity to geothermal sources for steel, zinc, aluminum, and copper. Atmospheric corrosion estimates are quantified by determining the corrosion rate and corresponding corrosion category in accordance with the ISOCORRAG and

the ISO 9223 standard.[38,39] The model applies the standard atmospheric normalization discussed in Section 1.3. Using the ET GIS information, the model determines the operating voltage for the asset and uses that information to calculate the hardware figure of merit, time to 1/3 wall loss, for the smallest cold-end component, the smallest hot end components, and the smallest galvanic couple. The DLRF is then assigned as discussed in Section 1.6. Cold-end components are typically only galvanized steel or cast iron, while hot-end components can also be copper or aluminum (e.g., suspension shoes and power-actuated connectors). A list of assets with the corrosion category and DLRF are the final AAC model output which are input to the TCM to adjust the dispersion of the fragility curves for each asset. Note that while corrosion on tie wires is not explicitly modeled since these components are not considered to be load bearing, a data "flag" is applied to alert the user when a tie-wire is present.

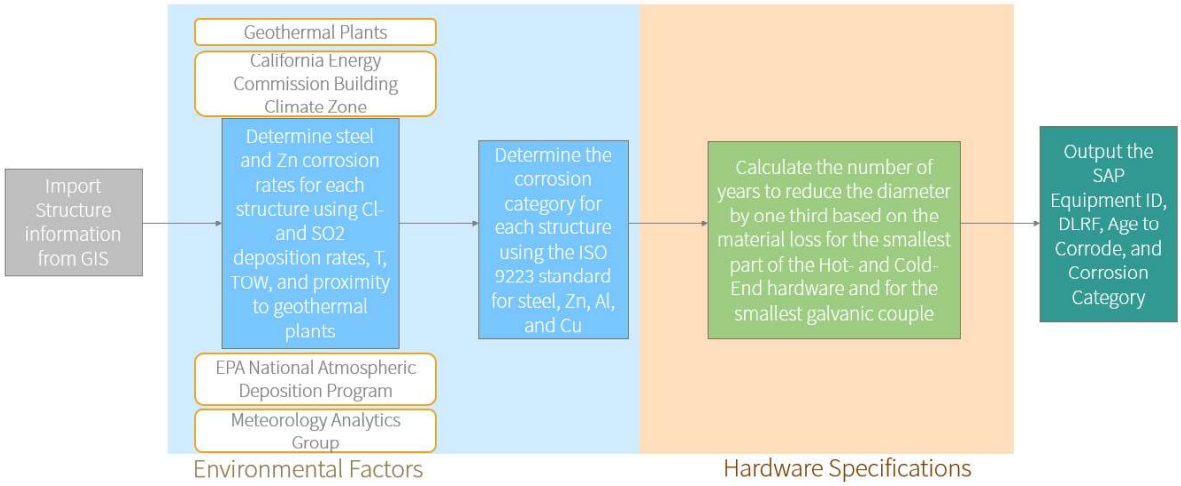

Figure 5.1 Overview of Process Flow of Above Grade Hardware AAC model

5.2 Calculating the corrosion category of the local environment

In general, the corrosion category assignment is done consistent with what was described previously in Section 1.3 Note that the helical rate adjustment discussed in Section 4.2 is also applicable to the guy wires. To accommodate this, two corrosion category assignment steps are performed in the hardware implementation for assets with guy wires: a flat plate corrosion category and a helical corrosion category. Although some guy systems utilize "Alumoweld" (aluminum-clad) steels, which exhibit improved levels of corrosion protection, explicit material

[38] Knotkova, D., Kreislova, K., Dean, S.W., "ISO CORRAG International Atmospheric Exposure Program: Summary of Results", ASTM Data Series 71. ASTM International, PA, USA, 2010.

[39] International Organization for Standards (ISO). (2012) 9223:2012 Corrosion of metals and alloys - Corrosivity of atmospheres - Classification, determination and estimation

data for guy systems is currently unavailable. Therefore, the model conservatively assumes all guy systems include galvanized steel wires, as these have the higher corrosion rates.

5.3 Calculating Material Loss due to Atmospheric Corrosion on Above Grade Hardware

To calculate the material loss for hardware, the model relies on ET GIS information to determine the asset's operating voltage, as this determines which specific hardware components should be present. After determining the operating voltage, the model identifies the thinnest critical dimensions on load bearing components. This process flow is shown schematically in Figure 5.2. As corrosion rates and categories often vary between different materials, the model calculates the material loss for the thinnest component of each metal. Note that to provide a more granular analysis of risk across the various groups of hardware, the hot-end and cold-end components are treated separately. Additionally, to provide an improved understanding of the possible risk associated with galvanic corrosion on aluminum components in contact with steel components, the thinnest galvanic couple is also treated independently. Galvanic couples are limited to the hot-end of the hardware linkage. Table 5.2 presents the components of interest for each operating voltage (or voltage group) considered and their critical dimensions.

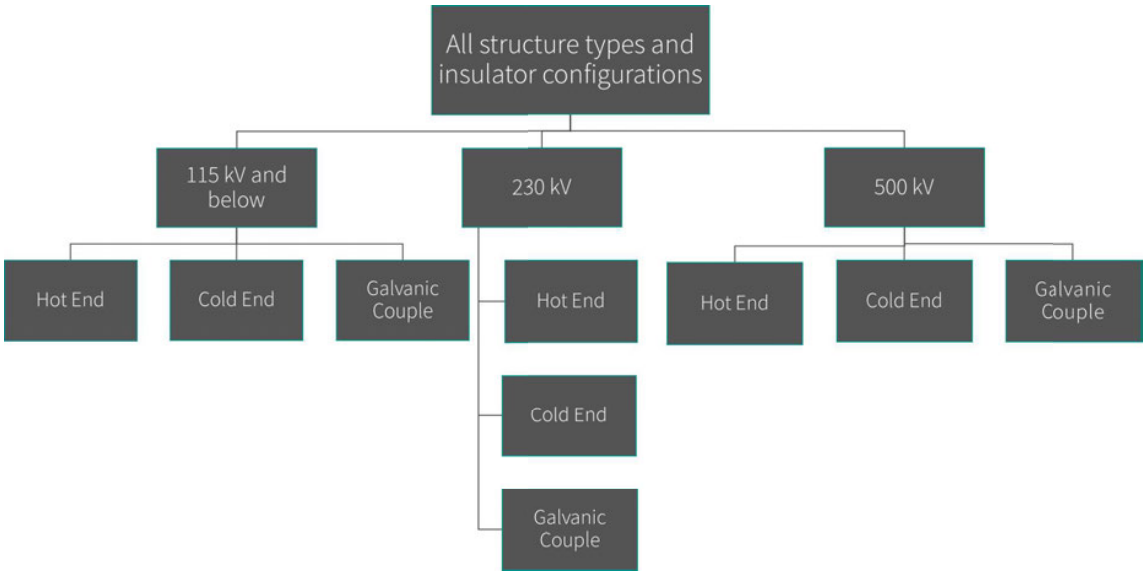

Figure 5.2 Process flow for identifying above grade hardware critical dimensions.

	115 kV and Below	230 kV towers	500 kV Towers
Cold End	Mounting Brackets (galvanized steel or galv. ductile Iron) critical thickness: 3/8"	Anhor Shackle (25 kip) (galvanized steel) critical thickness: 0.5"	Ball oval eye Class 52-8/52-11 (galvanized steel) critical thickness: 11/16"
Hot End	U Bolts on Clamps (galvanized steel) critical thickness: 0.5"	U Bolts on Clamps (galvanized steel) critical thickness: 0.5"	U Bolts on Clamps (galvanized steel) critical thickness: 0.5"
	Power-Actuated Connector (aluminum alloy) critical thickness: 0.25"	Power-Actuated Connector (aluminum alloy) critical thickness: 0.25"	Clamp Body (aluminum alloy) critical thickness: 0.5"
	Power-Actuated Connector (copper alloy) critical thickness: 0.2"	Power-Actuated Connector (copper alloy) critical thickness: 0.2"	N/A
Galvanic Couple	Clamp Body (galvanized steel) critical thickness: 0.5"	U Bolts on Clamps (galvanized steel) critical thickness: 0.5"	U Bolts on Clamps (galvanized steel) critical thickness: 0.5"
	Clamp Body (aluminum alloy) critical thickness: 0.5"	Clamp Body (aluminum alloy) critical thickness: 0.5"	Clamp Body (aluminum alloy) critical thickness: 0.5"

Table 5.2 Above grade hardware components of interest and their critical thicknesses.

To identify the components of interest and their critical thicknesses (Table 5.2), PG&E standards were used to identify technical specifications and drawings for components in Table 5.1. In many cases, the critical thicknesses for the components were directly reported in the technical specifications. However, in some cases, the critical thicknesses were not explicitly stated. In those cases, the critical dimension was estimated by image analysis on the technical drawings. Figure 5.3 presents an example of an aluminum connector, of the type used in hot-end assemblies on 230 kV towers and 115kV towers and below, whose critical dimension was estimated to be approximately 0.25” using the software image analysis program ImageJ.

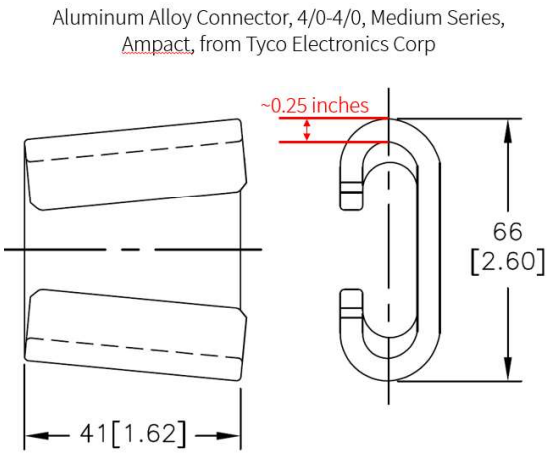

Figure 5.3 Estimate of critical thickness (0.25”) on an aluminum power actuated connector from scale drawing.

Asset-level data on guy wire sizes was also unavailable. Additionally, unlike the other hardware components, guy wire sizes can vary within a single operating voltage. Thus, the model assumes the smallest guy wire critical thickness currently in use on ET: 7/32 inches.

The time to 1/3 wall loss is then calculated for each of the components of interest according to the process outlined in Sections 1.5 and 1.6 except for the galvanic couples. In the hardware implementation, the thinnest galvanic couple always occurs between the same two components: the shoe clamps (aluminum) and their U-bolts (galvanized steel). Because the shoe clamp has a relatively large area compared to the galvanized steel bolt, there may initially be some increase in the corrosion rate of the zinc; however, laboratory analysis would be required to assess this increase. As such, the current model implementation assumes the increase is negligible. However, once the zinc layer has corroded away, the steel-aluminum couple will result in an increased corrosion rate for aluminum. The model considers two factors to quantify this: (1) the potential difference due to the galvanic series, and (2) the sample geometry. As discussed previously, the aluminum corrosion rate will increase by approximately four-fold when steel and aluminum are in a bimetallic couple with a 1:1 area ratio due to the potential difference. However, because the area of the aluminum is significantly larger than that of the steel in this case, the geometric factor should reduce the overall rate acceleration. Therefore, the model currently assumes the galvanic acceleration to be two-fold for the shoe clamp / U-bolt couple. Additional laboratory study would be required to refine this assumption. For additional information on galvanic corrosion, see Section 4.3.

5.4 Calculating Design Life Reduction Factor

To calculate the design life reduction factor for hardware, the model relies on the calculation outlined in Section 1.6. For above grade hardware, the model currently assumes the structure's notional design life of 150 years. As more nuanced information regarding the design life of individual components becomes available, the model may be modified to better reflect those values. The model chooses the shortest time to 1/3 wall loss from the five cases considered in the previous section for DLRF determination.

5.5 Example Above Grade Hardware Calculations

5.5.1 60kV Wood Pole Above Grade Hardware without a Guy System

An example structure is presented in the following section to demonstrate the AAC model above-grade hardware implementation calculations. A structure with SAP Equipment number of 40619424 is used for this example. For sake of argument, we initially assume that this asset does not have a guy system. Section 5.5.2 will treat the guy wires. This asset is a 60 kV wood pole that was installed in 2011. The location of the asset is shown below in Figure 5.4; it is ~ 240 km from the nearest plant in the Geysers. Referencing the EPA National Atmospheric Deposition Program, the SO_2 and Cl^- deposition rates at that location are 0.26 mg/m^2/day and 3.52 mg/m^2/day, respectively. This location is within Zone 1 of the California Energy Commission Building Climate Zone. Within Zone 1, the annual average temperature is 11.7 °C. The TOW at this location is 4657 hours.

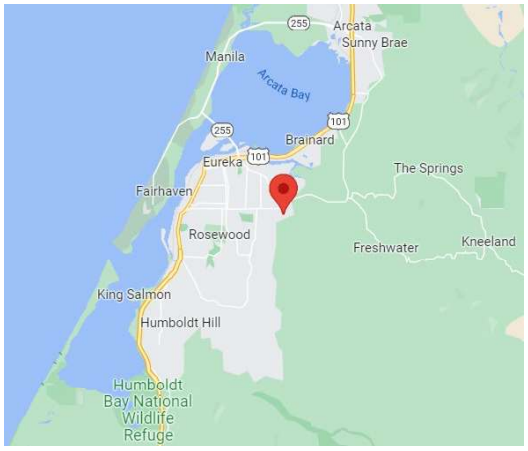

Figure 5.4 Location of Asset 40619424.

Using the equations from Sections 1.3 and 1.4, we calculate the non-normalized corrosion rates for steel, zinc, copper, and aluminum.

For carbon steel:

$$r_{corr\,St} = (0.085 \times 0.26^{0.56})(4657^{0.53})e^{f_{St}} + (0.24 \times 3.52^{0.47})(4657^{0.25})e^{0.049 \times 11.7} = 9.15\ \mu m/year$$
$$f_{St} = -0.087(11.7 - 10)$$

For zinc:

$$r_{corr\,Zn} = (0.0053 \times 0.26^{0.43})(4657^{0.53})e^{f_{Zn}} + (0.00071 \times 3.52^{0.68})(4657^{0.3})e^{0.11 \times 11.7} = 0.31\ \mu m/year$$
$$f_{Zn} = -0.032(11.7 - 10)$$

For copper:

$$r_{corr,Cu} = (0.00013 \times 0.26^{0.55})(4657^{0.84})e^{f_{Cu}} + (0.0024 \times 3.52^{0.31})(4657^{0.57})e^{0.03 \times 11.7} = 0.69\ \mu m/year$$
$$f_{Cu} = -0.029(11.7 - 10)$$

For aluminum:

$$r_{corr\,Al} = (0.00068 \times 0.26^{0.87})(4657^{0.38})e^{f_{Al}} + (0.00098 \times 3.52^{0.49})(4657^{0.38})e^{0.057 \times 11.7} = 0.09\ \mu m/year$$
$$f_{Al} = -0.031(11.7 - 10)$$

The corrosion rates were normalized to experimental data using the following equation:

$$r_{corr\_adj,X} = 3.91 \times 2.41 \times r_{corr,X}$$

$$r_{corr\_adj,St} = 86.22\ \mu m/year$$

$$r_{corr\_adj,Zn} = 2.91\ \mu m/year$$

$$r_{corr\_adj,Cu} = 6.46\ \mu m/year$$

$$r_{corr\_adj,Al} = 0.87\ \mu m/year$$

Comparing the calculated adjusted corrosion rates to Figure 1.3 and confirming that the nearest plant at The Geysers is ≥ 10 km, the corrosion categories are determined to be C5 for steel, C4 for zinc, C6 for copper, and C3 for aluminum.

As this structure is a 60 kV wood pole, the critical dimensions (from Table 5.2) are as follows:

- Cold-End
  - 3/8" galvanized steel
- Hot-End
  - 0.5" galvanized steel
  - 0.25" aluminum
  - 0.2" copper
- Galvanic Couple

  - 0.5” galvanized steel
  - 0.5” aluminum

Thus, for these components 1/3 wall loss is:

- Cold-End
  - 75 µm of zinc and 3100 µm of carbon steel (1/8” total)
- Hot-End
  - 75 µm of zinc and 4158 µm of carbon steel (1/6” total)
  - 2117 µm of aluminum (1/12”)
  - 1693 µm of copper (1/15”)
- Galvanic Couple
  - 75 µm of zinc and 4158 µm of carbon steel (1/6” total)
  - 4233 µm of aluminum (1/6”)

Setting the 1/3 wall losses to (D) from Equation 1.7 and solving for t yields the time to 1/3 wall loss for each component.

$$D(t > 20) = r_{cc,X}[20^{b_2} + b_2(20^{b_2-1})(t - 20)]$$

The values of b_2 are available in Table 1.1. Note that for galvanized steel components, the time to corrode the zinc and the time to corrode the remaining carbon steel must be solved for separately and then added together.

Thus, the time to 1/3 loss for each component above is found to be:

- Cold-End
  - Steel: $t_{atm\_corr} = 27 + 82 = 109\ years$
- Hot-End
  - Steel: $t_{atm\_corr} = 27 + 114 = 141\ years$
  - Aluminum: $t_{atm\_corr} = 6314\ years$
  - Copper: $t_{atm\_corr} = 522\ years$
- Galvanic Couple
  - Steel: $t_{atm\_corr} = 27 + 114 = 141\ years$
  - Aluminum: $t_{atm+galv\_corr} = 6287\ years$

To calculate the DLRF, the shortest time is chosen (109 years) and the DLRF is calculated for the structure.

$$atm\_corr_{DLRF} = 1 - \frac{109}{150} = 0.276$$

5.5.2 60kV Wood Pole Above Grade Hardware with a Guy System

Taking the same structure as before, the calculations through the experimental normalization step are identical. However, to assign corrosion categories for the guy wires, we must also perform the helical normalization described in Section 4.2. Using Table 4.1 we find that the helical factors are 1.51 and 1.73 for steel and zinc, respectively. Inserting these values and the previously calculated rates from Section 5.5.1 in Equation 4.1,

$$r_{h,X} = h_X(r_{corr,X})$$

we find that the helical rates are:

$r_{h,St} = 130.19\ \mu m/year$

$r_{h,Zn} = 5.03\ \mu m/year$

As we have already confirmed that this structure is far from The Geysers, comparing these values to those in Figure 1.3 yields the same corrosion category for steel (C5) but an increase in the corrosion category for zinc from C4 (flat panel) to C5 (helical). For guy wires, we assume a critical dimension of 7/32" (including our galvanizing layer thickness of 30 µm). Thus, 1/3 wall loss will be 30 µm of zinc and 1822 µm of carbon steel. Solving time using Equation 1.7, we find that for the guy wires:

$$t_{atm\_corr} = 4.3 + 65.7 = 70\ years$$

Comparing this to the previously calculated times to 1/3 wall loss, we find that guy wires are the shortest lifetime component. Using Equation 1.8, we find that

$$atm\_corr_{DLRF} = 1 - \frac{70}{150} = 0.536$$

Any calculated $atm\_corr_{DLRF} > 0.33$ is set to 0.33, thus the final Hardware DLRF for this structure is 0.33.

Limitations

The model described herein necessarily relies on simplifying engineering assumptions and idealized representations of complex engineering systems, threats and loads. The implications and limitations of these modeling decisions have been discussed and accepted by PG&E Subject Matter Experts. While we have made every effort to accurately capture key factors related to atmospheric corrosion that could adversely affect PG&E's transmission structures based on available information, this model is expected to be further refined as new idealizations, methods and/or data become available. Proper application of this model requires recognition and understanding of the limitations of both the scope and methodology.

The model described herein is intended to be incorporated into a comprehensive PG&E framework (TCM Framework) that was developed to inform PG&E risk mitigation decisions. Neither the Framework nor this model is intended to predict specific failures, and the actual performance of some assets may be materially different from that anticipated by the model.

For limitations associated with the Framework, see Revision 1 of Exponent's "PG&E's Composite Risk Model for Overhead Electric Transmission Components: A White Paper," dated March 31, 2022.

DRAFT: 31 March 2022, Revision 1

Appendix E

Underground Corrosion Models

Exponent®

EXTERNAL MEMORANDUM

TO:	[redacted] (PG&E)
FROM:	Exponent
DATE:	March 31, 2022
PROJECT:	Transmission Composite Model
SUBJECT:	Below-Grade Corrosion Model

Exponent has developed a below-grade corrosion model (BGC model) that incorporates environmental data and corrosion analysis to help evaluate and predict electric transmission line asset health, as a part of the larger Transmission Composite Model (TCM). The purpose of this memorandum is to provide a summary of the technical bases underpinning the BGC model and describe its implementation.

Motivation for BGC Model Implementation in the TCM

The TCM provides a risk-based framework for evaluating the health of transmission line assets subject to various hazards. The tool uses a variety of data to evaluate the current remaining strength of an asset (a tower or pole structure, plus the equipment it supports) relative to the strength of a new pristine asset. These data are used to adjust the median strength of an asset and/or the uncertainty (dispersion) associated with the asset strength, resulting in an estimate of the probability of failure at a given wind speed in the form of an asset-specific fragility curve.[1]

Adjustment of the dispersion in strength for an asset within the TCM is based primarily on its age relative to its design life. The design life of an asset is a function of its notional design life in a benign environment, currently set at 150 years for most component groupings, and the aggressiveness of the environment with respect to degradation mechanisms such as decay, corrosion, fatigue, and wear. Assets exposed to more aggressive environments are assigned greater "design life reduction factors" (DLRFs) than assets in more benign environments (e.g., the actual life of an asset in a highly corrosive environment will be significantly less than the notional design life of 150 years). For below-ground portions of steel structures, corrosion due to interactions with the surrounding soil is one of the primary degradation mechanisms resulting in a reduction in useful design life. Likewise, soil mediated corrosion is a key degradation

[1] For a more complete explanation of the OA model framework see Revision 1 of Exponent's "PG&E's Composite Risk Model for Overhead Electric Transmission Components: A White Paper."

mechanism for guy anchor systems. For this reason, the BGC model, and the TCM more broadly, represent a significant refinement to the original Operability Assessment tool fragility curves.

Technical Bases for BGC Model Development

Below-grade components of electric transmission towers are susceptible to corrosion due to the local underground environment. Many factors affect the extent of corrosive attack including: 1) soil properties, such as chemistry, texture, conductivity, and water content; 2) external factors, such as precipitation, soil drainage, and soil disruption/manipulation; and 3) structure properties, such as the structure age, alloy type, foundation type, coating types, and installed corrosion protection systems. The BGC model was developed to consider both the local environment and structure properties to better estimate the DLRF.

BGC Model Overview

An overview of the BGC model process is shown in Figure 1. Structure information from PG&E's Electric Transmission Geographic Information System (ETGIS) was collected to capture structure identifying numbers, ages, and locations. Using the location of each structure, the potential for soil corrosion of steel and concrete components was determined. The soil corrosivity was evaluated using the United States Department of Agriculture (USDA) Soil Survey Geographic Database (SSURGO) dataset. Inspection forms were used to determine the foundation type and foundation condition (when available) for each structure. The corrosivity, classified as high, moderate, or low, was determined for each structure based on the foundation type and condition, soil corrosivity, and structure age. A schematic showing how these factors were considered for each foundation type is shown in Figure 2. A more detailed discussion of this methodology is presented in later sections of this memorandum. This model currently applies to direct buried grillage, direct embedded, and concrete embedded foundations. Timber pile foundations or foundations located underwater are not considered in this model. Once the corrosivity was determined, the DLRF was assigned. A list of structures with the DLRF and soil corrosivity is the final BGC model output, which in turn serves as input to the TCM to adjust the dispersion of the fragility curve for each structure.

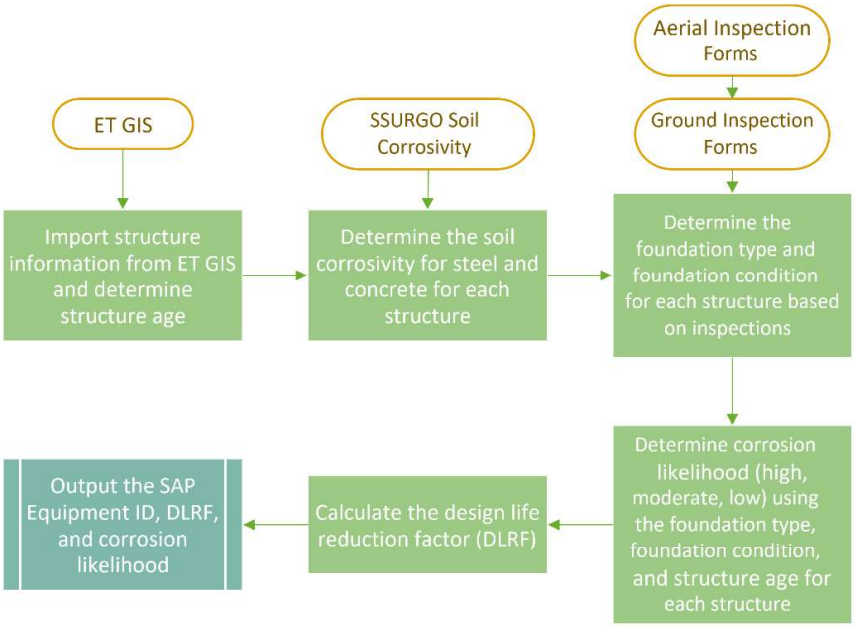

Figure 1 BGC Model process overview.

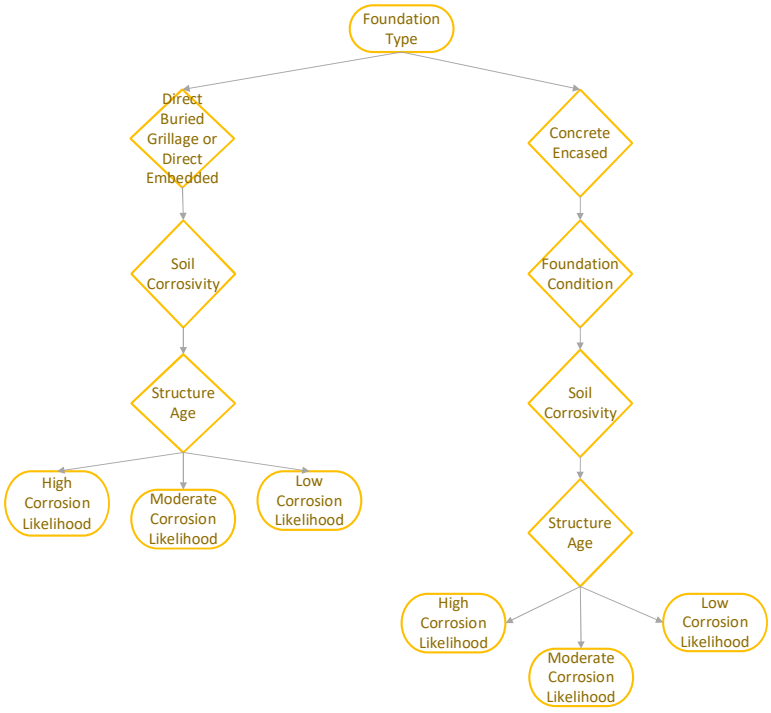

Figure 2 BGC model process overview for each foundation type.

Soil Corrosivity

Degradation of below-grade metal assets is mostly caused by corrosion due to the surrounding soils. Unlike atmospheric corrosion, where general regions have similar environments and therefore similar atmospheric corrosion likelihood, underground corrosivity is highly localized. Soil composition and properties can change drastically in relatively small regions, thereby causing large changes in the soil corrosivity. Additionally, seasonal changes (e.g., seasons with higher precipitation) and human use (e.g., farming or irrigation) can also have a large role in soil corrosivity changes.

Because soil testing data is not available across the entire PG&E electric transmission network at this time, the SSURGO database was used to characterize the soil corrosivity.[2] This database contains a detailed map of the state of California that characterizes a number of different soil parameters, two of which were used to identify the potential for soil corrosion in the BGC model: Corrosion – Concrete ('corcon'), and Corrosion – Uncoated Steel ('corsteel').

Corrosion – Concrete, and Corrosion – Uncoated Steel, are parameters that describe an interpretation rating of the propensity for concrete or uncoated steel to corrode when in contact with soil.[3] The likelihood of corrosion is expressed as low, moderate, or high for both parameters. The corrosivity of concrete is estimated in the SSURGO database based off Table 1, which takes into account the soil texture, pH, Na, Mg, sulfate, and NaCl concentrations.[4] SSURGO uses Table 2 to estimate the corrosivity for uncoated steel by characterizing soil texture, drainage class, acidity, and conductivity. Through the SSURGO database, maps of uncoated steel and concrete corrosivity are obtained for the state of California. The electric transmission steel structures are geospatially located on the maps and the corresponding steel and concrete corrosivity rankings are attributed to each asset. The resulting SSURGO maps of uncoated steel and concrete corrosivity are shown in Figure 3.

---

2 Additional information and documentation about this database can be found at the following website <https://www nrcs.usda.gov/wps/portal/nrcs/detail/soils/survey/geo/?cid=nrcs142p2_053627>

3 Additional details of the SSURGO database can be found at <https://www nrcs.usda.gov/wps/portal/nrcs/detail/soils/survey/geo/?cid=nrcs142p2_053631>

4 Muckel, G. "Understanding Soil Risk and Hazards" USDA, 2004 <https://www nrcs.usda.gov/Internet/FSE_DOCUMENTS/16/nrcs143_019308.pdf>

Guide for Estimating the Risk of Corrosion of Concrete [1]

Property	Limits		
	Low	Moderate	High
Texture and reaction	Sandy and organic soils with pH of >6.5 or medium and fine textured soils with pH of >6.0	Sandy and organic soils with pH of 5.5-6.5 or medium textured and fine textured soils with pH of 5.0 to 6.0	Sandy and organic soils with pH of <5.5 or medium textured and fine textured soils with pH of <5.0
Na and/or Mg sulfate (ppm) in soil	Less than 1,000	1,000 to 7,000	More than 7,000
NaCl (ppm) in soil	Less than 2,000	2,000 to 10,000	More than 10,000

[1] Based on data in "National Conservation Practice Standards," Standard 606, Subsurface Drain.

Table 1 USDA guide for estimating the risk of corrosion for concrete. (Obtained from Muckel, G. "Understanding Soil Risk and Hazards" USDA, 2004 https://www.nrcs.usda.gov/Internet/FSE_DOCUMENTS/16/nrcs143_019308.pdf)

Guide for Estimating the Risk of Corrosion of Uncoated Steel [1]

Property	Limits		
	Low	Moderate	High
Drainage class and texture	Excessively drained, coarse textured soils; well drained, coarse textured to medium textured soils; moderately well drained, coarse textured soils; or somewhat poorly drained, coarse textured soils	Well drained, moderately fine textured soils; moderately well drained, medium textured soils; somewhat poorly drained, moderately coarse textured soils; or very poorly drained soils with a stable high water table	Well drained, fine textured or stratified soils; moderately well drained, fine textured and moderately fine textured or stratified soils; somewhat poorly drained, medium textured to fine textured or stratified soils; or poorly drained soils with a fluctuating water table
Total acidity (meq/100g)	<8	8-12	≥12
Resistivity at saturation (ohm/cm)	≥5,000	2,000-5,000	<2,000
Conductivity of saturated extract (dSm^{-1})	<0.3	0.3-0.8	≥0.8

[1] Based on "Underground Corrosion," Circular 579, U.S. Department of Commerce, National Bureau of Standards.

Table 2 USDA guide for estimating the risk of corrosion for uncoated steel. (Obtained from Muckel, G. "Understanding Soil Risk and Hazards" USDA, 2004 https://www.nrcs.usda.gov/Internet/FSE_DOCUMENTS/16/nrcs143_019308.pdf)

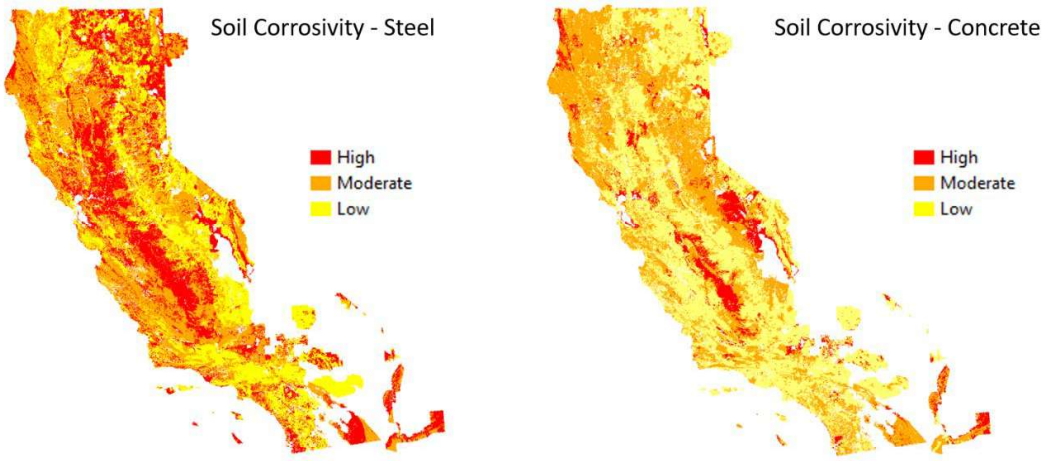

Figure 3 Soil corrosivity of steel and concrete showing high, moderate, and low corrosion risk, as taken from the SSURGO database.

Converting Corrosivity to DLRF

The BGC model outputs a high, moderate, or low corrosivity, which is then converted into a DLRF. Table 3 shows the conversion of corrosivity to DLRF.

Table 3 Conversion of corrosivity (output of the BGC model) to DLRF (used in the TCM).

Corrosion Likelihood	DLRF
High	0.33
Moderate	0.16
Low	0

Direct-Buried Foundations

The process for calculating the corrosion likelihood and DLRF for direct buried grillage or direct embedded foundations is shown in Figure 4. The model starts by determining if the foundation type is direct-buried grillage or direct embedded, as shown in Step 1 in Figure 4. For both foundation types, the steel grillage or steel member is assumed to be in direct contact with the surrounding soil. Based on SME input, foundations are also assumed to have no cathodic protection systems installed.[5] Due to these assumptions, the primary drivers for below-grade corrosion for direct buried structures are the soil corrosivity for steel, and the structure age.

[5] Based on discussions with PG&E SMEs. Some cathodic protection (CP) systems were known to be installed on a few structures; however, no CP system maintenance plans are known. Due to the low number of structures with potential CP systems and the lack of maintenance, the assumption was made that structures did not have CP systems installed.

In Step 2, the likelihood of steel corrosion was determined by geospatially linking each structure to the SSURGO soil corrosivity (as shown in Figure 3), as discussed in the section "Soil Corrosivity." The structure age was accounted for by adjusting the corrosion likelihood as a function of the age and soil corrosivity, as shown in Step 3 through 5 in Figure 4. If the structure was in a high steel soil corrosivity zone and the structure age was over 25 years old, the structure was assigned a corrosion likelihood of "high" (Step 3). If the structure was less than 25 years old and located in a high steel soil corrosivity zone, the structure was assigned a corrosion likelihood of "moderate" (Step 3). If the structure age was greater than 50 years old, the corrosion likelihood was increased from low to medium, or medium to high, as shown in Step 4 and 5 in Figure 4. Modifications to the corrosion likelihood for structure ages of 25 and 50 years were based on SME input and historical PG&E standard changes. The corrosion likelihood was then converted to a DLRF using Table 3.

Figure 5 shows the corrosion likelihood output for the direct buried grillage or direct embedded structures. Many structures are identified as having high or moderate corrosion likelihoods. This is mainly driven by the moderate and high level of soil corrosivity for steel from the SSURGO dataset, as shown in Figure 3.

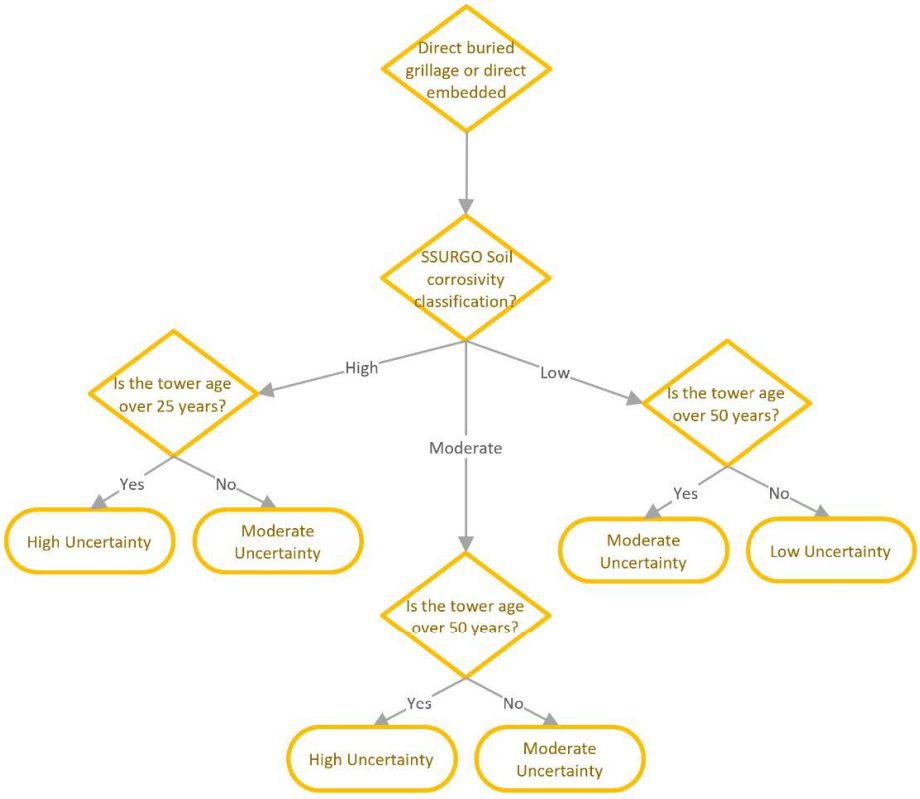

Figure 4 BGC model overview for direct-buried grillage and direct embedded foundations.

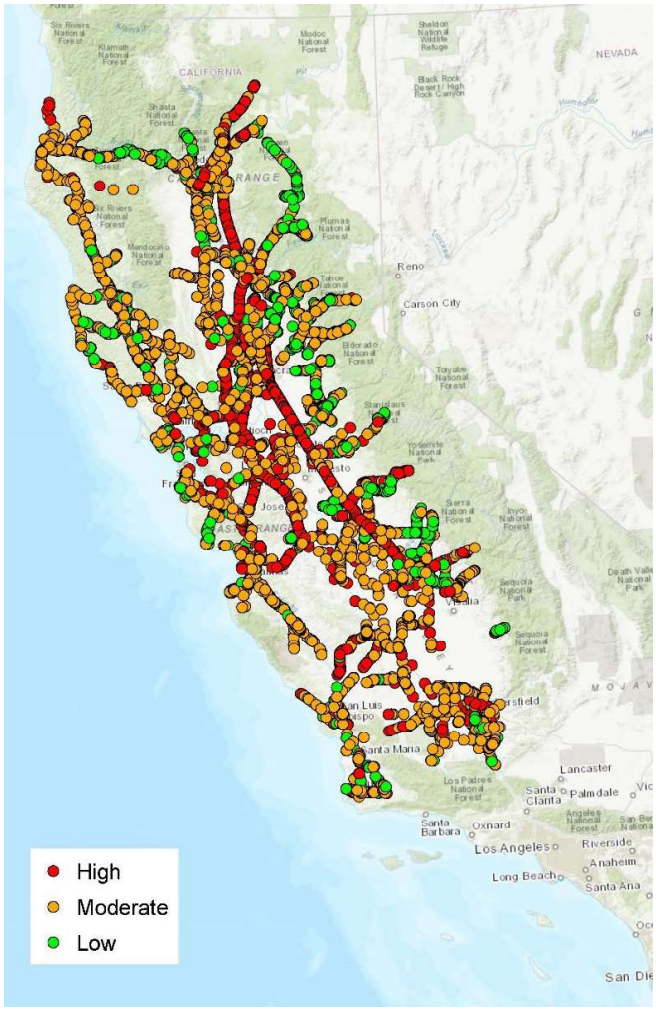

Figure 5 BGC model corrosion likelihood output for direct buried grillage and direct embedded foundations.

Concrete Encased Foundations

The process for calculating the corrosion likelihood and DLRF for concrete encased foundations is shown in Figure 6. The BGC model first determines if the foundation is a concrete encased foundation (Step 1). To determine the DLRF, the foundation condition, steel and concrete soil corrosivity, and structure age are taken into consideration as described in the following subsections.

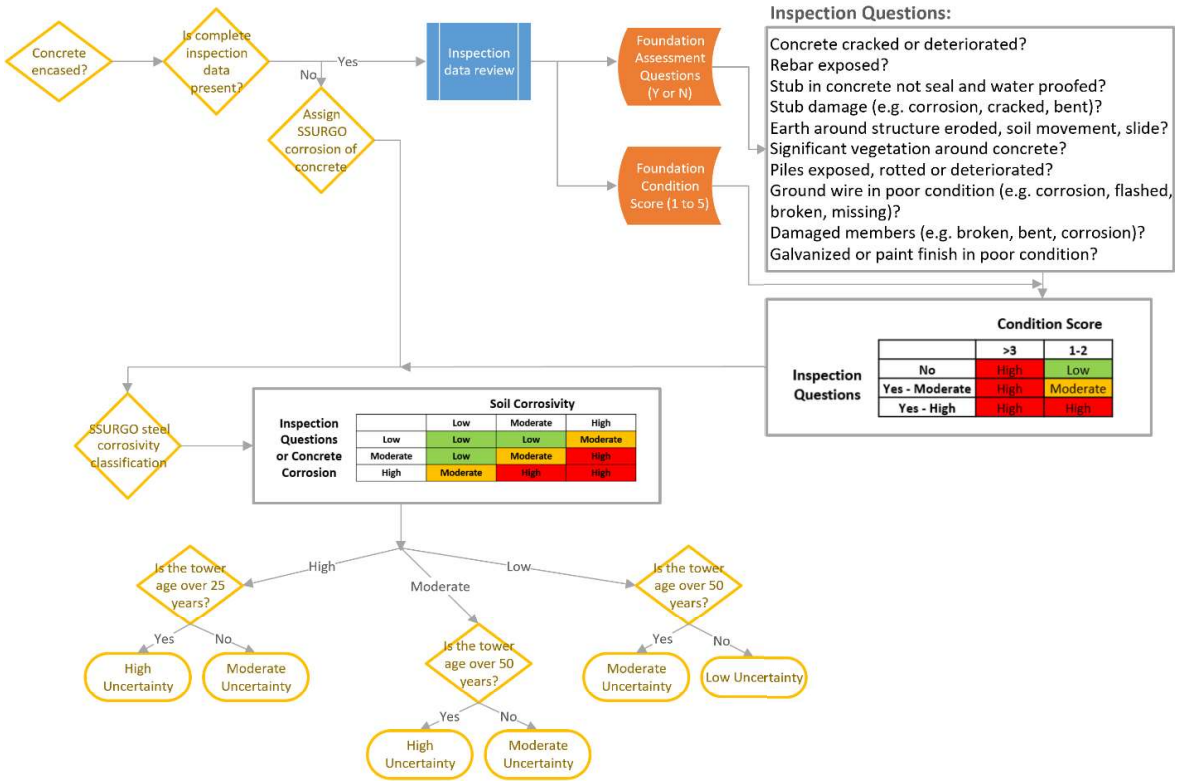

Figure 6 BGC Model overview for concrete encased foundations.

Foundation Condition

The foundation condition is assessed by using the relevant questions in the ground or aerial inspection forms. If the inspection data is incomplete (i.e. missing fields or no inspection completed) then the SSURGO concrete corrosivity was assigned, as shown in Steps 2 and 3 in Figure 6. If the inspection data is complete, Steps 4 to 7 are completed in Figure 6. Each inspection form collects information on any damage observed (cracks, deterioration, damage) and assigns an overall condition score to the foundation (Steps 4 through 6). The model assumes that a pristine concrete-encased foundation will protect the underlying steel from corrosion. As the concrete becomes damaged, the concrete no longer fully protects the steel from the surrounding environment and corrosion of the steel will likely occur.

The ground and aerial inspection form questions are mined to determine if damage has occurred to the foundation, shown in Steps 5 and 6 of Figure 6. If any of the ground inspection form questions concerning the steel structure foundations are answered "yes", then damage to the foundation is assumed. The aerial inspection form comments were mined to determine if foundation damage was indicated. The steel structure foundation condition score from both the ground and aerial inspections were determined for each structure, if available, as shown in Step 5 of Figure 6. A condition score less than three was assumed to have no significant damage while

a condition score greater than or equal to three was assumed to have damage. The condition scores and inspection questions were combined into an intermediate corrosion likelihood ranking using Step 7 in Figure 6.

Steel and Concrete Soil Corrosivity

The potential for concrete and steel degradation due to soil corrosion is estimated from the SSURGO concrete and uncoated steel corrosivity values, as discussed in the section "Soil Corrosivity." For concrete encased foundations, concrete is assumed to be initially in direct contact with the soil, therefore the concrete corrosivity is considered. As the concrete degrades or becomes damaged, the underlying steel structure may come in to contact with the soil and steel corrosion may occur. The SSURGO concrete and steel soil corrosivity potentials are determined for each structure, as discussed in the section "Soil Corrosivity." The concrete corrosivity value is used if the inspection form data is not present or incomplete, as shown in Step 2 and 3 of Figure 6. The steel corrosivity value is applied to all structures in the BGC model as shown in Step 8 of Figure 6. Step 9 shows the table used to combine the inspection data or concrete corrosivity values with the steel corrosivity values. The resulting output is a high, moderate, or low intermediate corrosion likelihood.

Structure Age

As with direct buried foundations, the structure age was accounted for by adjusting the corrosion likelihood as a function of the age and soil corrosivity, as shown in Step 10 and 11 of Figure 6. For structures with a high corrosion likelihood following Step 9, a structure age of 25 years was used to adjust the final corrosion likelihood output, as shown in Step 10. If the structure had a moderate or low corrosion likelihood following Step 9, a structure age of 50 years was used to adjust the final corrosion likelihood output, as shown in Step 11. The corrosion likelihood level was then converted to a DLRF using Table 3.

Concrete Encased Foundation Model Output

Figure 7 shows the corrosion likelihood output for the concrete encased foundation structures. Many structures are identified as having high corrosion likelihood. Data from the recently completed foundation pilot study will be used to validate this modeling work, and to inform possible improvements to the model.

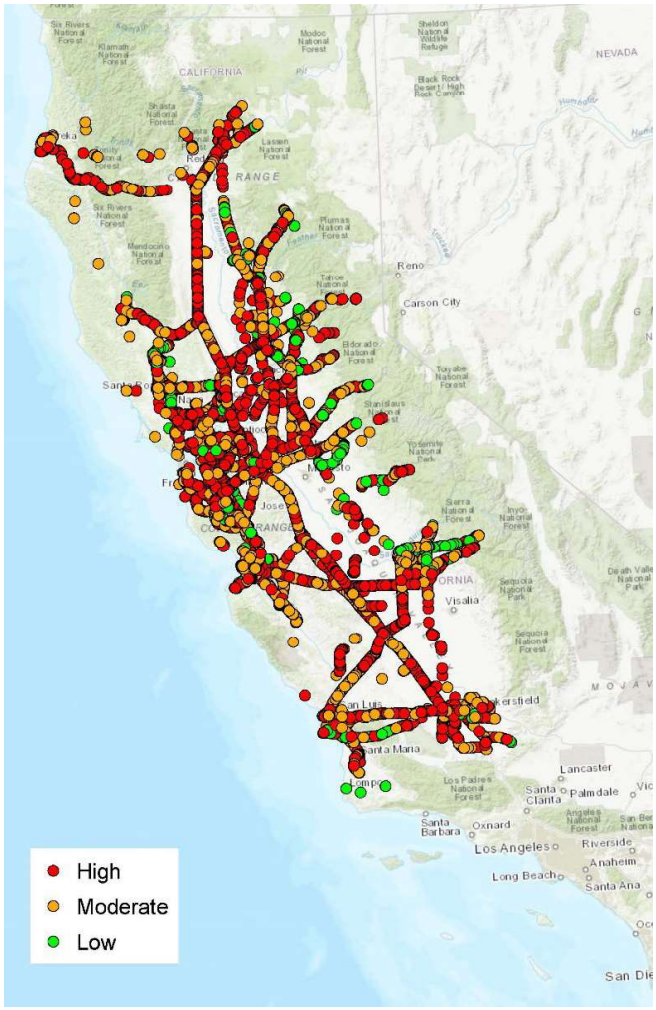

Figure 7 BGC model corrosion likelihood output for concrete encased foundations.

Below Grade Hardware (Guy Anchor Systems)

In general, the model implementation for below grade hardware (BGH) follows the same logic employed in the direct buried foundations implementation described previously. Based on a review of standards provided by PG&E, the only below grade hardware that is not part of the foundation is the guy anchor system. Therefore, this portion of the below grade model will focus specifically on guy anchors. Some structures such as lattice steel structures do not typically have guy systems, and therefore the below grade hardware corrosion model would not apply to those structures. As before, the model assumes BGH components are unpainted steel without cathodic protection systems. This is because, although paint is sometimes applied to various BGH components, information on BGH painting history is not currently available at the individual

asset level. Thus, the model provides a conservative estimate for corrosion risk on these components. As the assumptions for BGH components mirror those for direct buried foundations, the BGH implementation employs the same process flow outlined in Figure 4. That is, it relies on both the BGH system install date and the SSURGO soil corrosivity for uncoated steel to assign a corrosion risk category. Furthermore, this implementation employs the same 25-year and 50-year corrosion risk timepoints (see Figure 4 for specifics). Likewise, DLRF assignment remains consistent with the foundation implementation: high corrosion risk results in a 0.33 DLRF, moderate corrosion risk results in a 0.16 DLRF, and low corrosion risk results in a 0 DLRF. However, note that because BGH can have separate install dates from the structures themselves, a structure could have differing levels of corrosion risk (and thus DLRFs) for its foundation and its BGH. Thus, assigning two separate DLRFs better stratifies the risk BGC poses to the asset overall.

There are certain scenarios under which the BGH implementation will not output a DLRF. Figure 8 provides the BGH implementation outputs for these scenarios. As lattice steel towers are assumed not to have BGH, the model does not compute a DLRF for those structures. Similarly, if the SSURGO soil corrosivity is unknown, the model does not compute a DLRF. Otherwise, the BGH implementation outputs a DLRF, as described previously.

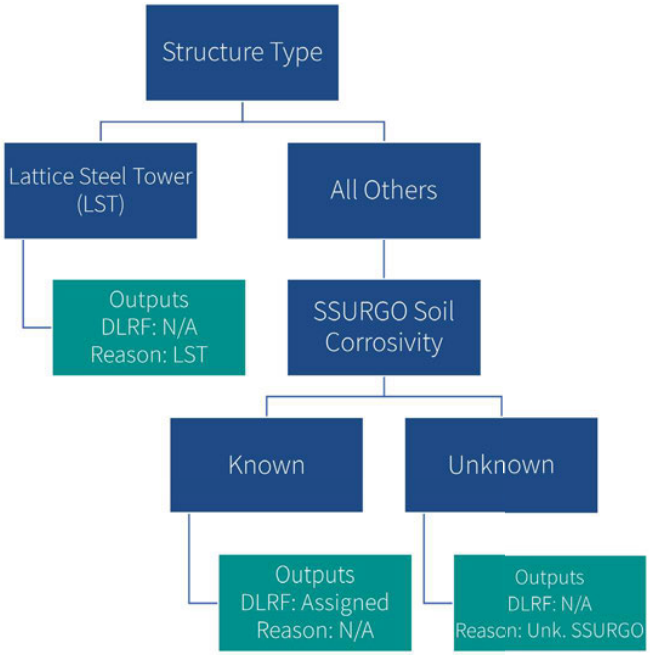

Figure 8 BGH implementation output assignment process flow.

Stray Current

Stray current is a phenomenon where cathodic protection systems from nearby pipelines can interact with the buried portions of a transmission tower. Depending on the direction of the current flow, this may accelerate corrosion on either the pipeline or the electric transmission tower. Both PG&E and Exponent SMEs have indicated that stray current should be considered to ensure the integrity of towers near pipelines. Exponent has performed an analysis to identify instances in which electric transmission towers were near buried pipelines. The considered pipelines were both those operated by PG&E and 'foreign' pipelines not owned or operated by PG&E. The identified towers were indexed across circuits where shield wires or optical ground wires (OPGW) were thought to be present, which was determined through a combination of SAP data, inspections, and arc fault data. Due to current data limitations, it is not possible to predict exactly how much corrosion acceleration may occur in these specific situations. However, a data "flag" has been implemented in the TCM interface to alert the user when such a situation exists.

Example Calculations

This section presents an example of the BGC model procedure used for direct buried foundation and for concrete encased foundations. As the process for BGH mirrors the direct buried process it is not explicitly treated.

Direct Buried Foundation

An example structure (SAP Equipment Number 40581755) is presented in the following section to demonstrate the BGC model for direct buried foundations. This asset is a light duty steel pole (LDSP) with a direct buried grillage foundation that was installed in 1997, making the age of the asset 24 years. The asset location is shown in Figure 9. Referencing the SSURGO dataset, the soil corrosivity for steel was found to be "Low." Following the direct-buried grillage foundation logic presented in Figure 4 and summarized for this asset in Figure 10, the corrosion likelihood for this asset was determined to be "Low."

Transmission Composite Model
March 31, 2022
Page 15

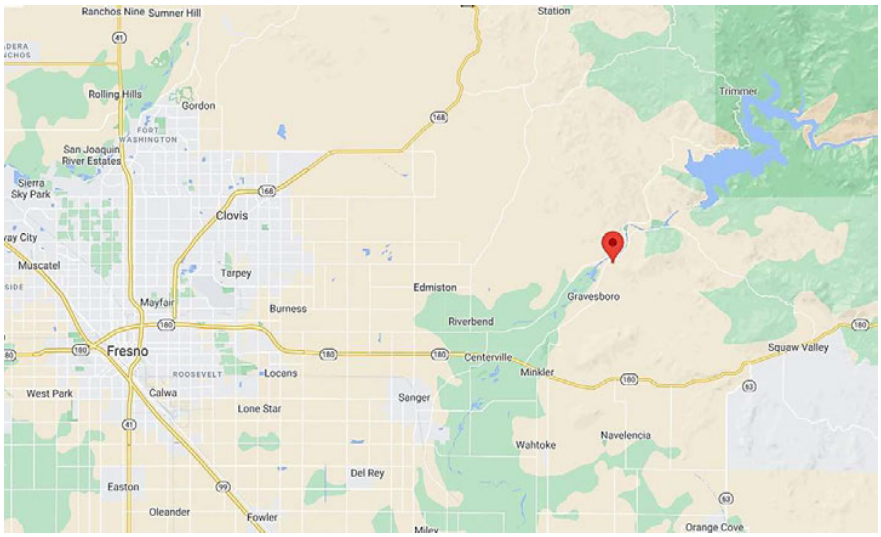

Figure 9 Location of the direct buried foundation structure with SAP Equipment number 40581755.

Figure 10 BGC model logic for direct buried foundation, asset 40581755.

Concrete Encased Foundation with Inspection Forms

An example structure (SAP Equipment Number 40872311) is presented in the following section to demonstrate the BGC model. This asset is a lattice steel tower with concrete encased foundations that was installed in 1950, making the age of the asset 71 years. The asset location is shown in Figure 11. Referencing the SSURGO dataset, the soil corrosivity for steel and concrete was found to be "High" and "Moderate", respectively. The aerial inspection form showed the foundation condition to be 3, and comments indicated the foundation exhibited damage ("concrete damaged or in poor condition"). Following the concrete encased foundation logic presented in Figure 6 and summarized for this asset in Figure 12, the corrosion likelihood for this asset was found to be "High."

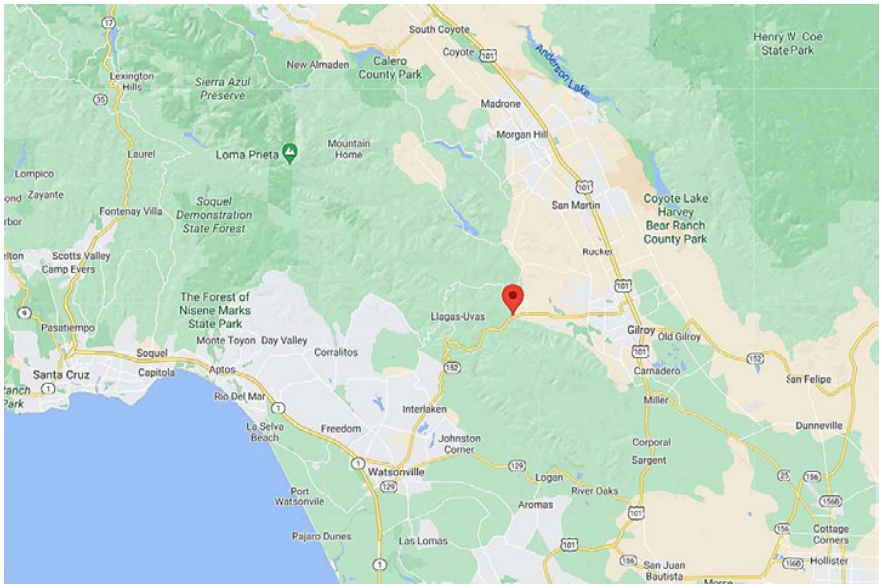

Figure 11 Location of the concrete encased structure with SAP Equipment number 40872311.

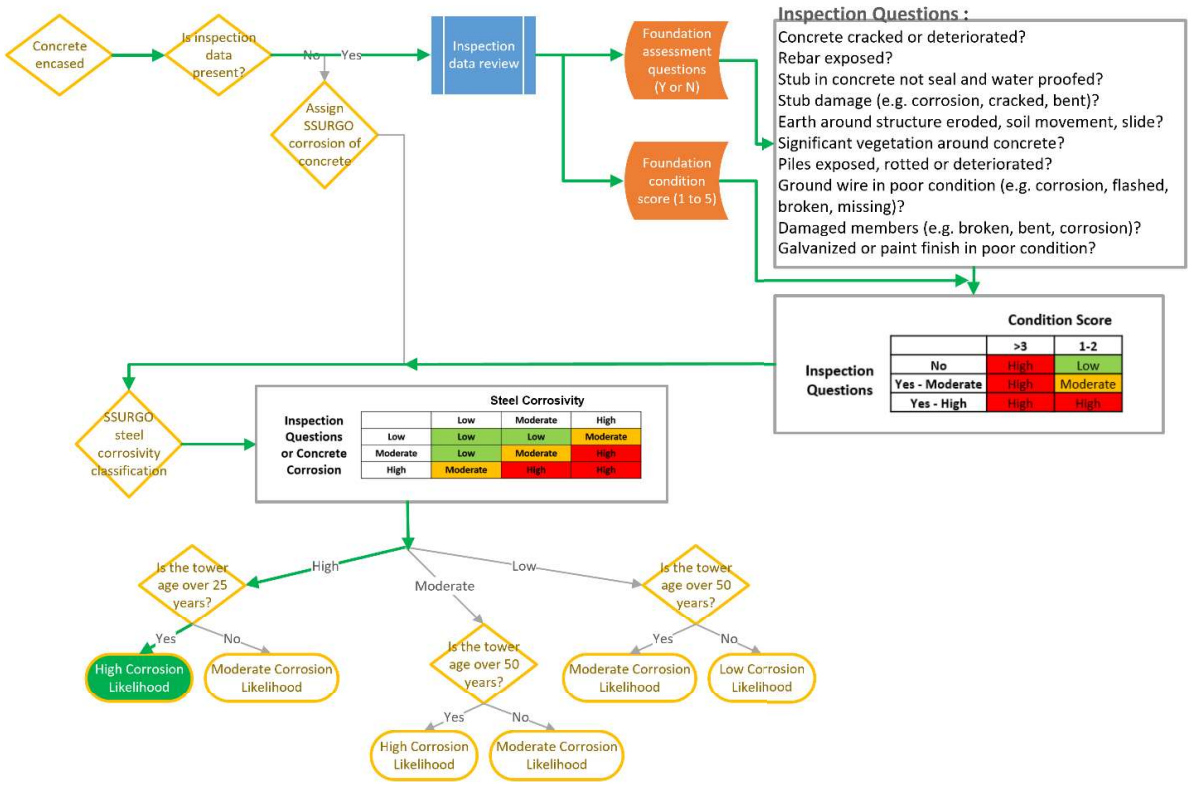

Figure 12 BGC model logic for concrete encased foundation, asset 40872311.

Concrete Encased Foundation with Incomplete Inspection Form Data

An example structure (SAP Equipment Number 43249877) is presented in the following section to demonstrate the BGC model. This asset is a lattice steel tower with concrete encased foundations that was installed in 1972, making the age of the asset 49 years. The asset location is shown in Figure 13. Referencing the SSURGO dataset, the soil corrosivity to steel and concrete was found to be "High" and "Low", respectively. No aerial inspection forms were found for this structure at the time of analysis. The ground inspection form indicated the steel structure foundation condition was 1. Incomplete information was found in the ground inspection form for the steel structure foundation questions. Due to the incomplete ground inspection form questions, the soil corrosivity for concrete was used in place of the inspection data. Following the concrete encased foundation logic presented in Figure 6 and summarized for this asset in Figure 14, the corrosion likelihood for this asset was found to be "Moderate."

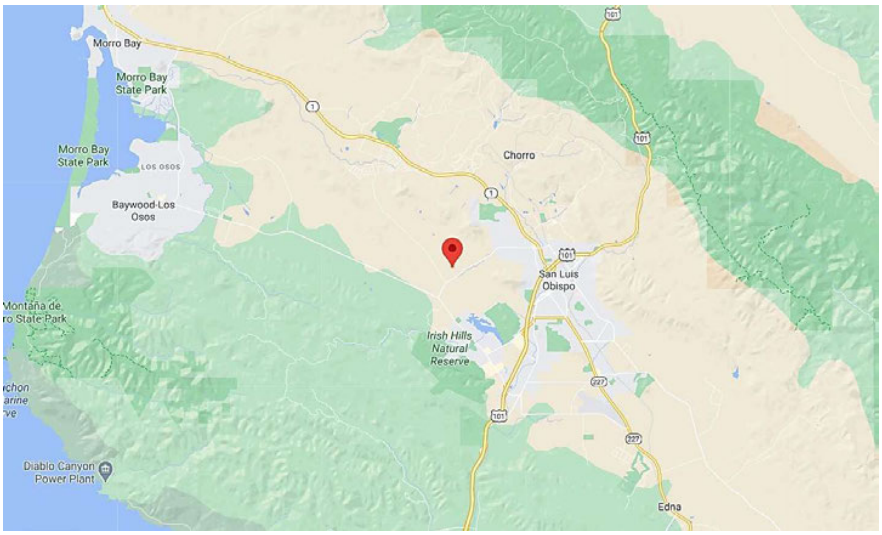

Figure 13 Location of the concrete encased structure with SAP Equipment number 43249877.

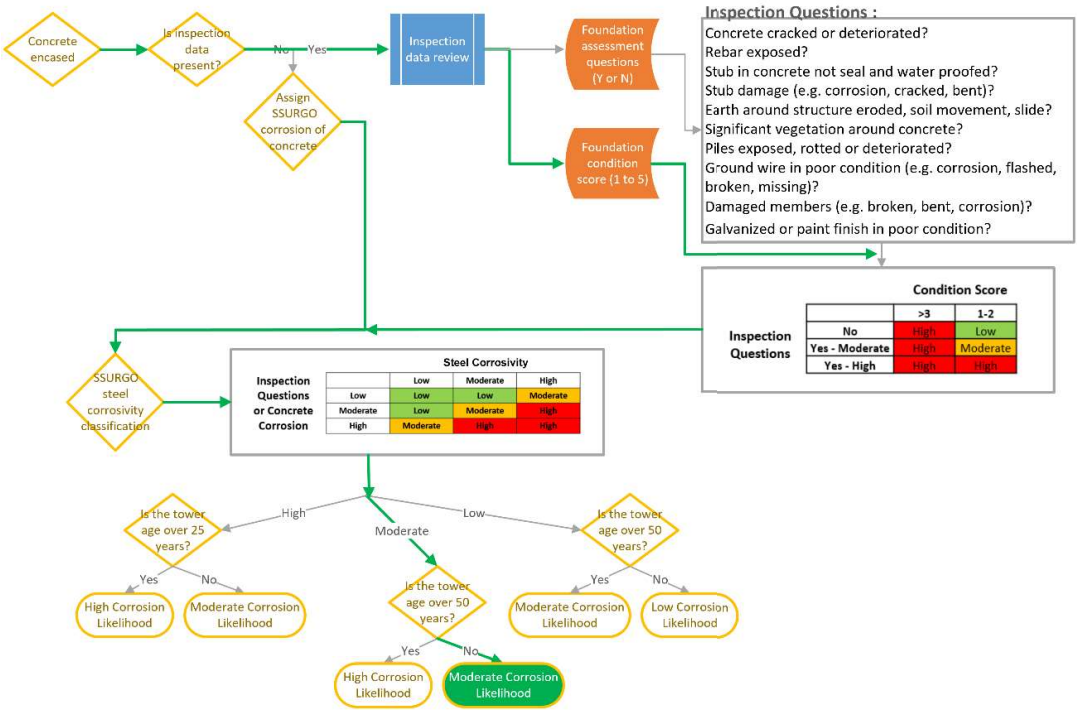

Figure 14 BGC model logic for concrete encased foundation, asset 43249877.

Limitations

The model described herein necessarily relies on simplifying engineering assumptions and idealized representations of complex engineering systems, threats and loads. The implications and limitations of these modeling decisions have been discussed and accepted by PG&E Subject Matter Experts. While we have made every effort to accurately capture key factors related to below-grade corrosion that could adversely affect PG&E's transmission structures based on available information, this model is expected to be further refined as new idealizations, methods and/or data become available. Proper application of this model requires recognition and understanding of the limitations of both the scope and methodology.

The model described herein is intended to be incorporated into a comprehensive PG&E framework (TCM Framework) that was developed to inform PG&E risk mitigation decisions. Neither the Framework nor this model is intended to predict specific failures, and the actual performance of some assets may be materially different from that anticipated by the model.

For limitations associated with the Framework, see Revision 1 of Exponent's "PG&E's Composite Risk Model for Overhead Electric Transmission Components: A White Paper," dated March 31, 2022.

DRAFT: 31 March 2022, Revision 1

Appendix F

Aeolian Vibration Model

Exponent®

EXTERNAL MEMORANDUM

TO:	[redacted] PG&E)
FROM:	Exponent
DATE:	March 31, 2022
PROJECT:	Transmission Composite Model
SUBJECT:	Aeolian Vibration Model

This memorandum describes the technical basis for design life reductions due to the susceptibility of spans to fatigue from wind-induced vibrations. Fundamental wind parameters provided by PG&E Meteorology on the POMMS grid define the site-specific hazard for steady, perpendicular winds that drive vibrations due to vortex shedding (Aeolian vibration). The fatigue amplitude and associated damage accumulation is calculated for each span in the transmission system.

Wind Environment and Near-Surface Wind Modeling

Aeolian vibration damage is chiefly due to a very large number of cycles of relatively low amplitude (low stress) vibrations. Vibrations are due to oscillating loads from alternating vortex shedding on opposite sides of the conductor transverse to the wind direction. The number and amplitude of vibration cycles are a function of how often steady winds of a given velocity blow perpendicular to the conductor, and thus the threat of Aeolian vibration is site-specific. The site-specific wind environment is modeled using site-specific parameters assigned to the nearest POMMS grid as provided by (or derived from) data accumulated and maintained by PG&E Meteorology.

The model adopts the basic logarithmic wind model to describe the site-specific wind profile. (It is called a wind profile because in most cases the wind speed increases with height z above the ground.)

$$U(z) = \frac{u^*}{\kappa} \times \ln\left(\frac{z - z_h}{z_0} + \Psi\right) \quad (1)$$

where u^* is the friction velocity, κ is the von Karman constant = 0.4, z_0 is the roughness length, z_h is the zero-plane displacement, and Ψ is a function that depends on the stability of rising air.

Because structural loads act close to the ground relative to the entire air column, some simplifications are applied that are common to wind engineering of structures. First, the Ψ

function is assumed to be negligible at the heights of interest to structural engineers. The term z_h depends on the height of surrounding structures and is conservatively taken to be zero herein, though that could be a future refinement should such data become available. A simplified model of the wind profile similar to that used in building codes remains.

$$U(z) = \frac{u^*}{\kappa} \times \ln\left(\frac{z}{z_0}\right) \quad (2)$$

A typical wind profile using Equation 2 is shown in Figure 1.

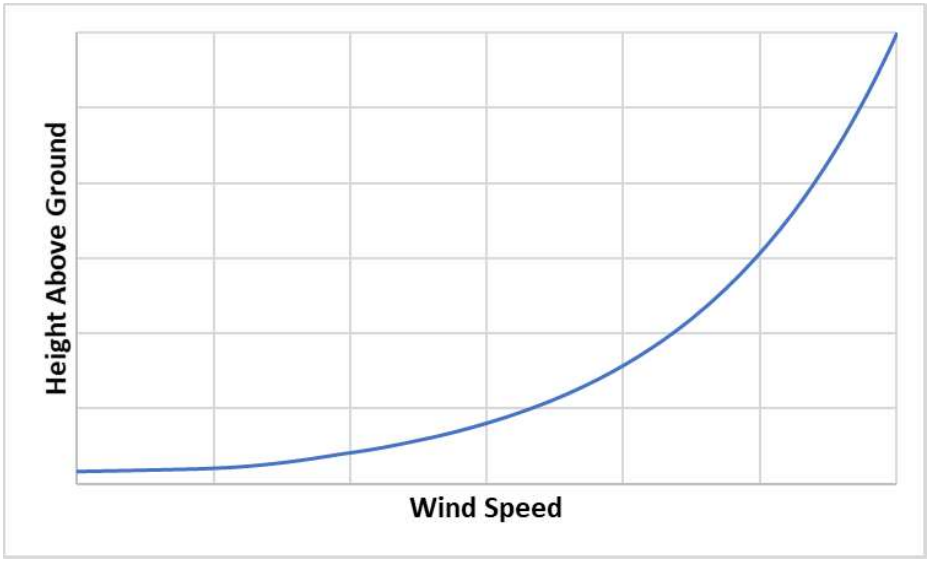

Figure 1. Typical wind profile using Equation 2

Note that the surface roughness that slows the wind due to surface friction is defined by the roughness length z_0. This parameter is currently being estimated for each structure by mapping the designated Land Use and Land Cover (LULC) type in ETGIS to typical z_0 values for similar LULC tabulated in ASCE 7-22. Efforts are underway to improve this estimate by incorporating data from PG&E Meteorology models (at each POMMS grid, then mapped to spans) or publicly available sources.[1]

In addition to the wind profile, the distribution of wind speeds and directions is also important. How often the wind blows at different speeds and from different directions is typically defined by a wind rose. Based on PG&E historical wind speed measurements, wind roses are derived for

[1] For instance, FEMA's HAZUS program has mapped surface roughness length nationwide based on land use maps, satellite imagery, and calibration.

each POMMS grid. Steady winds perpendicular to the conductors' span generate the vortices and therefore drive the vibrations and damage accumulation; herein only wind directions that are generally perpendicular to the span (90-degree wedge) are considered. A typical wind rose is shown in Figure 2.

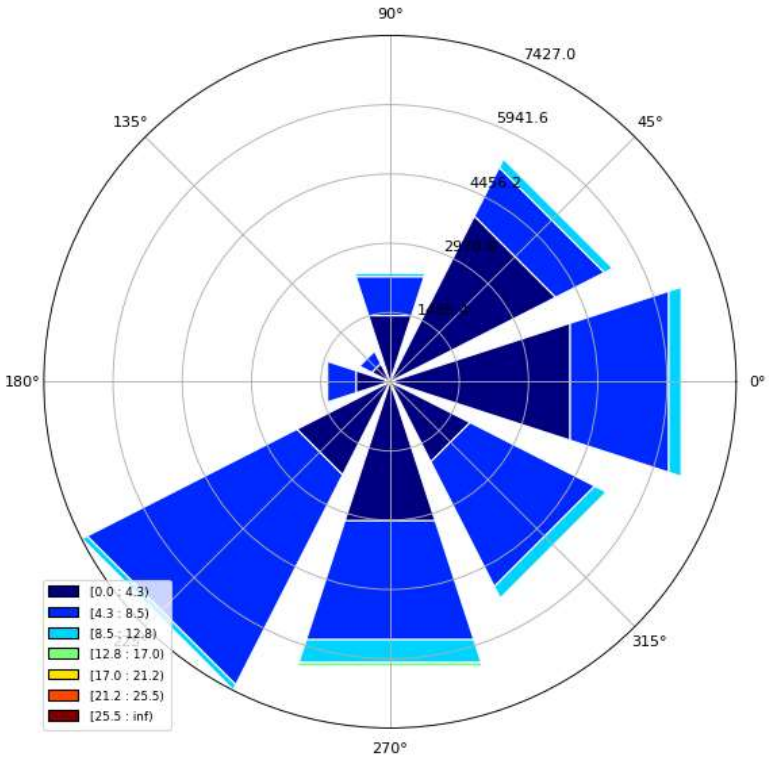

Figure 2. Example wind rose derived from PG&E meteorological data for POMMS Grid 281_189

As mentioned, steady winds cause the vortices to be shed at regular intervals. The frequency at which the vortices shed will excite one of the natural frequencies of the conductor, causing significant amplification by a mechanism known as resonance. As an example, resonance allows a child on a swing to achieve significant height with only a series of light pushes, as long as those pushes are applied at the right frequency. In contrast to steady (laminar) wind, turbulence (gusting) will disrupt the regular cycle of shedding and reduce the vibration amplitudes. Turbulence is caused by roughness of the ground surface; more roughness, such as trees or buildings rather than grasslands, causes more turbulence. The expected turbulence intensity is estimated on a site-specific basis as described in the following paragraphs.

Wind at any elevation above the ground can be considered to be composed of two components - a steady (stationary mean) wind *U* per Equation 2 above, and a dynamic component *u(t)* that is superposed on it (Figure 3). By definition *u(t)* has a mean of zero and a nonnegative standard deviation σ_u. Increasing standard deviation is associated with increasing gustiness (turbulence); the turbulence intensity I_u is defined as $\frac{\sigma_u}{U}$. The standard deviation of the dynamic component σ_u can be estimated from the friction velocity u^* provided by PG&E Meteorology. One simple relation is that $\sigma_u = 2.5 \times u^*$ and is adopted herein.

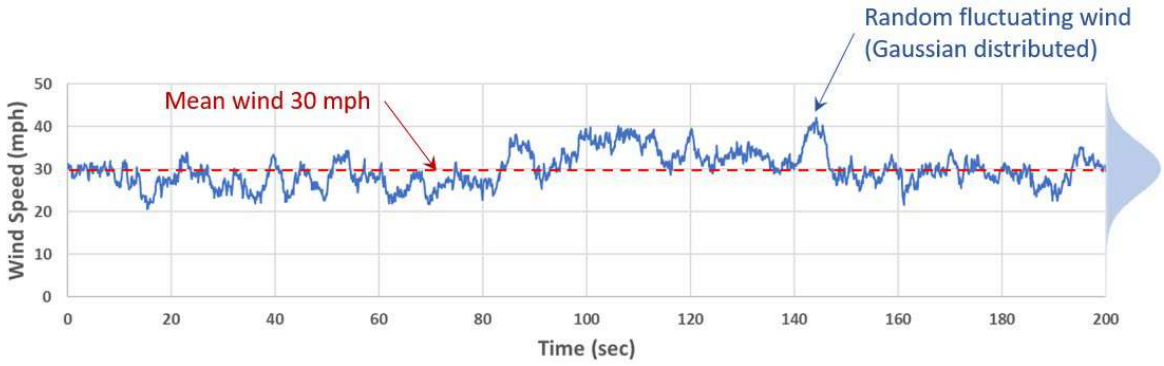

Figure 3. Dynamic model of wind as a random fluctuating component (**blue**) superposed on a steady mean wind (**red**)

According to EPRI,[2] the energy supplied by the wind to drive Aeolian vibration in the presence of turbulence is reduced by a factor β_w as determined by the following equation:

$$\beta_w = \frac{1}{\sqrt{1+(\frac{I_u}{I_L})^2}} \quad (3)$$

Where I_L is the lock-in index and is a function of the vibration amplitude, and is estimated herein to be 0.09, which is a common approximation in the technical literature.

[2] EPRI Transmission Line Reference Book: Wind-Induced Conductor Motion, 2017 Edition. EPRI, Palo Alto, CA: 2017. 3002010124 (i.e., the EPRI "Orange Book")

Structural Model

Each span is idealized as a level, taut string.[3] Taut strings have many natural modes of vibration of frequency f_n and wavelength λ_n (for the nth mode), as expressed in Equations 4 and 5, respectively.

$$f_n = \frac{S*V}{D} \tag{4}$$

where S is the Strouhal Number (estimated herein to be 0.185), D is the conductor diameter, and V is the wind Velocity.

$$\lambda_n = \frac{1}{f_n}\sqrt{\frac{T}{m}} \tag{5}$$

where T is the tension in the conductor and m is the mass per unit length of the conductor.

Equation 6 describes the snapshot shape of the nth mode of vibration at the time of maximum amplitude, where A_n is the amplitude (zero-to-peak) and y_n is the displacement at a distance x from the support.

$$y_n = A_n sin(\frac{2\pi}{\lambda_n}x) \tag{6}$$

An example application of Equations 4, 5 and 6 is shown in Figure 4.

All variables except A_n in Equations 4, 5 and 6 are completely defined by the wind rose and the conductor properties. The amplitude A_n is determined by the principle of conservation of energy, that is, the wind power input (site-specific) is set equal to the energy dissipation rate (conductor-specific) to determine the amplitude A_n. The associated math is too cumbersome for this memorandum, and instead the reader is referred to the reference document by Foti and Martinelli.[4]

There are several formulations in the technical literature for calculating the stress σ_a near a support. None present a clear advantage in terms of predicting fatigue life; the equation presented by EPRI is adopted in this model, reproduced here as Equation 7.

$$\sigma_a = \pi D E_A \sqrt{\frac{m}{EI}} f_n y_n \tag{7}$$

---

[3] The term string indicates that the bending stiffness of the conductor is taken to be zero, which is a standard approximation in sag-tension calculations and is consistent with PLSCADD calculations.

[4] Francesco Foti, Luca Martinelli, An enhanced unified model for the self-damping of stranded cables under aeolian vibrations, Journal of Wind Engineering & Industrial Aerodynamics 182 (2018) 72–86

where EA is the elastic modulus of the conductor, EI is the effective bending stiffness of the conductor (per EPRI, taken to be 95% of the maximum theoretical value), with other terms previously defined.

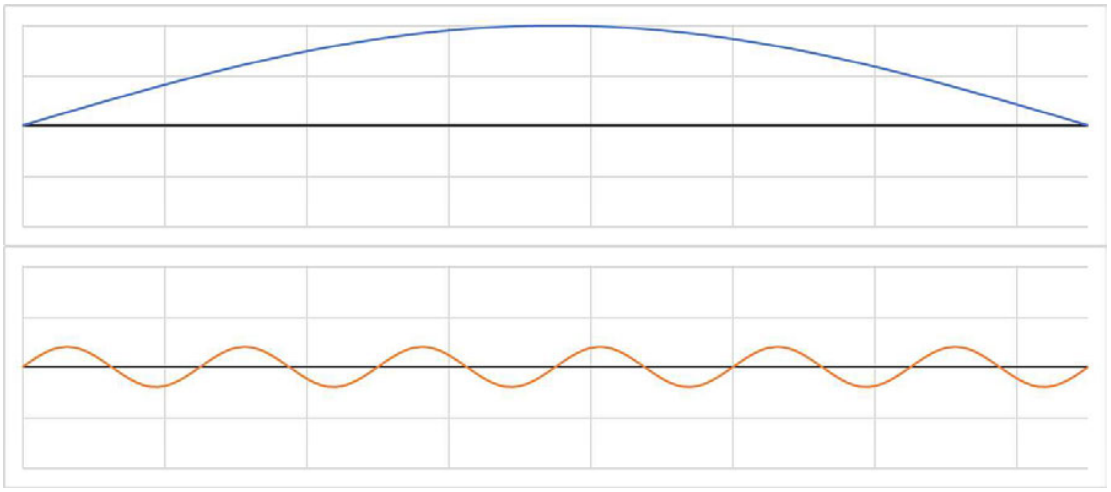

Figure 4. Example showing the 1st and 12th modes for a 150 m level span of Penguin conductor: diameter = 14mm, mass per length = 0.433 kg/m; tension = 5570 N (15% rated strength). The first mode (**blue**) is associated with a steady wind of 0.1 mph; the 12th mode (**orange**) is associated with a steady wind of 0.7 mph.

Stochastic Model for Fatigue Life

The fatigue life of a span consumed annually is calculated based on the number of cycles of vibration at each stress level (σ) and each wind direction (perpendicular to the span) using Miner's Rule (Equation 8).

$$\text{Miner}(\sigma) = \frac{Annual\ N_{cycles}(\sigma)}{N_{fail}(\sigma)} \quad (8)$$

where Annual N_{cycles} is the annual number of cycles based on the conductor's natural frequency of vibraion and characteristics of the wind rose. The number of cycles to failure of the first strand, N_{fail}, is for stress σ at the support and is based on SN curves[5] as available in the technical literature for each class of conductor.

[5] Fatigue life is generally given in the technical literature in the form of SN curves that plot the vibration stress amplitude (S) on one axis and the number of cycles to failure (N) on the other.

The SN curves for ACSR, Aluminum, and Copper conductors are defined probabilistically based on the scatter observed in laboratory testing. The test results are fit to a log-normal distribution and the mean, 95th percentile, and standard deviation are defined.[6] An example SN curve from the EPRI Orange Book appears in Figure 5.

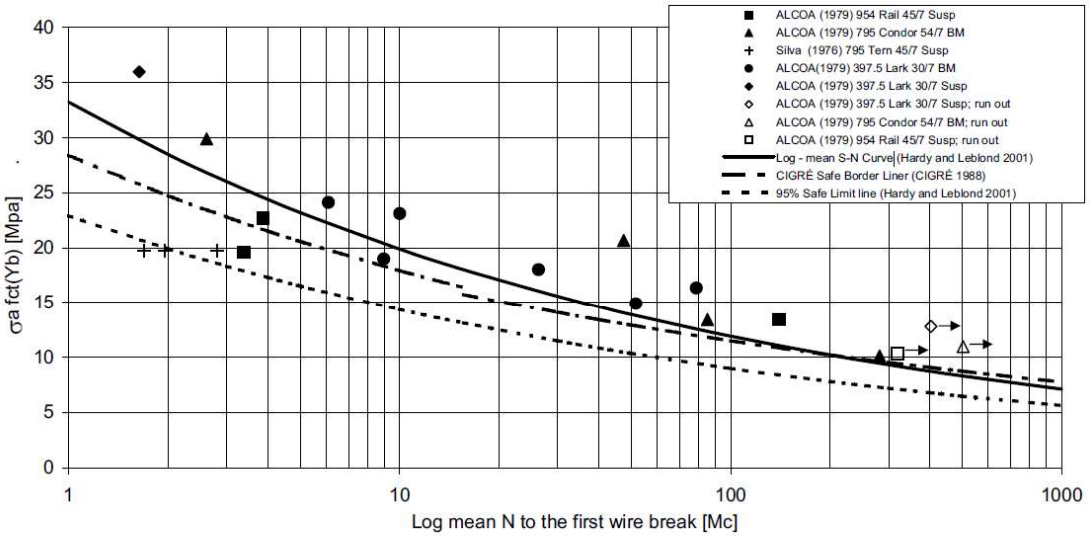

Figure 5. Example SN curve for multi-strand ACSR conductors

The aggregated Miner's rule for all stress levels is the sum of the Miner's rule for all of the vibration modes excited by different wind speeds and proportioned based on the amount of time that speed is expected to blow (per the wind rose). The mean and variance of Miner's rule for annual fatigue life consumption is calculated considering the variation in the corresponding SN curve.

The probability of first strand fatigue failure is based on the probabilistic limit state equation as follows:

$$p_f = Probability\ that\ (R - Q \leq 0) \quad (9)$$

Where R is the capacity (Resistance) and Q is the demand (Quantified effect of the vibration). The capacity is treated as a random variable defined by the SN curve log-normal fit; uncertainty in the demand is not currently considered but could be a future refinement.

[6] Hardy and Leblond (2001)

The annual failure probability is calculated as follows:

$$p_f(year) = \Phi\left(-\frac{\bar{R} - E[Miner(year)]}{\sqrt{\sigma_R^2 + Var[Miner(year)]}}\right)$$

An example failure curve computed for an ACSR conductor is depicted in Figure 6.

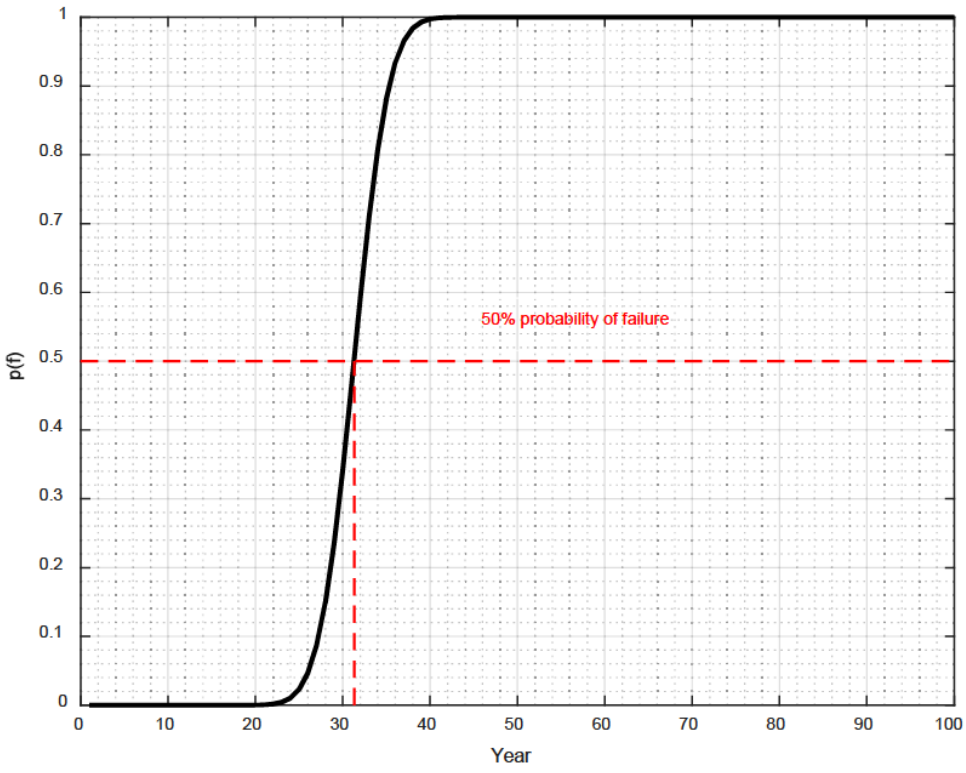

Figure 6. Aeolian vibration annual probability of failure for an example ACSR conductor

In Figure 6, the dashed horizontal line in red shows 50% probability of failure of the example ACSR conductor. For the conductor shown in Figure 6, as can be seen, the fatigue life corresponding to 50% probability of failure is about 31 years.

One of the reasons for the presence of a conductor splice is repair of fatigue damage. As such, for calibration of the model it is informative to consider whether there is correlation between low fatigue life and presence of splices. Figure 7 shows 50% fatigue life plotted against the existing number of splices (splice density) for each conductor. While establishing a definitive correlation between the two parameters is not meaningful because there are many reasons for

the presence of splices, it can be seen that, in general, lines with the highest splice densities tend to be lines with low predicted fatigue life, and lines with highest predicted fatigue lives tend to have low splice density.

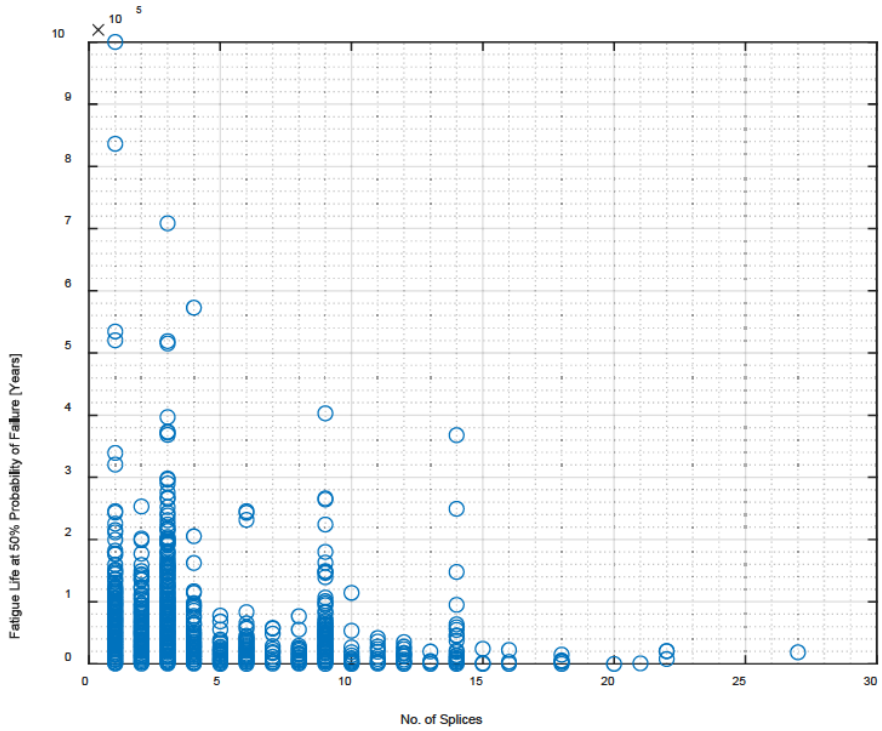

Figure 7. Relationship between the existing number of splices and fatigue life at 50% probability of failure for conductor spans.

Modeling Design Life Reduction from Aeolian Vibration Induced Fatigue

With the wind and structural models defined above, this section describes each step in the analysis. This process would be repeated for every span and for every cell (wind speed, direction, and duration) of the wind rose.

1. Estimate the turbulence intensity from the surface roughness using ETGIS (refinements in development).
2. Calculate the wind energy reduction β_w based on turbulence intensity.

3. Determine the frequency of vortex shedding from the wind velocity and conductor diameter.
4. Estimate the conductor tension based on the rated tensile strength or use the PLSCADD calculated tension, if available.
5. Calculate the wind power input as a function of vibration amplitude.
6. Calculate the self-damping of the conductor as a function of vibration amplitude.
7. Calculate the vibration amplitude by equating the wind power input to the self-damping energy dissipation rate.
8. Estimate the stress at the clamp based on mode shape and vibration amplitude.
9. Calculate the expected number of cycles until failure and uncertainty using the distribution fit to available laboratory SN curves for the given conductor type.
10. Calculate the mean and standard deviation of a damage index for the conductor for a particular year using Miner's rule.
11. Calculate the annual rate of failure assuming a normal distribution for the damage.
12. Calculate the expected times to first wire break with different levels of confidence corresponding to10%, 50% and 90% probabilities of failure.

Once this is done for all spans, they are ranked by expected time to first wire break. Based on the distribution of times to first break, outliers will be assigned the highest design life reduction (33%), with lesser design life reductions assigned as a function of the number of standard deviations below the median design life. Lines with close-to or greater-than median design life will have no modification to their expected design life.

A fully worked example MathCad calculation for a representative span is provided in Appendix B.

Given the large number of spans, calculations for all the spans are performed using a code written in MATLAB programming language. Simulation results for three spans with design life reduction factors ranging from 0% to 33% are chosen to verify the code written in MATLAB against the calculations done in MathCad. Properties of the chosen Spans as well as the failure curves computed for each span using both MATLAB and MathCad are shown in Appendix A.

Limitations

The model described herein necessarily relies on simplifying engineering assumptions and idealized representations of complex engineering systems, threats and loads. The implications and limitations of these modeling decisions have been discussed and accepted by PG&E Subject Matter Experts. While we have made every effort to accurately capture key factors related to Aeolian vibrations that could adversely affect PG&E's transmission structures based on available information, this model is expected to be further refined as new idealizations, methods and/or data become available. Proper application of this model requires recognition and understanding of the limitations of both the scope and methodology.

The model described herein is intended to be incorporated into a comprehensive PG&E framework (TCM Framework) that was developed to inform PG&E risk mitigation decisions. Neither the Framework nor this model is intended to predict specific failures, and the actual performance of some assets may be materially different from that anticipated by the model.

For limitations associated with the Framework, see Revision 1 of Exponent's "PG&E's Composite Risk Model for Overhead Electric Transmission Components: A White Paper," dated March 31, 2022.

Appendix A – MATLAB/MathCad Comparison

In this Appendix, calculation results obtained from the code written in MATLAB are verified against MathCad calculation results. Failure curves are chosen as the output measure used for doing this comparison. Three conductor spans with design life reduction factors ranging from 0% to 33% are chosen for the purpose of the verifications. Properties of the selected spans are shown in Table 1. Failure curves for the selected spans are shown in Figure 8 to Figure 10. As can be seen, complete agreement between the failure curves obtained from MATLAB and MathCad is achieved for all cases. Therefore, the code developed in MATLAB is considered reliable for performing aeolian vibration calculations shown in Appendix B of this memorandum.

Table 1. Properties of three conductor spans selected for MATLAB code verification.

Example No./Property	No. 1	No. 2	No. 3
ETL #	ETL.2392	ETL.7780	ETL.5440
SAP equipment ID	44905857	40660577	44931498
Conductor type	ACSR	ACSR	ACSR
Conductor name	Penguin	Ibis	Condor
Span length (ft)	393.081	433.246	3.404
Span direction (deg)	235.414	301.372	93.994
Conductor diameter (in)	0.563	0.783	1.092
Conductor mass (lb/ft)	0.291	0.546	1.023
Design Life Reduction Factor (DLRF)	33%	20%	0%

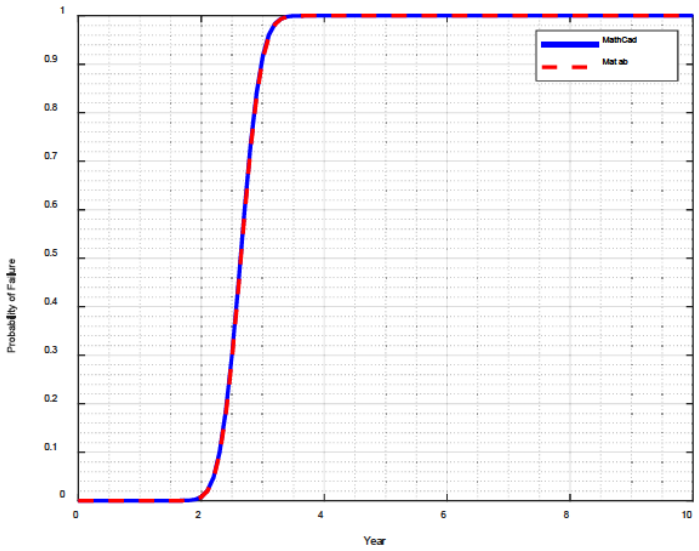

Figure 8. Failure curve for example No.1 which has a DLRF of 33%.

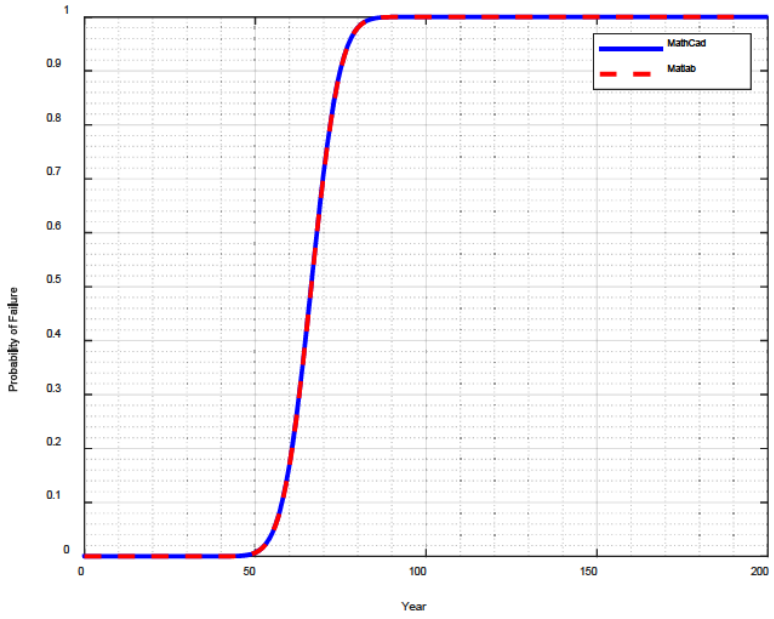

Figure 9. Failure curve for example No.2 which has a DLRF of 20%.

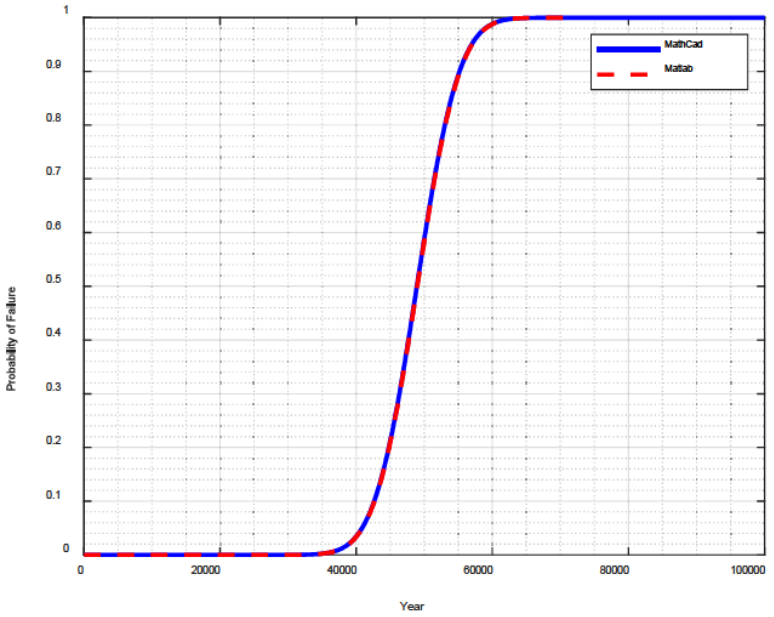

Figure 10. Failure curve for example No.3 which has a DLRF of 0%.

Appendix B – Worked Example (MathCad)

Aeolian Vibration and Fatigue of Overhead Conductors

This Mathcad calculation is intended to provide the engineering and mathematical basis for quantitatively assessing the risk of fatigue failure of overhead lines given the conductor properties and wind environment. The assessment is based on calculating the vibration amplitude and cyclic stress using the energy balance approach in which the amplitude is found by equating the power dissipated internally by the conductor to the external power input from the wind. The vibration amplitude and mode shapes allow the estimation of cyclic stresses and expected fatigue life. Much of the work and notation herein is based on that of Foti and Martinelli (2018), particularly regarding the internal power dissipation by the conductor, and the reader in encouraged to review that reference. Derivation of the wind power input is based somewhat on the work of Vandiver 2012). Wind roses are derived from PG&E Meteorological database.

Calculations presented herein will are codified in MATLAB programming language and are applied to all conductor spans. The useful output of such work is an annual probability of fatigue failure for all conductor spans.

This version of the calculation does not address the presence of dampers (e.g., Stockbridge dampers). Should that become a concern, inclusion of the power dissipation would be straightforward within this framework.

Brian McDonald, April 2022

Contents

References:
(1) Foti, Francesco, and Luca Martinelli. "An enhanced unified model for the self-damping of stranded cables under aeolian vibrations." Journal of Wind Engineering and Industrial Aerodynamics 182 (2018): 72-86.
(2) Vandiver, J. Kim. "Damping parameters for flow-induced vibration." Journal of fluids and structures 35 (2012): 105-119.

Section 1. Conductor Properties

For this calculation, we have chosen a conductor span with ETL# of 2392 and SAP equipment ID of 44905857.

$D := 0.563\ in$ conductor diameter

$d_A := 0.1878\ in$ Aluminum wire diameter

$mass := 0.291 \cdot \frac{\frac{lbf}{g}}{ft}$ mass per unit length

$w := mass \cdot g = 0.291\ \frac{lbf}{ft}$ weight per unit length

$c_0 := \frac{0.15}{m}$ parameter defining break in moment curve

$RTS := 8350\ lbf$ rated strength

$EI_{max} := 37.04251643 \cdot kip \cdot in^2$ maximum (composite) bending stiffness

$\beta_{EI} := 0.95$ effective bending stiffness as proportion of max bending stiffness

$EI_{maxref} := \beta_{EI} \cdot EI_{max}$ effective bending stiffness

$E_a := 69\ GPa$ Aluminum elastic moduli for conductor stranding

Proportion of rated strength RTS for which the fatigue is evaluated, typically 20% to 35%

$\eta := 0.3$

Friction coefficient for wire-to-wire slippage

$\mu := 0.5$

Curvature at which the internal friction mechanism transitions to global slippage
(kink in moment-curvature diagram)

$\chi_0 := c_0 \cdot \mu \cdot \eta = 0.023\ m^{-1}$

Span length and span direction

$span := 393.0812338\ ft$

$\theta_{span} := 235.4144142 \cdot deg$ clockwise angle from north

Section 2. Wind Environment

$i := 0 .. 7$ $j := 0 .. 5$

wind speed associated with each column of windRose

$speeds := \text{READEXCEL}(\text{".\chosen\_strcutures\_for\_validation.xlsx"}, \text{"Sheet1!K15:P15"})^{T} \cdot mph$

wind bearing from north for each row of windRose

$bearings := \text{READEXCEL}(\text{".\chosen\_strcutures\_for\_validation.xlsx"}, \text{"Sheet1!K11:R11"})^{T} \cdot deg$

Define the wind rose as the proportion of time the span experiences wind of speed j and bearing i. Check that the proportions all add to 1.0.

$windRose := \text{READEXCEL}(\text{".\chosen\_strcutures\_for\_validation.xlsx"}, \text{"Sheet1!J21:O28"})$

$calm := 0$

$\sum_{i=0}^{7} \sum_{j=0}^{5} windRose_{i,j} + calm = 1$

Find the wind speeds perpendicular to the span for each bearing i and speed j

$perpSpeed_{i,j} := speeds_{j} \cdot \left| \cos\left(bearings_{i}\right) \cdot \sin\left(\theta_{span}\right) - \sin\left(bearings_{i}\right) \cdot \cos\left(\theta_{span}\right) \right|$

$$perpSpeed = \begin{bmatrix} 1.06 & 3.16 & 5.26 & 7.36 & 9.46 & 11.56 \\ 0.41 & 1.22 & 2.03 & 2.84 & 3.65 & 4.46 \\ 1.64 & 4.88 & 8.13 & 11.37 & 14.62 & 17.86 \\ 1.91 & 5.69 & 9.47 & 13.25 & 17.03 & 20.81 \\ 1.06 & 3.16 & 5.26 & 7.36 & 9.46 & 11.56 \\ 0.41 & 1.22 & 2.03 & 2.84 & 3.65 & 4.46 \\ 1.64 & 4.88 & 8.13 & 11.37 & 14.62 & 17.86 \\ 1.91 & 5.69 & 9.47 & 13.25 & 17.03 & 20.81 \end{bmatrix} mph$$

Section 3. Conductor Vibration Modes

$St := 0.185$

$$f_{shed} := \frac{St \cdot perpSpeed}{D} = \begin{bmatrix} 6.12 & 18.27 & 30.42 & 42.57 & 54.72 & 66.88 \\ 2.36 & 7.04 & 11.72 & 16.4 & 21.09 & 25.77 \\ 9.46 & 28.23 & 47 & 65.77 & 84.54 & 103.32 \\ 11.02 & 32.88 & 54.75 & 76.61 & 98.48 & 120.34 \\ 6.12 & 18.27 & 30.42 & 42.57 & 54.72 & 66.88 \\ 2.36 & 7.04 & 11.72 & 16.4 & 21.09 & 25.77 \\ 9.46 & 28.23 & 47 & 65.77 & 84.54 & 103.32 \\ 11.02 & 32.88 & 54.75 & 76.61 & 98.48 & 120.34 \end{bmatrix} Hz$$

frequencies at which wind of the given velocity will shed from an infinitely long cylinder

$$\lambda_{shed_{i,j}} := \left\| \begin{array}{l} \text{if } f_{shed_{i,j}} < 1 \cdot Hz \\ \quad \| (2 \cdot span) \\ \text{else} \\ \quad \left\| \left(\frac{1}{f_{shed_{i,j}}} \cdot \sqrt{\frac{\eta \cdot RTS}{mass}} \right) \right. \end{array} \right\|$$

wavelength associated with vortex shed frequency

adjust wavelength such that there is an integer number of half wavelengths in a span (associated with the lock-in frequency)

$$\lambda_{i,j} := \frac{2 \cdot span}{\max\left(\left(\text{round}\left(\frac{2 \cdot span}{\lambda_{shed_{i,j}}}, 0 \right), 1 \right) \right)}$$

$$\lambda = \begin{bmatrix} 26.62 & 8.87 & 5.32 & 3.74 & 2.92 & 2.40 \\ 59.91 & 21.78 & 13.31 & 9.58 & 7.73 & 6.31 \\ 17.12 & 5.71 & 3.42 & 2.45 & 1.90 & 1.56 \\ 14.98 & 4.89 & 2.92 & 2.10 & 1.63 & 1.33 \\ 26.62 & 8.87 & 5.32 & 3.74 & 2.92 & 2.40 \\ 59.91 & 21.78 & 13.31 & 9.58 & 7.73 & 6.31 \\ 17.12 & 5.71 & 3.42 & 2.45 & 1.90 & 1.56 \\ 14.98 & 4.89 & 2.92 & 2.10 & 1.63 & 1.33 \end{bmatrix} m$$

$$f := \frac{1}{\lambda} \cdot \sqrt{\frac{\eta \cdot RTS}{mass}} = \begin{bmatrix} 6.02 & 18.07 & 30.12 & 42.84 & 54.89 & 66.94 \\ 2.68 & 7.36 & 12.05 & 16.74 & 20.75 & 25.44 \\ 9.37 & 28.12 & 46.86 & 65.60 & 84.35 & 103.09 \\ 10.71 & 32.80 & 54.89 & 76.31 & 98.40 & 120.50 \\ 6.02 & 18.07 & 30.12 & 42.84 & 54.89 & 66.94 \\ 2.68 & 7.36 & 12.05 & 16.74 & 20.75 & 25.44 \\ 9.37 & 28.12 & 46.86 & 65.60 & 84.35 & 103.09 \\ 10.71 & 32.80 & 54.89 & 76.31 & 98.40 & 120.50 \end{bmatrix} Hz$$

adjust frequency to match adjusted wavelengths associated with the lock-in frequencies

Section 4. Wind Power Input

Verify the the power is D4 f3 based on first principles - see You, Xie et al 2018

$C_L \cdot \frac{1}{2} \cdot \rho \cdot U^2 \cdot D \cdot \sin(2 \cdot \pi \cdot f \cdot t)$ wind force assumed constant along cylinder

$\alpha \cdot D \cdot \cos(\omega \cdot t - \varphi) \cdot \sin\left(\frac{x}{\lambda} \cdot 2 \cdot \pi\right)$ deflection along a full wavelength

Wind power input per length using a half wavelength over a half of a period

$$\frac{\int_0^{\frac{\lambda}{2}} \int_0^{\frac{1}{2 \cdot f}} C_L \cdot \frac{1}{2} \cdot \rho \cdot \left(\frac{f \cdot D}{S_t}\right)^2 \cdot D \cdot \sin(2 \cdot \pi \cdot f \cdot t) \cdot \left(\frac{\mathrm{d}}{\mathrm{d}t}(\alpha \cdot D \cdot \cos(2 \cdot \pi \cdot f \cdot t - \varphi))\right) \cdot \sin\left(\frac{x}{\lambda} \cdot 2 \cdot \pi\right) \mathrm{d}t \, \mathrm{d}x}{\frac{1}{2 \cdot f} \cdot \frac{\lambda}{2}}$$

The integral is evaluated symbolically by Mathcad:

$$-\frac{C_L \cdot D^4 \cdot \alpha \cdot \rho \cdot f^3 \cdot \cos(\varphi)}{S_t^2}$$

Verification that the wind power input is the product of a function of lift coefficient *fnc* times frequency3 and diameter4. In this case fcn = CL * α *ρ * cos(φ) / St2

The function fnc is taken from an empirical fit as provided by Foti and Martinelli 2018 based on Diana et al.

$$fnc(\alpha) := \begin{cases} \text{if } \alpha > 1 \\ \quad 10^{-16} \\ \text{also if } \alpha \le 0 \\ \quad 0 \\ \text{else} \\ \quad \left(-99.73 \cdot \alpha^3 + 101.62 \cdot \alpha^2 + .1627 \cdot \alpha + 0.2256\right) \end{cases}$$

Calculate the correction factor βturb associated with turbulence.

$$I_v := 0.131$$

$$\beta_{turb} := \left(1 + \left(\frac{I_v}{0.09}\right)^2\right)^{\frac{-1}{2}} = 0.566$$

$$P_w(f, \alpha) := \beta_{turb} \cdot \left(fnc(\alpha) \cdot \frac{W}{m} \cdot Hz^{-3} \cdot m^{-4}\right) \cdot f^3 \cdot D^4$$

$$\alpha Plot := 0.001, 0.002 .. 1.0$$

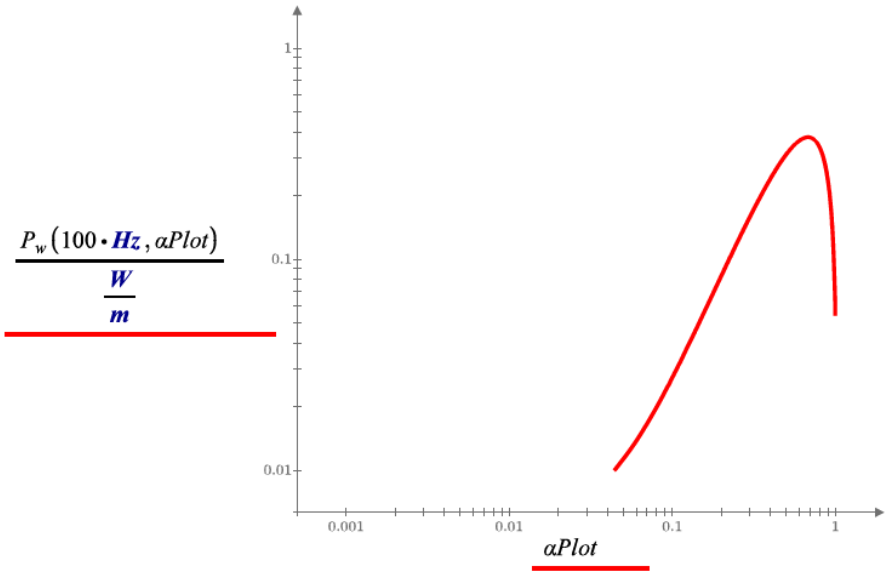

Section 5. Conductor Self-Damping

This section follows the self-damping derivation provided by Foti and Martinelli (2018)

$$x_0(\alpha,\lambda) := \left\| \begin{array}{l} \text{if } \chi_0 \geq \dfrac{4\cdot\pi^2}{\lambda^2}\cdot\alpha\cdot D \\ \quad \left\| \dfrac{\lambda}{4} \right. \\ \text{else} \\ \quad \left\| \dfrac{\lambda\cdot\operatorname{asin}\left(\dfrac{\lambda^2\cdot\chi_0}{4\cdot\pi^2\cdot\alpha\cdot D}\right)}{2\cdot\pi} \right. \end{array} \right.$$

If transition curvature χ0 is greater than the max curvature, then x0 = λ / 4 (at antinode) and the entire line is in a microslip mode with G1 = 1/3 and G2 = 0. Otherwise χ0 transition occurs at x0 within the half wavelength found by the equation.

$$G_1(\alpha,\lambda) := \left(\frac{1}{3} - \frac{3}{8}\cdot\cos\left(2\cdot\pi\cdot\frac{x_0(\alpha,\lambda)}{\lambda}\right)\right) + \frac{1}{24}\cdot\cos\left(6\cdot\pi\cdot\frac{x_0(\alpha,\lambda)}{\lambda}\right)$$

scales the damping from microsliding

$$G_2(\alpha,\lambda) := \pi - 4\cdot\pi\cdot\frac{x_0(\alpha,\lambda)}{\lambda} + \sin\left(4\cdot\pi\cdot\frac{x_0(\alpha,\lambda)}{\lambda}\right)$$

scales the damping from gross sliding

$$P_{d1}(\alpha,\lambda,f) := G_1(\alpha,\lambda)\cdot\left(\frac{128\cdot\pi^5\cdot(mass)^3\cdot RTS\cdot EI_{maxref}}{c_0\cdot\mu}\right)\cdot\frac{(\alpha\cdot D)^3\cdot f^7}{(\eta\cdot RTS)^4}$$

self-damping from micro-sliding

$$P_{d2}(\alpha,\lambda,f) := G_2(\alpha,\lambda)\cdot\left(4\cdot\pi^3\cdot(mass)^2\cdot EI_{maxref}\right)\cdot\frac{(\alpha\cdot D)^2\cdot f^5}{(\eta\cdot RTS)^2}$$

self-damping from gross sliding

$$P_d(f,\alpha) := P_{d1}\left(\alpha,\frac{1}{\lambda}\cdot\sqrt{\frac{\eta\cdot RTS}{\ }},f\right) + P_{d2}\left(\alpha,\frac{1}{\lambda}\cdot\sqrt{\frac{\eta\cdot RTS}{\ }},f\right)$$

total self-damping

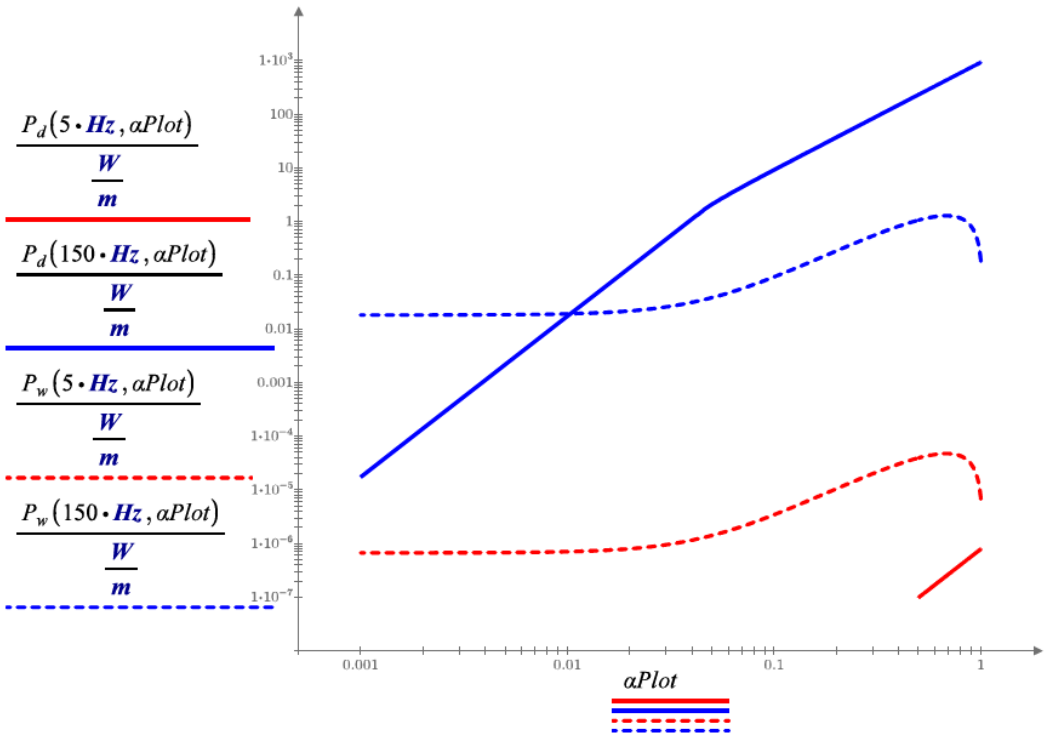
$\frac{P_d(5 \cdot Hz, \alpha Plot)}{\frac{W}{m}}$
$\frac{P_d(150 \cdot Hz, \alpha Plot)}{\frac{W}{m}}$
$\frac{P_w(5 \cdot Hz, \alpha Plot)}{\frac{W}{m}}$
$\frac{P_w(150 \cdot Hz, \alpha Plot)}{\frac{W}{m}}$
$1 \cdot 10^3$
100
10
1
0.1
0.01
0.001
$1 \cdot 10^{-4}$
$1 \cdot 10^{-5}$
$1 \cdot 10^{-6}$
$1 \cdot 10^{-7}$
0.001
0.01
0.1
1
αPlot

Section 6. Amplitudes and Stresses

Use the built built solver to determine the vibration amplitude at which the self-damping balances the wind power input

$a := 2$ guessing high seems to be more stable

Guess Values

Constraints

$$\left(\frac{P_d(f,a)}{\frac{W}{m}}\right) = \left(\frac{P_w(f,a)}{\frac{W}{m}}\right)$$

Solver

$$getα(\lambda, f) := \mathbf{Find}(a)$$

$$ymax_{i,j} := D \cdot getα\left(\lambda_{i,j}, f_{i,j}\right)$$

$$ymax = \begin{bmatrix} 14.300 & 10.085 & 3.383 & 1.245 & 0.710 & 0.492 \\ 14.300 & 14.300 & 13.427 & 10.986 & 8.218 & 5.340 \\ 14.162 & 4.108 & 0.999 & 0.509 & 0.338 & 0.251 \\ 13.853 & 2.638 & 0.710 & 0.396 & 0.269 & 0.201 \\ 14.300 & 10.085 & 3.383 & 1.245 & 0.710 & 0.492 \\ 14.300 & 14.300 & 13.427 & 10.986 & 8.218 & 5.340 \\ 14.162 & 4.108 & 0.999 & 0.509 & 0.338 & 0.251 \\ 13.853 & 2.638 & 0.710 & 0.396 & 0.269 & 0.201 \end{bmatrix} mm$$

$$curv_{i,j} := \frac{4 \cdot \pi^2}{\left(\lambda_{i,j}\right)^2} \cdot ymax_{i,j}$$

$$curv = \begin{bmatrix} 0.001 & 0.005 & 0.005 & 0.004 & 0.003 & 0.003 \\ 0.000 & 0.001 & 0.003 & 0.005 & 0.005 & 0.005 \\ 0.002 & 0.005 & 0.003 & 0.003 & 0.004 & 0.004 \\ 0.002 & 0.004 & 0.003 & 0.004 & 0.004 & 0.004 \\ 0.001 & 0.005 & 0.005 & 0.004 & 0.003 & 0.003 \\ 0.000 & 0.001 & 0.003 & 0.005 & 0.005 & 0.005 \\ 0.002 & 0.005 & 0.003 & 0.003 & 0.004 & 0.004 \\ 0.002 & 0.004 & 0.003 & 0.004 & 0.004 & 0.004 \end{bmatrix} \frac{1}{m}$$

$$\sigma_{a_{i,j}} := \pi \cdot d_A \cdot E_a \cdot \sqrt{\frac{mass}{\beta_{EI} \cdot EI_{max}}} \cdot f_{i,j} \cdot ymax_{i,j}$$

$$\sigma_a = \begin{bmatrix} 5.834 & 12.342 & 6.899 & 3.611 & 2.639 & 2.23 \\ 2.593 & 7.13 & 10.955 & 12.449 & 11.547 & 9.198 \\ 8.987 & 7.821 & 3.171 & 2.263 & 1.933 & 1.751 \\ 10.047 & 5.859 & 2.639 & 2.046 & 1.789 & 1.638 \\ 5.834 & 12.342 & 6.899 & 3.611 & 2.639 & 2.23 \\ 2.593 & 7.13 & 10.955 & 12.449 & 11.547 & 9.198 \\ 8.987 & 7.821 & 3.171 & 2.263 & 1.933 & 1.751 \\ 10.047 & 5.859 & 2.639 & 2.046 & 1.789 & 1.638 \end{bmatrix} MPa$$

$$AnnualN_{i,j} := windRose_{i,j} \cdot f_{i,j} \cdot 1 \cdot \mathbf{yr}$$

$$AnnualN = \begin{bmatrix} 4.54E+006 & 2.18E+007 & 3.13E+006 & 5.25E+005 & 1.71E+005 & 2.98E+004 \\ 3.55E+006 & 1.08E+007 & 3.77E+006 & 6.34E+004 & 3.24E+004 & 2.27E+004 \\ 1.18E+007 & 4.34E+007 & 9.28E+006 & 1.40E+006 & 1.88E+005 & 0.00 \\ 8.98E+006 & 4.28E+007 & 2.97E+007 & 1.63E+007 & 4.45E+006 & 5.91E+005 \\ 4.64E+006 & 1.99E+007 & 5.51E+006 & 6.49E+005 & 6.12E+004 & 0.00 \\ 2.30E+006 & 2.14E+007 & 3.96E+006 & 1.45E+005 & 2.31E+004 & 5.67E+003 \\ 7.00E+006 & 1.14E+008 & 1.01E+008 & 5.51E+006 & 1.50E+005 & 2.30E+004 \\ 5.22E+006 & 1.36E+008 & 1.28E+008 & 1.53E+007 & 1.78E+006 & 5.37E+004 \end{bmatrix}$$

$$AnnualN_{i,j} := \left\| \begin{array}{l} \text{if } perpSpeed_{i,j} > 15 \cdot mph \vee f_{i,j} > 150 \cdot Hz \\ \quad \| 0 \\ \text{also if } \left(perpSpeed_{i,j} < 2 \cdot mph\right) \vee \left(f_{i,j} < 3 \cdot Hz\right) \\ \quad \| 0 \\ \text{else} \\ \quad \| AnnualN_{i,j} \end{array} \right\|$$

Section 7. Miner's Rule Using Cigre Safe Border Line

The variables gmean is the expected value of the sum of the components of Miner's Rule most perpendicular to the span. For the conductor line of the current example, the most perpendicular components have been identified as component numbers 2, 3, 0, 6, 7, and 4. Participation factors of 0.7686, 1.0, 0.2314, 0.7686, 1.0, and 0.2314 are applied to each component to account for the portion of the component that is the most perpendicular to the span.

$$g_{mean} := 0.7686 \cdot \left(\sum_j \frac{AnnualN_{2,j}}{N_{mean}\left(\sigma_{a_{2,j}}\right)} \right) + 1.0 \cdot \left(\sum_j \frac{AnnualN_{3,j}}{N_{mean}\left(\sigma_{a_{3,j}}\right)} \right) + 0.2314 \cdot \left(\sum_j \frac{AnnualN_{0,j}}{N_{mean}\left(\sigma_{a_{0,j}}\right)} \right) = 0.379$$
$$+ 0.7686 \cdot \left(\sum_j \frac{AnnualN_{6,j}}{N_{mean}\left(\sigma_{a_{6,j}}\right)} \right) + 1.0 \cdot \left(\sum_j \frac{AnnualN_{7,j}}{N_{mean}\left(\sigma_{a_{7,j}}\right)} \right) + 0.2314 \cdot \left(\sum_j \frac{AnnualN_{4,j}}{N_{mean}\left(\sigma_{a_{4,j}}\right)} \right)$$

The variables gvar is the variance of the random variable that is the Miner's Rule aggregation. The grvar variance includes only the components most perpendicular to the span

$$g_{var} := 0.7686 \cdot \sum_j \left(\left(\frac{AnnualN_{2,j}}{N_{mean}\left(\sigma_{a_{2,j}}\right)^2} \right)^2 \cdot N_{var}\left(\sigma_{a_{2,j}}\right) \right) + 1.0 \cdot \sum_j \left(\left(\frac{AnnualN_{3,j}}{N_{mean}\left(\sigma_{a_{3,j}}\right)^2} \right)^2 \cdot N_{var}\left(\sigma_{a_{3,j}}\right) \right) = 4.775 \cdot 10^{-8}$$
$$+ 0.2314 \cdot \sum_j \left(\left(\frac{AnnualN_{0,j}}{N_{mean}\left(\sigma_{a_{0,j}}\right)^2} \right)^2 \cdot N_{var}\left(\sigma_{a_{0,j}}\right) \right) + 0.7686 \cdot \sum_j \left(\left(\frac{AnnualN_{6,j}}{N_{mean}\left(\sigma_{a_{6,j}}\right)^2} \right)^2 \cdot N_{var}\left(\sigma_{a_{6,j}}\right) \right)$$
$$+ 1.0 \cdot \sum_j \left(\left(\frac{AnnualN_{7,j}}{N_{mean}\left(\sigma_{a_{7,j}}\right)^2} \right)^2 \cdot N_{var}\left(\sigma_{a_{7,j}}\right) \right) + 0.2314 \cdot \sum_j \left(\left(\frac{AnnualN_{4,j}}{N_{mean}\left(\sigma_{a_{4,j}}\right)^2} \right)^2 \cdot N_{var}\left(\sigma_{a_{4,j}}\right) \right)$$

Fit to ACSR SN curves from Orange Book. Assume Gaussian Distribution.

$$N_{mean}(\sigma) \equiv 6.886 \cdot 10^{12} \cdot \left(\frac{\sigma}{MPa}\right)^{-4.502}$$

$$N_{var}(\sigma) \equiv 1 \cdot 10^{17} \cdot \left(\frac{\sigma}{MPa}\right)^{-6.454}$$

For Miner's Rule,the mean capacity is 1.0 (ratio of total cycles to cycles-to-failure) with a variance of 0.1 (assumed).

$R_{mean} := 1.0$ $R_{var} := 0.1$

Section 8. Failure Probability versus Age

Probability of failure as a function of age assuming Gaussian distributions.

$$p_f(age) := \text{pnorm}\left(-\frac{R_{mean} - age \cdot g_{mean}}{\sqrt{R_{var}{}^2 + age \cdot g_{var}}}, 0, 1\right)$$

$agePlot := 0, 0.1 .. 10$

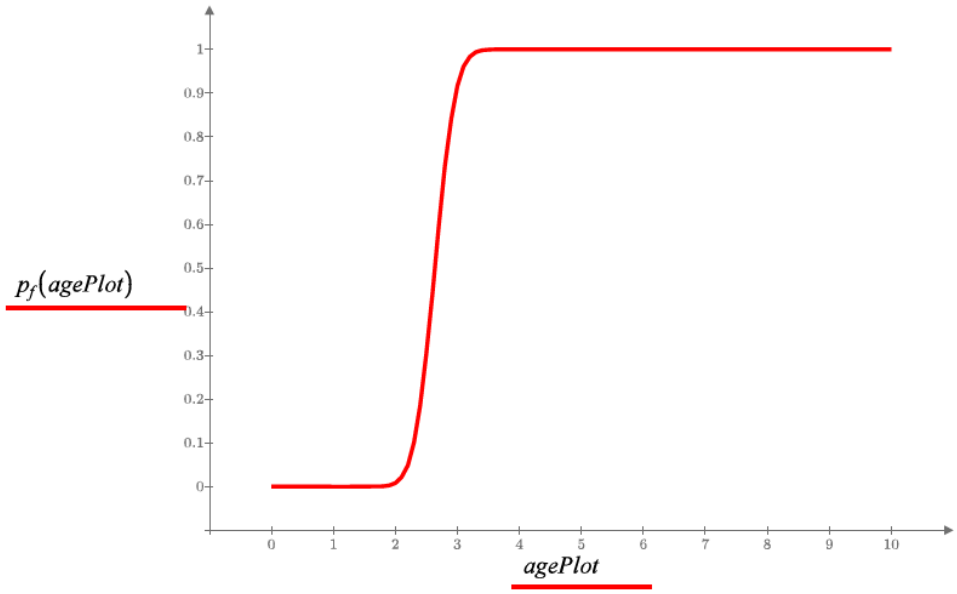

DRAFT: 31 March 2022, Revision 1

Appendix G

Wear Model

Exponent®

EXTERNAL MEMORANDUM

TO: [redacted] (PG&E)

FROM: Exponent

DATE: March 31, 2022

PROJECT: Transmission Composite Model

SUBJECT: Mechanical Wear Model

This memorandum describes the technical basis for design life reductions due to the susceptibility of components to wind-induced swinging and wear of connections.[1] Fundamental wind parameters provided by PG&E meteorology on the POMMS grid define the site-specific hazard for near-surface wind gusting (turbulence) and associated buffeting of components leading to wear. The swing amplitude and frequency is used to estimate wear damage accumulation, and the expected useful lives of components vulnerable to higher rates of wear damage are adjusted downward.

Wind Environment and Near-Surface Wind Modeling

Wear occurs chiefly due to large deflections and associated rubbing when relatively light, unbraced components are buffeted in turbulent (gusting) wind. Turbulence is due to roughness of the ground interrupting otherwise laminar wind flow. As such, the gustiness of the wind is site-specific and will differ at sites in wooded hills, open agricultural lands, and near large bodies of water. The characteristics of the gusting that are important to wear include both intensity and frequency content.

The wear model adopts the basic logarithmic wind model to describe the site-specific wind profile, which describes how wind speed varies with height z above the ground. Equation (1) gives this model,

$$U(z) = \frac{u^*}{\kappa} \times \ln\left(\frac{z - z_h}{z_0} + \Psi\right) \qquad (1)$$

where u^* is the friction velocity, κ is the von Karman constant = 0.4, z_0 is the roughness length, z_h is the zero-plane displacement, and Ψ is a function that depends on the stability of rising air.

[1] A discussion of the use of results from the Mechanical Wear Model to determine design life reduction factors in the Transmission Composite Model is provided in Revision 1 of Exponent's, "PG&E's Composite Risk Model for Overhead Electric Transmission Components: A White Paper."

Because wear occurs relatively close to the ground relative to the entire air column, some simplifications are applied that are common to wind engineering of structures. First, the Ψ function is assumed to be negligible at the heights of interest to structural engineers. The term z_h depends on the height of surrounding structures and is conservatively taken to be zero herein; the value of z_h could be refined in the future should additional data become available. These assumptions result in a simplified model of the wind profile, as given in Equation (2), that closely resembles the model used in building codes.

$$U(z) = \frac{u^*}{\kappa} \times \ln\left(\frac{z}{z_0}\right) \qquad (2)$$

Figure 1 shows a typical wind profile obtained using Equation (2).

Figure 1. Typical wind profile using Equation 2

The surface roughness that slows the wind due to surface friction is defined by the roughness length z_0. For each structure, this parameter can be estimated based on land-cover/land-use categories provided by PG&E using guidance in ASCE 7-22. The wind profile can be approximated for each asset based on the POMMS grid cell in which it is located .

In addition to the wind profile, the distribution of wind speeds and directions is also important. How often the wind blows at different speeds and from different directions is typically defined by a wind rose, which is a two-dimensional histogram. Based on PG&E historical wind speed

measurements, wind roses are derived for each POMMS grid. Because the compass orientation of jumpers or other components susceptible to wear is not known with sufficient certainty at this time, we make the conservative assumption that wind from any direction can cause gross deflections and associated wear. Figure 2 shows a sample wind rose.

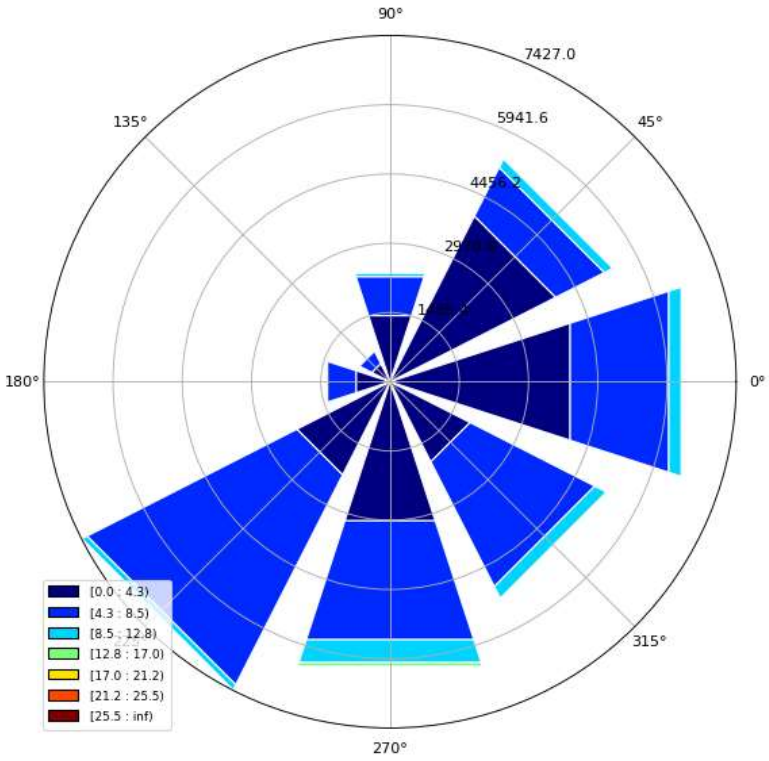

Figure 2. Example wind rose derived from PG&E meteorological data for POMMS Grid Cell 281_189.

Finally, the frequency content of the turbulence is determined using a standard gust spectrum. Frequency content is important because wind energy at the natural frequency of the component will cause significant displacement amplification by a mechanism known as resonance. As an example, resonance allows a child on a swing to achieve significant height with only a series of light pushes, as long as those pushes are applied at the right frequency.

Wind at any elevation above the ground can be decomposed into a steady (stationary mean) wind U (as given by Equation 2) and a dynamic component $u(t)$ that is superposed onto U, as diagrammed in Figure 3. By definition $u(t)$ has a mean of zero and a nonnegative standard deviation σ_u. Increasing standard deviation is associated with increasing gustiness (turbulence).

The turbulence intensity I_u is defined as $\frac{\sigma_u}{U}$ and is also equal to $\frac{1}{ln(\frac{z}{z_0})}$. These equations allow us to compute σ_u.

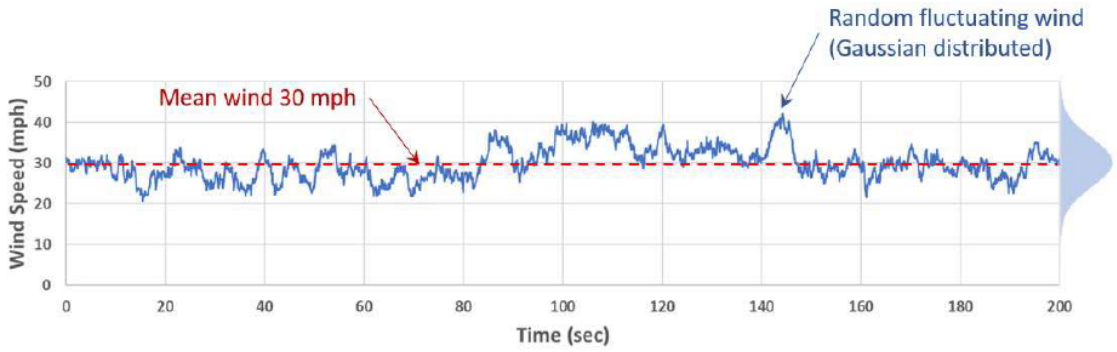

Figure 3. Dynamic model of wind as a random fluctuating component (**blue**) superposed on a steady mean wind (**red**).

The frequency content of the wind turbulence for a broad range of frequencies is the gust spectral density. There are several models available to define the spectrum, and herein we use the von Karman model as given in Equation 3,

$$S_u(f) = \frac{{\sigma_u}^2}{f} \frac{4(\frac{f*L_u}{U})}{[1+70.8*(\frac{f*L_u}{U})^2]^{\frac{5}{6}}} \qquad (3)$$

where f is the frequency and U is the mean wind speed defined above.

The input parameters of the von Karman gust spectrum are all defined above with the exception of L_u, the length scale. This parameter does not appear to be used by Meteorology and so we have adopted an empirical approximation by EDSU[2] that is a function of surface roughness and elevation above the ground.

$$Lu = 280m(\frac{z}{z_i})^{0\,35} \qquad (4)$$

Figure 4 shows a sample von Karman gust spectrum.

[2] As provided in Section 2.6.5 of the Wind Energy Handbook by Burton et all, 3rd Edition.

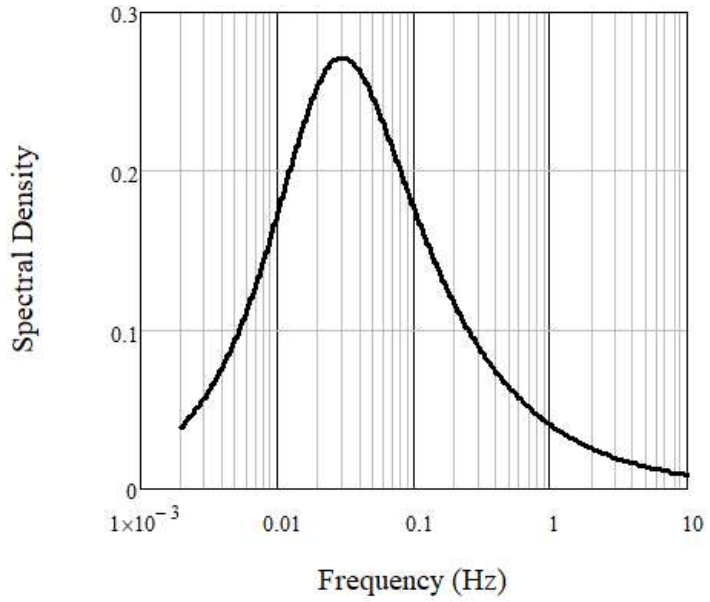

Figure 4. Example von Karman gust spectrum showing frequency content of the turbulent component of the wind

Component Structural Model

We expect that components subject to wear come in a variety of shapes and sizes, and no one structural model will represent all permutations. We instead use an idealized pendulum model whose parameters (mass, length, stiffness, damping, pin radius, plate thickness) can be varied to represent a wide range of components. The important parameters are summarized below:

- A pendulum has a natural period of vibration, that is, the time it takes to make one cycle of swing, there and back again. The inverse of the fundamental period is the fundamental frequency. The period of a pendulum T is defined solely by its length L.
- The weight of the pendulum is the product of its mass, m, and gravitational acceleration, g. A pendulum's weight defines the contact stress on the rubbing (faying) surfaces: all else being equal, the greater the mass of the pendulum, the faster wear occurs.
- The contact area on the rubbing surfaces, defined by the pin radius r and the plate thickness t, determines the contact stress for a given pendulum mass. Higher stress results in faster wear:. for instance, a thin plate will wear faster than a thick plate supporting the same hook radius, all else being equal.

- The rate at which the material will wear, that is, the rate at which material will be lost, is a function of the hardness of the material. The material type and the Brinell hardness parameters can be changed to represent different types or vintages of steel components.

We approximate the pendulum model with a standard single-degree-of-freedom (SDOF) model, which is typically depicted by a cart carrying mass connected to a fixed boundary through a spring and damper. In our model, the mass is set by the component mass *m*, and the stiffness *k* is chosen to match the pendulum period. The damping *c* is estimated based on the rubbing friction coefficient and other inherent energy-dissipation mechanisms. Figure 5 shows the analogous SDOF model.

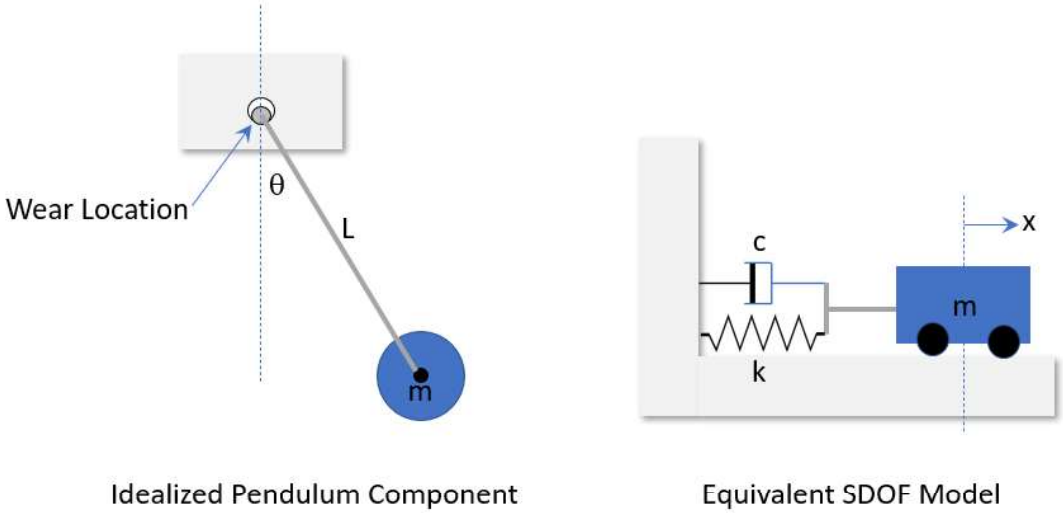

Figure 5. Single degree of freedom (SDOF) component idealizations

Given the natural period, equivalent stiffness, and damping of the analogous model, we estimate the displacement amplification due to resonance. This is done in the frequency domain by multiplying the gust spectrum and model mechanical admittance *H* (also known as the frequency response function). Equation 5 gives the mechanical admittance *H*,

$$H^2(f) = \frac{1}{\left[1-\left(\frac{f}{f_1}\right)^2\right]^2 + 4\eta^2\left(\frac{f}{f_1}\right)^2} \qquad (5)$$

where f_1 is the natural frequency of the equivalent model, and η is the fraction of critical damping.

The drag forces, stiffness, admittance, and gust spectrum allow calculation of the standard deviation of the pendulum displacement σ_x based on Parseval's Theorem, as given in Equation 6,

$$\sigma_x = \int_0^\infty \frac{1}{k^2} H(f)^2 \frac{4D^2}{U^2} S_u(f) df \qquad (6)$$

where D is the mean drag force on the component.

Wear is proportional to the total length of rubbing, which is the accumulation of very many cycles of pendulum swing. Given the amplitude of component displacement under all wind conditions of the wind rose, and given that the oscillating wind is normally distributed with known standard deviation, the number of cycles exceeding a given swing amplitude x can be calculated using the up-crossing frequency distribution f_p. For normally distributed displacements, the up-crossing frequency is Rayleigh distributed, according to Equation 7.

$$f_p(x) = \frac{x}{\sigma_x{}^2} e^{-\frac{x^2}{2\sigma_x{}^2}} \qquad (7)$$

Figure 6 shows an example up-crossing probability density as computed using Equation 7.

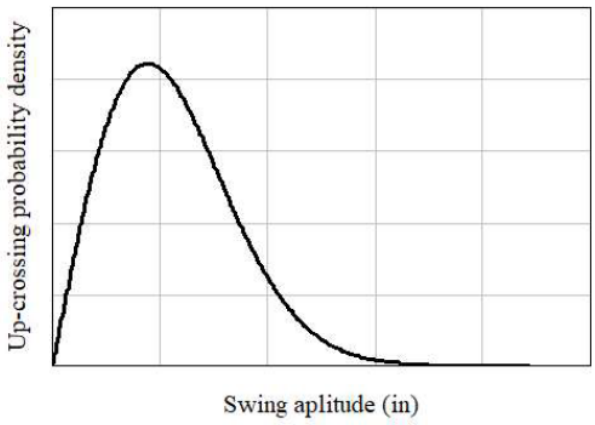

Figure 6. Example up-crossing distribution for pendulum swing amplitude

Finally, the total length of rubbing can be calculated by counting the number of swings that exceed a given amplitude over the age of the component. The accumulated length of rubbing, D, can be easily scaled from the total distance traveled by the pendulum,

$$D = f_1 \cdot age \cdot \frac{r}{L} \cdot \int_0^\infty x f_p(x) dx \qquad (8)$$

and the total volume of wear (material loss) V is given by the Archard wear equation,

$$V = \frac{K}{3 \cdot H} D \qquad (9)$$

where K is a wear rate constant (material property) and H is the Brinell hardness (kgf/m^2). The depth of wear is then simply the volume V divided by the faying area A_f, defined herein by the pin radius r and plate thickness t.

Modeling Wear from Gusting Winds

With the wind and structural models defined above, this section describes each step in the analysis for a single asset considering a single cell of the wind rose – that is, a single wind speed, wind direction, and the frequency with which that combination of wind speed and direction occurs. For each asset, the process described below is repeated for every cell (wind speed, direction, and duration) of the wind rose.

1. Define site-specific wind characteristics (wind rose, turbulence intensity) based on the POMMS grid cell in which the asset is located.
2. Estimate the length scale L_u and define the von Karman gust spectrum for the site at the elevation of the asset if known; absent data on the height of the asset from the ground, assume a height of 10 meters.
3. Define the mechanical admittance H based on the SDOF model properties (natural frequency, equivalent stiffness, critical damping ratio).
4. Calculate the response spectral density from the wind drag parameters, the admittance, and the gust spectrum.
5. Calculate the standard deviation σ_x of the dynamic component of the pendulum model displacement using Parseval's Theorem (Equation 6).
6. Assume the dynamic pendulum displacements are Gaussian, and define the crossing frequency as a Rayleigh distribution of displacement amplitude x. (This is only valid for an assumed narrow band process, and so up-crossings can be used to count cycles of different amplitudes.)
7. Calculate the total length of rubbing from the amplitude crossing frequency (Equation 8).
8. Calculate the volume of material lost to wear based on the rubbing distance, contact load, and material properties (Equation 9).
9. Calculate the depth of wear as the lost volume divided by the area of the faying surface.

Limitations

The model described herein necessarily relies on simplifying engineering assumptions and idealized representations of complex engineering systems, threats and loads. The implications and limitations of these modeling decisions have been discussed and accepted by PG&E Subject Matter Experts. While we have made every effort to accurately capture key factors related to mechanical wear that could adversely affect PG&E's transmission structures based on available information, this model is expected to be further refined as new idealizations, methods and/or data become available. Proper application of this model requires recognition and understanding of the limitations of both the scope and methodology.

The model described herein is intended to be incorporated into a comprehensive PG&E framework (TCM Framework) that was developed to inform PG&E risk mitigation decisions. Neither the Framework nor this model is intended to predict specific failures, and the actual performance of some assets may be materially different from that anticipated by the model.

For limitations associated with the Framework, see Revision 1 of Exponent's "PG&E's Composite Risk Model for Overhead Electric Transmission Components: A White Paper," dated March 31, 2022.

DRAFT: 31 March 2022, Revision 1

Appendix H

Insulator Contamination Model (In Progress)